ROLES OF MICROTUBULE POSTTRANSLATIONAL MODIFICATIONS IN ZEBRAFISH DEVELOPMENT AND BEHAVIOR

by

SUGANTHAN AMIRTHAGUNANATHAN

(Under the Direction of SCOTT T. DOUGAN)

ABSTRACT

Microtubules are one of the major cytoskeletons in eukaryotes. They are polymers of α- and β-tubulins heterodimers. Microtubules play many important roles in diverse cellular functions and establishing cellular structures like cilia, neuronal axons, and centrosomes. Microtubule Posttranslational modifications provide the diversity for microtubules to carry out these functions. Microtubule acetylation, glycylation, glutamylation, and detyrosination are the major PTMs in vertebrates. We generated mutants of enzymes that carry out these modifications to understand their roles in zebrafish development, ciliary functions, and neuronal functions.

Animal-vegetal (AV) axis formation occurs during oogenesis by forming the Balbiani body at the future vegetal pole. The formation of chromosomal bouquet during the zygotene stage is the initial asymmetry-breaking step, and precursors of the Balbianic body formed at the cytoplasmic site where this chromosomal bouquet is formed. A

zygotene stage-specific cilium plays a critical role in chromosomal bouquet formation. In our study, we found that mutants that lack both microtubule acetylation and glycylation show defects in the chromosomal bouquet formation, leading to reduced female fecundity and fertility. The zygotene cilia of *atat1; ttll3* double mutant does not show any ciliogenesis or ciliary maintenance defect. The loss of these modifications potentially alters the ciliary function by changing the physical properties of these microtubules. Additionally, we found that *ttll3* exhibits reduced progressive sperm motility and *atat1* mutants show altered behavior. Our data show that microtubule acetylation and glycylation play important roles in zebrafish ciliary and neuronal function, and also these modifications synergistically regulated oocyte polarization.

In this work, we generated mutants of microtubule detyrosinases *vash1* and *vash2* using CRISPR-Cas9 RNP mutagenesis. Single and double mutants of these genes showed reductions in microtubule detyrosination and *vash1; vash2* double mutant showed low penetrance microcephaly, curved body, and heart edema phenotypes. We also found a potential alteration in axonal transportation in the double mutant. Additionally, We generated a mutant of the *ttl* gene responsible for retyrosination and mutants of microtubule glutamylation initiases *ttll4*, *ttll5*, and *ttll7* to study the importance of these modifications in zebrafish ciliary and neuronal functions.

INDEX WORDS: Zebrafish, Microtubule, Posttranslational modification, Acetylation, Glycylation, Detyrosination, Glutamylation, Oocyte polarization, Asymmetry breaking, Aggression, Social anxiety, Stress, CRISPR-Cas9

ROLES OF MICROTUBULE POSTTRANSLATIONAL MODIFICATIONS IN ZEBRAFISH DEVELOPMENT AND BEHAVIOR

by

SUGANTHAN AMIRTHAGUNANATHAN

BS, WAYAMBA UNIVERSITY OF SRI LANKA, SRI LANKA, 2012

A Dissertation Submitted to the Graduate Faculty of The University of Georgia in Partial Fulfillment of the Requirements for the Degree

DOCTOR OF PHILOSOPHY

ATHENS, GEORGIA

2022

ROLES OF MICROTUBULE POSTTRANSLATIONAL MODIFICATIONS IN ZEBRAFISH DEVELOPMENT AND BEHAVIOR

by

SUGANTHAN AMIRTHAGUNANATHAN

Major Professor:	Scott T. Dougan
Committee:	Jacek Gaertig
	James D. Lauderdale
	Jonathan Eggenschwiler
	Daichi Kamiyama

Electronic Version Approved:

Ron Walcott
Vice Provost for Graduate Education and Dean of the Graduate School
The University of Georgia
August 2022

DEDICATION

I dedicate this work to my mother and late father for their unconditional love, hard work, and the sacrifices they made to provide my siblings and me with educational and life opportunities.

ACKNOWLEDGEMENTS

First, I would like to thank my major professor Scott T. Dougan for his enormous support and guidance during my time as his student. He has been very patient with me and allowed me to pursue the project I enjoyed. He has supported taking the projects in new directions and learning new techniques. Scott also helped me keep the direction of the project on the right path. He always has very communicative and replies to my emails. He has given valuable suggestions for my projects. I am very grateful for his contributions to my growth in my time as a graduate student.

I also like to thank my committee members Jacek Gaertig, Jim Lauderdale, Jonathan Eggenschwiler, and Daichi Kamiyama for their guidance and support. They helped me with problems I encountered in my experiments and kept me in the right direction. They also shared resources to carry out my experiments. I want to extend my gratitude to their lab members for helping me by providing chemicals and allowed to use their lab equipment.

I also thank Kojo Mensa-Wilmot, Karl F. Lechtreck, and their lab members for sharing resources and equipment. I also like to thank Muthugapatti Kandasamy for his help in the use of the confocal microscope. I also like to thank all the instructors I have worked with as TA and all the TAs and students who made my teaching labs enjoyable. I also want to thank the administrative staff of the Department of Cellular Biology, Carrie Hardin, Robin Fowler, Genia King, and Beverly Martin, for their help navigating graduate school.

I also want to thank Dougan lab members, Munisha, Nurgul, and Aimee for being great colleagues and friends. They helped me adapt to the lab when I joined it and, over the years, helped me with many laboratory activities. We also had great discussions on research ideas and life outside the lab.

I also like to thank my friends in Athens, Ishan, Afaq, Natasha, Zahra, Prasangi, TC, and Samanthi, for their help settling in Athens and making my stay enjoyable. We shared great memories, and I am very grateful for that.

I like to express my gratitude to my mother, brother, and sister for their support and encouragement in taking this endeavor. I also like to thank my wife, Baviththira Suganthan, for her support and encouragement. As a graduate student, she is also going through the same difficulties I have been through, but she is always there to support me, and I am grateful for that. I also like to thank my little daughter, who always makes me happy with her smiles and keeps me motivated.

TABLE OF CONTENTS

Page

LIST OF TABLES

Page

LIST OF FIGURES

Page

CHAPTER 1

INTRODUCTION AND LITERATURE REVIEW

Early embryonic development and microtubules

A fertilized egg undergoes a series of cell division, proliferation, migration, and differentiation to form a multicellular organism. A fertilized egg undergoes the cleavage stage, at which it undergoes rapid cell divisions into blastomeres. These blastomeres undergo gastrulation and form germ layers. Then tissues and organs are formed through organogenesis. Each step is tightly regulated and coordinated through cell signaling during these processes. During this process, the body axes and basic body plan are determined to direct morphogenesis. Microtubules and structures made out of microtubules, like cilia and spindle, play important roles in these processes.

Roles of microtubules during gastrulation

Microtubules play roles during zebrafish gastrulation. The progress of epiboly depends on the microtubule network of the yolk. Microtubules have been shown in the yolk syncytial layer (YSL) and yolk cytoplasmic layer (YCL). Disruption of these microtubules with taxol or nocodazole results in arrest in epiboly and movement of yolk syncytial nuclei (YSN) (Solnica-Krezel and Driever, 1994). The movement of YSN is shown to be carried out by motor proteins along the microtubules (Fei et al., 2019).

Another study in *Xenopus* gastrula shows the importance of opposite forces generated by F-actin and myosin-2 in the apical region and microtubule and myosin-10 in the basal region position the spindle for symmetric division of epithelium during early epiboly and even spread of cells (Woolner and Papalopulu, 2012).

Roles of microtubules in axis formation

Microtubules also play important roles in major axis formation during development. Microtubules have been shown to play critical roles during the initial establishment of the animal-vegetal axis. In zebrafish, the animal-vegetal axis formation is determined by the presence of the Balbiani body (Billett and Adam, 1976). During the oogenesis, oocyte polarization and asymmetry breaking occur during the zygotene stage of meiosis I. Chromosomal bouquet forms in one pole of the nucleus, and precursors of the Balbiani body accumulate in the cytoplasmic side of this nuclear pole and determine the future vegetal pole (Elkouby et al., 2016). Microtubules have been shown to play an important role in this chromosomal bouquet formation. Telomere movement during the bouquet formation is carried out by the dynein-driven movement of telomere along the perinuclear microtubule through the SUN-KASH complex (Shibuya et al., 2014). Depolymerizing these microtubules with nocodazole disrupt chromosomal bouquet formation (Elkouby et al., 2016). A zygotene stage cilium is also shown to play a critical role in this event. Chromosomal bouquet formation is disrupted when these cilia are disrupted (Mytlis et al., 2022). In vertebrates animal-vegetal axis influence the formation of the future dorsal-ventral and anterior-posterior axis as well (Miller et al., 1999, Kimelman and Martin, 2012).

Microtubules play an important role in dorsal-ventral axis formation. In Xenopus, dorsal determinants are localized in the vegetal pole. During the first cell cycle after fertilization, these determinants translocate to the future dorsal axis by microtubule-mediated cortical rotation (Elinson and Rowning, 1988, Miller et al., 1999). When fertilized eggs were treated with colchicine, it disrupted the cortical rotation and cortical microtubules (Manes et al., 1978, Elinson and Rowning, 1988). A similar role of cortical microtubules and cortical rotation is also reported in zebrafish (Tran et al., 2012). Microtubules also play an important role in Drosophila dorsal-ventral axis formation. In *Drosophila*, oocyte nuclei are pushed anteriorly and dorsally by growing microtubules (Zhao et al., 2012). This event influences gurken mRNA's localization and the Gurken protein distribution to establish the D-V axis (Norvell et al., 2015).

Studies in *Drosophila* and *C.elegans* show the roles of microtubules in anterior-posterior (AP) axis formation. In *C.elegans* AP axis is established after fertilization and the position of the sperm-derived centrosome determines the posterior end. Studies with mutants that arrest after fertilization and RNAi knockdown of tubulin show microtubules play a role in polarity signaling to regulate polarity proteins (PAR) and establish the AP axis (Wallenfang and Seydoux, 2000, Tsai and Ahringer, 2007). The determination of the AP axis takes place during oogenesis. *Bicoid* and *oskar* mRNAs localization at the anterior and posterior determines the axis. A weakly polarized microtubules-based cytoskeleton network plays an important role in the transportation of *oskar* mRNA to the posterior (Zimyanin et al., 2008). A noncetrosomal MTOC plays an important role in establishing the weak polarization toward the posterior (Nashchekin et al., 2016).

Internal organs in vertebrates show left-right asymmetry (Burdine and Schier, 2000). Cilia play an important role in Left-Right (L-R) axis formation. Asymmetric fluid flow generated by monocilia in the node of mice embryo plays a role in the asymmetric expression of Lefty-2, which defines the left side. Knockdown of *Kif3a* or *Kif3b* results in node cells that lack monocilia, and these embryos had bilateral or absent *Lefty-2* expression (Hirokawa et al., 2006). A similar role of cilia generating asymmetric fluid flow to determine in L-R pattern was shown in kupffer's vesicle of zebrafish (Essner et al., 2005).

Roles of microtubules in cell signaling

Cilia are also shown to play the role of signaling centers. Cilia play an important role in the hedgehog signaling pathway. In vertebrates, the localization of the hedgehog signaling pathway component to cilia regulates whether it is activated or not. When the ligand binds to the receptor Patched, it is removed from the ciliary membrane, allowing the Smoothened to accumulate at the ciliary membrane. Smoothened relieves the repression of Gli proteins by Sufu. These activator Gli proteins would promote the transcription of hedgehog signaling targets (Drummond, 2012). Studies have shown the role of cilia in Wnt signaling. Its role in the canonical Wnt signaling pathway is controversial, with some studies showing that cilia are important and others refuting that notion. There is some evidence showing the role of cilia in the non-canonical PCP signaling pathway (Eggenschwiler and Anderson, 2007).

Microtubules

Microtubules are one of the major components of eukaryotic cytoskeletons, defined by their hollow tubular structure and are 25 nm in diameter (Colantonio et al., 2014). Heterodimers of α-tubulin and β-tubulin polymerized to form linear protofilaments, and incorporation of α-tubulin and β-tubulin dimer into the polymer results in hydrolysis of GTP associated with β-tubulin. In most cases, thirteen protofilaments assemble into microtubules, which are polarized and arranged in the same orientation. Microtubules are dynamic and undergo phases of shrinkage and growth named catastrophe and rescue. Microtubules grow and shrink at the ends, and microtubule dynamics are regulated by microtubule-associated proteins (MAPs) to carry out their functions (Horio and Murata, 2014).

Microtubule diversity

Microtubules carry out many cellular functions in maintaining cell shape, establishing cell polarity, intracellular transportation, cell division, cell signaling, and motility. Microtubules play essential roles in establishing cellular structures like centrosomes, cilia, and axons of neurons (Magiera et al., 2018b). These different cellular functions require microtubules that have differences in dynamic nature, mechanics, and associated MAPs (Roll-Mecak, 2020). The diversity of microtubules needed to carry out these diverse functions is achieved using different gene-encoded isotypes of α-tubulin and β-tubulin and posttranslational modifications (PTMs) of these tubulins (Janke, 2014). Microtubule diversity is generated using a combination of tubulin isotypes and microtubule PTMs called the "Tubulin code" (Verhey and Gaertig, 2007, Janke, 2014).

Tubulin code is suggested to act as a fine regulator of microtubule functions (Janke and Magiera, 2020).

Tubulin isotypes

The existence of gene-encoded α- and β-tubulins isotypes were initially identified based on the heterogeneity in amino acid sequencing (Ponstingl et al., 1981, Krauhs et al., 1981). Many tubulin isotypes have been reported across diverse model organisms (Nsamba and Gupta Jr, 2022). There is no evidence to show that these isotypes form homogeneous microtubules for one type of isotype. Studies in mammalian cells show different isotypes of microtubules into heterogenous microtubules (Lewis et al., 1987). But levels and combinations of varying α- and β-tubulins isotypes could result in diverse microtubules that differed in physical properties and associated MAPs to carry out specific functions. Several tubulin isotypes express abundantly in specific tissues, indicating the importance of those isotypes in tissue-specific functions. Studies have shown enrichment of *Tubb1, 2,* and *4* in mice neurons, *Tubb4* in bovine connecting cilia of photoreceptors, *Tuba3* and *7* in mice testis, and *tuba7l* in zebrafish testis (Joshi and Cleveland, 1989, Renthal et al., 1993, Villasante et al., 1986, Atienzar-Aroca et al., 2021). Differential temporal and spatial expression of both α- and β-tubulins is also reported during embryonic development, indicating specific roles of tubulin isotypes during organogenesis (Denoulet et al., 1986, Lewis et al., 1985, Ginzburg et al., 1985, Buttgereit et al., 2003).

Mutations in α-tubulin isotypes *Tuba1a, Tuba8*, and β-tubulin isotypes *Tubb2b* and *Tubb3* of human are associated with neurological disorders that result in aberrant

neuronal differentiation, migration, axon guidance, and migration (Tischfield et al., 2011). These studies indicate the importance of tubulin isotypes in unique microtubule functions.

Tubulin posttranslational modifications

Phosphorylation was the first microtubule PTM identified (Murray and Froscio, 1971). Since then, many other microtubule posttranslational modifications and enzymes that add or remove these modifications have been identified. Most of these PTMs and enzymes are conserved in many organisms. Some PTMs like, acetylation, methylation, phosphorylation, and methylation occur in the tubulin body (Figure 1.1). Others like detyrosination, glutamylation, and glycylation take place in the C-terminal tails of tubulins (Figure 1.1). In addition to these major modifications, many other microtubule PTMs were also identified (Table 1.1). Most of these modifications occur preferentially on microtubules over tubulin heterodimers, and most are associated with stable microtubules. These modifications alter the physical properties of microtubules and preferential associations of MAPs with microtubules, making them an essential component in generating microtubule diversity.

Microtubule acetylation

Microtubule acetylation was initially reported on *Chlamydomonas reinhardtii* flagella (L'Hernault and Rosenbaum, 1983, L'Hernault and Rosenbaum, 1985), and the modification site was identified as lysine 40 of α-tubulin (LeDizet and Piperno, 1987). The occurrence of α-tubulin acetylation was reported in the axons of cerebellar neurons

(Cambray-Deakin and Burgoyne, 1987) and mouse brain (Eddé et al., 1989). This modification is conserved in sea urchins, *Drosophila*, humans (Piperno and Fuller, 1985), rats (Cambray-Deakin and Burgoyne, 1987), mice (Eddé et al., 1989), *Tetrahymena thermophila* (Gaertig et al., 1995), *C. elegans*, zebrafish (Akella et al., 2010), and in plants (Nakagawa et al., 2013). Unlike most other microtubule posttranslational modifications, acetylation of α-tubulin lysine 40 occurs on the luminal surface of the microtubule (Nogales et al., 1999).

The presence of α-tubulin acetyltransferase and tubulin deacetylase activities were reported in *Chlamydomonas reinhardtii* flagella and cytoplasm, respectively (Greer et al., 1985, Maruta et al., 1986). α-tubulin acetyltransferase acts preferentially on polymerized microtubules over α/β tubulin dimers (Maruta et al., 1986). The major enzyme involved in α-tubulin K40 acetylation is α-tubulin acetyltransferase (ATAT1) (Figure 1.2) (Akella et al., 2010, Shida et al., 2010). Other proteins like ARD1-NAT1 N-acetyltransferase complex (Ohkawa et al., 2008), ELP3 (Creppe et al., 2009), and GCN5 (Conacci-Sorrell et al., 2010, Ouyang et al., 2021) have been shown to acetylate α-tubulin K40 in vitro. Histone deacetylases HDAC6 (Hubbert et al., 2002), SIRT2 (North et al., 2003), and HDAC5 (Cho and Cavalli, 2012) carry out the deacetylation of α-tubulin K40 acetylation.

Microtubule α-tubulin K40 acetylation provides flexibility and resistance against breakage under mechanical stress. The weaker lateral interaction and sliding between protofilaments in acetylated microtubules contribute to the increased flexibility and mechanical stress resistance (Xu et al., 2017, Portran et al., 2017). Acetylated microtubule shows more resistance to depolymerization for cold, nocodazole, colchicine,

and oryzalin treatment, indicating their importance in microtubule dynamics (LeDizet and Piperno, 1987, Akella et al., 2010). Motor proteins preferentially associate with acetylated microtubules, and this modification regulates the motility of kinesin-1 and dynein (Table1.2) (Balabanian et al., 2017, Reed et al., 2006, Alper et al., 2014).

A new tubulin acetylation site was reported on β-tubulin. Acetylation of β-tubulin K252 site is carried out by San acetyltransferase. This modification was shown to prefer α/ β-tubulin dimers over polymerized microtubules. This modification alters microtubule dynamics by slowing down microtubule incorporation of tubulin dimer (Chu et al., 2011). It is unknown whether this acetyl group could be removed by known deacetylases.

Microtubule glutamylation

Microtubule glutamylation was initially reported in neuronal tubulins with mass spectrometry (Edde et al., 1990). The occurrence of microtubule glutamylation in the ciliary axoneme was first reported in mouse spermatozoa (Fouquet et al., 1994) and sea urchin sperm (Mary et al., 1996). This modification takes place in the C-terminal tail (CTT) domain of both α and β-tubulins, and glutamate residues are added to CTT glutamic acid residues E443 and E445 of α tubulins and E434, E435, E438, and E441 of β-tubulins (Edde et al., 1990, Redeker et al., 1998, Alexander et al., 1991, Mary et al., 1994, Rüdiger et al., 1992). Microtubule glutamylation is carried out in two steps. The first glutamate is added to the γ-carboxyl group of gene-encoded glutamates in tubulin CTT as an initiation step for branching. Additional glutamates added to the first glutamate to elongate the branch (Mahalingan et al., 2020). Microtubule glutamylation is carried out by tubulin tyrosine ligase-like (TTLL) family proteins (Figure1.2) (Janke et

al., 2005). Branching glutamates are added by initiases, TTLL4, TTLL5, and TTLL7 (Figure 1.2) (Van Dijk et al., 2007, Ikegami et al., 2006, Mahalingan et al., 2020). Extension of branch glutamates is carried out by elongases TTLL1, TTLL2, TTLL6, TTLL9, TTLL11, and TTLL13 (Figure 1.2) (Van Dijk et al., 2007). Cytosolic carboxypeptidase family proteins carry out Deglutamylation. CCP1, CCP2, CCP3, CCP4, and CCP6 shorten the long polyglutamate side chain. CCP5 specifically removes the branching point glutamates upon which long side chains are elongated (Rogowski et al., 2010, Tort et al., 2014).

Microtubule glycylation

Microtubule glycylation was initially identified in axonemal tubulin of *Paramecium* with mass spectrometry. Tubulin mono and polyglycylation are modifications in the c-terminal tail (CTT) domain of both α- and β-tubulins. Glycine residues are added to the γ-carboxyl group of glutamyl residues of CTT (Redeker et al., 1994). Glycines are added to glutamate residues at 445-447 (E445, E446, and E447) of α-tubulins and glutamate residues at 438, 439, 441, and 442 (E438, E439, E441, and E442) of β-tubulins (Garnham et al., 2017). Microtubule glycylation was reported exclusively on the axoneme of cilia and flagella (Levilliers et al., 1995). Microtubule glycylation was reported in axonemes of Tetrahymena (Xia et al., 2000), sea urchin (Mary et al., 1996), *Drosophila* (Bressac et al., 1995), humans, mice (Kann et al., 1998), and zebrafish (Wloga et al., 2009). Glycylation of microtubules is carried out by tubulin tyrosine ligase-like family proteins (TTLL). TTLL3 and TTLL8 add the first glycine to the glutamic acid residues of C-terminal tails of α- and β-tubulin (Figure 1.2) (Rogowski et al., 2009). Zebrafish lacks

ortholog of mammalian TTLL8, making TTLL3 the only monoglycylase (Pathak et al., 2011). TTLL10 elongates α- and β-tubulin monoglycylated by TTLL3 and TTLL8 (Ikegami and Setou, 2009, Rogowski et al., 2009, Wloga et al., 2009). In humans, two mutations in the TTL domain inactivate TTLL10, resulting in a loss of polygycylation activity (Rogowski et al., 2009). Deglycylases that would remove the glycine residues from the c-terminal tails of α- and β-tubulin have not been identified yet. Microtubule glycylation increases microtubule stiffness, and it is hypothesized that changes in stiffness occur due to the alterations in CTT and tubulin dimer body interaction (Wall et al., 2020). MAPs that are preferentially associated with glycylated microtubules and the role of glycylation on microtubule dynamics are unknown.

Microtubule detyrosination/ tyrosination

Removal of terminal tyrosine of α-tubulin (Rodriguez et al., 1973, Hallak et al., 1977) and addition of tyrosine back to α-tubulin was reported in rat brain (Argaraña et al., 1977). The subsets of tyrosinated and detyrosinated microtubules occur during the cell cycle, and neurons confirm the simultaneous presence of microtubules in both forms (Gundersen et al., 1984, Gundersen and Bulinski, 1986, Robson and Burgoyne, 1989). Detyrosinated microtubules occur in stable microtubules of neurons (Cambray-Deakin and Burgoyne, 1987, Robson and Burgoyne, 1989) and axonemal microtubules (Mary et al., 1996). Tyrosinated microtubules were also reported along axons in a subset of less acetylated microtubules, a marker of stable microtubules (Brown et al., 1993). Major enzymes that carry out the detyrosination of microtubules are VASH1 and VASH2 (Figure 1.2) (Aillaud et al., 2017, Nieuwenhuis et al., 2017). Knock out of both VASH1,

and VASH2 showed complete loss of microtubule detyrosination in the CHL-1 cell line, while HEK293T had a small amount of detyrosinated α-tubulin (Nieuwenhuis et al., 2017). This observation raises the possibility of other enzymes that can remove the C-terminal tyrosine of α-tubulin. The presence of α-tubulin isotype TUBA4A, which lacks C-terminal tyrosine (Valenzuela et al., 1981) could be another reason for non-complete loss of microtubule detyrosination in some cell lines. Retyrosination of α-tubulin is carried out by tubulin tyrosine ligase (TTL) (Figure 1.2) (Raybin and Flavin, 1977, Ersfeld et al., 1993).

Removal of penultimate glutamate of the CTT domain of detyrosinated tubulin results in Δ2-tubulin (Paturle-Lafanechere et al., 1991). Δ2-tubulin cannot be retyrosinated (Paturle et al., 1989). Δ2-tubulin is enriched in stable microtubules of neurons and ciliary axoneme (Paturle-Lafanechère et al., 1994). Further removal of C-terminal residues results in Δ3-tubulin (Berezniuk et al., 2013). Cytosolic carboxypeptidase family proteins CCP1 (Rogowski et al., 2010), CCP2, CCP3 (Tort et al., 2014), CCP4 (Rogowski et al., 2010), CCP5 (Berezniuk et al., 2013), and CCP6 (Rogowski et al., 2010) involve in the removal of glutamate from α-tubulin to generate Δ2 modification. Generation of Δ3 modification is carried out by CCP1 (Berezniuk et al., 2012) and CCP5 proteins (Berezniuk et al., 2013). There is no report on the ability of CCP2, CCP3, CCP4, and CCP6 to generate Δ3 α-tubulin.

Detyrosinated microtubules are enriched in long-lasting microtubules, while dynamic microtubules are enriched in tyrosinated microtubules (Webster et al., 1987). Detyrosinated microtubules alter microtubule dynamics. They show lower microtubule depolymerization with nocodazole treatment (Peris et al., 2006). Tyrosinated/

Detyrosinated state of microtubule shows preferential association with plus-end proteins and motor proteins. Tyrosinated microtubules preferentially associate with microtubule plus-end proteins like CLIP170, CLIP115 and p150 Glued through cytoskeleton-associated protein glycin-rich (CAP-Gly) microtubule-binding domain (Peris et al., 2009). Motor proteins kinesin-1 and CENP-E preferentially associate with detyrosinated microtubules, while kinesin-3 and kinesin-5 prefer tyrosinated tubulins (Table 1.2) (Tas et al., 2017, Guardia et al., 2016, Kahn et al., 2015, Barisic et al., 2015).

Microtubule methylation

Methylation of tubulin was reported during mitosis in mouse embryonic fibroblasts. Methylation was reported at K40 of α-tubulin, the site acetylated by ATAT1. Methylation of this site is carried out by histone methyltransferase SET-domain-containing 2 (SETD2). An inverse relationship between K40 acetylation and methylation was observed in the midbody during cytokinesis (Park et al., 2016). Methylation is also reported on both α- and β-tubulin CTT domains of *Toxoplasma gondii*. The presence of methylation in the CTT domain of tubulins in other organisms is unknown (Xiao et al., 2010).

Microtubule phosphorylation

Microtubule phosphorylation was initially reported in rat brains (Eipper, 1974). Both α- and β-tubulins are phosphorylated. α-tubulin is phosphorylated at Y432 by spleen tyrosine kinase syk (Peters et al., 1996), and β-tubulin is phosphorylated at S172 by Cdk1 and DYRK1a (Fourest-Lieuvin et al., 2006, Ori-McKenney et al., 2016).

Phosphorylation of β-tubulin at S172 regulates microtubule dynamics by inhibiting microtubule polymerization (Ori-McKenney et al., 2016).

Microtubule polyamination

Polyamination of microtubules by transglutaminases was reported on rat neurons. The major site of this modification is Q15 of β-tubulin, which is adjacent to hydrolyzable GTP of β-tubulin. This site is conserved in both mice and human β-tubulin. α-tubulin residues Q31, Q128, Q133, Q256, and Q285 were identified as sites for this modification (Song et al., 2013). The same study shows that polyaminated microtubules exhibit resistance to cold-induced depolymerization.

Roles of microtubule PTMs in ciliogenesis and ciliary functions

Cilia are conserved structures made out of the microtubule axoneme backbone. Cilia are divided into motile and primary cilia based on their functions. Most motile cilia have 9+2 axonemal structure and carry out motility functions. Primary cilia have 9+0 axonemal structure and carry out functions like cell signaling and sensory role. Axonemes of cilia are enriched in many microtubule PTMs including acetylation, detyrosination, glutamylation, and glycylation.

Multiple studies in different model organisms show the importance of microtubule acetylation in ciliogenesis and ciliary function. Knockdown of *ATAT1* shows delayed ciliary biogenesis and assembly in human cells (Shida et al., 2010, Rao et al., 2014). In *Tetrahymena*, knockout and alteration of acetylation site K40R showed normal ciliated structures and function. But these mutants showed increased sensitivity to microtubule

depolymerizing chemicals (Gaertig et al., 1995, Akella et al., 2010). Knockout of *Atat1* in mice resulted in reduced progressive movement in sperm motility, and sperm flagella showed altered flagellar beat properties (Kalebic et al., 2013). In zebrafish, morpholino knockdown of *atat1* resulted in curved body axis and hydrocephalus phenotypes that indicate ciliary defects (Akella et al., 2010).

In human cells, overexpression of *HDAC6* was shown to cause ciliary disassembly, reduced ciliated cells, and reduced ciliary length, potentially due to deacetylation of α-tubulin. (Ran et al., 2015, Yang et al., 2014). Overexpression of *SIRT2* was shown to reduce the number of ciliated cells and ciliary length, while knockdown of *SIRT2* increased both the number of ciliated cells and ciliary length in both human cells and zebrafish embryos (Zhou et al., 2014).

Unlike other microtubule modifications like acetylation, glutamylation, and detyrosination, microtubule glycylation occurs only on axonemes of ciliated structures (Levilliers et al., 1995). Depleting microtubule glycylation by knocking down *TTLL3* reduces primary cilia length in MDCK cells (Gadadhar et al., 2017). *Ttll3* knockout mice show the reduced occurrence of primary cilia and increased cell proliferation in colon epithelial cells. Increased proliferation has been implicated in promoting tumor development in mice, and decreased *ttll3* expression was observed in human colon tumor samples (Rocha et al., 2014). Loss of glycylation leads to shortening of connecting cilia in the retina and causes progressive retinal degeneration in mice. Hyperglutamylation of microtubule due to the loss of microtubule glycylation was suggested to cause retinal degeneration as a similar phenotype was reported in *Pcd* mutant, which lacks CCP1, a deglutamylase. *Pcd* mutant also shows hyperglutamylation of microtubules due to

deficiency in deglutamylation (Bosch Grau et al., 2017). These studies show the importance of glycylation in assembly and maintenance of primary cilia.

In *Tetrahymena,* the knockout of microtubule glycylation initiase TTLL3 paralogs resulted in progressive shortening of the cilia axoneme (Wloga et al., 2009). Depleting glycylation in mice by knocking out *Ttll3* and knockdown of *Ttll8* resulted in a near-complete loss of ependymal cilia (Bosch Grau et al., 2013). In zebrafish, morpholino knockdown of *ttll3* resulted in mild ciliary defect phenotypes like curled body axis and pronephric cysts. (Pathak et al., 2011). These studies show the importance of microtubule glycylation in the establishment and maintenance of motile cilia. In mice, knockout of both *Ttll3* and *Ttll8,* microtubule glycylation initiases, results in subfertility in males due to reducing progressive movement of sperm. Even though sperm axonemes were normal, flagella beating was altered due to the increased occurrence of post-power stroke configuration of outer and inner dynein (Gadadhar et al., 2021). In zebrafish, knockdown of both *ttll3* and *ttll6* resulted in a severe reduction in pronephric cilia motility (Pathak et al., 2011). These studies show the importance of microtubule glycylation in the ciliary beating of motile cilia.

Multiple studies show the importance of microtubule glutamylation in ciliogenesis and ciliary functions. Microtubule glutamylation elongase gene *Ttll1* mutants in mice exhibit infertility and reduced sperm motility. Most of the spermatozoa had short or no flagella indicating the importance of microtubule glutamylation by *Ttll1* in sperm flagella establishment or maintenance. Even though these mutants had normal-looking cilia in nasal passages and sinuses, exudates accumulated in these tissues indicating defects in the function of these cilia (Vogel et al., 2010). *Ttll1* mutant mice by another group also

showed similar respiratory phenotypes and attributed the observed phenotypes to alteration in ciliary beat asymmetry in the mutant tracheal cilia (Ikegami et al., 2010). In mice, *Ttll5* mutants showed reduced progressive sperm motility and defects in axonemal architecture (Lee et al., 2013). Microtubule glutamylation initiase *TTLL5* variants in humans were also associated with reduced sperm motility (Bedoni et al., 2016). In *Tetrahymena,* loss of microtubule glutamylation elongases TTLL1 and TTLL9 showed a mild phenotype of reduced motile velocity, but no axonemal architecture defect was not reported. These mutants also showed basal body maturation defects (Wloga et al., 2008). In *Tetrahymena,* the knockout of microtubule glutamylation elongase- TTLL6 paralogs resulted in shorter cilia, severely affecting their motility. Diminished ciliary motility in TTLL6 mutants was attributed to altered inner dynein arm activity (Suryavanshi et al., 2010). Knockdown of *ttll6* in zebrafish resulted in ciliary defects like axis curvature, pronephric cysts, abnormal otolith number, and a near-complete loss of cilia in the olfactory placode (Pathak et al., 2011, Pathak et al., 2007). Knockdown of *Ttll6* in mice ependymal cilia was shown to alter ciliary beating frequency (Bosch Grau et al., 2013). In *Chlamydomonas reingardtii*, loss of TTLL9, a microtubule glutamylation elongase, resulted in reduced flagella beating. Even though axonemal architecture was normal in these mutants, inner-arm dynein function was affected (Kubo et al., 2010). *Ttll9* mutant in mice showed infertility. These mice had reduced sperm count and defective motility. Ultrastructure of axoneme of these sperms showed shortening in doublet 7 (Konno et al., 2016). In zebrafish, knockdown and knockout of *ttll11* resulted in a scoliosis-like phenotype. Human fibroblast cells that lack TTLL11, a microtubule glutamylation elongase, showed reduced cilia length and emphasized the role of TTLL11 in ciliary

establishment or maintenance (Mathieu et al., 2021). The axonemal architecture of EV-releasing cephalic male (CEM) cilia was altered when *C. elegans* ttll11 mutant (O'Hagan et al., 2017).

Purkinje cell degeneration (*pcd*) mice lacking CCP1, a microtubule deglutamylase, had shortened connecting cilium of photoreceptors associated with retinal degeneration (Bosch Grau et al., 2017). In *C. elegans*, ccp1 mutants show progressive defects in CEM cilia and alteration in the ultrastructure of the axoneme (O'Hagan et al., 2011). In mice, knockdown of *Ccp5* results in spermatogenesis defect, abnormality in sperm flagella, and abnormal axoneme architecture (Giordano et al., 2019, Wu et al., 2017). In zebrafish, knockdown of *ccp5* results in ciliary defect phenotypes like curved body axis, pronephric cysts, and hydrocephalus brain. Alteration in ciliary beat amplitude was responsible for these phenotypes (Lyons et al., 2013, Pathak et al., 2014).

In *Chlamydomonas*, during the flagellar disassembly, K304 of α-tubulin is polyubiquitylated. Polyubiquitylation of this site results in the release of the flagellar axoneme and transportation of tubulins to the cell through intraflagellar transport (Wang et al., 2019).

Roles of microtubule PTMs in neurogenesis and neuronal functions

Neuronal axons and dendrites are made out of paraxially arranged arrays of microtubules. These microtubules play critical roles in maintaining the structure, axonal transport, and many other normal functions of neurons. Neuronal microtubules are enriched in microtubule PTMs acetylation, detyrosination, and glutamylation.

Ttl null mice died immediately after birth. The brain of this *Ttl* mutant showed abnormal axonal differentiation and axonal projections that led to defects in cortico-thalamic loop. *Ttl* null neurons also showed an abnormal distribution of microtubule tip protein CLIP170 (Erck et al., 2005). This mutant exhibits defects in axonal pathfinding and cytoskeletal organization of growth cones (Marcos et al., 2009). Tyrosinated tubulin was also shown to play an important role in polarized axonal transport of kinesin-1, which discriminate axon from dendrites. Recognition of tyrosinated tubulin by the beta5-loop8 region of kinesin-1 transports kinesin away from tyrosinated tubulin-rich dendrites to the detyrosinated tubulin-rich axon. Knockdown of *Ttl* in rat hippocampal neurons shows alteration in this polarization (Konishi and Setou, 2009). Knockdown of *Vash1* and *Vash2* in neurons showed defects in neuronal differentiation and radial migration of cortical neurons in the neocortex (Aillaud et al., 2017). A truncated variant of small vasohibin binding protein (*SVBP),* a chaperone that transports and stabilizes the vasohibins, was shown to be associated with microcephaly, intellectual disability, and delayed gross motor and speech development in humans. Mutation of *SVBP* in human cell lines shows increased tyrosinated tubulin levels and decreased detyrosinated and Δ2 tubulin. *Svbp* knockout mice showed defects in brain structure and behavior (Pagnamenta et al., 2019). These studies show the importance of microtubule detyrosination/tyrosination in neurogenesis and neuronal differentiation.

Microtubule detyrosination/tyrosination was also shown to influence axonal transportation. Tyrosination of microtubule was shown to initiate dynein-dynactin motility. CAP-Gly domain of dynactin subunit p150 mediates the interaction of dynein-dynactin with tyrosinated tubulin. Once the motility is initiated presence of detyrosinated

tubulin does not affect the processive motility of the complex (McKenney et al., 2016). Microtubule tyrosination in the distal end of the axon was shown to play an important role in the initiation of dynein-mediated retrograde transportation. Preferential binding of phosphorylated CLIP-170 to tyrosinated microtubule recruits $p150^{glued}$ associated vesicles for retrograde transportation (Nirschl et al., 2016). In rat hippocampal neurons dendrites, minus-end-out oriented microtubules are enriched in acetylation and detyrosination, while plus-end-out microtubules are tyrosinated. It was also shown that Kinesin-1 preferentially interacts with a subset of microtubules enriched in acetylation and detyrosination and Kinesin-3 with tyrosinated microtubules. This would explain the selectivity of Kinesin-1 to axons and the presence of Kinesin-3 in both axons and dendrites (Tas et al., 2017, Guardia et al., 2016). Kinesin-5 was shown to preferentially associate with tyrosinated microtubules over detyrosinated microtubules. Knockdown of *Ttl* showed reduced kinesin-5 levels in dendrites and exhibited similar defects shown by Kinesin-5 knockdown dendrites (Kahn et al., 2015). Mice mutant of spastin gene, a microtubule severing protein, showed axonal swelling in the central nervous system and abnormal axonal transportation. Axon swelling occurs in the distal region before the growth cone, whether transition occurs from a region enriched in detyrosinated microtubules to a region enriched in the tyrosinated microtubules. Axon swelling was enriched in detyrosinated, and immediately after swelling distal region was tyrosinated (Tarrade et al., 2006). Injury to the sciatic nerve was shown to have TTL mediate the increase in tyrosinated microtubules. Increased tyrosination increases the recruitment of +TIPs like CLIP170, $P150^{Glued,}$ and EB1, retrograde transport of injury signaling, and ultimate axon regeneration (Song et al., 2015).

Studies also show the importance of microtubule tyrosination/ detyrosiantion on neuronal degeneration and regeneration. Parthenolide-mediated inhibition of microtubule detyrosination was shown to accelerate the regeneration of crushed sciatic nerve (Gobrecht et al., 2016). Oligomeric $A\beta_{1-42}$ was shown to induce the increase of detyrosinated tubulin in cells that do not express tau, resulting in neurotoxicity independent of tau showing the potential for a higher level of detyrosinated tubulin to result in neuronal death (Pianu et al., 2014). Another study showed that transgenic mice with mutated Cu/Zn superoxidase dismutase (SOD1) showed Golgi apparatus fragmentation, disruption of cytoplasmic dynein, and tau aggregation mediated decrease in detyrosination that leads to cell death (Gonatas et al., 2006).

Atat1 mutant in mice showed a mild defect in the dentate gyrus (Kim et al., 2013b). Another *Atat1* mice mutant showed ventricular dilation due to the defect in neuronal migration during septal and striatal development (Li et al., 2019). Loss of *Atat1* resulted in axon over branching and outgrowth in hippocampal neurons and growth cone defects due to hyperdynamic microtubules due to loss of microtubule acetylation (Wei et al., 2018). Knockout of *atat1* in *Drosophila* neurons increased the number of branches in dendrites but not in the axon. The level of MAP1B homolog in dendrites was shown to be reduced in *atat1* mutant (Jenkins et al., 2017). *Atat1* was down-regulated by axon growth-inhibitory factors chondroitin sulfate proteoglycan and myelin-associated glycoprotein, resulting in decreased neurite length (Wong et al., 2018).0020

Loss of *Atat1* in mice, *C.elegans* and *Drosophila*, resulted in defects in touch sensation or mechanosensation (Morley et al., 2016, Akella et al., 2010, Shida et al., 2010, Yan et al., 2018). In both mice and *Drosophila*, it was shown that alteration in microtubule physical

properties due to loss of acetylation of microtubules associated with mechanosensitive ion channels contributes to the reduced mechanosensation. While in *C. elegans*, the non-enzymatic activity of mec-17 was suggested to contribute to the altered mechanosensation. Knockdown of *atat1* in Zebrafish resulted in no or reduced touched evoked response indicating potential neuromuscular and mechanosensation defects (Akella et al., 2010).

The role of microtubule acetylation on axonal transport has been shown in multiple studies. In *c. elegans*, loss of atat1 leads to altered axon transportation and axon degeneration caused by microtubule instability (Neumann and Hilliard, 2014). Microtubule acetylation was shown in multiple studies to enhance the binding of kinesin-1 to microtubule and its motility on microtubule (Balabanian et al., 2017, Reed et al., 2006, Kaul et al., 2014), while another that showed no difference between kinesin-1 motility between acetylated microtubule and non-acetylated microtubule (Walter et al., 2012). Loss of *Atat1* altered the axonal transport in mice neurons, and *Atat1* knockout neurons showed reduced vesicle and organelle transport (Even et al., 2019). Axon injury in peripheral neurons induces tubulin acetylation mediated by HDAC5 and contributes to axonal growth and regeneration through controlling growth cone dynamics (Cho and Cavalli, 2012).

Microtubule acetylation has been shown to alleviate neurodegenerative diseases. Inhibition of HDAC6 improved neurodegenerative diseases like Huntington's disease (Dompierre et al., 2007), Charcot-Marie-Tooth (d'Ydewalle et al., 2011), Parkinson's disease (Godena et al., 2014) and Alzheimer's disease (Kim et al., 2012, Tseng et al., 2017). In some cases, it was shown that an increase in microtubule acetylation due to

inhibition contributed to the improvement. It was shown to enhance autophagy response in response to HDAC6 inhibition and helps to alleviate these diseases (Lee et al., 2010, Pandey et al., 2007). Other studies point toward improved neuronal transportation in improving the diseases (Dompierre et al., 2007, d'Ydewalle et al., 2011, Kim et al., 2012, Godena et al., 2014). It is not known whether loss or reduction in microtubule acetylation could cause any neurodegenerative diseases.

Differentiating PC12 cells with neuronal growth factors increased the TTLL7 and β-tubulin glutamylation levels. Knockdown of *Ttll7* was shown to repress MAP2-positive neurite growth (Ikegami et al., 2006). In mice, ROSA22 mutant that lacks PGs1, a subunit of polyglutamylase activity, reduced KIF1A in neurites. These mice also showed reduced synaptic vesicles and impaired synaptic transmission (Ikegami et al., 2007). These studies show the role played by microtubule glutamylation during neurogenesis. Microtubule glutamylation is also important for normal axonal transportation. Reduced microtubule polyglutamylation was shown to reduce the landing rate and pausing behavior of KIF1A (Lessard et al., 2019). It was shown that polyglutamylation of microtubules could increase MAP2 binding to microtubules and negatively regulate the KIF5 mobility and KIF5 mediated transport (Maas et al., 2009). Spastin mutant mice increased microtubule glutamylation and reduced binding and processivity of KIF5. This mutant showed defects in synapse number, motor performance, and associative memory (Lopes et al., 2020). *Pcd* mice that lack CCP1 showed altered microtubule growing rate and catastrophe frequency. The biallelic variant of *Ccp1* resulted in motor neuron degeneration and cerebellar atrophy (Karakaya et al., 2019). These mutants showed increased cell death in the cerebellum and their motor coordination, long-term memory,

and social preference (Muñoz-Castañeda et al., 2018). Cell death reported in this mutant was attributed to apoptosis due to increased ER stress and protein synthesis inhibition (Li et al., 2020).

Studies have shown the roles of microtubule glutamylation in neurodegeneration. In *Ccp1* and *Ccp6* mutants, *Ttll1*-mediated excessive polyglutamylation was shown to cause neurodegeneration. These mutants also showed defects in axonal transportation as well (Magiera et al., 2018a). Loss of *Ttll1* in hippocampal neurons increased mitochondrial motility, while *Ttll7* did not significantly differ in mitochondrial motility (Bodakuntla et al., 2021). Amyloid-β oligomer induces polyglutamylation using TTLL6, and the increase in polyglutamylation results in the increased spastin-mediated severing of microtubules (Zempel et al., 2013). Increased glutamylation due to loss of *Ccp1* in cultured hippocampal neurons alters mitochondrial and lysosomal particles (Bodakuntla et al., 2020). Studies on humans associate TTLL7 with Alzheimer's disease (Leidinger et al., 2013, Heinzen et al., 2010) and familial clustering of schizophrenia, bipolar disorder, and major depressive disorder (Zhang and Chen, 2020). An increase in glutamylated Δ2 tubulin was seen in the hippocampal region of Alzheimer's disease (Vu et al., 2017).

Roles of microtubule PTMs in cell division

During cell division, microtubules and associated MAPs play a critical role in forming spindles that equally divide chromatids between daughter cells, and they are also important for cytokinesis. Most of the dynamic microtubules involved in cell division lack microtubule PTMs. But subsets of microtubules enriched in PTMs play a critical role in proper cell division. Enrichment of microtubule acetylation (Schatten et al., 1988,

Wilson and Forer, 1997), glutamylation (Bobinnec et al., 1998), tyrosinated, and detyrosination (Gundersen et al., 1984, Gundersen and Bulinski, 1986) in mitotic and meiotic spindle were reported.

Inhibition of microtubule detyrosination resulted in dissociation of kinetochore kinesin motor, CENP-E. CENP-E was proposed to allow the congression of the chromosome from poles to the equator during metaphase plate formation. CENP-E moves faster on detyrosinated microtubules than over tyrosinated microtubules. Reduction in detyrosinated tubulin delayed mitotic progression (Barisic et al., 2015). Detyrosination of microtubules occurs only in microtubule regions proximal to kinetochore once stable amphitelic attachment is formed. Overexpression of TTL RNAi or VASH1-SVBP led to microtubule detyrosination of microtubules associated with unstable kinetochore attachment and mitotic errors. It has been shown detyrosination affects error correction by suppressing Kinesin13 MCAK activity (Ferreira et al., 2020). Microtubule detyrosination also suppresses microtubule disassembly by inhibiting MCAK activity (Peris et al., 2009).

TTL-null mammalian fibroblasts show misaligned spindle and defects in cell morphology during interphase. The +TIPs proteins- CLIP-170, CLIP-115, and p150 Glued localize exclusively to the tyrosinated microtubule, and failure of their recruitment to microtubule plus ends in TTL-null mammalian fibroblasts hypothesized to contribute to the phenotype (Peris et al., 2006). A CDC42-driven asymmetry of tyrosination/ detyrosination between cortical and egg side spindle microtubules results in the segregation of selfish elements to the egg side and contributes to the meiotic drive during oogenesis. It was shown that

selfish centromeres interact with tyrosinated microtubules, which contributes to the flipping of those selfish centromeres towards the future egg (Akera et al., 2017). Knockdown of ATAT1 in pig kidney epithelial cells showed an increased occurrence of monopolar spindle caused by reduced recruitment of PLK1 to centrosome (Rasamizafy et al., 2021). The same study also showed inefficient kinetochore-microtubule attachment that activated the spindle checkpoint when ATAT1 was knocked down.

During the mice oogenesis, increased microtubule acetylation resulted in a defect in spindle organization (Tang et al., 2018, Jeon and Oh, 2020) and defects in the kinetochore-microtubule attachment (Jeon and Oh, 2020).

Microtubule methylation of α-tubulin K40 occurs on the spindle microtubule during mitosis. During the metaphase, methylation occurs on the microtubule close to the spindle and midbody during cytokinesis. Loss of SETD-mediated microtubule methylation showed a wide range of mitosis and cytokinesis defects in MEF cells. The occurrence of methylation on the same residue of acetylation and low level of acetylation observed on methylated tubulin indicates a potentially opposite role of α-tubulin K40 methylation and acetylation during mitosis (Park et al., 2016).

In *Saccharomyces cerevisiae*, mutation of cysteine 377 of α-tubulin to serine resulted in reduced palmitoylation of the site, and cells showed abnormal microtubule spindle and nuclear positioning (Caron et al., 2001). Even though the mechanism behind the mitotic defects is unknown, these observations indicate an important role of microtubule palmitoylation during mitosis.

Roles of microtubule PTMs muscle contraction

Microtubule PTMs modulate muscle stiffness. Detyrosinated microtubules are enriched in striated muscle, and pharmacological reduction of microtubule detyrosination was shown to reduce microtubule stiffness (Kerr et al., 2015). Microtubule detyrosination increases the stiffness of cardiomyocytes through the association with desmin and regulates microtubule buckling during cardiomyocyte contraction. An increase in detyrosination by TTL knockdown reduces cardiomyocyte contractibility. Elevated levels of detyrosination are associated with hypertrophic cardiomyopathy patients (Robison et al., 2016). Both pharmacological and genetic approaches to reduce detyrosination in failing human cardiomyocytes lower the stiffness and improve the contractibility (Chen et al., 2018). Additionally, the knockdown of VASH1 reduces microtubule stiffness and improves contractibility (Chen et al., 2020). MARK4 knockout improves cardiomyocytes' contractibility after myocardial infraction by reducing VASH2-mediated detyrosination (Yu et al., 2021).

An increase in microtubule acetylation increased cytoskeletal stiffness in striated muscle. It also reduces contraction (Coleman et al., 2021).

Roles of microtubule PTMs in platelet function

Platelets are produced from mature megakaryocytes. Megakaryocytes form long and branched cytoplasmic processes called proplatelets as intermediaries during platelet production. The generation of proplatelet depends on microtubule bundling and sliding. In mice, depletion of microtubule acetylation leads to defects in proplatelet generation (Van Dijk et al., 2018). Platelets switch from their disc-shaped to sphere and spread on an

injured vessel upon activation by injury. In resting platelets, the disc shape is maintained by marginal bands. During the activation of the platelet, microtubules of marginal bands undergo rapid deacetylation. Extension of microtubule acetylation by knocking out HDAC6 alters the dynamic of platelet spreading upon activation (Sadoul et al., 2012, Ribba et al., 2021).

Depletion of microtubule glutamylation also showed defects in protoplast generation. TTLL5 is responsible for the glutamylation of microtubules during this process. Microtubule glutamylation colocalizes with microtubule bundling at the leading edge of the cytoplasmic process (Van Dijk et al., 2018). Microtubule glutamylation is also present in the marginal band of mature platelets, but its role during platelet activation is unknown (Patel-Hett et al., 2008).

Microtubule detyrosination is present in marginal platelet bands, but its functional importance in platelet functions is yet to be studied (Patel-Hett et al., 2008).

Roles of microtubule PTMs in angiogenesis

In zebrafish, detyrosinated microtubules are enriched in endothelial microtubules of secondary sprouts from posterior cardinal veins (PCV). Knockdown of *vash1* shows increased secondary sprouting and suggests that detyrosinated microtubules regulate secondary sprouting. Knockout of *vash1* also shows defects in lymphatic vessel formation (de Oliveira et al., 2021). Overexpression Vash1 also results in defects in angiogenesis. Increased detyrosination impairs endocytosis and trafficking of VEGF receptor 2 and endothelial cell migration (Kobayashi et al., 2021).

Microtubule acetylation is shown to regulate endothelial tubulogenesis during angiogenesis. Overexpression of deacetylases HDAC6 and SIRT2 affect lumen formation (Kim et al., 2013a).

Microtubule glutamylation is also shown to regulate angiogenesis in zebrafish and human cells by regulating the deciliation of endothelial cilia. Deciliation of this mechanosensing cilia allows migration and tubulogenesis of endothelial cells (Ki et al., 2020).

Roles of microtubule PTMs in stress response

Microtubule PTMs play roles in stress response. Starvation and osmotic stress in HeLa cells resulted in hyperacetylation of microtubules and increased recruitment of kinesin-1 and JNK activation. This leads to the initiation of autophagy (Geeraert et al., 2010, Mackeh et al., 2014). Environmental stresses induce miceotubule acetylation mediated autophagy in *Arabidopsis thaliana* (Olenieva et al., 2019). *Atat1* knockout cells show reduced survival under stress (Mackeh et al., 2014). Acetylated microtubules have also been shown to play a role in fusing the autophagosome with lysosomes (Xie et al., 2010). Loss of microtubule acetylation increases cellular stress, and in breast cancer cell progression, increased acetylation allows cells to overcome cellular stress (Ko et al., 2021).

In mice, hyperglutamylation of microtubule due to loss of a deglutamylase increased ER stress due to increased free tubulins. This mutant was also shown to inhibit protein synthesis and increased cell death (Li et al., 2020). In *C. elegans*, levels of microtubule glutamylation in sensory cilia elevate in response to environmental stress and starvation.

This elevation is mediated by the p38 MAPK pathway and carried out by ttll4. Elevating glutamylation in response to stress increases intraflagellar transport (Kimura et al., 2018).

Concluding remarks

Microtubules play critical roles in carrying out various cellular functions. Diverse cellular functions require a diverse set of microtubules optimized to have proper physical properties and associated MAPs to carry out specific functions efficiently. Tubulin isotypes and microtubule PTMs are suggested to play a role in generating these diverse microtubules. Since the 1970s, a large number of microtubule PTMs and enzymes that carry out these modifications have been identified. In vitro and in vivo studies have illuminated the roles of these PTMs on cellular functions. Even though genetic deletion of enzymes that carry out showed that these modifications are not required in cellular function, they show the role of these modifications in fine-tuning cellular function to perform them efficiently. Studies also show alteration in these modifications associated with human diseases as well. Studying the roles of one PTM on microtubule functions is challenging as most stable microtubules are enriched in multiple PTMs. Many studies show alteration in one modification leads to alteration in other microtubule PTMs. These observations also raise the possibility of these modifications' redundant or compensatory roles. This could explain milder phenotypes with genetic approaches to knockdown or knockout the enzymes. Further studies must understand how these modifications interact to perform cellular functions.

REFERENCES

AILLAUD, C., BOSC, C., PERIS, L., BOSSON, A., HEEMERYCK, P., VAN DIJK, J., LE FRIEC, J., BOULAN, B., VOSSIER, F. & SANMAN, L. E. 2017. Vasohibins/SVBP are tubulin carboxypeptidases (TCPs) that regulate neuron differentiation. *Science,* 358**,** 1448-1453.

AKELLA, J. S., WLOGA, D., KIM, J., STAROSTINA, N. G., LYONS-ABBOTT, S., MORRISSETTE, N. S., DOUGAN, S. T., KIPREOS, E. T. & GAERTIG, J. 2010. MEC-17 is an α-tubulin acetyltransferase. *Nature,* 467**,** 218-222.

AKERA, T., CHMÁTAL, L., TRIMM, E., YANG, K., AONBANGKHEN, C., CHENOWETH, D. M., JANKE, C., SCHULTZ, R. M. & LAMPSON, M. A. 2017. Spindle asymmetry drives non-Mendelian chromosome segregation. *Science,* 358**,** 668-672.

ALEXANDER, J. E., HUNT, D. F., LEE, M. K., SHABANOWITZ, J., MICHEL, H., BERLIN, S. C., MACDONALD, T. L., SUNDBERG, R. J., REBHUN, L. I. & FRANKFURTER, A. 1991. Characterization of posttranslational modifications in neuron-specific class III beta-tubulin by mass spectrometry. *Proceedings of the National Academy of Sciences,* 88**,** 4685-4689.

ALPER, J. D., DECKER, F., AGANA, B. & HOWARD, J. 2014. The motility of axonemal dynein is regulated by the tubulin code. *Biophysical journal,* 107**,** 2872-2880.

ARGARAÑA, C. E., ARCE, C. A., BARRA, H. S. & CAPUTTO, R. 1977. In vivo incorporation of [14C] tyrosine into the C-terminal position of the α subunit of tubulin. *Archives of Biochemistry and Biophysics,* 180**,** 264-268.

ATIENZAR-AROCA, R., AROCA-AGUILAR, J.-D., ALEXANDRE-MORENO, S., FERRE-FERNÁNDEZ, J.-J., BONET-FERNÁNDEZ, J.-M., CABAÑERO-VARELA, M.-J. & ESCRIBANO, J. 2021. Knockout of myoc Provides Evidence for the Role of Myocilin in Zebrafish Sex Determination Associated with Wnt Signalling Downregulation. *Biology,* 10**,** 98.

BALABANIAN, L., BERGER, C. L. & HENDRICKS, A. G. 2017. Acetylated microtubules are preferentially bundled leading to enhanced kinesin-1 motility. *Biophysical journal,* 113**,** 1551-1560.

BARISIC, M., E SOUSA, R. S., TRIPATHY, S. K., MAGIERA, M. M., ZAYTSEV, A. V., PEREIRA, A. L., JANKE, C., GRISHCHUK, E. L. & MAIATO, H. 2015. Microtubule detyrosination guides chromosomes during mitosis. *Science,* 348**,** 799-803.

BEDONI, N., HAER-WIGMAN, L., VACLAVIK, V., TRAN, V. H., FARINELLI, P., BALZANO, S., ROYER-BERTRAND, B., EL-ASRAG, M. E., BONNY, O. & IKONOMIDIS, C. 2016. Mutations in the polyglutamylase gene TTLL5, expressed in photoreceptor cells and spermatozoa, are associated with cone-rod degeneration and reduced male fertility. *Human molecular genetics,* 25**,** 4546-4555.

BEREZNIUK, I., LYONS, P. J., SIRONI, J. J., XIAO, H., SETOU, M., ANGELETTI, R. H., IKEGAMI, K. & FRICKER, L. D. 2013. Cytosolic carboxypeptidase 5

removes α-and γ-linked glutamates from tubulin. *Journal of Biological Chemistry,* 288**,** 30445-30453.

BEREZNIUK, I., VU, H. T., LYONS, P. J., SIRONI, J. J., XIAO, H., BURD, B., SETOU, M., ANGELETTI, R. H., IKEGAMI, K. & FRICKER, L. D. 2012. Cytosolic carboxypeptidase 1 is involved in processing α-and β-tubulin. *Journal of Biological Chemistry,* 287**,** 6503-6517.

BILLETT, F. & ADAM, E. 1976. The structure of the mitochondrial cloud of Xenopus laevis oocytes.

BOBINNEC, Y., MOUDJOU, M., FOUQUET, J., DESBRUYERES, E., EDDÉ, B. & BORNENS, M. 1998. Glutamylation of centriole and cytoplasmic tubulin in proliferating non-neuronal cells. *Cell motility and the cytoskeleton,* 39**,** 223-232.

BODAKUNTLA, S., SCHNITZLER, A., VILLABLANCA, C., GONZALEZ-BILLAULT, C., BIECHE, I., JANKE, C. & MAGIERA, M. M. 2020. Tubulin polyglutamylation is a general traffic-control mechanism in hippocampal neurons. *Journal of cell science,* 133**,** jcs241802.

BODAKUNTLA, S., YUAN, X., GENOVA, M., GADADHAR, S., LEBOUCHER, S., BIRLING, M. C., KLEIN, D., MARTINI, R., JANKE, C. & MAGIERA, M. M. 2021. Distinct roles of α-and β-tubulin polyglutamylation in controlling axonal transport and in neurodegeneration. *The EMBO journal,* 40**,** e108498.

BOSCH GRAU, M., GONZALEZ CURTO, G., ROCHA, C., MAGIERA, M. M., MARQUES SOUSA, P., GIORDANO, T., SPASSKY, N. & JANKE, C. 2013. Tubulin glycylases and glutamylases have distinct functions in stabilization and motility of ependymal cilia. *Journal of Cell Biology,* 202**,** 441-451.

BOSCH GRAU, M., MASSON, C., GADADHAR, S., ROCHA, C., TORT, O., MARQUES SOUSA, P., VACHER, S., BIECHE, I. & JANKE, C. 2017. Alterations in the balance of tubulin glycylation and glutamylation in photoreceptors leads to retinal degeneration. *Journal of cell science,* 130**,** 938-949.

BRESSAC, C., BRÉ, M., DARMANADEN-DELORME, J., LAURENT, M., LEVILLIERS, N. & FLEURY, A. 1995. A massive new posttranslational modification occurs on axonemal tubulin at the final step of spermatogenesis in Drosophila. *European journal of cell biology,* 67**,** 346-355.

BROWN, A., LI, Y., SLAUGHTER, T. & BLACK, M. M. 1993. Composite microtubules of the axon: quantitative analysis of tyrosinated and acetylated tubulin along individual axonal microtubules. *Journal of cell science,* 104**,** 339-352.

BURDINE, R. D. & SCHIER, A. F. 2000. Conserved and divergent mechanisms in left–right axis formation. *Genes & development,* 14**,** 763-776.

BUTTGEREIT, D., PAULULAT, A. & RENKAWITZ-POHL, R. 2003. Muscle development and attachment to the epidermis is accompanied by expression of beta 3 and beta 1 tubulin isotypes, respectively. *International Journal of Developmental Biology,* 40**,** 189-196.

CALLEN, A.-M., ADOUTTE, A., ANDREW, J. M., BAROIN-TOURANCHEAU, A., BRÉ, M.-H., RUIZ, P. C., CLÉROT, J.-C., DELGADO, P., FLEURY, A. & JEANMAIRE-WOLF, R. 1994. Isolation and characterization of libraries of

monoclonal antibodies directed against various forms of tubulin in Paramecium. *Biology of the Cell,* 81**,** 95-119.

CAMBRAY-DEAKIN, M. A. & BURGOYNE, R. D. 1987. Posttranslational modifications of alpha-tubulin: acetylated and detyrosinated forms in axons of rat cerebellum. *The Journal of cell biology,* 104**,** 1569-1574.

CARON, J. M. 1997. Posttranslational modification of tubulin by palmitoylation: I. In vivo and cell-free studies. *Molecular biology of the cell,* 8**,** 621-636.

CARON, J. M., VEGA, L. R., FLEMING, J., BISHOP, R. & SOLOMON, F. 2001. Single site α-tubulin mutation affects astral microtubules and nuclear positioning during anaphase in Saccharomyces cerevisiae: possible role for palmitoylation of α-tubulin. *Molecular biology of the cell,* 12**,** 2672-2687.

CHEN, C. Y., CAPORIZZO, M. A., BEDI, K., VITE, A., BOGUSH, A. I., ROBISON, P., HEFFLER, J. G., SALOMON, A. K., KELLY, N. A. & BABU, A. 2018. Suppression of detyrosinated microtubules improves cardiomyocyte function in human heart failure. *Nature medicine,* 24**,** 1225-1233.

CHEN, C. Y., SALOMON, A. K., CAPORIZZO, M. A., CURRY, S., KELLY, N. A., BEDI, K., BOGUSH, A. I., KRÄMER, E., SCHLOSSAREK, S. & JANIAK, P. 2020. Depletion of vasohibin 1 speeds contraction and relaxation in failing human cardiomyocytes. *Circulation research,* 127**,** e14-e27.

CHO, Y. & CAVALLI, V. 2012. HDAC5 is a novel injury-regulated tubulin deacetylase controlling axon regeneration. *The EMBO journal,* 31**,** 3063-3078.

CHU, C.-W., HOU, F., ZHANG, J., PHU, L., LOKTEV, A. V., KIRKPATRICK, D. S., JACKSON, P. K., ZHAO, Y. & ZOU, H. 2011. A novel acetylation of β-tubulin

by San modulates microtubule polymerization via down-regulating tubulin incorporation. *Molecular biology of the cell,* 22**,** 448-456.

COLANTONIO, S., D'ACUNTO, M., RIGHI, M. & SALVETTI, O. SuperResolution-aided Recognition of Cytoskeletons in Scanning Probe Microscopy Images. ICPRAM, 2014. 703-709.

COLEMAN, A. K., JOCA, H. C., SHI, G., LEDERER, W. J. & WARD, C. W. 2021. Tubulin acetylation increases cytoskeletal stiffness to regulate mechanotransduction in striated muscle. *Journal of General Physiology,* 153.

CONACCI-SORRELL, M., NGOUENET, C. & EISENMAN, R. N. 2010. Myc-nick: a cytoplasmic cleavage product of Myc that promotes α-tubulin acetylation and cell differentiation. *Cell,* 142**,** 480-493.

CREPPE, C., MALINOUSKAYA, L., VOLVERT, M.-L., GILLARD, M., CLOSE, P., MALAISE, O., LAGUESSE, S., CORNEZ, I., RAHMOUNI, S. & ORMENESE, S. 2009. Elongator controls the migration and differentiation of cortical neurons through acetylation of α-tubulin. *Cell,* 136**,** 551-564.

D'YDEWALLE, C., KRISHNAN, J., CHIHEB, D. M., VAN DAMME, P., IROBI, J., KOZIKOWSKI, A. P., BERGHE, P. V., TIMMERMAN, V., ROBBERECHT, W. & VAN DEN BOSCH, L. 2011. HDAC6 inhibitors reverse axonal loss in a mouse model of mutant HSPB1–induced Charcot-Marie-Tooth disease. *Nature medicine,* 17**,** 968-974.

DE OLIVEIRA, M. B., MEIER, K., JUNG, S., BARTELS-KLEIN, E., COXAM, B., GEUDENS, I., SZYMBORSKA, A., SKOCZYLAS, R., FECHNER, I. &

KOLTOWSKA, K. 2021. Vasohibin 1 selectively regulates secondary sprouting and lymphangiogenesis in the zebrafish trunk. *Development,* 148**,** dev194993.

DENOULET, P., EDDÉ, B. & GROS, F. 1986. Differential expression of several neurospecific β-tubulin mRNAs in the mouse brain during development. *Gene,* 50**,** 289-297.

DOMPIERRE, J. P., GODIN, J. D., CHARRIN, B. C., CORDELIERES, F. P., KING, S. J., HUMBERT, S. & SAUDOU, F. 2007. Histone deacetylase 6 inhibition compensates for the transport deficit in Huntington's disease by increasing tubulin acetylation. *Journal of Neuroscience,* 27**,** 3571-3583.

DRUMMOND, I. A. 2012. Cilia functions in development. *Current opinion in cell biology,* 24**,** 24-30.

DUAN, J. & GOROVSKY, M. A. 2002. Both carboxy-terminal tails of α-and β-tubulin are essential, but either one will suffice. *Current biology,* 12**,** 313-316.

EDDÉ, B., DENOULET, P., DE NÉCHAUD, B., KOULAKOFF, A., BERWALD-NETTER, Y. & GROS, F. 1989. Posttranslational modifications of tubulin in cultured mouse brain neurons and astroglia. *Biology of the Cell,* 65**,** 109-117.

EDDE, B., ROSSIER, J., LE CAER, J.-P., DESBRUYERES, E., GROS, F. & DENOULET, P. 1990. Posttranslational glutamylation of α-tubulin. *Science,* 247**,** 83-85.

EGGENSCHWILER, J. T. & ANDERSON, K. V. 2007. Cilia and developmental signaling. *Annual review of cell and developmental biology,* 23**,** 345.

EIPPER, B. A. 1974. Properties of rat brain tubulin. *Journal of Biological Chemistry,* 249**,** 1407-1416.

ELINSON, R. P. & ROWNING, B. 1988. A transient array of parallel microtubules in frog eggs: potential tracks for a cytoplasmic rotation that specifies the dorso-ventral axis. *Developmental biology,* 128**,** 185-197.

ELKOUBY, Y. M., JAMIESON-LUCY, A. & MULLINS, M. C. 2016. Oocyte polarization is coupled to the chromosomal bouquet, a conserved polarized nuclear configuration in meiosis. *PLoS biology,* 14**,** e1002335.

ERCK, C., PERIS, L., ANDRIEUX, A., MEISSIREL, C., GRUBER, A. D., VERNET, M., SCHWEITZER, A., SAOUDI, Y., POINTU, H. & BOSC, C. 2005. A vital role of tubulin-tyrosine-ligase for neuronal organization. *Proceedings of the National Academy of Sciences,* 102**,** 7853-7858.

ERSFELD, K., WEHLAND, J., PLESSMANN, U., DODEMONT, H., GERKE, V. & WEBER, K. 1993. Characterization of the tubulin-tyrosine ligase. *The Journal of cell biology,* 120**,** 725-732.

ESSNER, J. J., AMACK, J. D., NYHOLM, M. K., HARRIS, E. B. & YOST, H. J. 2005. Kupffer's vesicle is a ciliated organ of asymmetry in the zebrafish embryo that initiates left-right development of the brain, heart and gut.

EVEN, A., MORELLI, G., BROIX, L., SCARAMUZZINO, C., TURCHETTO, S., GLADWYN-NG, I., LE BAIL, R., SHILIAN, M., FREEMAN, S. & MAGIERA, M. M. 2019. ATAT1-enriched vesicles promote microtubule acetylation via axonal transport. *Science advances,* 5**,** eaax2705.

FEI, Z., BAE, K., PARENT, S. E., WAN, H., GOODWIN, K., THEISEN, U., TANENTZAPF, G. & BRUCE, A. E. 2019. A cargo model of yolk syncytial nuclear migration during zebrafish epiboly. *Development,* 146**,** dev169664.

FERREIRA, L. T., ORR, B., RAJENDRAPRASAD, G., PEREIRA, A. J., LEMOS, C., LIMA, J. T., GUASCH BOLDÚ, C., FERREIRA, J. G., BARISIC, M. & MAIATO, H. 2020. α-Tubulin detyrosination impairs mitotic error correction by suppressing MCAK centromeric activity. *Journal of Cell Biology,* 219.

FOUQUET, J. P., KANN, M. L., EDDE, B., WOLFF, A., DESBRUYERES, E. & DENOULET, P. 1994. Differential distribution of glutamylated tubulin during spermatogenesis in mammalian testis. *Cell motility and the cytoskeleton,* 27**,** 49-58.

FOUREST-LIEUVIN, A., PERIS, L., GACHE, V., GARCIA-SAEZ, I., JUILLAN-BINARD, C., LANTEZ, V. & JOB, D. 2006. Microtubule regulation in mitosis: tubulin phosphorylation by the cyclin-dependent kinase Cdk1. *Molecular biology of the cell,* 17**,** 1041-1050.

GADADHAR, S., ALVAREZ VIAR, G., HANSEN, J. N., GONG, A., KOSTAREV, A., IALY-RADIO, C., LEBOUCHER, S., WHITFIELD, M., ZIYYAT, A. & TOURÉ, A. 2021. Tubulin glycylation controls axonemal dynein activity, flagellar beat, and male fertility. *Science,* 371**,** eabd4914.

GADADHAR, S., DADI, H., BODAKUNTLA, S., SCHNITZLER, A., BIÈCHE, I., RUSCONI, F. & JANKE, C. 2017. Tubulin glycylation controls primary cilia length. *Journal of Cell Biology,* 216**,** 2701-2713.

GAERTIG, J., CRUZ, M. A., BOWEN, J., GU, L., PENNOCK, D. G. & GOROVSKY, M. A. 1995. Acetylation of lysine 40 in alpha-tubulin is not essential in Tetrahymena thermophila. *The Journal of Cell Biology,* 129**,** 1301-1310.

GARNHAM, C. P., YU, I., LI, Y. & ROLL-MECAK, A. 2017. Crystal structure of tubulin tyrosine ligase-like 3 reveals essential architectural elements unique to tubulin monoglycylases. *Proceedings of the National Academy of Sciences,* 114**,** 6545-6550.

GEERAERT, C., RATIER, A., PFISTERER, S. G., PERDIZ, D., CANTALOUBE, I., ROUAULT, A., PATTINGRE, S., PROIKAS-CEZANNE, T., CODOGNO, P. & POÜS, C. 2010. Starvation-induced hyperacetylation of tubulin is required for the stimulation of autophagy by nutrient deprivation. *Journal of Biological Chemistry,* 285**,** 24184-24194.

GINZBURG, I., TEICHMAN, A., DODEMONT, H., BEHAR, L. & LITTAUER, U. 1985. Regulation of three beta-tubulin mRNAs during rat brain development. *The EMBO Journal,* 4**,** 3667-3673.

GIORDANO, T., GADADHAR, S., BODAKUNTLA, S., STRAUB, J., LEBOUCHER, S., MARTINEZ, G., CHEMLALI, W., BOSC, C., ANDRIEUX, A. & BIECHE, I. 2019. Loss of the deglutamylase CCP5 perturbs multiple steps of spermatogenesis and leads to male infertility. *Journal of cell science,* 132**,** jcs226951.

GOBRECHT, P., ANDREADAKI, A., DIEKMANN, H., HESKAMP, A., LEIBINGER, M. & FISCHER, D. 2016. Promotion of functional nerve regeneration by inhibition of microtubule detyrosination. *Journal of Neuroscience,* 36**,** 3890-3902.

GODENA, V. K., BROOKES-HOCKING, N., MOLLER, A., SHAW, G., OSWALD, M., SANCHO, R. M., MILLER, C. C., WHITWORTH, A. J. & DE VOS, K. J. 2014. Increasing microtubule acetylation rescues axonal transport and locomotor

deficits caused by LRRK2 Roc-COR domain mutations. *Nature communications,* 5**,** 1-11.

GONATAS, N. K., STIEBER, A. & GONATAS, J. O. 2006. Fragmentation of the Golgi apparatus in neurodegenerative diseases and cell death. *Journal of the neurological sciences,* 246**,** 21-30.

GREER, K., MARUTA, H., L'HERNAULT, S. W. & ROSENBAUM, J. L. 1985. Alpha-tubulin acetylase activity in isolated Chlamydomonas flagella. *The Journal of cell biology,* 101**,** 2081-2084.

GUARDIA, C. M., FARÍAS, G. G., JIA, R., PU, J. & BONIFACINO, J. S. 2016. BORC functions upstream of kinesins 1 and 3 to coordinate regional movement of lysosomes along different microtubule tracks. *Cell reports,* 17**,** 1950-1961.

GUNDERSEN, G. G. & BULINSKI, J. C. 1986. Distribution of tyrosinated and nontyrosinated alpha-tubulin during mitosis. *The Journal of cell biology,* 102**,** 1118-1126.

GUNDERSEN, G. G., KALNOSKI, M. H. & BULINSKI, J. C. 1984. Distinct populations of microtubules: tyrosinated and nontyrosinated alpha tubulin are distributed differently in vivo. *Cell,* 38**,** 779-789.

HALLAK, M. E., RODRIGUEZ, J., BARRA, H. & CAPUTTO, R. 1977. Release of tyrosine from tyrosinated tubulin. Some common factors that affect this process and the assembly of tubulin. *FEBS letters,* 73**,** 147-150.

HEINZEN, E. L., NEED, A. C., HAYDEN, K. M., CHIBA-FALEK, O., ROSES, A. D., STRITTMATTER, W. J., BURKE, J. R., HULETTE, C. M., WELSH-BOHMER,

K. A. & GOLDSTEIN, D. B. 2010. Genome-wide scan of copy number variation in late-onset Alzheimer's disease. *Journal of Alzheimer's Disease,* 19**,** 69-77.

HIROKAWA, N., TANAKA, Y., OKADA, Y. & TAKEDA, S. 2006. Nodal flow and the generation of left-right asymmetry. *Cell,* 125**,** 33-45.

HORIO, T. & MURATA, T. 2014. The role of dynamic instability in microtubule organization. *Frontiers in plant science,* 5**,** 511.

HUANG, K., DIENER, D. R. & ROSENBAUM, J. L. 2009. The ubiquitin conjugation system is involved in the disassembly of cilia and flagella. *Journal of Cell Biology,* 186**,** 601-613.

HUBBERT, C., GUARDIOLA, A., SHAO, R., KAWAGUCHI, Y., ITO, A., NIXON, A., YOSHIDA, M., WANG, X.-F. & YAO, T.-P. 2002. HDAC6 is a microtubule-associated deacetylase. *Nature,* 417**,** 455-458.

IKEGAMI, K., HEIER, R. L., TARUISHI, M., TAKAGI, H., MUKAI, M., SHIMMA, S., TAIRA, S., HATANAKA, K., MORONE, N. & YAO, I. 2007. Loss of α-tubulin polyglutamylation in ROSA22 mice is associated with abnormal targeting of KIF1A and modulated synaptic function. *Proceedings of the National Academy of Sciences,* 104**,** 3213-3218.

IKEGAMI, K., MUKAI, M., TSUCHIDA, J.-I., HEIER, R. L., MACGREGOR, G. R. & SETOU, M. 2006. TTLL7 is a mammalian β-tubulin polyglutamylase required for growth of MAP2-positive neurites. *Journal of Biological Chemistry,* 281**,** 30707-30716.

IKEGAMI, K., SATO, S., NAKAMURA, K., OSTROWSKI, L. E. & SETOU, M. 2010. Tubulin polyglutamylation is essential for airway ciliary function through the

regulation of beating asymmetry. *Proceedings of the National Academy of Sciences,* 107**,** 10490-10495.

IKEGAMI, K. & SETOU, M. 2009. TTLL10 can perform tubulin glycylation when co-expressed with TTLL8. *FEBS letters,* 583**,** 1957-1963.

JANKE, C. 2014. The tubulin code: molecular components, readout mechanisms, and functions. *Journal of Cell Biology,* 206**,** 461-472.

JANKE, C. & MAGIERA, M. M. 2020. The tubulin code and its role in controlling microtubule properties and functions. *Nature Reviews Molecular Cell Biology,* 21**,** 307-326.

JANKE, C., ROGOWSKI, K., WLOGA, D., REGNARD, C., KAJAVA, A. V., STRUB, J.-M., TEMURAK, N., VAN DIJK, J., BOUCHER, D. & VAN DORSSELAER, A. 2005. Tubulin polyglutamylase enzymes are members of the TTL domain protein family. *Science,* 308**,** 1758-1762.

JENKINS, B. V., SAUNDERS, H. A., RECORD, H. L., JOHNSON-SCHLITZ, D. M. & WILDONGER, J. 2017. Effects of mutating α-tubulin lysine 40 on sensory dendrite development. *Journal of cell science,* 130**,** 4120-4131.

JEON, H.-J. & OH, J. S. 2020. RASSF1A Regulates Spindle Organization by Modulating Tubulin Acetylation via SIRT2 and HDAC6 in Mouse Oocytes. *Frontiers in cell and developmental biology***,** 1222.

JI, S., KANG, J. G., PARK, S. Y., LEE, J., OH, Y. J. & CHO, J. W. 2011. O-GlcNAcylation of tubulin inhibits its polymerization. *Amino acids,* 40**,** 809-818.

JOSHI, H. C. & CLEVELAND, D. W. 1989. Differential utilization of beta-tubulin isotypes in differentiating neurites. *The Journal of cell biology,* 109**,** 663-673.

KAHN, O. I., SHARMA, V., GONZÁLEZ-BILLAULT, C. & BAAS, P. W. 2015. Effects of kinesin-5 inhibition on dendritic architecture and microtubule organization. *Molecular biology of the cell,* 26**,** 66-77.

KALEBIC, N., SORRENTINO, S., PERLAS, E., BOLASCO, G., MARTINEZ, C. & HEPPENSTALL, P. A. 2013. αTAT1 is the major α-tubulin acetyltransferase in mice. *Nature communications,* 4**,** 1-10.

KANN, M. L., PRIGENT, Y., LEVILLIERS, N., BRÉ, M. H. & FOUQUET, J. P. 1998. Expression of glycylated tubulin during the differentiation of spermatozoa in mammals. *Cell motility and the cytoskeleton,* 41**,** 341-352.

KARAKAYA, M., PAKETCI, C., ALTMUELLER, J., THIELE, H., HOELKER, I., YIS, U. & WIRTH, B. 2019. Biallelic variant in AGTPBP1 causes infantile lower motor neuron degeneration and cerebellar atrophy. *American Journal of Medical Genetics Part A,* 179**,** 1580-1584.

KAUL, N., SOPPINA, V. & VERHEY, K. J. 2014. Effects of α-tubulin K40 acetylation and detyrosination on kinesin-1 motility in a purified system. *Biophysical journal,* 106**,** 2636-2643.

KERR, J. P., ROBISON, P., SHI, G., BOGUSH, A. I., KEMPEMA, A. M., HEXUM, J. K., BECERRA, N., HARKI, D. A., MARTIN, S. S. & RAITERI, R. 2015. Detyrosinated microtubules modulate mechanotransduction in heart and skeletal muscle. *Nature communications,* 6**,** 1-14.

KI, S. M., KIM, J. H., WON, S. Y., OH, S. J., LEE, I. Y., BAE, Y. K., CHUNG, K. W., CHOI, B. O., PARK, B. & CHOI, E. J. 2020. CEP 41-mediated ciliary tubulin

glutamylation drives angiogenesis through AURKA-dependent deciliation. *EMBO reports,* 21**,** e48290.

KIM, C., CHOI, H., JUNG, E. S., LEE, W., OH, S., JEON, N. L. & MOOK-JUNG, I. 2012. HDAC6 inhibitor blocks amyloid beta-induced impairment of mitochondrial transport in hippocampal neurons.

KIM, D. J., MARTINEZ-LEMUS, L. A. & DAVIS, G. E. 2013a. EB1, p150Glued, and Clasp1 control endothelial tubulogenesis through microtubule assembly, acetylation, and apical polarization. *Blood, The Journal of the American Society of Hematology,* 121**,** 3521-3530.

KIM, G.-W., LI, L., GORBANI, M., YOU, L. & YANG, X.-J. 2013b. Mice lacking α-tubulin acetyltransferase 1 are viable but display α-tubulin acetylation deficiency and dentate gyrus distortion. *Journal of Biological Chemistry,* 288**,** 20334-20350.

KIMELMAN, D. & MARTIN, B. L. 2012. Anterior–posterior patterning in early development: three strategies. *Wiley Interdisciplinary Reviews: Developmental Biology,* 1**,** 253-266.

KIMURA, Y., TSUTSUMI, K., KONNO, A., IKEGAMI, K., HAMEED, S., KANEKO, T., KAPLAN, O. I., TERAMOTO, T., FUJIWARA, M. & ISHIHARA, T. 2018. Environmental responsiveness of tubulin glutamylation in sensory cilia is regulated by the p38 MAPK pathway. *Scientific reports,* 8**,** 1-13.

KO, P., CHOI, J.-H., SONG, S., KEUM, S., JEONG, J., HWANG, Y. E., KIM, J. W. & RHEE, S. 2021. Microtubule acetylation controls MDA-MB-231 breast cancer cell invasion through the modulation of endoplasmic reticulum stress. *International journal of molecular sciences,* 22**,** 6018.

KOBAYASHI, M., WAKABAYASHI, I., SUZUKI, Y., FUJIWARA, K., NAKAYAMA, M., WATABE, T. & SATO, Y. 2021. Tubulin carboxypeptidase activity of vasohibin-1 inhibits angiogenesis by interfering with endocytosis and trafficking of pro-angiogenic factor receptors. *Angiogenesis,* 24**,** 159-176.

KONISHI, Y. & SETOU, M. 2009. Tubulin tyrosination navigates the kinesin-1 motor domain to axons. *Nature neuroscience,* 12**,** 559-567.

KONNO, A., IKEGAMI, K., KONISHI, Y., YANG, H.-J., ABE, M., YAMAZAKI, M., SAKIMURA, K., YAO, I., SHIBA, K. & INABA, K. 2016. Ttll9−/− mice sperm flagella show shortening of doublet 7, reduction of doublet 5 polyglutamylation and a stall in beating. *Journal of Cell Science,* 129**,** 2757-2766.

KRAUHS, E., LITTLE, M., KEMPF, T., HOFER-WARBINEK, R., ADE, W. & PONSTINGL, H. 1981. Complete amino acid sequence of beta-tubulin from porcine brain. *Proceedings of the National Academy of Sciences,* 78**,** 4156-4160.

KUBO, T., YANAGISAWA, H.-A., YAGI, T., HIRONO, M. & KAMIYA, R. 2010. Tubulin polyglutamylation regulates axonemal motility by modulating activities of inner-arm dyneins. *Current Biology,* 20**,** 441-445.

L'HERNAULT, S. W. & ROSENBAUM, J. L. 1983. Chlamydomonas alpha-tubulin is posttranslationally modified in the flagella during flagellar assembly. *The Journal of cell biology,* 97**,** 258-263.

L'HERNAULT, S. W. & ROSENBAUM, J. L. 1985. Chlamydomonas. alpha.-tubulin is posttranslationally modified by acetylation on the. epsilon.-amino group of a lysine. *Biochemistry,* 24**,** 473-478.

LEDIZET, M. & PIPERNO, G. 1987. Identification of an acetylation site of Chlamydomonas alpha-tubulin. *Proceedings of the National Academy of Sciences,* 84**,** 5720-5724.

LEE, G.-S., HE, Y., DOUGHERTY, E. J., JIMENEZ-MOVILLA, M., AVELLA, M., GRULLON, S., SHARLIN, D. S., GUO, C., BLACKFORD, J. A. & AWASTHI, S. 2013. Disruption of Ttll5/stamp gene (tubulin tyrosine ligase-like protein 5/SRC-1 and TIF2-associated modulatory protein gene) in male mice causes sperm malformation and infertility. *Journal of Biological Chemistry,* 288**,** 15167-15180.

LEE, J. Y., KOGA, H., KAWAGUCHI, Y., TANG, W., WONG, E., GAO, Y. S., PANDEY, U. B., KAUSHIK, S., TRESSE, E. & LU, J. 2010. HDAC6 controls autophagosome maturation essential for ubiquitin-selective quality-control autophagy. *The EMBO journal,* 29**,** 969-980.

LEIDINGER, P., BACKES, C., DEUTSCHER, S., SCHMITT, K., MUELLER, S. C., FRESE, K., HAAS, J., RUPRECHT, K., PAUL, F. & STÄHLER, C. 2013. A blood based 12-miRNA signature of Alzheimer disease patients. *Genome biology,* 14**,** 1-16.

LESSARD, D. V., ZINDER, O. J., HOTTA, T., VERHEY, K. J., OHI, R. & BERGER, C. L. 2019. Polyglutamylation of tubulin's C-terminal tail controls pausing and motility of kinesin-3 family member KIF1A. *Journal of Biological Chemistry,* 294**,** 6353-6363.

LEVILLIERS, N., FLEURY, A. & HILL, A.-M. 1995. Monoclonal and polyclonal antibodies detect a new type of post-translational modification of axonemal tubulin. *Journal of Cell Science,* 108**,** 3013-3028.

LEWIS, S. A., GU, W. & COWAN, N. J. 1987. Free intermingling of mammalian β-tubulin isotypes among functionally distinct microtubules. *Cell,* 49**,** 539-548.

LEWIS, S. A., LEE, M. G.-S. & COWAN, N. J. 1985. Five mouse tubulin isotypes and their regulated expression during development. *The Journal of cell biology,* 101**,** 852-861.

LI, J., SNYDER, E. Y., TANG, F. H., PASQUALINI, R., ARAP, W. & SIDMAN, R. L. 2020. Nna1 gene deficiency triggers Purkinje neuron death by tubulin hyperglutamylation and ER dysfunction. *JCI insight,* 5.

LI, L., JAYABAL, S., GHORBANI, M., LEGAULT, L.-M., MCGRAW, S., WATT, A. J. & YANG, X.-J. 2019. ATAT1 regulates forebrain development and stress-induced tubulin hyperacetylation. *Cellular and molecular life sciences,* 76**,** 3621-3640.

LOPES, A. T., HAUSRAT, T. J., HEISLER, F. F., GROMOVA, K. V., LOMBINO, F. L., FISCHER, T., RUSCHKIES, L., BREIDEN, P., THIES, E. & HERMANS-BORGMEYER, I. 2020. Spastin depletion increases tubulin polyglutamylation and impairs kinesin-mediated neuronal transport, leading to working and associative memory deficits. *PLoS biology,* 18**,** e3000820.

LYONS, P. J., SAPIO, M. R. & FRICKER, L. D. 2013. Zebrafish cytosolic carboxypeptidases 1 and 5 are essential for embryonic development. *Journal of Biological Chemistry,* 288**,** 30454-30462.

MAAS, C., BELGARDT, D., LEE, H. K., HEISLER, F. F., LAPPE-SIEFKE, C., MAGIERA, M. M., VAN DIJK, J., HAUSRAT, T. J., JANKE, C. & KNEUSSEL, M. 2009. Synaptic activation modifies microtubules underlying transport of postsynaptic cargo. *Proceedings of the National Academy of Sciences,* 106**,** 8731-8736.

MACKEH, R., LORIN, S., RATIER, A., MEJDOUBI-CHAREF, N., BAILLET, A., BRUNEEL, A., HAMAÏ, A., CODOGNO, P., POÜS, C. & PERDIZ, D. 2014. Reactive oxygen species, AMP-activated protein kinase, and the transcription cofactor p300 regulate α-tubulin acetyltransferase-1 (αTAT-1/MEC-17)-dependent microtubule hyperacetylation during cell stress. *Journal of Biological Chemistry,* 289**,** 11816-11828.

MAGIERA, M. M., BODAKUNTLA, S., ŽIAK, J., LACOMME, S., MARQUES SOUSA, P., LEBOUCHER, S., HAUSRAT, T. J., BOSC, C., ANDRIEUX, A. & KNEUSSEL, M. 2018a. Excessive tubulin polyglutamylation causes neurodegeneration and perturbs neuronal transport. *The EMBO journal,* 37**,** e100440.

MAGIERA, M. M., SINGH, P., GADADHAR, S. & JANKE, C. 2018b. Tubulin posttranslational modifications and emerging links to human disease. *Cell,* 173**,** 1323-1327.

MAHALINGAN, K. K., KEITH KEENAN, E., STRICKLAND, M., LI, Y., LIU, Y., BALL, H. L., TANNER, M. E., TJANDRA, N. & ROLL-MECAK, A. 2020. Structural basis for polyglutamate chain initiation and elongation by TTLL family enzymes. *Nature Structural & Molecular Biology,* 27**,** 802-813.

MANES, M. E., ELINSON, R. P. & BARBIERI, F. D. 1978. Formation of the amphibian grey crescent: effects of colchicine and cytochalasin B. *Wilhelm Roux's archives of developmental biology,* 185**,** 99-104.

MARCOS, S., MOREAU, J., BACKER, S., JOB, D., ANDRIEUX, A. & BLOCH-GALLEGO, E. 2009. Tubulin tyrosination is required for the proper organization and pathfinding of the growth cone. *PloS one,* 4**,** e5405.

MARUTA, H., GREER, K. & ROSENBAUM, J. L. 1986. The acetylation of alpha-tubulin and its relationship to the assembly and disassembly of microtubules. *The Journal of cell biology,* 103**,** 571-579.

MARY, J., REDEKER, V., LE CAER, J.-P., PROMÉ, J.-C. & ROSSIER, J. 1994. Class I and IVa β-tubulin isotypes expressed in adult mouse brain are glutamylated. *FEBS letters,* 353**,** 89-94.

MARY, J., REDEKER, V., LE CAER, J.-P., ROSSIER, J. & SCHMITTER, J.-M. 1996. Posttranslational Modifications in the C-terminal Tail of Axonemal Tubulin from Sea Urchin Sperm (∗). *Journal of Biological Chemistry,* 271**,** 9928-9933.

MATHIEU, H., PATTEN, S. A., ARAGON-MARTIN, J. A., OCAKA, L., SIMPSON, M., CHILD, A. & MOLDOVAN, F. 2021. Genetic variant of TTLL11 gene and subsequent ciliary defects are associated with idiopathic scoliosis in a 5-generation UK family. *Scientific reports,* 11**,** 1-15.

MCKENNEY, R. J., HUYNH, W., VALE, R. D. & SIRAJUDDIN, M. 2016. Tyrosination of α-tubulin controls the initiation of processive dynein–dynactin motility. *The EMBO journal,* 35**,** 1175-1185.

MILLER, J. R., ROWNING, B. A., LARABELL, C. A., YANG-SNYDER, J. A., BATES, R. L. & MOON, R. T. 1999. Establishment of the dorsal–ventral axis in Xenopus embryos coincides with the dorsal enrichment of dishevelled that is dependent on cortical rotation. *The Journal of cell biology,* 146**,** 427-438.

MORLEY, S. J., QI, Y., IOVINO, L., ANDOLFI, L., GUO, D., KALEBIC, N., CASTALDI, L., TISCHER, C., PORTULANO, C. & BOLASCO, G. 2016. Acetylated tubulin is essential for touch sensation in mice. *Elife,* 5**,** e20813.

MUÑOZ-CASTAÑEDA, R., DÍAZ, D., PERIS, L., ANDRIEUX, A., BOSC, C., MUÑOZ-CASTAÑEDA, J. M., JANKE, C., ALONSO, J. R., MOUTIN, M.-J. & WERUAGA, E. 2018. Cytoskeleton stability is essential for the integrity of the cerebellum and its motor-and affective-related behaviors. *Scientific reports,* 8**,** 1-14.

MURRAY, A. W. & FROSCIO, M. 1971. Cyclic adenosine 3′: 5′-monophosphate and microtubule function: Specific interaction of the phosphorylated protein subunits with a soluble brain component. *Biochemical and Biophysical Research Communications,* 44**,** 1089-1095.

MYTLIS, A., KUMAR, V., QIU, T., DEIS, R., HART, N., LEVY, K., MASEK, M., SHAWAHNY, A., AHMAD, A., EITAN, H., NATHER, F., ADAR-LEVOR, S., BIRNBAUM, R. Y., ELIA, N., BACHMANN-GAGESCU, R., ROY, S. & ELKOUBY, Y. M. 2022. Control of meiotic chromosomal bouquet and germ cell morphogenesis by the zygotene cilium. *Science,* 0**,** eabh3104.

NAKAGAWA, U., SUZUKI, D., ISHIKAWA, M., SATO, H., KAMEMURA, K. & IMAMURA, A. 2013. Acetylation of α-tubulin on Lys40 is a widespread post-

translational modification in angiosperms. *Bioscience, biotechnology, and biochemistry,* 77**,** 1602-1605.

NASHCHEKIN, D., FERNANDES, A. R. & ST JOHNSTON, D. 2016. Patronin/Shot cortical foci assemble the noncentrosomal microtubule array that specifies the Drosophila anterior-posterior axis. *Developmental cell,* 38**,** 61-72.

NEUMANN, B. & HILLIARD, M. A. 2014. Loss of MEC-17 leads to microtubule instability and axonal degeneration. *Cell reports,* 6**,** 93-103.

NIEUWENHUIS, J., ADAMOPOULOS, A., BLEIJERVELD, O. B., MAZOUZI, A., STICKEL, E., CELIE, P., ALTELAAR, M., KNIPSCHEER, P., PERRAKIS, A. & BLOMEN, V. A. 2017. Vasohibins encode tubulin detyrosinating activity. *Science,* 358**,** 1453-1456.

NIRSCHL, J. J., MAGIERA, M. M., LAZARUS, J. E., JANKE, C. & HOLZBAUR, E. L. 2016. α-Tubulin tyrosination and CLIP-170 phosphorylation regulate the initiation of dynein-driven transport in neurons. *Cell reports,* 14**,** 2637-2652.

NOGALES, E., WHITTAKER, M., MILLIGAN, R. A. & DOWNING, K. H. 1999. High-resolution model of the microtubule. *Cell,* 96**,** 79-88.

NORTH, B. J., MARSHALL, B. L., BORRA, M. T., DENU, J. M. & VERDIN, E. 2003. The human Sir2 ortholog, SIRT2, is an NAD+-dependent tubulin deacetylase. *Molecular cell,* 11**,** 437-444.

NORVELL, A., WONG, J., RANDOLPH, K. & THOMPSON, L. 2015. Wispy and Orb cooperate in the cytoplasmic polyadenylation of localized gurken mRNA. *Developmental Dynamics,* 244**,** 1276-1285.

NSAMBA, E. T. & GUPTA JR, M. L. 2022. Tubulin isotypes–functional insights from model organisms. *Journal of Cell Science,* 135**,** jcs259539.

O'HAGAN, R., PIASECKI, B. P., SILVA, M., PHIRKE, P., NGUYEN, K. C., HALL, D. H., SWOBODA, P. & BARR, M. M. 2011. The tubulin deglutamylase CCPP-1 regulates the function and stability of sensory cilia in C. elegans. *Current biology,* 21**,** 1685-1694.

O'HAGAN, R., SILVA, M., NGUYEN, K. C., ZHANG, W., BELLOTTI, S., RAMADAN, Y. H., HALL, D. H. & BARR, M. M. 2017. Glutamylation regulates transport, specializes function, and sculpts the structure of cilia. *Current Biology,* 27**,** 3430-3441. e6.

OHKAWA, N., SUGISAKI, S., TOKUNAGA, E., FUJITANI, K., HAYASAKA, T., SETOU, M. & INOKUCHI, K. 2008. N-acetyltransferase ARD1-NAT1 regulates neuronal dendritic development. *Genes to Cells,* 13**,** 1171-1183.

OLENIEVA, V., LYTVYN, D., YEMETS, A., BERGOUNIOUX, C. & BLUME, Y. 2019. Tubulin acetylation accompanies autophagy development induced by different abiotic stimuli in Arabidopsis thaliana. *Cell Biology International,* 43**,** 1056-1064.

ORI-MCKENNEY, K. M., MCKENNEY, R. J., HUANG, H. H., LI, T., MELTZER, S., JAN, L. Y., VALE, R. D., WIITA, A. P. & JAN, Y. N. 2016. Phosphorylation of β-tubulin by the Down syndrome kinase, minibrain/DYRK1a, regulates microtubule dynamics and dendrite morphogenesis. *Neuron,* 90**,** 551-563.

OUYANG, C., LI, J., ZHENG, X., MU, J., TORRES, G., WANG, Q., ZOU, M.-H. & XIE, Z. 2021. Deletion of Ulk1 inhibits neointima formation by enhancing

KAT2A/GCN5-mediated acetylation of TUBA/α-tubulin in vivo. *Autophagy,* 17**,** 4305-4322.

OZOLS, J. & CARON, J. 1997. Posttranslational modification of tubulin by palmitoylation: II. Identification of sites of palmitoylation. *Molecular biology of the cell,* 8**,** 637-645.

PAGNAMENTA, A. T., HEEMERYCK, P., MARTIN, H. C., BOSC, C., PERIS, L., USZYNSKI, I., GORY-FAURÉ, S., COULY, S., DESHPANDE, C. & SIDDIQUI, A. 2019. Defective tubulin detyrosination causes structural brain abnormalities with cognitive deficiency in humans and mice. *Human molecular genetics,* 28**,** 3391-3405.

PANDEY, U. B., NIE, Z., BATLEVI, Y., MCCRAY, B. A., RITSON, G. P., NEDELSKY, N. B., SCHWARTZ, S. L., DIPROSPERO, N. A., KNIGHT, M. A. & SCHULDINER, O. 2007. HDAC6 rescues neurodegeneration and provides an essential link between autophagy and the UPS. *Nature,* 447**,** 860-864.

PARK, I. Y., POWELL, R. T., TRIPATHI, D. N., DERE, R., HO, T. H., BLASIUS, T. L., CHIANG, Y.-C., DAVIS, I. J., FAHEY, C. C. & HACKER, K. E. 2016. Dual chromatin and cytoskeletal remodeling by SETD2. *Cell,* 166**,** 950-962.

PATEL-HETT, S., RICHARDSON, J. L., SCHULZE, H., DRABEK, K., ISAAC, N. A., HOFFMEISTER, K., SHIVDASANI, R. A., BULINSKI, J. C., GALJART, N. & HARTWIG, J. H. 2008. Visualization of microtubule growth in living platelets reveals a dynamic marginal band with multiple microtubules. *Blood, The Journal of the American Society of Hematology,* 111**,** 4605-4616.

PATHAK, N., AUSTIN-TSE, C. A., LIU, Y., VASILYEV, A. & DRUMMOND, I. A. 2014. Cytoplasmic carboxypeptidase 5 regulates tubulin glutamylation and zebrafish cilia formation and function. *Molecular biology of the cell,* 25**,** 1836-1844.

PATHAK, N., AUSTIN, C. A. & DRUMMOND, I. A. 2011. Tubulin tyrosine ligase-like genes ttll3 and ttll6 maintain zebrafish cilia structure and motility. *Journal of Biological Chemistry,* 286**,** 11685-11695.

PATHAK, N., OBARA, T., MANGOS, S., LIU, Y. & DRUMMOND, I. A. 2007. The zebrafish fleer gene encodes an essential regulator of cilia tubulin polyglutamylation. *Molecular biology of the cell,* 18**,** 4353-4364.

PATURLE-LAFANECHERE, L., EDDE, B., DENOULET, P., VAN DORSSELAER, A., MAZARGUIL, H., LE CAER, J. P., WEHLAND, J. & JOB, D. 1991. Characterization of a major brain tubulin variant which cannot be tyrosinated. *Biochemistry,* 30**,** 10523-10528.

PATURLE-LAFANECHÈRE, L., MANIER, M., TRIGAULT, N., PIROLLET, F., MAZARGUIL, H. & JOB, D. 1994. Accumulation of delta 2-tubulin, a major tubulin variant that cannot be tyrosinated, in neuronal tissues and in stable microtubule assemblies. *Journal of cell science,* 107**,** 1529-1543.

PATURLE, L., WEHLAND, J., MARGOLIS, R. L. & JOB, D. 1989. Complete separation of tyrosinated, detyrosinated, and nontyrosinatable brain tubulin subpopulations using affinity chromatography. *Biochemistry,* 28**,** 2698-2704.

PERIS, L., THERY, M., FAURÉ, J., SAOUDI, Y., LAFANECHÈRE, L., CHILTON, J. K., GORDON-WEEKS, P., GALJART, N., BORNENS, M. & WORDEMAN, L.

2006. Tubulin tyrosination is a major factor affecting the recruitment of CAP-Gly proteins at microtubule plus ends. *The Journal of cell biology,* 174**,** 839-849.

PERIS, L., WAGENBACH, M., LAFANECHÈRE, L., BROCARD, J., MOORE, A. T., KOZIELSKI, F., JOB, D., WORDEMAN, L. & ANDRIEUX, A. 2009. Motor-dependent microtubule disassembly driven by tubulin tyrosination. *Journal of Cell Biology,* 185**,** 1159-1166.

PETERS, J. D., FURLONG, M. T., ASAI, D. J., HARRISON, M. L. & GEAHLEN, R. L. 1996. Syk, Activated by Cross-linking the B-cell Antigen Receptor, Localizes to the Cytosol Where It Interacts with and Phosphorylates α-Tubulin on Tyrosine (∗). *Journal of Biological Chemistry,* 271**,** 4755-4762.

PIANU, B., LEFORT, R., THUILIERE, L., TABOURIER, E. & BARTOLINI, F. 2014. The Aβ1-42 peptide regulates microtubule stability independently of tau. *Journal of Cell Science,* 127**,** 1117-1127.

PIPERNO, G. & FULLER, M. T. 1985. Monoclonal antibodies specific for an acetylated form of alpha-tubulin recognize the antigen in cilia and flagella from a variety of organisms. *The Journal of cell biology,* 101**,** 2085-2094.

PONSTINGL, H., KRAUHS, E., LITTLE, M. & KEMPF, T. 1981. Complete amino acid sequence of alpha-tubulin from porcine brain. *Proceedings of the National Academy of Sciences,* 78**,** 2757-2761.

PORTRAN, D., SCHAEDEL, L., XU, Z., THÉRY, M. & NACHURY, M. V. 2017. Tubulin acetylation protects long-lived microtubules against mechanical ageing. *Nature cell biology,* 19**,** 391-398.

RAN, J., YANG, Y., LI, D., LIU, M. & ZHOU, J. 2015. Deacetylation of α-tubulin and cortactin is required for HDAC6 to trigger ciliary disassembly. *Scientific reports,* 5**,** 1-13.

RAO, Y., HAO, R., WANG, B. & YAO, T.-P. 2014. A Mec17-Myosin II effector axis coordinates microtubule acetylation and actin dynamics to control primary cilium biogenesis. *PloS one,* 9**,** e114087.

RASAMIZAFY, S. F., DELSERT, C., RABEHARIVELO, G., CAU, J., MORIN, N. & VAN DIJK, J. 2021. Mitotic Acetylation of Microtubules Promotes Centrosomal PLK1 Recruitment and Is Required to Maintain Bipolar Spindle Homeostasis. *Cells,* 10**,** 1859.

RAYBIN, D. & FLAVIN, M. 1977. Enzyme which specifically adds tyrosine to the α chain of tubulin. *Biochemistry,* 16**,** 2189-2194.

REDEKER, V., LEVILLIERS, N., SCHMITTER, J.-M., LE CAER, J.-P., ROSSIER, J., ADOUTTE, A. & BRE, M.-H. 1994. Polyglycylation of tubulin: a posttranslational modification in axonemal microtubules. *Science,* 266**,** 1688-1691.

REDEKER, V., ROSSIER, J. & FRANKFURTER, A. 1998. Posttranslational modifications of the C-terminus of α-tubulin in adult rat brain: α4 is glutamylated at two residues. *Biochemistry,* 37**,** 14838-14844.

REED, N. A., CAI, D., BLASIUS, T. L., JIH, G. T., MEYHOFER, E., GAERTIG, J. & VERHEY, K. J. 2006. Microtubule acetylation promotes kinesin-1 binding and transport. *Current biology,* 16**,** 2166-2172.

REN, Y., ZHAO, J. & FENG, J. 2003. Parkin binds to α/β tubulin and increases their ubiquitination and degradation. *Journal of Neuroscience,* 23**,** 3316-3324.

RENTHAL, R., SCHNEIDER, B. G., MILLER, M. M. & LUDUEÑA, R. F. 1993. βIV is the major β-tubulin isotype in bovine cilia. *Cell motility and the cytoskeleton,* 25**,** 19-29.

RIBBA, A.-S., BATZENSCHLAGER, M., RABAT, C., BUCHOU, T., MOOG, S., KHOCHBIN, S., BOUROVA-FLIN, E., LAFANECHÈRE, L., LANZA, F. & SADOUL, K. 2021. Marginal band microtubules are acetylated by αTAT1. *Platelets,* 32**,** 568-572.

ROBISON, P., CAPORIZZO, M. A., AHMADZADEH, H., BOGUSH, A. I., CHEN, C. Y., MARGULIES, K. B., SHENOY, V. B. & PROSSER, B. L. 2016. Detyrosinated microtubules buckle and bear load in contracting cardiomyocytes. *Science,* 352**,** aaf0659.

ROBSON, S. J. & BURGOYNE, R. D. 1989. Differential localisation of tyrosinated, detyrosinated, and acetylated α-tubulins in neurites and growth cones of dorsal root ganglion neurons. *Cell motility and the cytoskeleton,* 12**,** 273-282.

ROCHA, C., PAPON, L., CACHEUX, W., MARQUES SOUSA, P., LASCANO, V., TORT, O., GIORDANO, T., VACHER, S., LEMMERS, B. & MARIANI, P. 2014. Tubulin glycylases are required for primary cilia, control of cell proliferation and tumor development in colon. *The EMBO journal,* 33**,** 2247-2260.

RODRIGUEZ, J., ARCE, C., BARRA, H. & CAPUTTO, R. 1973. Release of tyrosine incorporated as a single unit into rat brain protein. *Biochemical and Biophysical Research Communications,* 54**,** 335-340.

ROGOWSKI, K., JUGE, F., VAN DIJK, J., WLOGA, D., STRUB, J.-M., LEVILLIERS, N., THOMAS, D., BRÉ, M.-H., VAN DORSSELAER, A. & GAERTIG, J. 2009. Evolutionary divergence of enzymatic mechanisms for posttranslational polyglycylation. *Cell,* 137**,** 1076-1087.

ROGOWSKI, K., VAN DIJK, J., MAGIERA, M. M., BOSC, C., DELOULME, J.-C., BOSSON, A., PERIS, L., GOLD, N. D., LACROIX, B. & GRAU, M. B. 2010. A family of protein-deglutamylating enzymes associated with neurodegeneration. *Cell,* 143**,** 564-578.

ROLL-MECAK, A. 2020. The tubulin code in microtubule dynamics and information encoding. *Developmental cell,* 54**,** 7-20.

ROSAS-ACOSTA, G., RUSSELL, W. K., DEYRIEUX, A., RUSSELL, D. H. & WILSON, V. G. 2005. A universal strategy for proteomic studies of SUMO and other ubiquitin-like modifiers. *Molecular & Cellular Proteomics,* 4**,** 56-72.

RÜDIGER, M., PLESSMAN, U., KLÖPPEL, K.-D., WEHLAND, J. & WEBER, K. 1992. Class II tubulin, the major brain β tubulin isotype is polyglutamylated on glutamic acid residue 435. *FEBS letters,* 308**,** 101-105.

SADOUL, K., WANG, J., DIAGOURAGA, B., VITTE, A.-L., BUCHOU, T., ROSSINI, T., POLACK, B., XI, X., MATTHIAS, P. & KHOCHBIN, S. 2012. HDAC6 controls the kinetics of platelet activation. *Blood, The Journal of the American Society of Hematology,* 120**,** 4215-4218.

SCHATTEN, G., SIMERLY, C., ASAI, D. J., SZÖKE, E., COOKE, P. & SCHATTEN, H. 1988. Acetylated α-tubulin in microtubules during mouse fertilization and early development. *Developmental biology,* 130**,** 74-86.

SHANG, Y., LI, B. & GOROVSKY, M. A. 2002. Tetrahymena thermophila contains a conventional γ-tubulin that is differentially required for the maintenance of different microtubule-organizing centers. *The Journal of cell biology,* 158**,** 1195-1206.

SHIBUYA, H., MORIMOTO, A. & WATANABE, Y. 2014. The dissection of meiotic chromosome movement in mice using an in vivo electroporation technique. *PLoS genetics,* 10**,** e1004821.

SHIDA, T., CUEVA, J. G., XU, Z., GOODMAN, M. B. & NACHURY, M. V. 2010. The major α-tubulin K40 acetyltransferase αTAT1 promotes rapid ciliogenesis and efficient mechanosensation. *Proceedings of the National Academy of Sciences,* 107**,** 21517-21522.

SOLNICA-KREZEL, L. & DRIEVER, W. 1994. Microtubule arrays of the zebrafish yolk cell: organization and function during epiboly. *Development,* 120**,** 2443-2455.

SONG, W., CHO, Y., WATT, D. & CAVALLI, V. 2015. Tubulin-tyrosine ligase (TTL)-mediated increase in tyrosinated α-tubulin in injured axons is required for retrograde injury signaling and axon regeneration. *Journal of Biological Chemistry,* 290**,** 14765-14775.

SONG, Y., KIRKPATRICK, L. L., SCHILLING, A. B., HELSETH, D. L., CHABOT, N., KEILLOR, J. W., JOHNSON, G. V. & BRADY, S. T. 2013.

Transglutaminase and polyamination of tubulin: posttranslational modification for stabilizing axonal microtubules. *Neuron,* 78**,** 109-123.

SURYAVANSHI, S., EDDÉ, B., FOX, L. A., GUERRERO, S., HARD, R., HENNESSEY, T., KABI, A., MALISON, D., PENNOCK, D. & SALE, W. S. 2010. Tubulin glutamylation regulates ciliary motility by altering inner dynein arm activity. *Current biology,* 20**,** 435-440.

TANG, F., PAN, M.-H., WAN, X., LU, Y., ZHANG, Y. & SUN, S.-C. 2018. Kif18a regulates Sirt2-mediated tubulin acetylation for spindle organization during mouse oocyte meiosis. *Cell Division,* 13**,** 1-9.

TARRADE, A., FASSIER, C., COURAGEOT, S., CHARVIN, D., VITTE, J., PERIS, L., THOREL, A., MOUISEL, E., FONKNECHTEN, N. & ROBLOT, N. 2006. A mutation of spastin is responsible for swellings and impairment of transport in a region of axon characterized by changes in microtubule composition. *Human molecular genetics,* 15**,** 3544-3558.

TAS, R. P., CHAZEAU, A., CLOIN, B. M., LAMBERS, M. L., HOOGENRAAD, C. C. & KAPITEIN, L. C. 2017. Differentiation between oppositely oriented microtubules controls polarized neuronal transport. *Neuron,* 96**,** 1264-1271. e5.

TISCHFIELD, M. A., CEDERQUIST, G. Y., GUPTA JR, M. L. & ENGLE, E. C. 2011. Phenotypic spectrum of the tubulin-related disorders and functional implications of disease-causing mutations. *Current opinion in genetics & development,* 21**,** 286-294.

TORT, O., TANCO, S., ROCHA, C., BIÈCHE, I., SEIXAS, C., BOSC, C., ANDRIEUX, A., MOUTIN, M.-J., AVILÉS, F. X. & LORENZO, J. 2014. The cytosolic

carboxypeptidases CCP2 and CCP3 catalyze posttranslational removal of acidic amino acids. *Molecular biology of the cell,* 25**,** 3017-3027.

TRAN, L. D., HINO, H., QUACH, H., LIM, S., SHINDO, A., MIMORI-KIYOSUE, Y., MIONE, M., UENO, N., WINKLER, C. & HIBI, M. 2012. Dynamic microtubules at the vegetal cortex predict the embryonic axis in zebrafish. *Development,* 139**,** 3644-3652.

TSAI, M.-C. & AHRINGER, J. 2007. Microtubules are involved in anterior-posterior axis formation in C. elegans embryos. *The Journal of cell biology,* 179**,** 397-402.

TSENG, J.-H., XIE, L., SONG, S., XIE, Y., ALLEN, L., AJIT, D., HONG, J.-S., CHEN, X., MEEKER, R. B. & COHEN, T. J. 2017. The deacetylase HDAC6 mediates endogenous neuritic tau pathology. *Cell reports,* 20**,** 2169-2183.

VALENZUELA, P., QUIROGA, M., ZALDIVAR, J., RUTTER, W., KIRSCHNER, M. & CLEVELAND, D. 1981. Nucleotide and corresponding amino acid sequences encoded by α and β tubulin mRNAs. *Nature,* 289**,** 650-655.

VAN DIJK, J., BOMPARD, G., CAU, J., KUNISHIMA, S., RABEHARIVELO, G., MATEOS-LANGERAK, J., CAZEVIEILLE, C., CAVELIER, P., BOIZET-BONHOURE, B. & DELSERT, C. 2018. Microtubule polyglutamylation and acetylation drive microtubule dynamics critical for platelet formation. *BMC biology,* 16**,** 1-17.

VAN DIJK, J., ROGOWSKI, K., MIRO, J., LACROIX, B., EDDÉ, B. & JANKE, C. 2007. A targeted multienzyme mechanism for selective microtubule polyglutamylation. *Molecular cell,* 26**,** 437-448.

VERHEY, K. J. & GAERTIG, J. 2007. The tubulin code. *Cell cycle,* 6**,** 2152-2160.

VILLASANTE, A., WANG, D., DOBNER, P., DOLPH, P., LEWIS, S. & COWAN, N. 1986. Six mouse alpha-tubulin mRNAs encode five distinct isotypes: testis-specific expression of two sister genes. *Molecular and Cellular Biology,* 6**,** 2409-2419.

VOGEL, P., HANSEN, G., FONTENOT, G. & READ, R. 2010. Tubulin Tyrosine Ligase–Like 1 Deficiency Results in Chronic Rhinosinusitis and Abnormal Development of Spermatid Flagella in Mice. *Veterinary pathology,* 47**,** 703-712.

VU, H. T., AKATSU, H., HASHIZUME, Y., SETOU, M. & IKEGAMI, K. 2017. Increase in α-tubulin modifications in the neuronal processes of hippocampal neurons in both kainic acid-induced epileptic seizure and Alzheimer's disease. *Scientific reports,* 7**,** 1-14.

WALGREN, J. L., VINCENT, T. S., SCHEY, K. L. & BUSE, M. G. 2003. High glucose and insulin promote O-GlcNAc modification of proteins, including α-tubulin. *American Journal of Physiology-Endocrinology and Metabolism,* 284**,** E424-E434.

WALL, K. P., HART, H., LEE, T., PAGE, C., HAWKINS, T. L. & HOUGH, L. E. 2020. C-terminal tail polyglycylation and polyglutamylation alter microtubule mechanical properties. *Biophysical journal,* 119**,** 2219-2230.

WALLENFANG, M. R. & SEYDOUX, G. 2000. Polarization of the anterior–posterior axis of C. elegans is a microtubule-directed process. *Nature,* 408**,** 89-92.

WALTER, W. J., BERANEK, V., FISCHERMEIER, E. & DIEZ, S. 2012. Tubulin acetylation alone does not affect kinesin-1 velocity and run length in vitro.

WANG, Q., PENG, Z., LONG, H., DENG, X. & HUANG, K. 2019. Polyubiquitylation of α-tubulin at K304 is required for flagellar disassembly in Chlamydomonas. *Journal of Cell Science,* 132**,** jcs229047.

WEBSTER, D. R., GUNDERSEN, G. G., BULINSKI, J. C. & BORISY, G. G. 1987. Differential turnover of tyrosinated and detyrosinated microtubules. *Proceedings of the National Academy of Sciences,* 84**,** 9040-9044.

WEHLAND, J., WILLINGHAM, M. C. & SANDOVAL, I. V. 1983. A rat monoclonal antibody reacting specifically with the tyrosylated form of alpha-tubulin. I. Biochemical characterization, effects on microtubule polymerization in vitro, and microtubule polymerization and organization in vivo. *The Journal of cell biology,* 97**,** 1467-1475.

WEI, D., GAO, N., LI, L., ZHU, J.-X., DIAO, L., HUANG, J., HAN, Q.-J., WANG, S., XUE, H. & WANG, Q. 2018. α-Tubulin acetylation restricts axon overbranching by dampening microtubule plus-end dynamics in neurons. *Cerebral cortex,* 28**,** 3332-3346.

WILSON, P. J. & FORER, A. 1997. Effects of Nanomolar taxol on crane-fly spermatocyte spindles indicate that acetylation of kinetochore microtubules can be used as a marker of poleward tubulin flux. *Cell motility and the cytoskeleton,* 37**,** 20-32.

WLOGA, D., ROGOWSKI, K., SHARMA, N., VAN DIJK, J., JANKE, C., EDDÉ, B., BRÉ, M.-H., LEVILLIERS, N., REDEKER, V. & DUAN, J. 2008. Glutamylation on α-tubulin is not essential but affects the assembly and functions of a subset of microtubules in Tetrahymena thermophila. *Eukaryotic cell,* 7**,** 1362-1372.

WLOGA, D., WEBSTER, D. M., ROGOWSKI, K., BRÉ, M.-H., LEVILLIERS, N., JERKA-DZIADOSZ, M., JANKE, C., DOUGAN, S. T. & GAERTIG, J. 2009. TTLL3 Is a tubulin glycine ligase that regulates the assembly of cilia. *Developmental cell,* 16**,** 867-876.

WOLFF, A., DE NÉCHAUD, B., CHILLET, D., MAZARGUIL, H., DESBRUYÈRES, E., AUDEBERT, S., EDDÉ, B., GROS, F. & DENOULET, P. 1992. Distribution of glutamylated alpha and beta-tubulin in mouse tissues using a specific monoclonal antibody, GT335. *European journal of cell biology,* 59**,** 425-432.

WONG, C. C. L., XU, T., RAI, R., BAILEY, A. O., YATES 3RD, J. R., WOLF, Y. I., ZEBROSKI, H. & KASHINA, A. 2007. Global analysis of posttranslational protein arginylation. *PLoS biology,* 5**,** e258.

WONG, V. S., PICCI, C., SWIFT, M., LEVINSON, M., WILLIS, D. & LANGLEY, B. 2018. α-tubulin acetyltransferase is a novel target mediating neurite growth inhibitory effects of chondroitin sulfate proteoglycans and myelin-associated glycoprotein. *eneuro,* 5.

WOOLNER, S. & PAPALOPULU, N. 2012. Spindle position in symmetric cell divisions during epiboly is controlled by opposing and dynamic apicobasal forces. *Developmental cell,* 22**,** 775-787.

WU, H.-Y., WEI, P. & MORGAN, J. I. 2017. Role of cytosolic carboxypeptidase 5 in neuronal survival and spermatogenesis. *Scientific reports,* 7**,** 1-14.

XIA, L., HAI, B., GAO, Y., BURNETTE, D., THAZHATH, R., DUAN, J., BRÉ, M.-H., LEVILLIERS, N., GOROVSKY, M. A. & GAERTIG, J. 2000. Polyglycylation

of tubulin is essential and affects cell motility and division in Tetrahymena thermophila. *The Journal of cell biology,* 149**,** 1097-1106.

XIAO, H., EL BISSATI, K., VERDIER-PINARD, P., BURD, B., ZHANG, H., KIM, K., FISER, A., ANGELETTI, R. H. & WEISS, L. M. 2010. Post-translational modifications to Toxoplasma gondii α-and β-tubulins include novel C-terminal methylation. *Journal of proteome research,* 9**,** 359-372.

XIE, R., NGUYEN, S., MCKEEHAN, W. L. & LIU, L. 2010. Acetylated microtubules are required for fusion of autophagosomes with lysosomes. *BMC cell biology,* 11**,** 1-12.

XU, G., PAIGE, J. S. & JAFFREY, S. R. 2010. Global analysis of lysine ubiquitination by ubiquitin remnant immunoaffinity profiling. *Nature biotechnology,* 28**,** 868-873.

XU, Z., SCHAEDEL, L., PORTRAN, D., AGUILAR, A., GAILLARD, J., MARINKOVICH, M. P., THÉRY, M. & NACHURY, M. V. 2017. Microtubules acquire resistance from mechanical breakage through intralumenal acetylation. *Science,* 356**,** 328-332.

YAN, C., WANG, F., PENG, Y., WILLIAMS, C. R., JENKINS, B., WILDONGER, J., KIM, H.-J., PERR, J. B., VAUGHAN, J. C. & KERN, M. E. 2018. Microtubule acetylation is required for mechanosensation in Drosophila. *Cell reports,* 25**,** 1051-1065. e6.

YANG, Y., RAN, J., LIU, M., LI, D., LI, Y., SHI, X., MENG, D., PAN, J., OU, G. & ANEJA, R. 2014. CYLD mediates ciliogenesis in multiple organs by deubiquitinating Cep70 and inactivating HDAC6. *Cell research,* 24**,** 1342-1353.

YU, X., CHEN, X., AMRUTE-NAYAK, M., ALLGEYER, E., ZHAO, A., CHENOWETH, H., CLEMENT, M., HARRISON, J., DORETH, C. & SIRINAKIS, G. 2021. MARK4 controls ischaemic heart failure through microtubule detyrosination. *Nature,* 594**,** 560-565.

ZEMPEL, H., LUEDTKE, J., KUMAR, Y., BIERNAT, J., DAWSON, H., MANDELKOW, E. & MANDELKOW, E. M. 2013. Amyloid-β oligomers induce synaptic damage via Tau-dependent microtubule severing by TTLL6 and spastin. *The EMBO journal,* 32**,** 2920-2937.

ZHANG, Z. & CHEN, G. 2020. A logical relationship for schizophrenia, bipolar, and major depressive disorder. Part 1: Evidence from chromosome 1 high density association screen. *Journal of Comparative Neurology,* 528**,** 2620-2635.

ZHAO, T., GRAHAM, O. S., RAPOSO, A. & ST JOHNSTON, D. 2012. Growing microtubules push the oocyte nucleus to polarize the Drosophila dorsal-ventral axis. *Science,* 336**,** 999-1003.

ZHOU, X., FAN, L. X., LI, K., RAMCHANDRAN, R., CALVET, J. P. & LI, X. 2014. SIRT2 regulates ciliogenesis and contributes to abnormal centrosome amplification caused by loss of polycystin-1. *Human molecular genetics,* 23**,** 1644-1655.

ZIMYANIN, V. L., BELAYA, K., PECREAUX, J., GILCHRIST, M. J., CLARK, A., DAVIS, I. & ST JOHNSTON, D. 2008. In vivo imaging of oskar mRNA transport reveals the mechanism of posterior localization. *Cell,* 134**,** 843-853.

TABLES AND TABLE DESCRIPTIONS

Table 1.1. Other Posttranslational modifications of microtubules

Modification	**Site of modification**	**Function**	**Reference**
Arginylation	α- and β-tubulin	Proteasome dependent degradation	(Wong et al., 2007)
Glycosylation	α- and β-tubulin	Negatively regulate dimerization and incorporation into microtubule	(Walgren et al., 2003, Ji et al., 2011)
Palmitoylation	α- tubulin (C377)	Alters astral microtubule and nuclear positioning	(Caron, 1997, Ozols and Caron, 1997, Caron et al., 2001)
Sumoylation	α- tubulin		(Rosas-Acosta et al., 2005)
Ubiquitinylation	α- tubulin (K304)	Tubulin degradation, Flagellar disassembly	(Ren et al., 2003, Huang et al., 2009, Xu et al., 2010, Wang et al., 2019)

Table 1.2. Proteins that preferentially associate/dissociate with major microtubule PTMs

Modification	Proteins	Reference
Acetylation	PLK1 MAP1B Kinesin-1	(Rasamizafy et al., 2021) (Jenkins et al., 2017) (Balabanian et al., 2017, Kaul et al., 2014)
Glutamylation	KIF1A MAP2, KIF5	(Lessard et al., 2019) (Maas et al., 2009)
Detyrosination	CENP-E, Kinesin-1	(Barisic et al., 2015) (Tas et al., 2017, Guardia et al., 2016)
Tyrosination	CLIP-170, CLIP-115, p150 Glued Kinesin-3 Kinesin-5	(Peris et al., 2006) (Tas et al., 2017, Guardia et al., 2016) (Kahn et al., 2015)
Glycylation	Unknown	

FIGURES AND FIGURE LEGENDS

Figure 1.1. Major microtubule posttranslational modifications

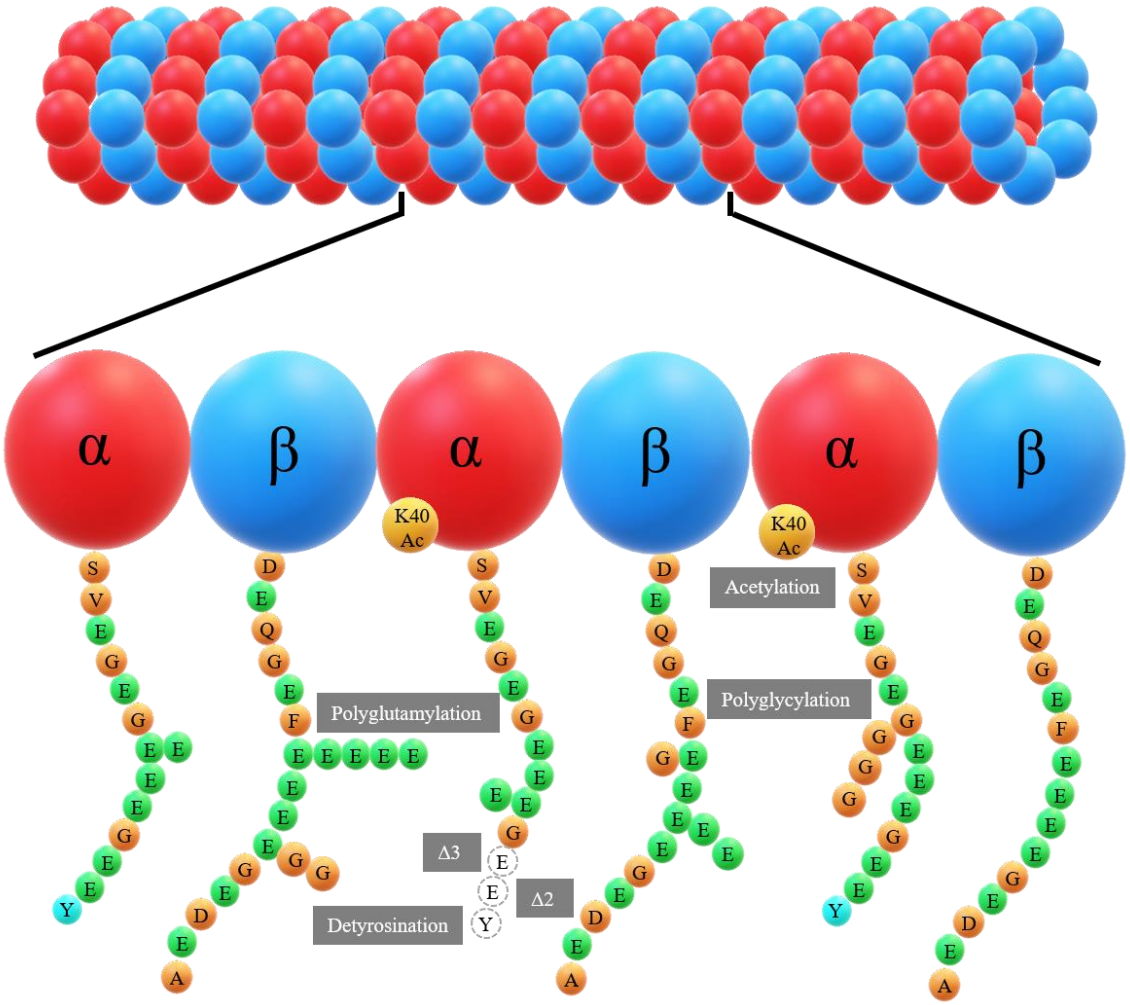
α
β
α
β
α
β
K40
Ac
K40
Ac
Acetylation
Polyglutamylation
Polyglycylation
Δ3
Δ2
Detyrosination

Figure 1.2. Enzymes of major microtubule posttranslational modifications

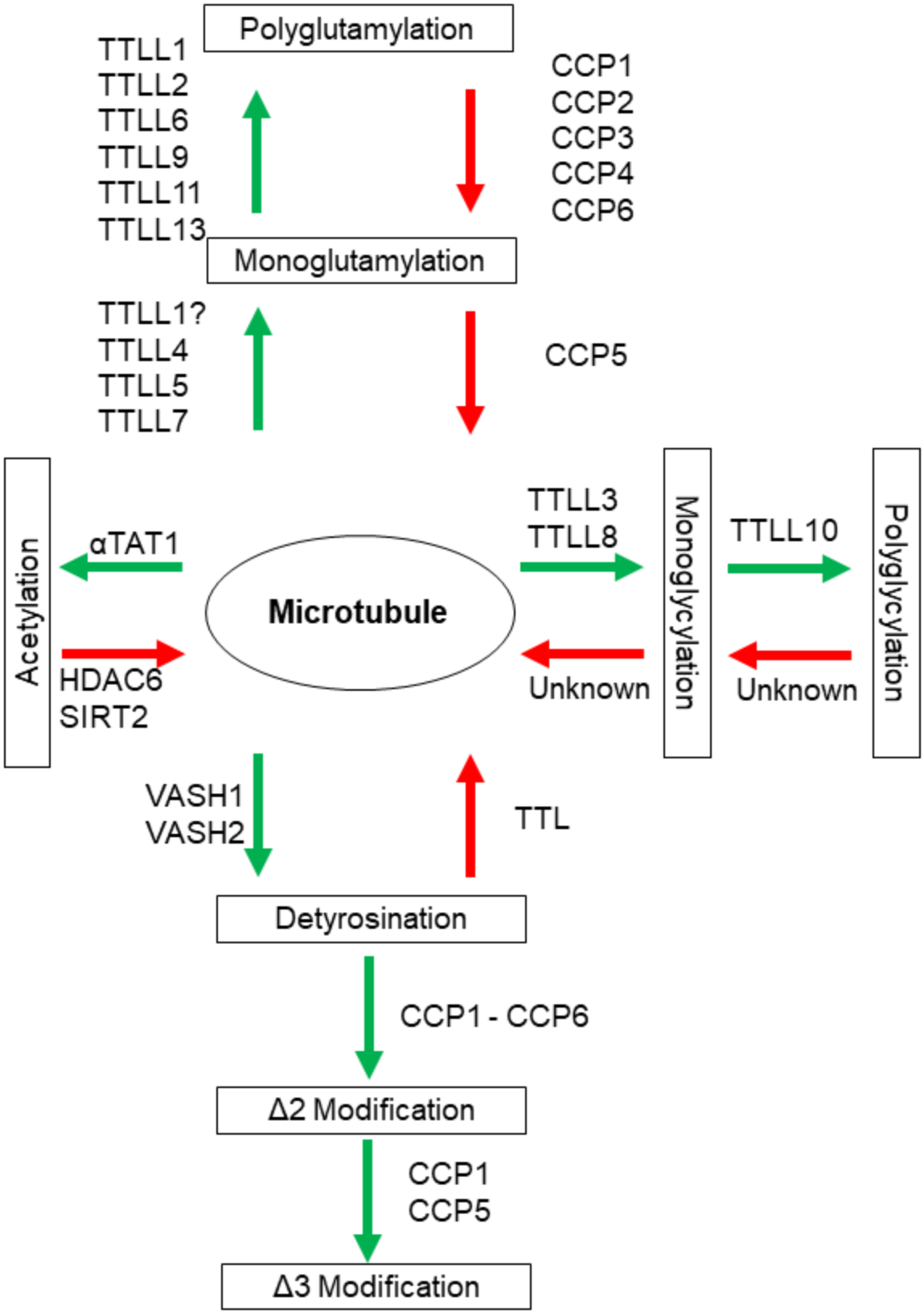
Polyglutamylation
TTLL1
TTLL2
TTLL6
TTLL9
TTLL11
TTLL13
CCP1
CCP2
CCP3
CCP4
CCP6
Monoglutamylation
TTLL1?
TTLL4
TTLL5
TTLL7
CCP5
Acetylation
αTAT1
HDAC6
SIRT2
Microtubule
TTLL3
TTLL8
Unknown
Monoglycylation
TTLL10
Unknown
Polyglycylation
VASH1
VASH2
TTL
Detyrosination
CCP1 - CCP6
Δ2 Modification
CCP1
CCP5
Δ3 Modification

SUPPLEMENTARY TABLES AND TABLE DESCRIPTIONS

Table S1.1. Major microtubule posttranslational modification-specific antibodies

Modification	Antibody	Reference
α-tubulin K40 acetylation	6-11-1B	(Piperno and Fuller, 1985)
Glutamylation	GT355	(Wolff et al., 1992)
	R-poly E (2304)	(Shang et al., 2002)
Glycylation	TAP952	(Callen et al., 1994)
	AXO49	(Callen et al., 1994)
	R-poly G (2302)	(Duan and Gorovsky, 2002)
Detyrosination	Glu antibody	(Gundersen et al., 1984)
	AA12	
Tyrosination	YL1/2	(Wehland et al., 1983)

CHAPTER 2

MICROTUBULE POSTTRANSLATIONAL MODIFICATIONS ARE REQUIRED TO BREAK SYMMETRY DURING ZEBRAFISH OOGENESIS[1]

[1] Amirthagunanathan S., Tseng WC., Grant MK., Gaertig J., and Dougan ST. To be submitted to Developmental Biology

ABSTRACT

Microtubules play important roles in axis determination during embryonic development. Animal-vegetal (AV) axis formation occurs during oogenesis, and the presence of the Balbiani body determines the future vegetal pole. Initial symmetry breaking of the AV axis coincides with the chromosomal bouquet formation during the zygotene stage of meiosis I. A zygotene stage transient cilia play an important role in forming the chromosomal bouquet. These cilia are enriched in microtubule posttranslational modifications (PTMs)- acetylation and glycylation. In our study, we found that female mutant that lacks both microtubule acetylation and glycylation showed defects in chromosomal bouquet formation. Altered chromosomal bouquet configuration leads to reduced female fecundity and fertility due to cell death. The loss of these modifications did not affect the ciliogenesis of zygotene cilia. Our data show microtubule acetylation and glycylation play a critical role in zygotene cilia function.

INTRODUCTION

Microtubules play important roles in many tightly regulated events during embryonic development. Like in other vertebrates, microtubules are important for body axis formation. Establishing the animal-vegetal axis is the initial asymmetry generated during development. Animal-vegetal axis is established during the oogenesis, with the vegetal pole defined by the presence of the Balbiani body. The Balbiani body is an aggregate of proteins, mRNA, and organelles that specifies the vegetal pole during zebrafish oogenesis

(Billett and Adam, 1976, Guraya, 1979, Marlow and Mullins, 2008). The Balbiani body is present in many other vertebrates (Billett and Adam, 1976, Pepling et al., 2007, Marlow, 2010). In zebrafish, initial precursors of the Balbiani body are present during the zygotene stage of prophase I. Mature Balbiani body forms during the diplotene stage (Elkouby et al., 2016).

The chromosomal bouquet is a chromosomal arrangement that occurs during prophase I, where telomeres aggregate in one pole of the nuclear envelope and subtelomeric regions loop in the opposite direction. It is a conserved structure in eukaryotes (Scherthan, 2001). The formation of the chromosomal bouquet is the initial symmetry-breaking event during zebrafish oogenesis. Balbiani body precursors localize adjacent to the nuclear pole, where telomere aggregation occurs during the bouquet formation. Pharmacological disruption of microtubules alters both the chromosol bouquet formation and localization of Balbiani body precursors (Elkouby et al., 2016). Telomeres interact with inner and out nuclear membrane protein complex SUN-KASH through telomere binding protein TERB1 (Shibuya and Watanabe, 2014). These telomeres are pulled towards the pole where the centrosome is present. Telomere-associated SUN-KASH complex driven by Dynein-dynactin complex through perinuclear microtubules originates from the centrosome (Shibuya et al., 2014).

A novel non-motile cilium associated with chromosomal bouquet formation in zebrafish was recently identified at the zygotene stage of prophase I. This zygotene cilium plays a role in anchoring the centrosome of the bouquet. Loss of this cilia by genetic approaches and laser excision showed its importance in bouquet formation by anchoring the centrosome and facilitating the movement of telomeres toward the centrosome. This

cilium is enriched in acetylated and glutamylated microtubules (Mytlis et al., 2022a). Ciliary structures are also enriched in glycylated tubulin (Levilliers et al., 1995). Microtubule acetylation of Lysine 40 residue of α-tubulin is carried out by α-tubulin acetyltransferase I (ATAT1) (LeDizet and Piperno, 1987, Akella et al., 2010, Shida et al., 2010). Microtubule acetylation is enriched in neurons and ciliated structures (Cambray-Deakin and Burgoyne, 1987, Gaertig et al., 1995, Akella et al., 2010). Microtubule acetylation plays a role during cilia biogenesis and maintenance (Akella et al., 2010, Shida et al., 2010, Kalebic et al., 2013, Rao et al., 2014). Microtubule glycylation is a modification that occurs in the c-terminal tail of both α- and β-tubulin (Redeker et al., 1994, Levilliers et al., 1995). Microtubule glycylation is initiated by TTLL3 and TTLL8 by adding the first glycine and elongated by TTLL10 (Rogowski et al., 2009, Wloga et al., 2009). Microtubule glycylation has been shown to play a role in normal ciliary structure and functions (Wloga et al., 2009, Pathak et al., 2011, Bosch Grau et al., 2013, Rocha et al., 2014, Bosch Grau et al., 2017, Gadadhar et al., 2017, Gadadhar et al., 2021). The reduction of acetylated tubulin in cilia increased the level of monoglycylated tubulin in zebrafish (Tseng, 2015, Łysyganicz et al., 2021). These modifications could play potential redundant roles in ciliary functions.

In this study, we used a genetic approach to study the role of microtubule posttranslational modifications in ciliary biogenesis and functions in zebrafish. We show that female double mutants of *atat1* and *ttll3* genes show defects in fecundity and fertility. These modifications are enriched in zygotene cilia that play an essential role in chromosomal bouquet formation during oogenesis. Our data show that even though the zygotene cilia are established normally, chromosomal bouquet configuration is altered in

atat1 and *ttll3* double mutants. Our result indicates a potential role of microtubule acetylation and glycylation in the normal function of zygotene cilia.

MATERIAL AND METHODS

Zebrafish Maintenance, Embryo Collection, and Adult Tissue Collection

Zebrafish lines were maintained in Paul D. Coverdell Biomedical Center fish facility in accordance with the Animal Use Protocols (AUPs) A2014 07-005-Y3-A6, A2017 08-020-Y3-A0 and A2020 08-002-Y1-A0, approved by the Institutional Animal Care and Use Committee (IACUC) of the University of Georgia. Embryos were collected using single or multiple-pair mating and maintained at 28.5 ^{o}C in egg water (60 µg/ml Instant Ocean sea salt and 0.3 µg/ml Methylene Blue). Embryos used in experimental procedures were treated with 1-phenyl 2-thiourea for optical clarity. Embryos were staged using a Leica S6E stereomicroscope (Leica Microsystems, Germany) as previously described (Kimmel et al., 1995). Appropriately aged fishes were euthanized for adult tissue collection by rapid chilling in ice water.

gRNA design and cloning

A sequence (5’-TGGCAATCGCCGCTCCACCC-3') located within the *ttll3* exon 4 was identified as a target for gRNA designing. The target sequence was amplified using two DNA oligonucleotides (Forward: 5'- TAGGGTGGAGCGGCGATTGCCA-3' and Reverse: 5'- AAACTGGCAATCGCCGCTCCAC-3') and cloned to pT7-gRNA plasmid as previously described (Jao et al., 2013).

gRNA synthesis and microinjection

gRNA was synthesized with 1 µg of linearized plasmid using a MEGAshortscript™ T7 transcription kit (Life Technologies, Carlsbad, CA). Capped *cas9* mRNA synthesis was performed with 1 µg of linearized pCS2+-nls-zCas9-nls plasmid using an mMESSAGE mMACHINE™ SP6 transcription kit (AM1340, Life Technologies, Carlsbad, CA). Microinjection was carried out as a mixture of 150 pg *cas9* mRNA, 100 pg of gRNA, 0.1 M KCl, and 0.1 % phenol red. This mixture was injected into 1-cell stage wild-type zebrafish embryos. Unfertilized eggs and dead embryos were discarded around 5hpf.

Screening of Mutants

Twelve gRNA and Cas9 mRNA injected adult fishes (F_0) were outcrossed to wild-type fishes to obtain F1 embryos with germline transmitted mutant alleles. Adult F1 fishes were screened for mutant alleles with T7 Endonuclease 1 (T7E1) assay using fin-clip genomic DNA. Potential mutant alleles identified by the T7E1 assay were confirmed with DNA sequencing (Georgia Genomics and Bioinformatics Core, Athens, GA). F1 fishes with the same mutant alleles were crossed to generate F2 generation. Adult F2 fishes were genotyped, and mutant fishes were identified to establish a mutant fish line.

Genomic DNA Extraction

Genomic DNA extraction was performed with either 72hpf larva or fin clips from adult fishes. Samples were initially incubated with DNA extraction buffer (10 mM Tris pH 8.2, 10 mM EDTA, 200 mM NaCl, and 0.5% SDS) at 95 ^{o}C for 20 minutes before the addition of 200 µg/ ml proteinase K. This step was followed by incubation at 55 ^{o}C for

3-16 hours. Finally, proteinase K activity was terminated with incubation at 95 ^{o}C for 20 minutes. Extracted DNA was stored at -20 ^{o}C and diluted 25 times before use as a template in PCR reactions.

T7 Endonuclease 1 (T7E1) assay

PCR reaction was carried out to amplify a region of 267 bp that includes that gRNA with forward primer 5'-TTGTGTCGATCATGCTGTAGG-3' and reverse primer 5'-CAGGGAATAGCCAACAATCC-3'. PCR amplification condition used as given below. Initial denaturation: 94^{o}C for 2 minutes, 35 cycles of denaturation: 94^{o}C for 20 seconds, annealing: 51^{o}C for 20 seconds, extension: 72^{o}C for 30 seconds and final extension: 72^{o}C for 5 minutes. PCR products were T7 Endonuclease 1 (New England Biolabs, Ipswich, MA) at 37 ^{o}C for 2 hours following an initial denaturation at 95 ^{o}C for 10 minutes and annealing from 95 ^{o}C-85 ^{o}C at the rate of -2 ^{o}C/s and 85 ^{o}C-25 ^{o}C at the rate of -0.1 ^{o}C/s. T7E1 digested products were resolved on 2% agarose gel.

Genotyping

Genotyping of the *atat1* mutant allele was carried out with PCR using TALENTEST3F (5'-CATTGATAAGACCGCTACTACA-3') and TALENTEST3F (5'-GTGCATGTAGCGAACCAGAT-3') under following PCR conditions and digestion with *BsmI* (New England Biolabs, Ipswich, MA). Initial denaturation: 94^{o}C for 2 minutes, denaturation: 94^{o}C for 20 seconds, annealing: 57^{o}C for 20 seconds, extension: 72^{o}C for 30 seconds for 35 cycles and final extension: 72^{o}C for 5 minutes. Genotyping of *ttll3* mutant alleles were genotyped with PCR using forward primer *ttll3*-geno-F (5'-

TCTGTGGTTTCAGTTTCATGGT-3') and reverse primer *ttll3*-geno R (5'-AAGGCCCGTATCCTGTGA-3') under the PCR condition as given below. Initial denaturation: 94^{o}C for 2 minutes, denaturation: 94^{o}C for 20 seconds, annealing: 51^{o}C for 20 seconds, extension: 72^{o}C for 30 seconds for 35 cycles and final extension: 72^{o}C for 5 minutes. PCR products were resolved on 15% polyacrylamide gel (VanLeuven et al., 2018).

Total RNA extraction

Total RNA extraction was performed with embryos, larva, and adult tissues. Total RNA was extracted by homogenizing the samples with TRIzol reagent (Life Technologies, Carlsbad, CA), followed by chloroform extraction and total RNA precipitation with isopropanol. Extracted total RNA preparation was treated with DNAase to eliminate any genomic DNA extraction with TURBO DNA-*free* Kit (Life Technologies, Carlsbad, CA). Total RNA was quantified using NanoDrop 2000 (Thermo Scientific, Waltham, MA) and stored at -80 ^{o}C.

Reverse Transcriptase PCR

First-strand cDNA was synthesized using a RevertAid First Strand cDNA synthesis kit (Thermo Scientific, Waltham, MA) per the manufacturer's instruction. 500 ng of total RNA was used as the template for first-strand cDNA synthesis. PCR reactions were carried out with 1 µl of first-strand cDNA. The level of *ttll3* transcripts was determined using forward primer *ttll3*cDNA F (5'- TGTGGTTCTACCGTGAGTGC -3') and reverse primer *ttll3*cDNA R (5'- AGCGAGGACTTGTGATTGGT -3'). The *gadph* gene was used

as a control. zGADPH long F (5'- CGTCTGGTGACCCGTGCTGC -3') and zGADPH long R (5'-TGGGGGTGGGGACACGGAAG-3') used for the PCR amplification. RT-PCR was carried out with PCR conditions as follows: initial denaturation- 94^{o}C for 2 minutes, 35cycles of denaturation- 94^{o}C for 20 seconds, annealing- 51^{o}C for 20 seconds, extension- 72^{o}C for 30 seconds and final extension: 72^{o}C for 5 minutes. Amplified PCR products were resolved on 2% agarose gel.

Immunofluorescence

Zebrafish embryos, larvae, and ovaries were fixed with fresh 4% paraformaldehyde in PBT (1x PBS, 0.5% Triton X-100) overnight. Fixed specimens were gradually dehydrated and stored in 100% methanol at -20 ^{o}C until the use. Specimens were gradually rehydrated and washed with PBT before being blocked for 2 hours in blocking reagent (2% Bovine Serum Albumin, 1% DMSO, 0.5% Triton X-100, 0.5% Normal Goat Serum in 1X PBS). Specimens were incubated with primary antibodies and secondary antibodies in blocking reagent overnight at 4 ^{o}C. Primary antibodies used were mouse monoclonal anti-monoglycylated tubulin antibody TAP952 (1:1000), mouse monoclonal anti-monoglutamylated tubulin GT355 (1:500), and mouse monoclonal anti-acetylated tubulin 6-11-1B (1:500). FITC conjugated anti-mouse IgG (1:500) was used as secondary antibodies.

Western blots

Protein extraction was carried out by homogenization and incubation of deyolked larvae and adult tissues with Lysis buffer (RIPA buffer (Sigma-Aldrich, St. Louis, MO), NaF,

Na3VO4, Protease inhibitor) followed by centrifugation to removed cell debris. Isolated protein concentration was determined using the manufacturer's protocol by the Pierce BCA Protein Assay kit (Thermo Scientific, Waltham, MA). SDS-PAGE was carried out on 4%-20% precast gel (Bio-Rad Laboratories, Hercules, CA) with 10 µg of total protein of each sample. Resolved proteins were transferred to the Hybond-P PVDF membrane (GE Healthcare, Piscataway, NJ). Membranes were incubated at 4 ^{o}C overnight with primary antibodies at dilutions as follows: mouse monoclonal anti-monoglycylated tubulin antibody TAP952 (1:2000), Rabbit polyclonal Poly G antibody R2302 (1:1000),: mouse monoclonal anti-monoglutamylated tubulin antibody GT335 (1:1000), Rabbit polyclonal Poly E antibody R2304 (1:1000) and mouse monoclonal anti-acetylated tubulin 6-11-1B (1:1000). Primary antibody incubation followed by incubation with either HRP-conjugated anti-mouse IgG or HRP-conjugated anti-rabbit IgG secondary antibody at 4 ^{o}C overnight. Following secondary antibody incubation, blots were treated with Clarity Western ECL substrate (Bio-Rad Laboratories, Hercules, CA) and detected X-OMAT LS films (Carestream, Rochester, NY).

Longevity assay

Longevity studies for atat1 and ttll3 mutants were carried out with mutant and heterozygous fishes obtained by crossing heterozygous fishes. Fishes were genotyped at three months and kept in separate adjacent tanks. The number of fish in each tank was counted weekly. The number of fishes in mutant and control tanks was maintained by adding Long Fin (TL) fishes.

NMDi14 treatment

Nonsense-mediated mRNA decay was inhibited by treating 8hpf embryos with 5μM NMDi14. DMSO was used as the vehicle. Embryos were observed under a dissecting microscope for any phenotypes at 24hpf, 48hpf, and 72hpf.

Fertility assay

Fertility assays were carried out by crossing four to six months old male or female sibling fishes of desired genotypes with wild-type female or male fishes as a single cross. Eggs were collected 20 minutes after collecting, and the total number of laid eggs was counted. After two hours number of unfertilized eggs was counted and removed.

TUNEL assay

Cell Death in ovaries was analyzed with DeadEnd™ Fluorometric TUNEL System (Promega, Madison, Wisconsin). Ovaries collected from 6-8 week old females were fixed in 4% PFA at 4°C overnight. Fixed ovaries were dehydrated gradually with a series of methanol and stored in 100% Methanol at -20°C. Ovaries were rehydrated with a methanol series and washed twice with 1X PBS. Ovaries were permeabilized with 20μg/ml of Proteinase K (in 1X PBS at room temperature for 5 minutes. Permeabilized ovaries were fixed with 4%PFA for 20min at room temperature to inactivate Proteinase K. Then ovaries were analyzed for cell death using Manufacture's protocol and counterstained with DAPI (1:2000).

DNA-FISH assay

TelC-Cy3 DNA probe (PNA Bio, Newbury Park, CA) was used for Telomere DNA-FISH using a previously reported protocol (Elkouby et al., 2016, Elkouby and Mullins, 2017).

Sperm motility assay

Testes of 6 months old adult zebrafish males were dissected and transferred to sperm extender buffer (10 mM HEPES, 80 mM KCl, 45 mM NaCl, 45 mM $C_2H_3NaO_2$, 0.4 mM $CaCl_2$, and 0.2 mM $MgCl_2$) and maintained at 4^oC. Testes were crushed just before the experiment, and 1 µl of the extract was mixed with 9 µl of prewarmed sterile water, transferred to a prewarmed slide, and coverslipped. Sperm motility was recorded under bright field conditions at 60 frames/second. Sperm motility was analyzed using the ImageJ MT Tracker plugin.

RESULTS

Monoglycylated tubulin enriched in ciliated tissues in zebrafish embryos

To understand the spatial enrichment of microtubule glycylation during zebrafish embryonic development, we carried out wholemount immunofluorescence with an antibody specific for monoglycylated tubulin. In *Danio rerio*, monoglycylated microtubules are enriched in ciliated structures. At 24 hpf, monoglycylated microtubules are present in pronephros but not in any other ciliated structure (Data not shown). By 48 hpf, monoglycylated microtubules are enriched in the olfactory placode (Figure 2.1A),

otic vesicle (Figure 2.1B), pronephros (Figure 2.1C), ependymal cilia (Figure 2.1D), and hair cells of lateral line system (Data not shown). Enrichment of monoglycylated microtubules in ciliary structures in multiple tissues suggests a potential role of this modification in the assembly and maintenance of cilia, thereby playing an important role in cilia biogenesis and function. During development, *ttll3* is expressed maternally, and zygotic expression of the gene is observed by 24 hpf (Figure S2.1). *ttll3* is expressed in the adult brain, testes, ovary, kidney, heart, gut, and liver tissues (Figure S2.2).

Generation of *ttll3* mutant using CRISPR/Cas9 mutagenesis

To study the roles of microtubule glycylation, we generated null mutants of *ttll3.* To generate *ttll3* mutant, we targeted exon 4 of the *ttll3* gene with CRISPR sgRNAs (Figure 2.2A). We generated two alleles of the *ttll3* gene, a two bp deletion allele (*ttll3*^{ga231}) and a four bp insertion allele (*ttll3*^{ga232}) (Figure S2.2A). Both alleles are frameshift mutation and result in premature stop codons leading to truncated proteins with altered amino acid sequences downstream of the target sites (Figure 2.2B). All the alleles were confirmed to be null alleles with immunofluorescence and western blotting (Figure 2.3C and Figure S2.2A).

Further analyses were carried out with *ttll3*^{ga232} alleles. *ttll3* mutants did not exhibit any obvious phenotype during embryonic development and were viable (Figure 2.3A). Mutants showed comparable growth to sibling heterozygous fishes (Figure S2.5D & S2.5E). Males of *ttll3* mutants showed subfertility compared to wild-type siblings (Figure S2.7), and females exhibited normal fertility (Data not shown). *ttll3* mutants showed reduced longevity compared to heterozygous siblings (Figure S2.6B).

Knockdown of *ttll3* by morpholino resulted in ciliary defects during zebrafish embryogenesis (Wloga et al., 2009, Pathak et al., 2011). In contrast, *ttll3* mutants did not exhibit ciliary defects like curved body axis, hydrocephalous, or kidney cyst, as reported with morphants (Figure 2.3A). Typical olfactory cilia were seen in *ttll3* mutant, confirming normal cilia biogenesis and maintenance (Figure 2.3B).

Deleterious mutation of genes could lead to nonsense-mediated mRNA decay (NMD) driven transcriptional adaptation to minimize the effect of the mutation (El-Brolosy et al., 2019). To test whether NMD-mediated genetic compensation occurs in our mutants, we treated the *ttll3* mutant with an NMD inhibitor. No obvious phenotypes were seen when the mutant was treated with NMD inhibitor NMDi14, confirming that the absence of phenotype in the mutant is not an outcome of NMD-mediated genetic compensation (Figure S2.4).

The level of microtubule acetylation increased in *ttll3* mutants

Cilia are enriched in microtubule acetylation, detyrosination, glutamylation, glycylation, and other posttranslational modifications. Previous studies have shown alteration of one modification alters levels of other microtubule posttranslational modifications. Reduction in microtubule acetylation in zebrafish was shown to increase the level of monoglycylation in zebrafish (Tseng, 2015, Łysyganicz et al., 2021). Reduction in the levels of glycylation increases microtubule acetylation and glutamylation (Wloga et al., 2009, Rogowski et al., 2009). We examined the levels of different microtubule posttranslational modifications in adult testes of the mutant, which are rich in ciliary microtubules from sperm flagella, and found alterations in them. In *ttll3* mutants,

microtubule acetylation, mono-, and polyglutamylation levels have increased (Figure 2.4). Our data and previous reports show a reciprocal increase in microtubule glycylation and acetylation in *atat* and *ttll3* mutants. This result suggests that the increased acetylation in our mutants could functionally compensate for the loss of glycylation. To test this, we generated a double mutant of *atat1* and *ttll3* mutants.

We used a previously reported *atat1*^{ga4} mutant to generate the double mutant (Tseng, 2015). Unlike previous reports on zebrafish *atat1* morphants (Akella et al., 2010), the *atat1* mutant did not exhibit any obvious phenotype during embryonic development and was viable (Data not shown). Mutant embryos showed no apparent phenotypes when treated with NMD inhibitor NMDi14 (Figure S2.4). This mutant showed comparable growth to sibling heterozygous fishes (Figure S2.5B & S2.5C). Interestingly, like *ttll3* mutants, this *atat1* mutant also showed reduced longevity compared to heterozygous siblings (Figure S2.6A).

We crossed double heterozygous of *atat* and *ttll3* mutant alleles. We did not see any embryos with obvious phenotypes, and double mutants were viable. We observed the presence of olfactory cilia in double heterozygous, single mutants, and double mutants of these genes, confirming normal ciliary establishment and maintenance. Interestingly, *atat1*; *ttll3* double mutant females showed fertility problems and rarely laid eggs. None of the maternal and zygotic double mutants survived into adulthood.

Loss of microtubule acetylation and glycylation affects female fecundity

To understand the roles of these modifications on female fertility, we crossed four to six months old fishes with wild-type males and counted the number of eggs laid and the

number of unfertilized eggs. Double mutant female fishes laid significantly fewer eggs than double heterozygous and single mutant siblings when they were crossed with wild-type males (p value<0.05, One-way ANOVA with Tukey's test) (Figure 2.5A). On average *atat1*$^{+/-}$*; ttll3*$^{+/-}$, *atat1*$^{-/-}$*; ttll3*$^{+/+}$, and *atat1*$^{+/+}$*; ttll3*$^{-/-}$fishes laid 88.09 (11 crosses), 73.5 (6 crosses), and 72.71 (7 crosses) eggs, respectively, compared to 12.6 (10 crosses) eggs laid by *atat1*$^{-/-}$*; ttll3*$^{-/-}$ fishes. Double mutant female fishes also laid a significantly higher unfertile egg when crossed with wild-type males (p value<0.05, One-way ANOVA with Tukey's test) than other genotypes (Figure 2.5B). It indicates the subfertility of *atat1*$^{-/-}$*; ttll3*$^{-/-}$ females compared to double heterozygous and single mutants. Zebrafish ciliary gene mutants result in reduced female fertility due to p53-mediated apoptosis (Mytlis et al., 2022b, Xie et al., 2022). To test the occurrence of apoptosis, we performed TUNEL assay in ovaries of 6-8 wpf *atat1*$^{+/-}$*; ttll3*$^{+/-}$, *atat1*$^{-/-}$*; ttll3*$^{+/+}$, and *atat1*$^{+/+}$*; ttll3*$^{-/-}$ and *atat1*$^{-/-}$*; ttll3*$^{-/-}$ fishes. Ovaries of double mutant fishes (n=3) showed increased TUNEL positive puncta compared to ovaries of double heterozygous and single mutants (Figure 2.5C). This data indicates that increased cell death of oocytes causes the reduced fecundity in the double mutant.

Microtubule acetylation and glycylation are enriched in the early stages of oocytes

To understand the role of microtubule acetylation and glycylation during oogenesis, we studied the expression of *atat1* and *ttll3* genes in wild-type ovaries and the enrichment of acetylated and glycylated microtubules during oogenesis. RT-PCR of total RNA extracted from various tissues showed that both genes were expressed in wild-type zebrafish ovaries (Figure S2.1B). To check the enrichment of microtubule acetylation and

glycylation, we extracted protein from manually separated stage I, stage II, and stage III oocytes from wild-type ovaries and carried out western blotting. Both stage I and stage II oocytes showed acetylated and monoglycylated microtubule enrichment, and both modifications were absent in stage III oocytes (Figure 2.6A). Interestingly, we also observed a reduction in levels of α-tubulin in stage III oocytes, even though total protein amounts were the same for all three stages (Figure 2.6A). This reduction could be potentially due to the accumulation of yolk proteins. Wholemount immunofluorescence of ovaries from 6-7 week-old fishes showed cilia-like structures enriched in microtubule acetylation and monoglycylation (Figure 2.6B), consistent with previously published results demonstrating the presence of cilia at this stage (Mytlis et al., 2022b).

Loss of both microtubule acetylation and monoglycylation results in expansion of chromosomal bouquet configuration

Loss of zygotene cilium in ciliary mutants in zebrafish has been shown to affect the chromosomal bouquet formation during the zygotene stage of meiosis (Mytlis et al., 2022b). To understand whether chromosomal bouquet is affected in our mutants, we carried out DNA in situ hybridization of telomere with telo-cy3 probe (PNA Bio). Double mutant female fishes showed significant expansion of chromosomal bouquets compared to double heterozygous and single mutants (Figure 2.7A). On average chromosomal bouquet of *atat1*$^{+/-}$*; ttll3*$^{+/-}$, *atat1*$^{-/-}$*; ttll3*$^{+/+}$, and *atat1*$^{+/+}$*; ttll3*$^{-/-}$ oocytes showed an average angle of chromosomal bouquet to the center of 77.62 (n=165), 81.81 (n=61), and 79.57 (n=65), respectively, compared to110.51 (n=138) of *atat1*$^{-/-}$*; ttll3*$^{-/-}$ chromosomal bouquet (Figure 2.7B). Oocytes of different genotypes were confirmed to be in the same

stage with the diameter of the nucleus (Figure 2.7C). This data indicates that loss of microtubule posttranslational modifications acetylation and glycylation result in chromosomal bouquet configuration defects similar to that reported in ciliary mutants.

Loss of both microtubule acetylation and monoglycylation does not affect zygotene cilia establishment and maintenance

To test whether the zygotene cilia are affected, we carried out wholemount immunofluorescence of ovaries from 6-8 wpf old fishes with an antibody that labels monoglutamylated tubulins. We found cilia-like structures present in ovaries of *atat1*$^{+/-}$*; ttll3*$^{+/-}$, *atat1*$^{-/-}$*; ttll3*$^{+/+}$, and *atat1*$^{+/+}$*; ttll3*$^{-/-}$ and *atat1*$^{-/-}$*; ttll3*$^{-/-}$ fishes (Figure 2.8A). We did not find any significant difference between the cilia length, indicating that loss of microtubule acetylation and glycylation has not affected the establishment and maintenance of the zygotene cilia as seen in the olfactory cilia during embryonic development (Figure 2.8B). On average, the length of cilia of ovaries from *atat1*$^{+/-}$*; ttll3*$^{+/-}$, *atat1*$^{-/-}$*; ttll3*$^{+/+}$, and *atat1*$^{+/+}$*; ttll3*$^{-/-}$ and *atat1*$^{-/-}$*; ttll3*$^{-/-}$ fishes were 6.57 μm (n=30), 6.40 μm (n=30), 6.02 μm (n=30), and 6.18 μm (n=30), respectively (Figure2.8B). Oocytes of different genotypes were confirmed to be in the same stage with the diameter of the nucleus (Figure 2.8C). Ciliary mutants that result in loss of or short zygotene cilia were shown to result in expanded and dispersed zygotene bouquet configurations confirming the functional importance of cilia in proper chromosomal bouquet formation (Mytlis et al., 2022b). In our study, we find that loss of microtubule acetylation and glycylation affect the function of these cilia without affecting the establishment and maintenance of the cilia.

DISCUSSION

Chromosomal bouquet formation during the zygotene stage of meiosis plays the initial symmetry-breaking role during animal-vegetal axis formation (Elkouby et al., 2016). Zygotene stage transient cilia are essential in proper chromosomal bouquet formation by anchoring the MTOC involved in bouquet formation (Mytlis et al., 2022b). Our study demonstrated that microtubule posttranslational modifications play an important role in proper chromosomal bouquet formation.

Previous works on morpholino-based depletion of *atat1* or *ttll3* showed ciliary defect phenotypes like curved body axis, kidney cyst, and hydrocephalous brain (Akella et al., 2010, Wloga et al., 2009, Pathak et al., 2011). Our study found that the *atat1* or *ttll3* single mutants were viable and did not show any apparent defects during embryonic development. To eliminate the role of NMD-mediated genetic compensation, we treated these mutants with an NMD inhibitor, and these single mutants did not phenocopy the morphants' phenotype. Interestingly, Both mutants showed reduced longevity, and *ttll3* males exhibited subfertility. In mouse *Atat1* mutant that lacks acetylation and *Ttll3 Ttll8* double mutant that lack glycylation did not show any severe ciliary phenotypes except sperm motility defects (Kalebic et al., 2013, Kim et al., 2013, Gadadhar et al., 2021). Our data on single mutants of these genes result in similar phenotypes.

In our study, *atat1;ttll3* double mutant females showed reduced female fecundity and fertility. They also showed increased apoptosis compared to double heterozygous and single mutants. A similar phenotype was reported in zebrafish *cep290* and *cep290;kif7* mutants (Mytlis et al., 2022b). These mutants lacked or had short zygotene cilium, which

was shown to anchor the centrosome involved in chromosomal bouquet formation. We found that the zygotene cilium was present in *atat1;ttll3* double mutants. We did not see any significant difference in length of cilia compared double heterozygous or single mutants. Loss of microtubule acetylation and monoglycylation has not affected the establishment and maintenance of this zygotene cilia. Even though *atat1;ttll3* double mutant has normal zygotene cilium, they phenocopy the shortening of cilium reported previously and indicating an essential functional role played by microtubule acetylation and glycylation in the formation of normal chromosomal bouquet.

The formation of chromosomal bouquet plays an important role in chromosomal pairing and homologous recombination (Harper et al., 2004). Mice mutant of SUN protein plays an essential role in chromosomal bouquet formation and shows impaired chromosomal pairing, synapsis, and homologous recombination (Ding et al., 2007). Defects in zygotene cilia in zebrafish spermatocytes alter double-strand break repair and cross-over during homologous recombination (Xie et al., 2022). Loss of zygotene cilia also affects the loading of synaptonemal complex protein, Sycp3, to chromosomes and the proper formation of synaptonemal complexes during oogenesis (Mytlis et al., 2022b). Mutants of proteins involved in the meiotic recombination show pachytene checkpoint-mediated arrest and cell death apoptosis during the gametogenesis (Di Giacomo et al., 2005, Roeder and Bailis, 2000). We presume that reduced fecundity caused by cell death was due to homologous recombination defects resulting from altered chromosomal bouquet formation. Further studies directly label synaptonemal complex proteins are needed to confirm the alteration in chromosomal pairing and homologous recombinations in *atat1;ttll3* double mutant.

Laser ablation of zygotene cilia results in dislocation of centrosome that involves the chromosomal bouquet formation and confirms its role as an anchor of the centrosome. It also affirms that perinuclear microtubules exert enormous force on centrosomes (Mytlis et al., 2022b). Loss of cilia in ciliary mutants shows that loss of anchoring results in expansion and dispersion of chromosomal bouquet. Even though zygotene cilia is still intact in *atat1;ttll3* double mutant, the chromosomal bouquet takes expanded configuration. Loss of microtubule acetylation and glycylation could alter the zygotene cilia's ability to anchor the centrosome efficiently. Microtubule posttranslational modifications are known to alter the physical properties of microtubules. Microtubule acetylation was shown to stabilize mechanically and minimize the occurrence of breakage under repeated mechanical stresses (Xu et al., 2017, Portran et al., 2017). Microtubule glycylation improves the stiffness and integrity of microtubules (Wall et al., 2020). There are no reports on the mechanical properties of microtubules with acetylation and glycylation compared to the loss of one or both modifications. Reciprocal increases in these modifications in *atat1* and *ttll3* mutants raise the possibility of redundant roles played by these two modifications. Loss of both modifications could result in a weaker anchoring that could result weaker pulling of telomere towards the centrosome. Further studies has to be conducted to study how loss of both microtubule acetylation and glycylation could alter physical properties of microtubule. Effects of lacking these modifications on the centrosome and migration of telomere towards the centrosome could be further studied with live imaging.

Our study demonstrates that microtubule posttranslational modifications acetylation and glycylation play a critical role in normal zygotene cilia function in chromosomal bouquet

formation. Loss of these modifications alters chromosomal bouquet formation and reduces female fecundity and fertility.

REFERENCES

AKELLA, J. S., WLOGA, D., KIM, J., STAROSTINA, N. G., LYONS-ABBOTT, S., MORRISSETTE, N. S., DOUGAN, S. T., KIPREOS, E. T. & GAERTIG, J. 2010. MEC-17 is an α-tubulin acetyltransferase. *Nature,* 467**,** 218-222.

BILLETT, F. & ADAM, E. 1976. The structure of the mitochondrial cloud of Xenopus laevis oocytes.

BOSCH GRAU, M., GONZALEZ CURTO, G., ROCHA, C., MAGIERA, M. M., MARQUES SOUSA, P., GIORDANO, T., SPASSKY, N. & JANKE, C. 2013. Tubulin glycylases and glutamylases have distinct functions in stabilization and motility of ependymal cilia. *Journal of Cell Biology,* 202**,** 441-451.

BOSCH GRAU, M., MASSON, C., GADADHAR, S., ROCHA, C., TORT, O., MARQUES SOUSA, P., VACHER, S., BIECHE, I. & JANKE, C. 2017. Alterations in the balance of tubulin glycylation and glutamylation in photoreceptors leads to retinal degeneration. *Journal of cell science,* 130**,** 938-949.

CAMBRAY-DEAKIN, M. A. & BURGOYNE, R. D. 1987. Posttranslational modifications of alpha-tubulin: acetylated and detyrosinated forms in axons of rat cerebellum. *The Journal of cell biology,* 104**,** 1569-1574.

DI GIACOMO, M., BARCHI, M., BAUDAT, F., EDELMANN, W., KEENEY, S. & JASIN, M. 2005. Distinct DNA-damage-dependent and-independent responses drive the loss of oocytes in recombination-defective mouse mutants. *Proceedings of the National Academy of Sciences,* 102**,** 737-742.

DING, X., XU, R., YU, J., XU, T., ZHUANG, Y. & HAN, M. 2007. SUN1 is required for telomere attachment to nuclear envelope and gametogenesis in mice. *Developmental cell,* 12**,** 863-872.

EL-BROLOSY, M. A., KONTARAKIS, Z., ROSSI, A., KUENNE, C., GÜNTHER, S., FUKUDA, N., KIKHI, K., BOEZIO, G. L., TAKACS, C. M. & LAI, S.-L. 2019. Genetic compensation triggered by mutant mRNA degradation. *Nature,* 568**,** 193-197.

ELKOUBY, Y. M., JAMIESON-LUCY, A. & MULLINS, M. C. 2016. Oocyte polarization is coupled to the chromosomal bouquet, a conserved polarized nuclear configuration in meiosis. *PLoS biology,* 14**,** e1002335.

ELKOUBY, Y. M. & MULLINS, M. C. 2017. Methods for the analysis of early oogenesis in Zebrafish. *Developmental biology,* 430**,** 310-324.

GADADHAR, S., ALVAREZ VIAR, G., HANSEN, J. N., GONG, A., KOSTAREV, A., IALY-RADIO, C., LEBOUCHER, S., WHITFIELD, M., ZIYYAT, A. & TOURÉ, A. 2021. Tubulin glycylation controls axonemal dynein activity, flagellar beat, and male fertility. *Science,* 371**,** eabd4914.

GADADHAR, S., DADI, H., BODAKUNTLA, S., SCHNITZLER, A., BIÈCHE, I., RUSCONI, F. & JANKE, C. 2017. Tubulin glycylation controls primary cilia length. *Journal of Cell Biology,* 216**,** 2701-2713.

GAERTIG, J., CRUZ, M. A., BOWEN, J., GU, L., PENNOCK, D. G. & GOROVSKY, M. A. 1995. Acetylation of lysine 40 in alpha-tubulin is not essential in Tetrahymena thermophila. *The Journal of Cell Biology,* 129**,** 1301-1310.

GURAYA, S. S. 1979. Recent advances in the morphology, cytochemistry, and function of Balbiani's vitelline body in animal oocytes. *International review of cytology,* 59**,** 249-321.

HARPER, L., GOLUBOVSKAYA, I. & CANDE, W. Z. 2004. A bouquet of chromosomes. *Journal of cell science,* 117**,** 4025-4032.

JAO, L.-E., WENTE, S. R. & CHEN, W. 2013. Efficient multiplex biallelic zebrafish genome editing using a CRISPR nuclease system. *Proceedings of the National Academy of Sciences,* 110**,** 13904-13909.

KALEBIC, N., SORRENTINO, S., PERLAS, E., BOLASCO, G., MARTINEZ, C. & HEPPENSTALL, P. A. 2013. αTAT1 is the major α-tubulin acetyltransferase in mice. *Nature communications,* 4**,** 1-10.

KIM, G.-W., LI, L., GORBANI, M., YOU, L. & YANG, X.-J. 2013. Mice lacking α-tubulin acetyltransferase 1 are viable but display α-tubulin acetylation deficiency and dentate gyrus distortion. *Journal of Biological Chemistry,* 288**,** 20334-20350.

KIMMEL, C. B., BALLARD, W. W., KIMMEL, S. R., ULLMANN, B. & SCHILLING, T. F. 1995. Stages of embryonic development of the zebrafish. *Developmental dynamics,* 203**,** 253-310.

LEDIZET, M. & PIPERNO, G. 1987. Identification of an acetylation site of Chlamydomonas alpha-tubulin. *Proceedings of the National Academy of Sciences,* 84**,** 5720-5724.

LEVILLIERS, N., FLEURY, A. & HILL, A.-M. 1995. Monoclonal and polyclonal antibodies detect a new type of posttranslational modification of axonemal tubulin. *Journal of Cell Science,* 108**,** 3013-3028.

ŁYSYGANICZ, P. K., POORANACHANDRAN, N., LIU, X., ADAMSON, K. I., ZIELONKA, K., ELWORTHY, S., VAN EEDEN, F. J., GRIERSON, A. J. & MALICKI, J. J. 2021. Loss of Deacetylation Enzymes Hdac6 and Sirt2 Promotes Acetylation of Cytoplasmic Tubulin, but Suppresses Axonemal Acetylation in Zebrafish Cilia. *Frontiers in Cell and Developmental Biology*, 9.

MARLOW, F. 2010. Oocyte polarity and the embryonic axes: the balbiani body, an ancient oocyte asymmetry. *Maternal Control of Development in Vertebrates: My Mother Made Me Do It***,** 1-6.

MARLOW, F. L. & MULLINS, M. C. 2008. Bucky ball functions in Balbiani body assembly and animal–vegetal polarity in the oocyte and follicle cell layer in zebrafish. *Developmental biology,* 321**,** 40-50.

MYTLIS, A., KUMAR, V., QIU, T., DEIS, R., HART, N., LEVY, K., MASEK, M., SHAWAHNY, A., AHMAD, A., EITAN, H., NATHER, F., ADAR-LEVOR, S., BIRNBAUM, R. Y., ELIA, N., BACHMANN-GAGESCU, R., ROY, S. & ELKOUBY, Y. M. 2022a. Control of meiotic chromosomal bouquet and germ cell morphogenesis by the zygotene cilium. *Science,* 0**,** eabh3104.

MYTLIS, A., KUMAR, V., TAO, Q., DEIS, R., HART, N., LEVY, K., MASEK, M., SHAWAHNY, A., AHMAD, A., EITAN, H., NATHER, F., ADAR-LEVOR, S., BIRNBAUM, R. Y., ELIA, N., BACHMANN-GAGESCU, R., ROY, S. & ELKOUBY, Y. M. 2022b. Biomechanical control of meiotic chromosomal bouquet and germ cell morphogenesis by the zygotene cilium. *bioRxiv***,** 2021.02.08.430249.

PATHAK, N., AUSTIN, C. A. & DRUMMOND, I. A. 2011. Tubulin tyrosine ligase-like genes ttll3 and ttll6 maintain zebrafish cilia structure and motility. *Journal of Biological Chemistry,* 286**,** 11685-11695.

PEPLING, M. E., WILHELM, J. E., O'HARA, A. L., GEPHARDT, G. W. & SPRADLING, A. C. 2007. Mouse oocytes within germ cell cysts and primordial follicles contain a Balbiani body. *Proceedings of the National Academy of Sciences,* 104**,** 187-192.

PORTRAN, D., SCHAEDEL, L., XU, Z., THÉRY, M. & NACHURY, M. V. 2017. Tubulin acetylation protects long-lived microtubules against mechanical ageing. *Nature cell biology,* 19**,** 391-398.

RAO, Y., HAO, R., WANG, B. & YAO, T.-P. 2014. A Mec17-Myosin II effector axis coordinates microtubule acetylation and actin dynamics to control primary cilium biogenesis. *PloS one,* 9**,** e114087.

REDEKER, V., LEVILLIERS, N., SCHMITTER, J.-M., LE CAER, J.-P., ROSSIER, J., ADOUTTE, A. & BRE, M.-H. 1994. Polyglycylation of tubulin: a posttranslational modification in axonemal microtubules. *Science,* 266**,** 1688-1691.

ROCHA, C., PAPON, L., CACHEUX, W., MARQUES SOUSA, P., LASCANO, V., TORT, O., GIORDANO, T., VACHER, S., LEMMERS, B. & MARIANI, P. 2014. Tubulin glycylases are required for primary cilia, control of cell proliferation and tumor development in colon. *The EMBO journal,* 33**,** 2247-2260.

ROEDER, G. S. & BAILIS, J. M. 2000. The pachytene checkpoint. *Trends in genetics,* 16**,** 395-403.

ROGOWSKI, K., JUGE, F., VAN DIJK, J., WLOGA, D., STRUB, J.-M., LEVILLIERS, N., THOMAS, D., BRÉ, M.-H., VAN DORSSELAER, A. & GAERTIG, J. 2009. Evolutionary divergence of enzymatic mechanisms for posttranslational polyglycylation. *Cell,* 137**,** 1076-1087.

SCHERTHAN, H. 2001. A bouquet makes ends meet. *Nature reviews Molecular cell biology,* 2**,** 621-627.

SHIBUYA, H., MORIMOTO, A. & WATANABE, Y. 2014. The dissection of meiotic chromosome movement in mice using an in vivo electroporation technique. *PLoS genetics,* 10**,** e1004821.

SHIBUYA, H. & WATANABE, Y. 2014. The meiosis-specific modification of mammalian telomeres. *Cell Cycle,* 13**,** 2024-2028.

SHIDA, T., CUEVA, J. G., XU, Z., GOODMAN, M. B. & NACHURY, M. V. 2010. The major α-tubulin K40 acetyltransferase αTAT1 promotes rapid ciliogenesis and efficient mechanosensation. *Proceedings of the National Academy of Sciences,* 107**,** 21517-21522.

TSENG, W. 2015. *Neural crest specification by Max's giant associated protein and regulation of microtubule's function by alpha-tubulin acetyltransferase 1 in zebrafish.* Doctor of Philosophy (PHD), University of Georgia.

VANLEUVEN, A. J., PARK, S., MENKE, D. B. & LAUDERDALE, J. D. 2018. A PAGE screening approach for identifying CRISPR-Cas9-induced mutations in zebrafish. *Biotechniques,* 64**,** 275-278.

WALL, K. P., HART, H., LEE, T., PAGE, C., HAWKINS, T. L. & HOUGH, L. E. 2020. C-terminal tail polyglycylation and polyglutamylation alter microtubule mechanical properties. *Biophysical journal,* 119**,** 2219-2230.

WLOGA, D., WEBSTER, D. M., ROGOWSKI, K., BRÉ, M.-H., LEVILLIERS, N., JERKA-DZIADOSZ, M., JANKE, C., DOUGAN, S. T. & GAERTIG, J. 2009. TTLL3 Is a tubulin glycine ligase that regulates the assembly of cilia. *Developmental cell,* 16**,** 867-876.

XIE, H., WANG, X., JIN, M., LI, L., ZHU, J., KANG, Y., CHEN, Z., SUN, Y. & ZHAO, C. 2022. Cilia regulate meiotic recombination in zebrafish. *bioRxiv***,** 2022.03.05.482955.

XU, Z., SCHAEDEL, L., PORTRAN, D., AGUILAR, A., GAILLARD, J., MARINKOVICH, M. P., THÉRY, M. & NACHURY, M. V. 2017. Microtubules acquire resistance from mechanical breakage through intralumenal acetylation. *Science,* 356**,** 328-332.

FIGURES AND FIGURE LEGENDS

Figure 2.1. The distribution of monoglycylated tubulin in 48hpf *Danio rerio* embryo. Wholemount immunofluorescence of 48hpf wild-type embryos with monoglycylated tubulin-specific TAP952 antibody. Monoglycylated tubulin is enriched in ciliated structures olfactory placode (A), otic vesicle (B), pronephros (C), and ependymal cilia (D).

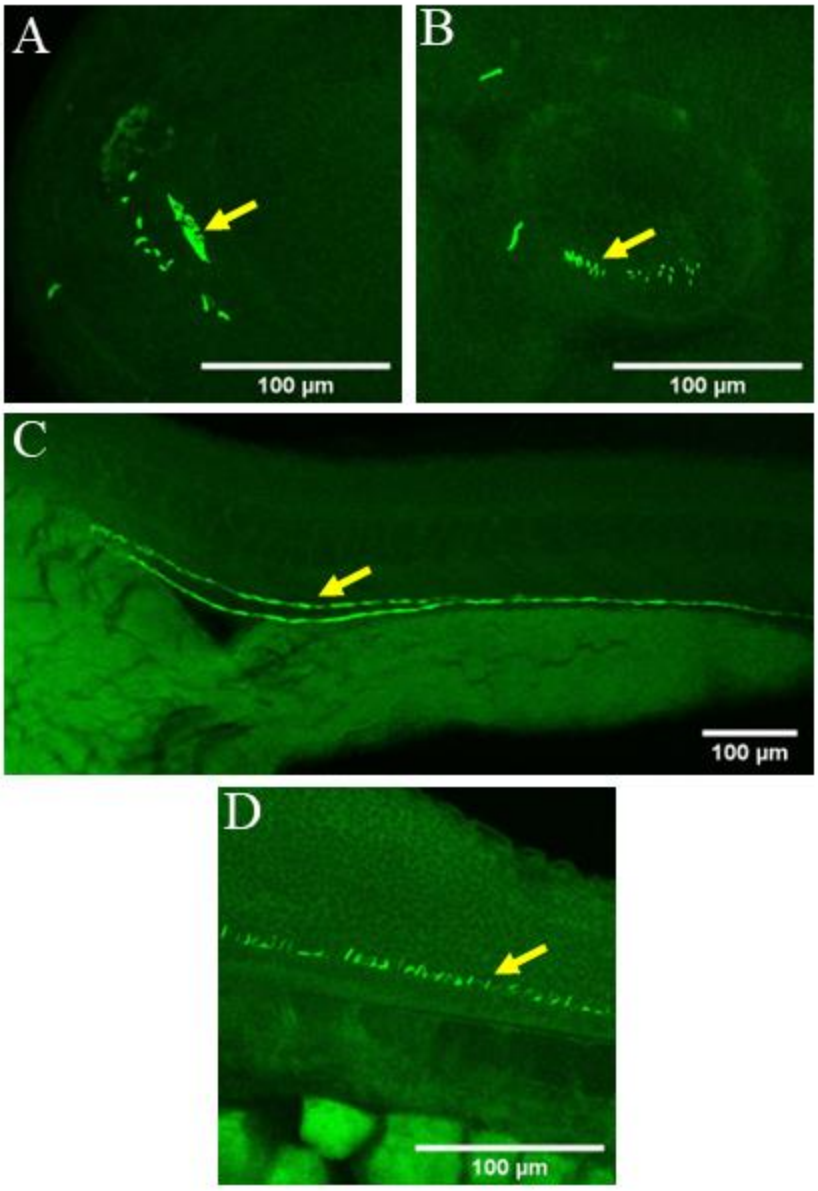
A
100 µm
B
100 µm
C
100 µm
D
100 µm

Figure 2.2. Generation of *ttll3* mutant zebrafish lines using CRISPR/Cas9 mediated mutagenesis. (A). Schematic representation of *ttll3* gene and TTLL3 protein. Red arrows represent the gRNA target sites. (B). Two mutant alleles, $ttll3^{ga231}$ (2 nucleotide deletion) and $ttll3^{ga232}$ (4 nucleotide insertion) were identified in F1 screening. (C). Both alleles were confirmed null alleles with wholemount immunofluorescence with monoglycylated tubulin-specific TAP952 antibody. Red arrow: olfactory placode and yellow arrow: pronephros.

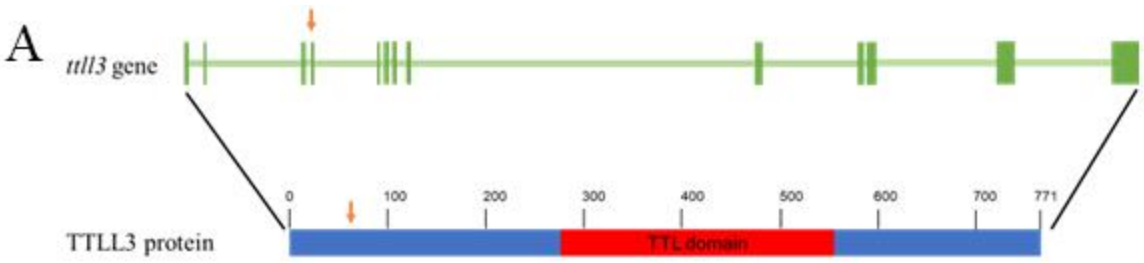
A
ttll3 gene
0
100
200
300
400
500
600
700
771
TTLL3 protein
TTL domain


B
5′ TGGCAATCGCCGCTCCACCC 3′
ttll3wt
CGAGGCTGTGAGAAAGAGGGCCTTGGCAATCGCCGCTCCACCCATCCTCT
2 nt deletion
ttll3ga231
CGAGGCTGTGAGAAAGAGGGCCTTG--AATCGCCGCTCCACCCATCCTCT
5′ TGGCAATCGCCGCTCCACCC 3′
ttll3wt
CGAGGCTGTGAGAAAGAGGGCCTTGG-CA---ATCGCCGCTCCACCCATCCTCT
4 nt insertion
ttll3ga232
CGAGGCTGTGAGAAAGAGGGCCTTTCTCACAGATCGCCGCTCCACCCATCCTCT

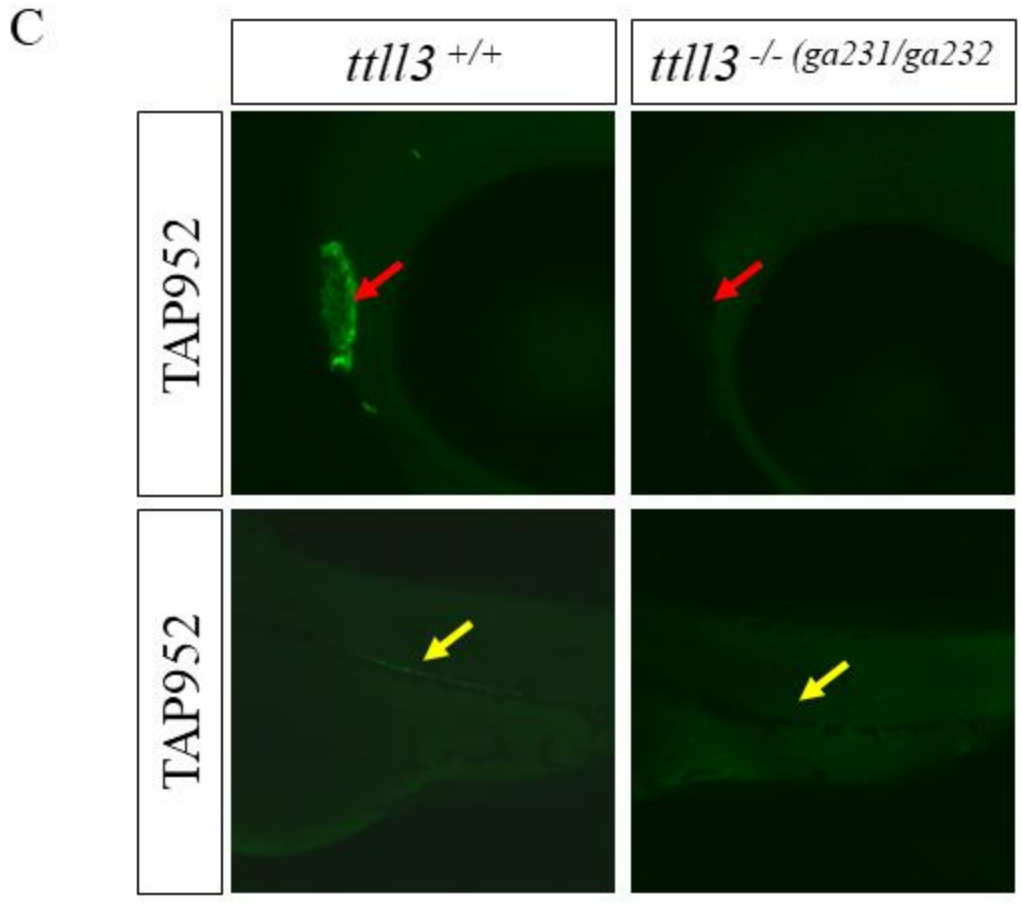
C
ttll3 +/+
ttll3 -/- (ga231/ga232
TAP952
TAP952

Figure 2.3. *ttll3* mutant does not exhibit any apparent defects. (A). Bright-field images of 48hpf wild type and *ttll3* $^{-/-\ ga231/ga232}$ embryos. Mutants do not show any obvious defects (B). Wholemount immunofluorescence of 48hpf wild-type and *ttll3* $^{-/-\ ga231/ga232}$ embryos with acetylated α-tubulin-specific 6-11-1B antibody. Olfactory cilia are present in both wild-type and *ttll3* $^{-/-}$ embryos.

A

B

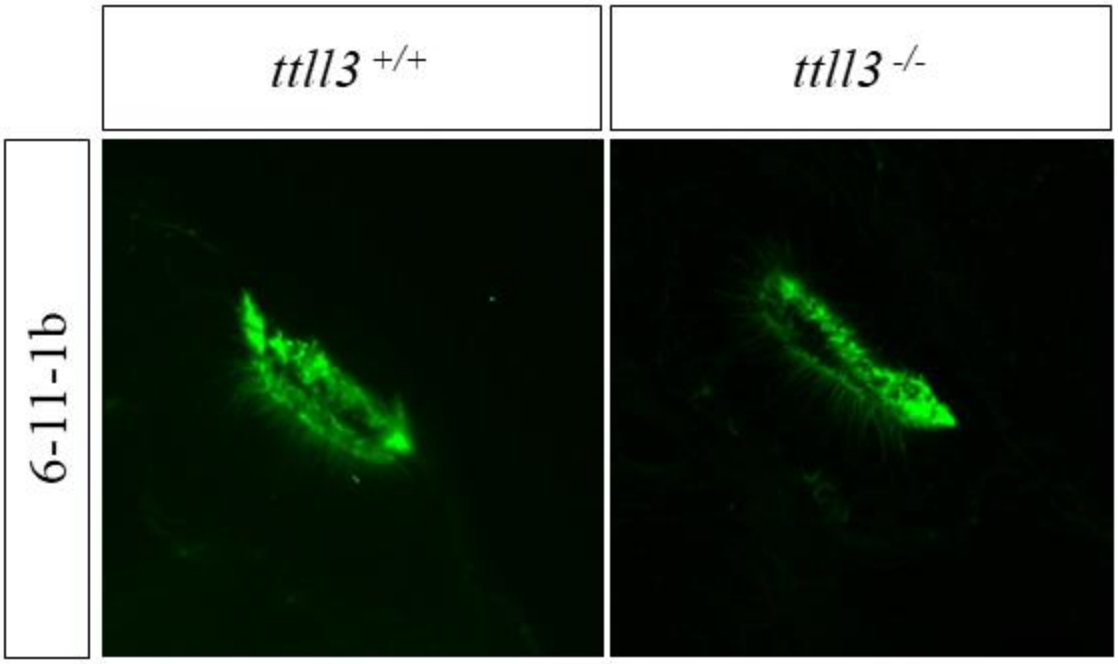

Figure 2.4: Levels of other microtubule PTMs altered in *ttll3* $^{-/-}$ mutants. Western blot with antibodies specific mono-, polyglycylated tubulin, mono-, polyglutamylated tubulin, acetylated α-tubulin, and α-tubulin for total protein extracted from *ttll3* $^{+/+}$ and *ttll3* $^{-/-}$ testes. Levels of acetylated α-tubulin, mono- and polyuglycylated tubulin levels were increased in *ttll3* $^{-/-}$ mutant.

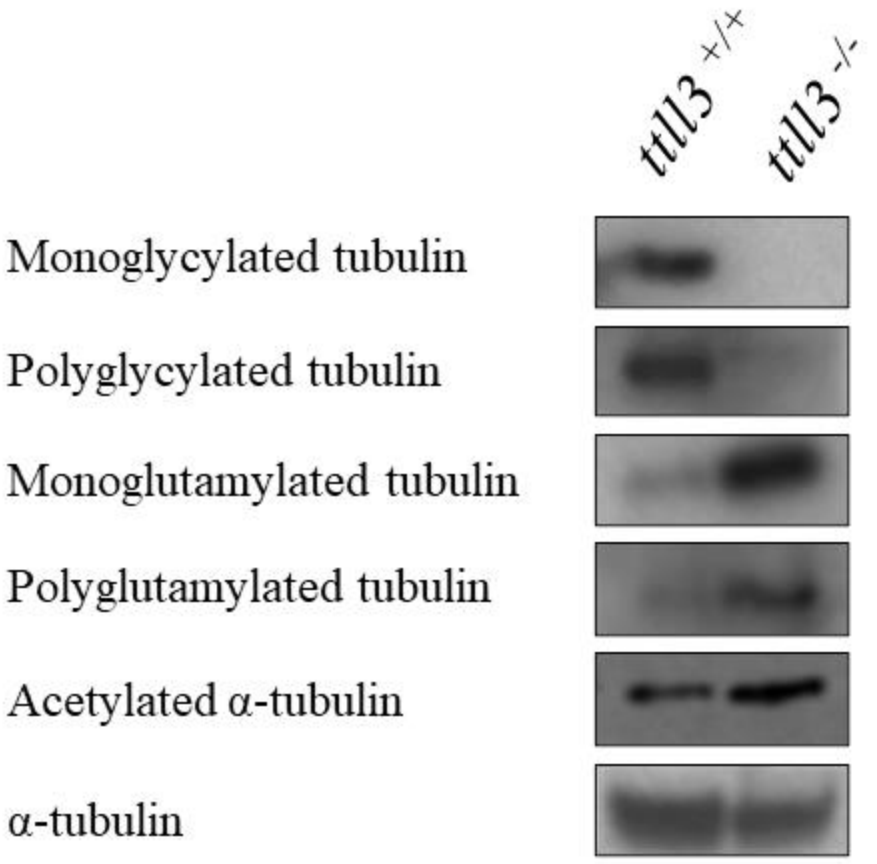
ttll3 +/+
ttll3 -/-
Monoglycylated tubulin
Polyglycylated tubulin
Monoglutamylated tubulin
Polyglutamylated tubulin
Acetylated α-tubulin
α-tubulin

Figure 2.5. *atat1* $^{-/-}$; *ttll3* $^{-/-}$ double mutant shows reduced fecundity and fertility. (A). Cross of *atat1* $^{-/-}$; *ttll3* $^{-/-}$ females with wild type males laid significantly lower number of eggs compared to sibling *atat1* $^{+/-}$; *ttll3* $^{+/-}$, *atat1* $^{-/-}$; *ttll3* $^{+/+}$,and *atat1* $^{+/+}$; *ttll3* $^{-/-}$ females. (B). Unfertilized eggs laid by *atat1* $^{-/-}$; *ttll3* $^{-/-}$ females were significantly higher than the unfertilized eggs laid by sibling *atat1* $^{+/-}$; *ttll3* $^{+/-}$, *atat1* $^{-/-}$; *ttll3* $^{+/+}$,and *atat1* $^{+/+}$; *ttll3* $^{-/-}$ females. (C). Apoptotic cells were stained in *atat1* $^{+/-}$; *ttll3* $^{+/-}$, *atat1* $^{-/-}$; *ttll3* $^{+/+}$, *atat1* $^{+/+}$; *ttll3* $^{-/-}$ and *atat1* $^{-/-}$; *ttll3* $^{-/-}$ ovaries was analyzed using TUNEL assay. Increased TUNEL puncta in *atat1* $^{-/-}$; *ttll3* $^{-/-}$ ovaries show increased cell death compared to other genotypes.

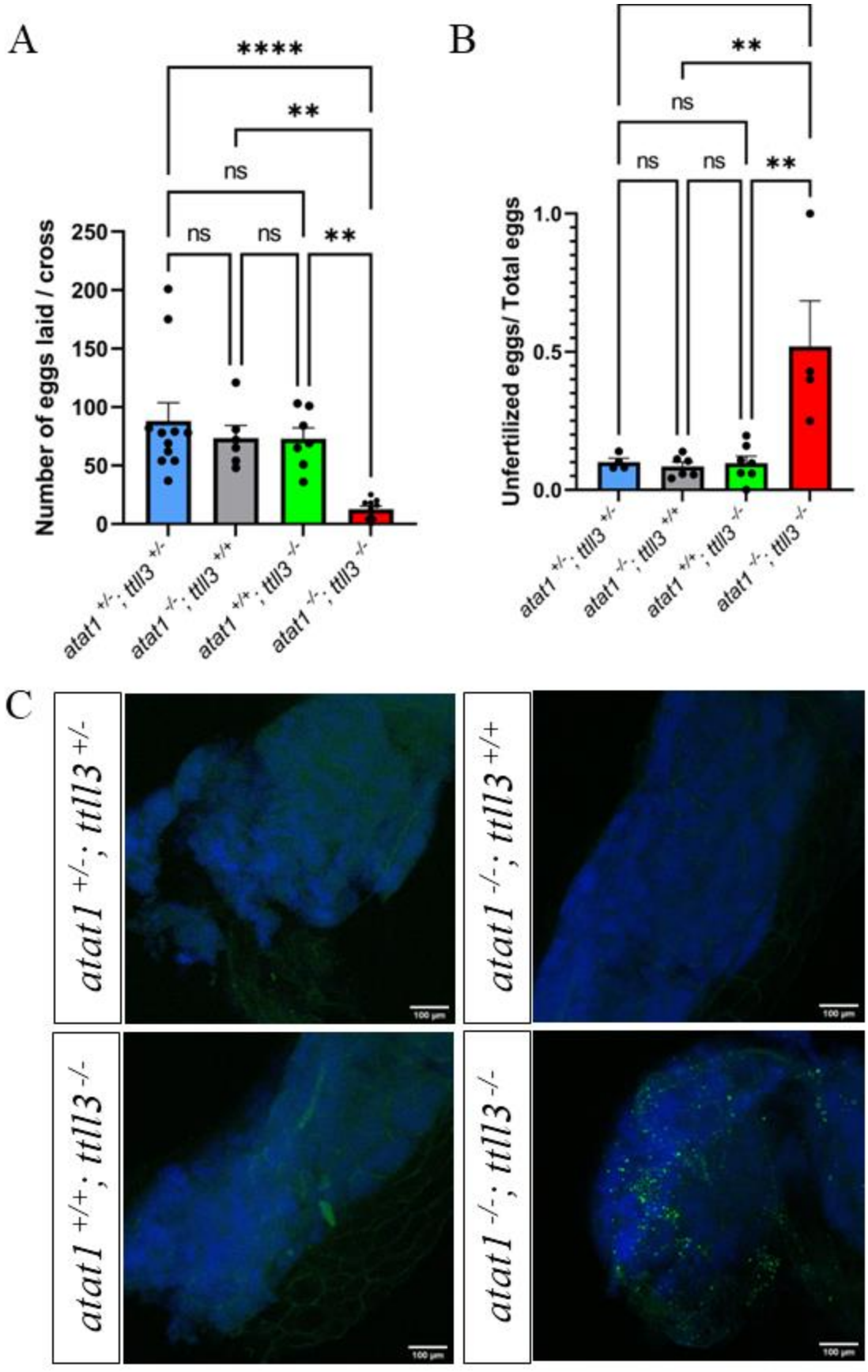
A
****
**
ns
ns
ns
**
Number of eggs laid / cross
250
200
150
100
50
0
atat1 +/-; ttll3 +/-
atat1 -/-; ttll3 +/+
atat1 +/+; ttll3 -/-
atat1 -/-; ttll3 -/-
B
**
ns
ns
ns
**
Unfertilized eggs/ Total eggs
1.0
0.5
0.0
atat1 +/-; ttll3 +/-
atat1 -/-; ttll3 +/+
atat1 +/+; ttll3 -/-
atat1 -/-; ttll3 -/-
C
atat1 +/-; ttll3 +/-
atat1 -/-; ttll3 +/+
atat1 +/+; ttll3 -/-
atat1 -/-; ttll3 -/-
100 µm

Figure 2.6. Microtubule acetylation and monoglycylation are enriched during the early stages of oogenesis. (A) Western blot with antibodies specific acetylated α-tubulin monoglycylated tubulin and α-tubulin for total protein extracted from wild-type stage I, II, and III oocytes. (B). Wholemount immunofluorescence of six-week-old wild-type ovaries with acetylated α-tubulin and monoglycylated tubulin-specific antibodies. Both antibodies stain cilia-like structures.

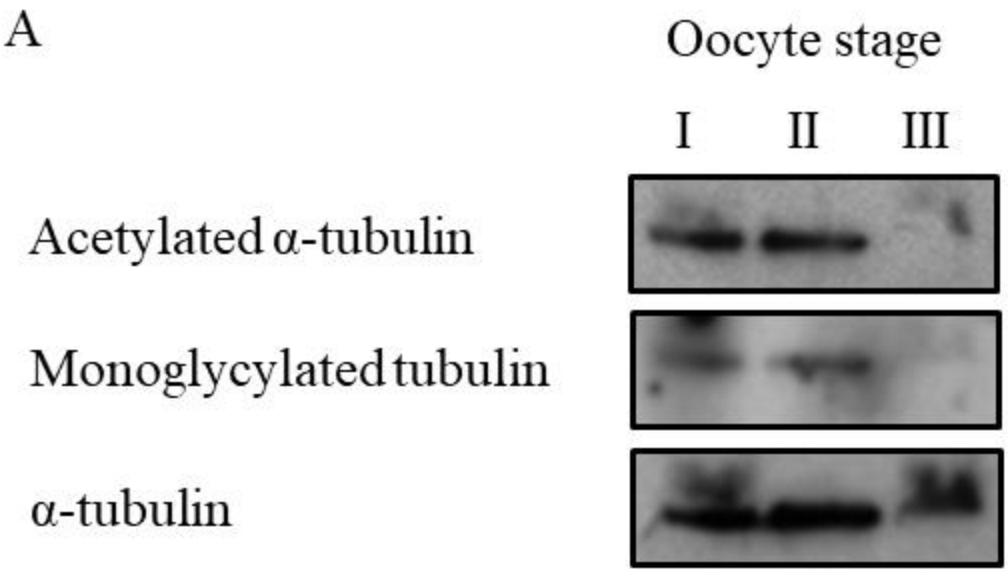
A
Oocyte stage
I
II
III
Acetylated α-tubulin
Monoglycylated tubulin
α-tubulin

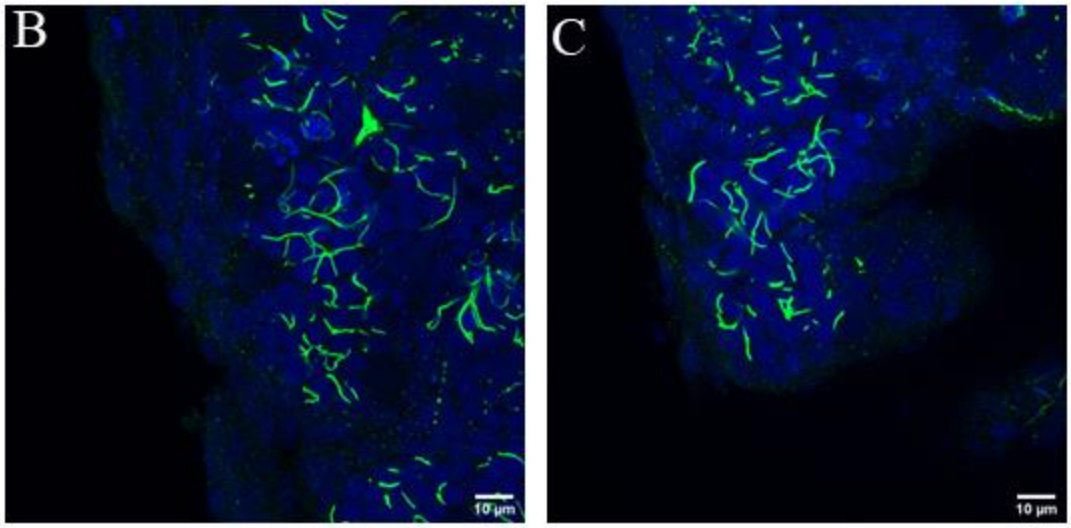
B
C
10 μm
10 μm

Figure 2.7. *atat1* $^{-/-}$; *ttll3* $^{-/-}$ double mutant show expanded chromosomal bouquet configuration. (A) Chromosomal bouquet of *atat1* $^{+/-}$; *ttll3* $^{+/-}$, *atat1* $^{-/-}$; *ttll3* $^{+/+}$, *atat1* $^{+/+}$; *ttll3* $^{-/-}$ and *atat1* $^{-/-}$; *ttll3* $^{-/-}$ ovaries were stained with Telo-Cy3 DNA probe (PNABio) that labels telomere regions. DRAQ5 was used to stain nuclei (Pseudocolored to blue). Chromosomal bouquet of *atat1* $^{-/-}$; *ttll3* $^{-/-}$ expanded configuration compared to other genotypes. (B) Quantification of chromosomal bouquet angle to the center in *atat1* $^{+/-}$; *ttll3* $^{+/-}$, *atat1* $^{-/-}$; *ttll3* $^{+/+}$, *atat1* $^{+/+}$; *ttll3* $^{-/-}$ and *atat1* $^{-/-}$; *ttll3* $^{-/-}$ ovaries show significant increase the angle of chromosomal bouquet to the center in *atat1* $^{-/-}$; *ttll3* $^{-/-}$. Statistical analysis was carried out with one-way ANOVA and Tukey's multiple comparison test (P-value <0.0001). (C). Quantification of nuclear diameter of nuclei in *atat1* $^{+/-}$; *ttll3* $^{+/-}$, *atat1* $^{-/-}$; *ttll3* $^{+/+}$, *atat1* $^{+/+}$; *ttll3* $^{-/-}$ and *atat1* $^{-/-}$; *ttll3* $^{-/-}$ ovaries. Statistical analysis was carried out with one-way ANOVA and Tukey's multiple comparison test (p-value=0.2170).

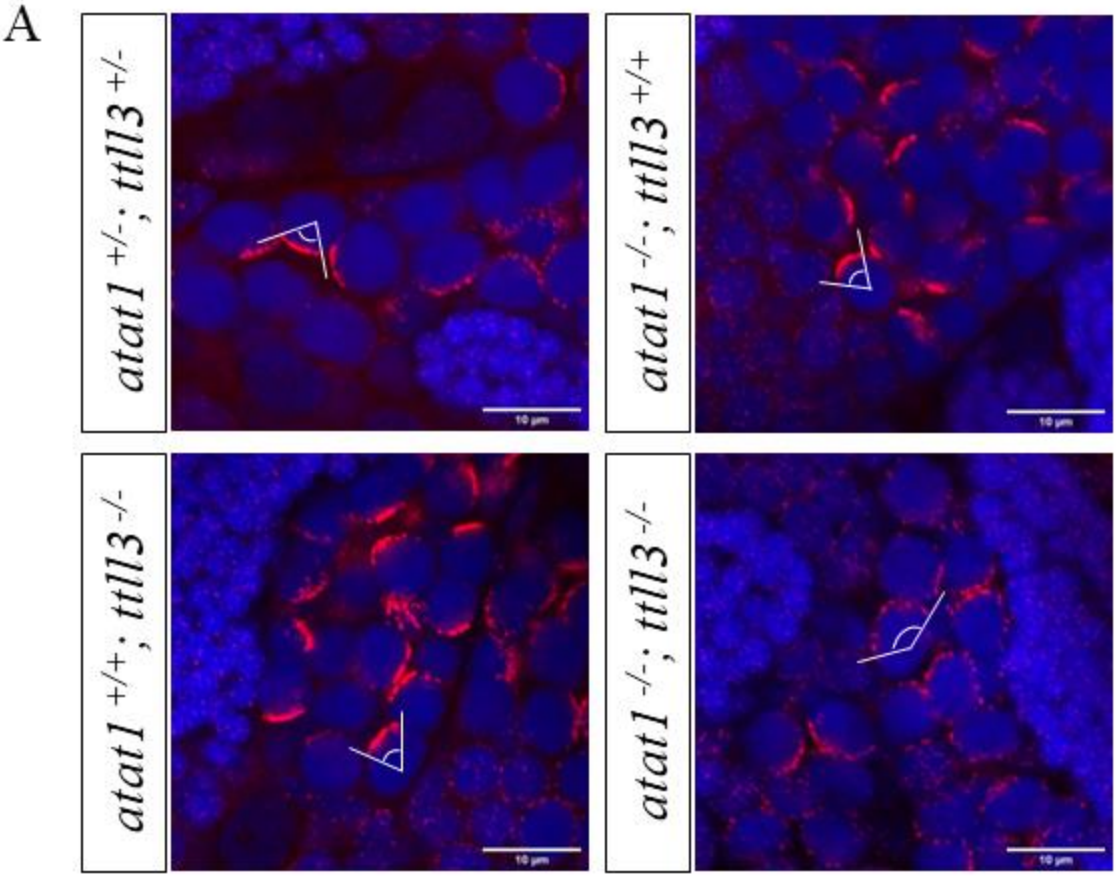
A
atat1 +/-; ttll3 +/-
atat1 -/-; ttll3 +/+
atat1 +/+; ttll3 -/-
atat1 -/-; ttll3 -/-
10 µm

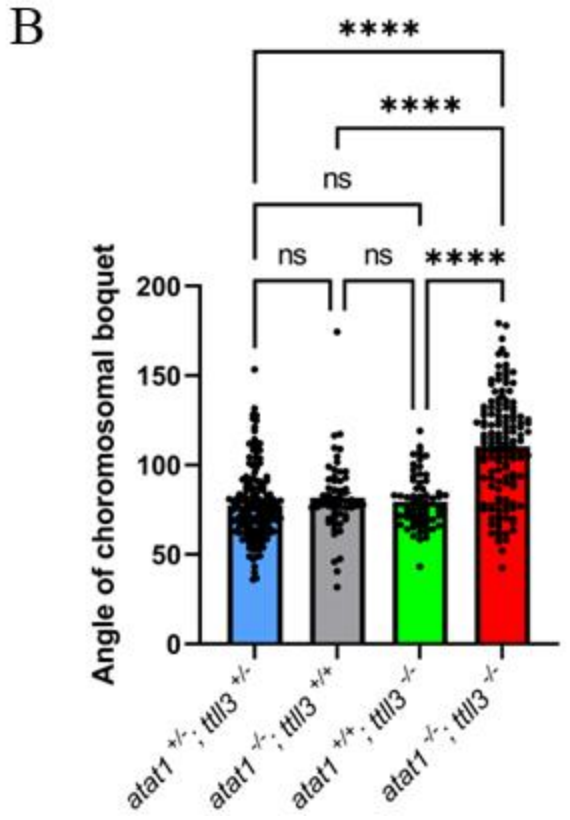
B
****
****
ns
ns
ns
****
Angle of choromosomal boquet
200
150
100
50
0
atat1 +/-; ttll3 +/-
atat1 -/-; ttll3 +/+
atat1 +/+; ttll3 -/-
atat1 -/-; ttll3 -/-

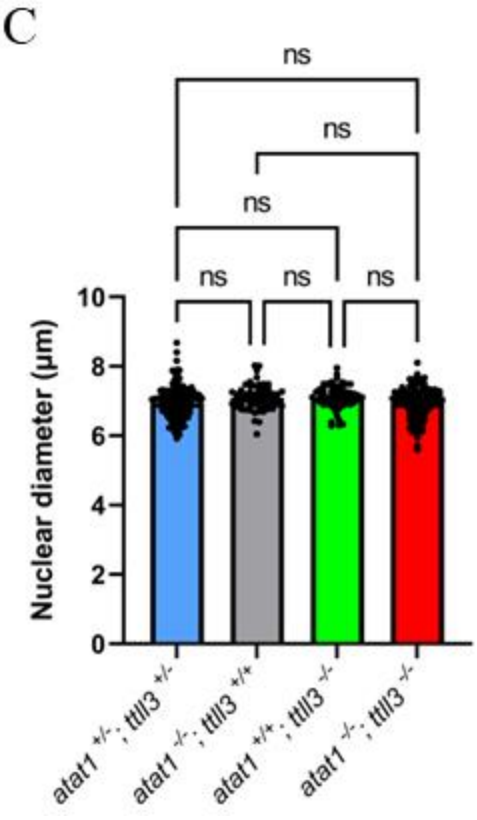
C
ns
ns
ns
ns
ns
ns
ns
Nuclear diameter (µm)
10
8
6
4
2
0
atat1 +/-; ttll3 +/-
atat1 -/-; ttll3 +/+
atat1 +/+; ttll3 -/-
atat1 -/-; ttll3 -/-

Figure 2.8. *atat1* $^{-/-}$; *ttll3* $^{-/-}$ double mutant has normal zygotene cilia. (A) Zygotene cilia of *atat1* $^{+/-}$; *ttll3* $^{+/-}$, *atat1* $^{-/-}$; *ttll3* $^{+/+}$, *atat1* $^{+/+}$; *ttll3* $^{-/-}$ and *atat1* $^{-/-}$; *ttll3* $^{-/-}$ ovaries were stained with monoglutamylated tubulin specific antibody GT355 (Green). DRAQ5 was used to stain nuclei (Pseudocolored to blue). Ovaries of all genotypes showed the presence of similar zygotene cilia. (B) Quantification of cilia length of zygotene cilia in *atat1* $^{+/-}$; *ttll3* $^{+/-}$, *atat1* $^{-/-}$; *ttll3* $^{+/+}$, *atat1* $^{+/+}$; *ttll3* $^{-/-}$ and *atat1* $^{-/-}$; *ttll3* $^{-/-}$ ovaries. Statistical analysis was carried out with one-way ANOVA and Tukey's multiple comparison test (P-value=0.6371). (C). Quantification of nuclear diameter of nuclei associated with zygotene cilia in *atat1* $^{+/-}$; *ttll3* $^{+/-}$, *atat1* $^{-/-}$; *ttll3* $^{+/+}$, *atat1* $^{+/+}$; *ttll3* $^{-/-}$ and *atat1* $^{-/-}$; *ttll3* $^{-/-}$ ovaries. Statistical analysis was carried out with one-way ANOVA and Tukey's multiple comparison test (p-value=0.2170).

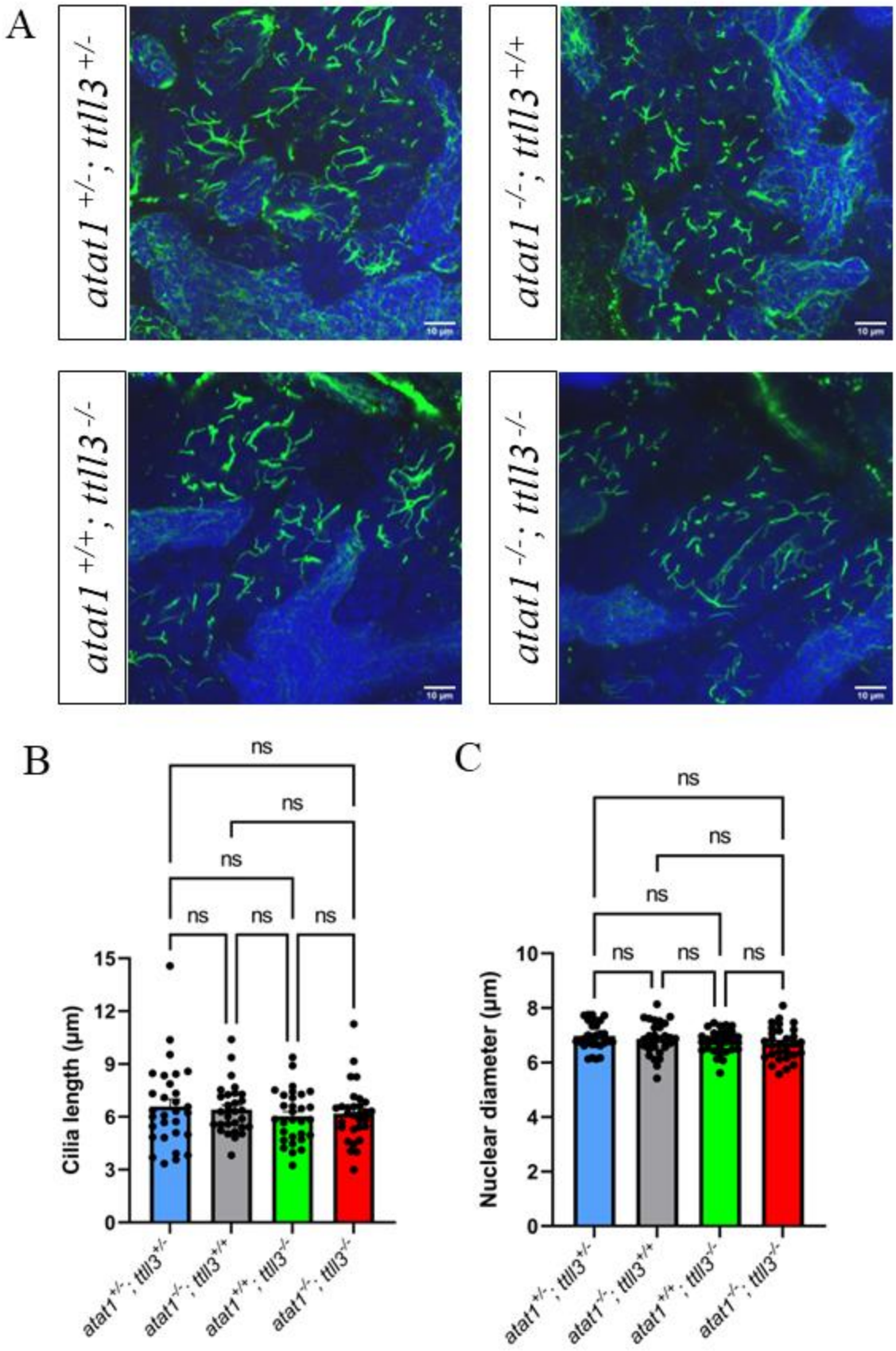
A
atat1 +/-; ttll3 +/-
atat1 -/-; ttll3 +/+
atat1 +/+; ttll3 -/-
atat1 -/-; ttll3 -/-
10 µm
B
Cilia length (µm)
0
3
6
9
12
15
ns
atat1+/-; ttll3+/-
atat1-/-; ttll3+/+
atat1+/+; ttll3-/-
atat1-/-; ttll3-/-
C
Nuclear diameter (µm)
0
2
4
6
8
10

SUPPLEMENTAL FIGURES

Figure S2.1. Expression of *atat1* and *ttll3* mRNAs in *Danio rerio*. (A). *atat1* and *ttll3* mRNA expression in zebrafish embryonic stages from 8-cell to 72hpf and larval stages from 96hpf-144hpf. (B). *atat1* and *ttll3* mRNA expression in zebrafish adult tissues-brain, testis, ovary, kidney, heart, gut, and liver.

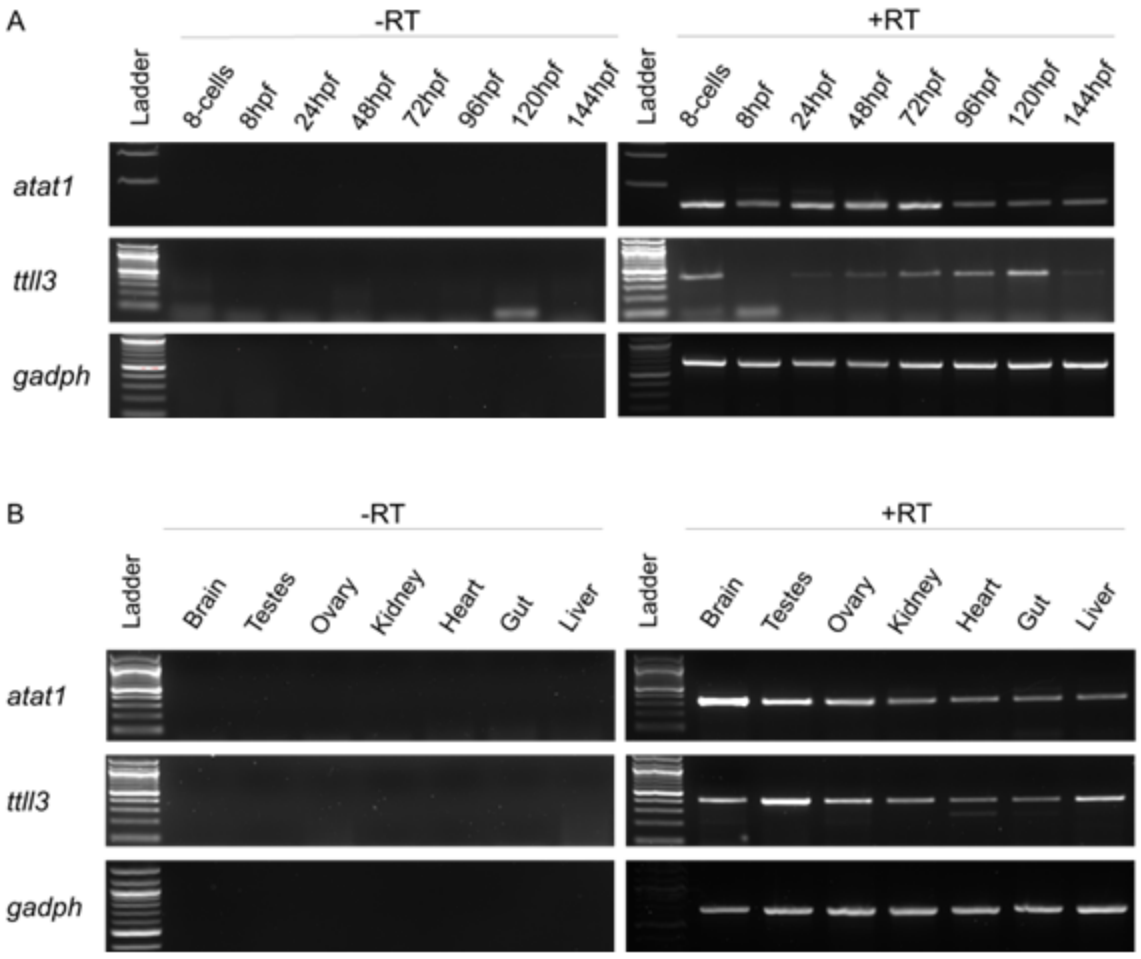
A
-RT
+RT
Ladder
8-cells
8hpf
24hpf
48hpf
72hpf
96hpf
120hpf
144hpf
atat1
ttll3
gadph
B
Brain
Testes
Ovary
Kidney
Heart
Gut
Liver

Figure S2.2. Screening of *ttll3* specific CRISPR-Cas9 mediated mutations in F1. (A). Potential null alleles were identified by crossing F0 females with wild-type males. Randomly selected eight embryos out of resulting F1 embryos were screened using the T7E1 assay to detect DNA mismatches. (B). Alleles were confirmed to be null by crossing heterozygous fishes of identified alleles, and the resulting embryos were stained with monoglycylated tubulin-specific TAP952 antibody. Embryos that lacked antibody staining were genotyped to confirm as a mutant of a specific allele.

A

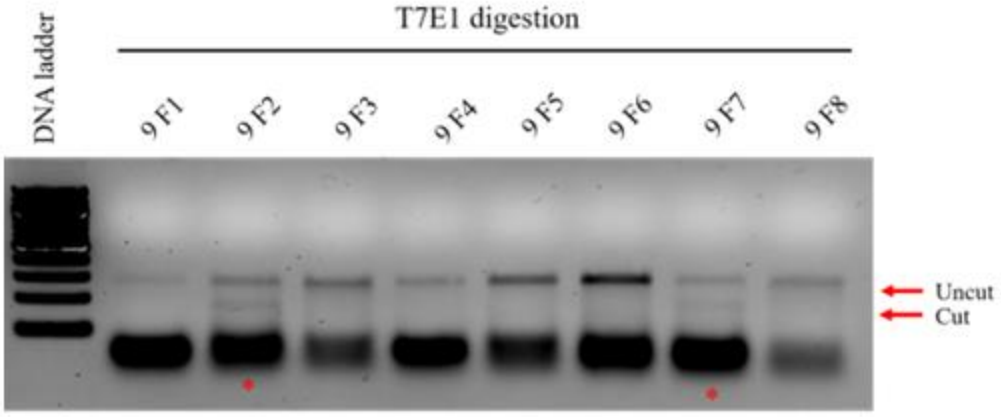
T7E1 digestion
DNA ladder
9 F1
9 F2
9 F3
9 F4
9 F5
9 F6
9 F7
9 F8
Uncut
Cut

B

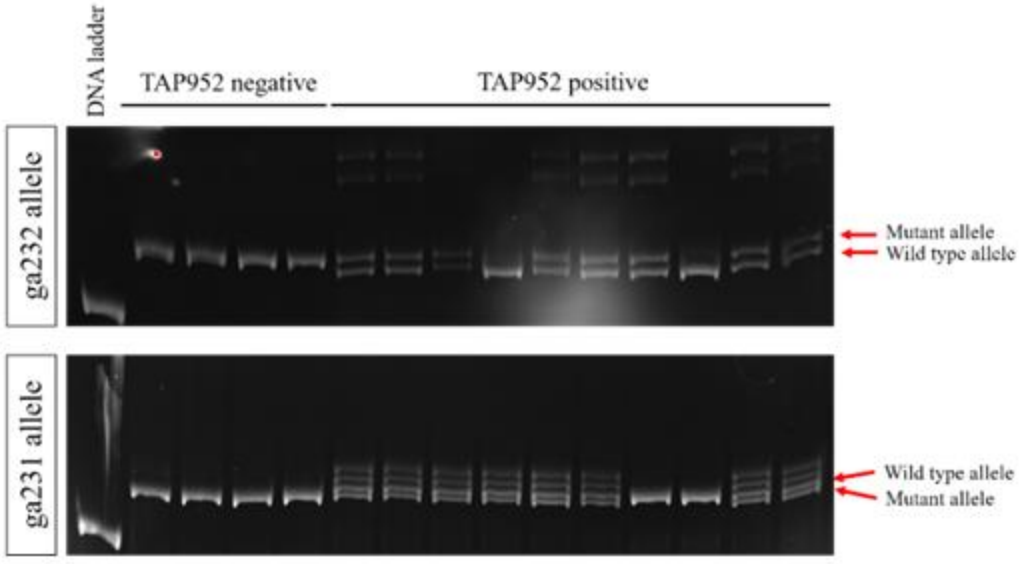
DNA ladder
TAP952 negative
TAP952 positive
ga232 allele
Mutant allele
Wild type allele
ga231 allele
Wild type allele
Mutant allele

Figure S2.3. *atat1* mutant has normal-looking cilia. Wholemount immunofluorescence of 48hpf wild-type and *atat1* $^{-/-\ ga4}$ embryos with monoglycylated tubulin-specific TAP952 antibody. Olfactory cilia, renal cilia, and ependymal cilia are present in wild-type and *ttll3* $^{-/-}$ embryos.

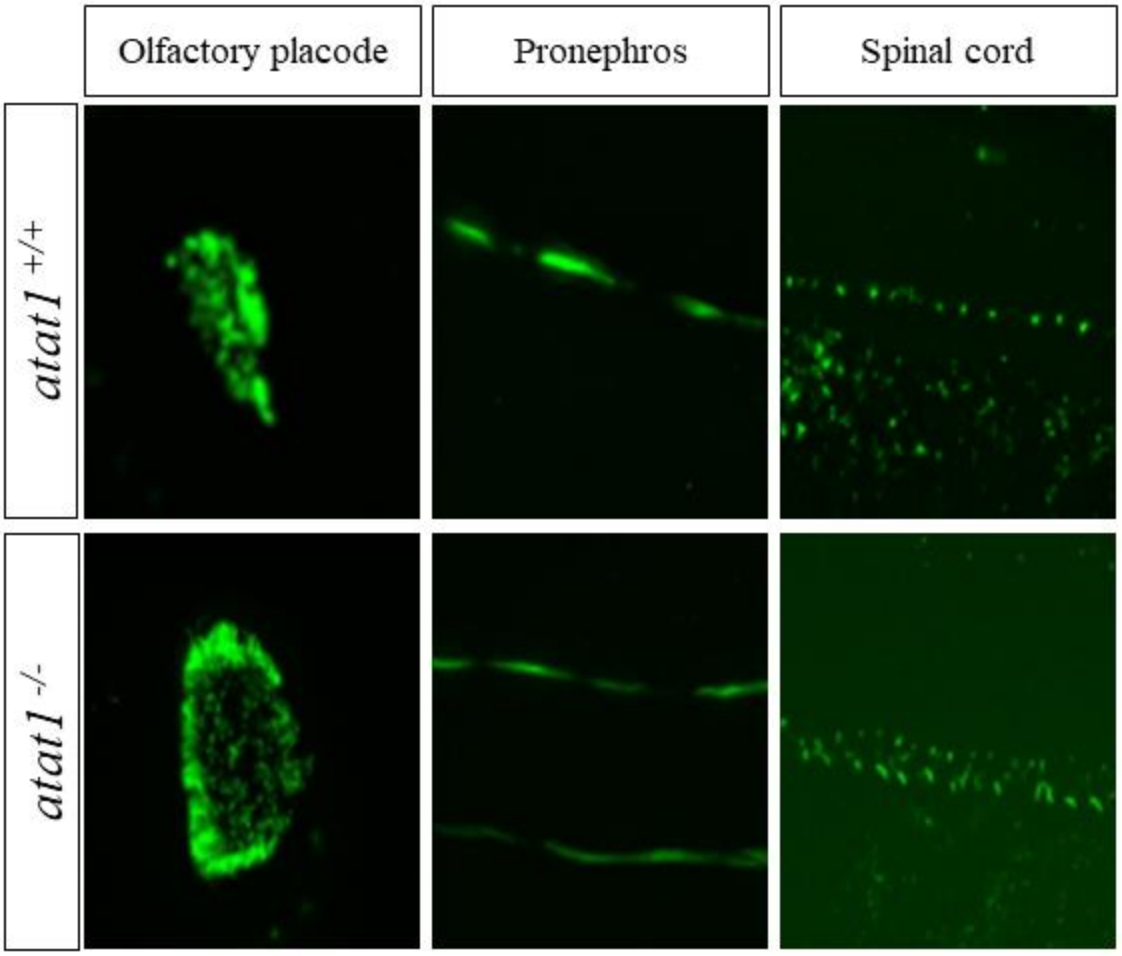
Olfactory placode
Pronephros
Spinal cord
atat1 +/+
atat1 -/-

Figure S2.4. Inhibition of nonsense-mediated mRNA decay (NMD) does not result in severe phenotypes in *atat1* $^{-/-}$ or ttll3 $^{-/-}$ embryos. Wild-type (n=20), *atat1*$^{-/-}$ (n=20), and *ttll3* $^{-/-}$ (n=20) embryos were treated with NMDi14 or DMSO at 8hpf and observed for morphological defects during embryonic development. Neither mutant showed any severe phenotype that differs from the DMSO treated controls.

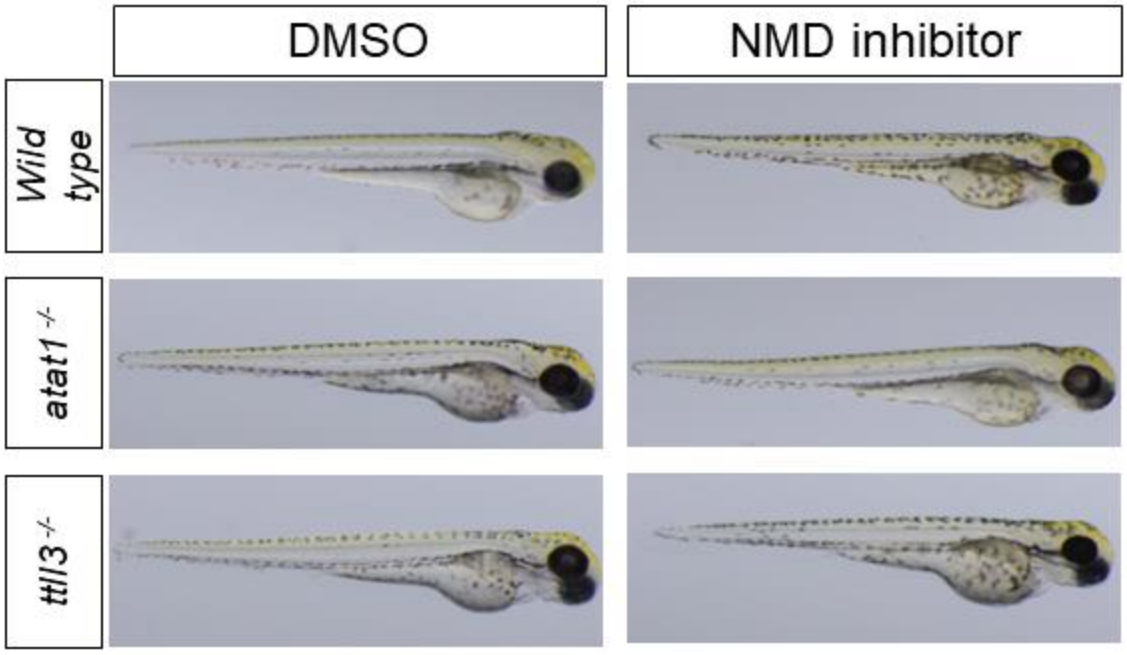
DMSO
NMD inhibitor
Wild type
atat1 -/-
ttll3 -/-

Figure S2.5. *atat1* or *ttll3* mutant adults do not exhibit any morphological or growth defects. (A). Bright-field images of 9 months old wild type, *atat1* $^{-/-}$ and *ttll3* $^{-/-}$ male and female fishes. (B) Body weights of 4 months old sibling *atat* $^{+/-}$ (n=7) and *atat1*$^{-/-}$ (n=5) are not significantly different different (Student's t-test, p-value= 0.4841). (C) Body length of 4 months old sibling *atat* $^{+/-}$ (n=7) and *atat1*$^{-/-}$ (n=5) are not significantly (Student's t-test, p-value= 0.3414). (D) Body weight of 4 months old sibling *ttll3* $^{+/-}$ (n=8) and *ttll3* $^{-/-}$ (n=10) are not significantly different (Student's t-test, p-value= 0.5383). (E) Body length of 4 months old sibling *ttll3* $^{+/-}$ (n=8) and *ttll3* $^{-/-}$ (n=10) are not significantly different (Student's t-test, p-value= 0.9280).

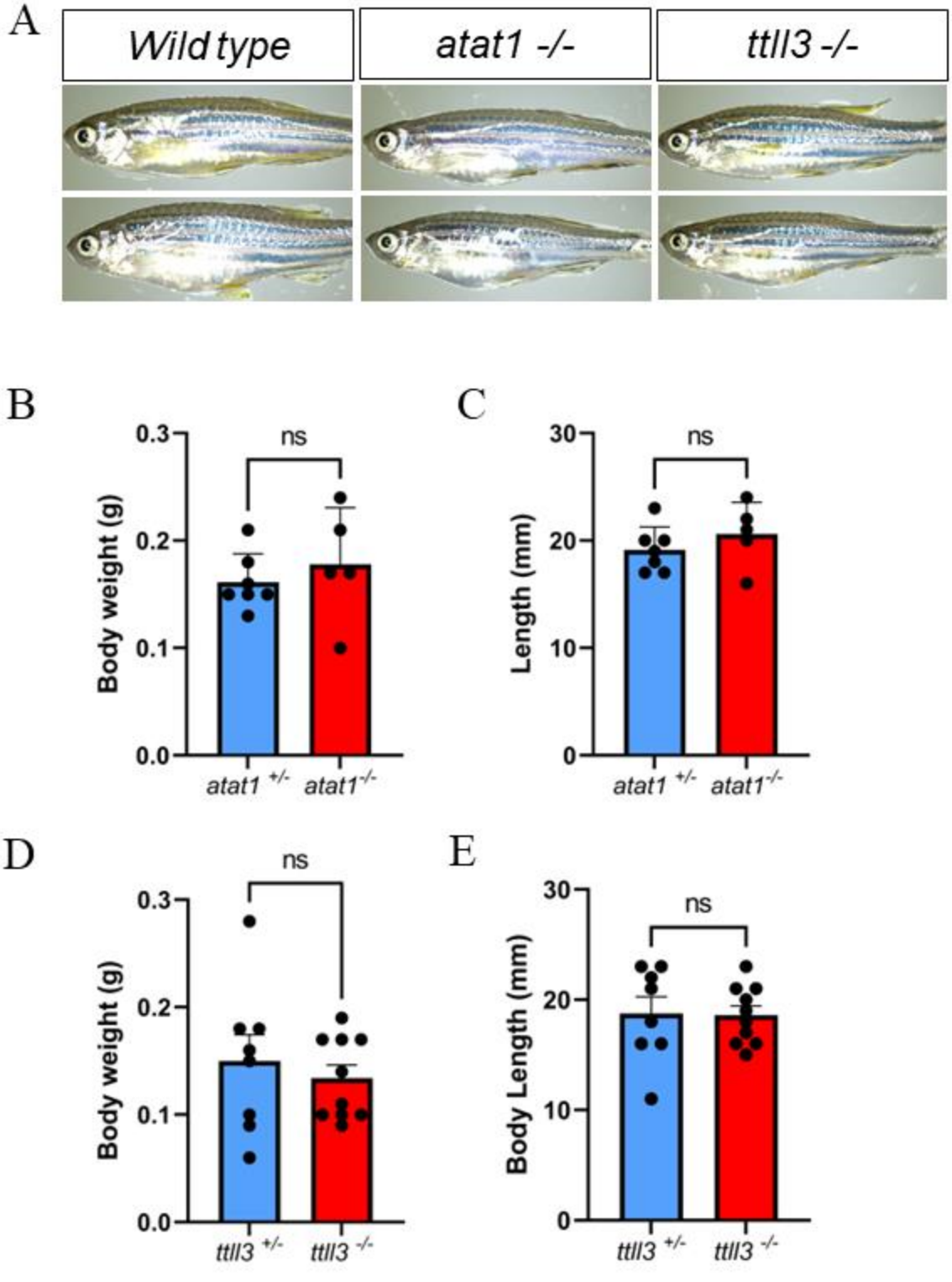
A
Wild type
atat1 -/-
ttll3 -/-
B
Body weight (g)
0.3
0.2
0.1
0.0
ns
atat1 +/-
atat1-/-
C
Length (mm)
30
20
10
0
ns
atat1 +/-
atat1-/-
D
Body weight (g)
0.3
0.2
0.1
0.0
ns
ttll3 +/-
ttll3 -/-
E
Body Length (mm)
30
20
10
0
ns
ttll3 +/-
ttll3 -/-

Figure S2.6. *atat1* and *ttll3* mutants show reduced survival. (A). Survival probability of *atat1*$^{-/-}$ (n=29) was lower than sibling *atat* $^{+/-}$ (n=25) (Log-rank test, p-value =0.0126). (B). Survival probability of *ttll3*$^{-/-}$ (n=11) was lower than sibling *ttll3* $^{+/-}$ (n=12) (Log-rank test, p-value =0.0070).

A

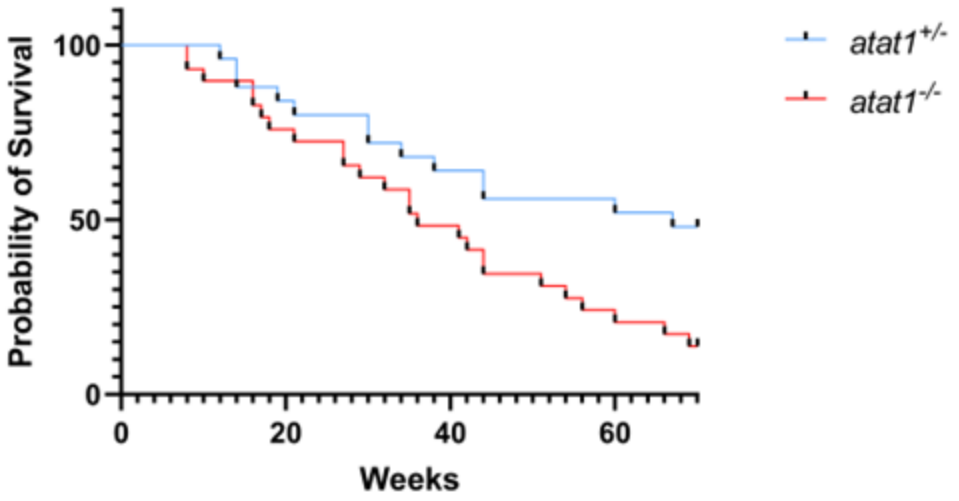
Probability of Survival
100
50
0
0
20
40
60
Weeks
atat1+/-
atat1-/-

B

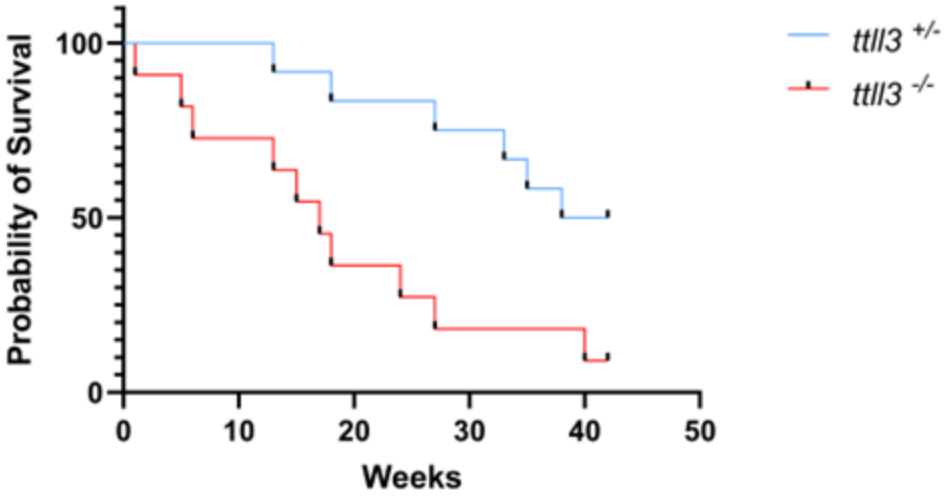
Probability of Survival
100
50
0
0
10
20
30
40
50
Weeks
ttll3 +/-
ttll3 -/-

Figure S2.7. *ttll3* mutants show reduced progressive sperm motility. (A). Proportion of fertilized eggs of *ttll3* $^{-/-}$ (n=6 crosses) was lower than sibling *ttll3* $^{+/+}$ (n=6 crosses) (Student's t-test, p-value =0.0001). (B). *ttll3* $^{-/-}$ does not show any obvious histological defects compared to sibling *ttll3* $^{+/+}$. (C). Spermatozoa of *ttll3* $^{-/-}$ mutants (n=4) show reduced progressive sperm motility compared to sibling *ttll3* $^{+/+}$ (n=4). (D). Quantification of sperm motility assay (Student's t-test, p-value =0.0001).

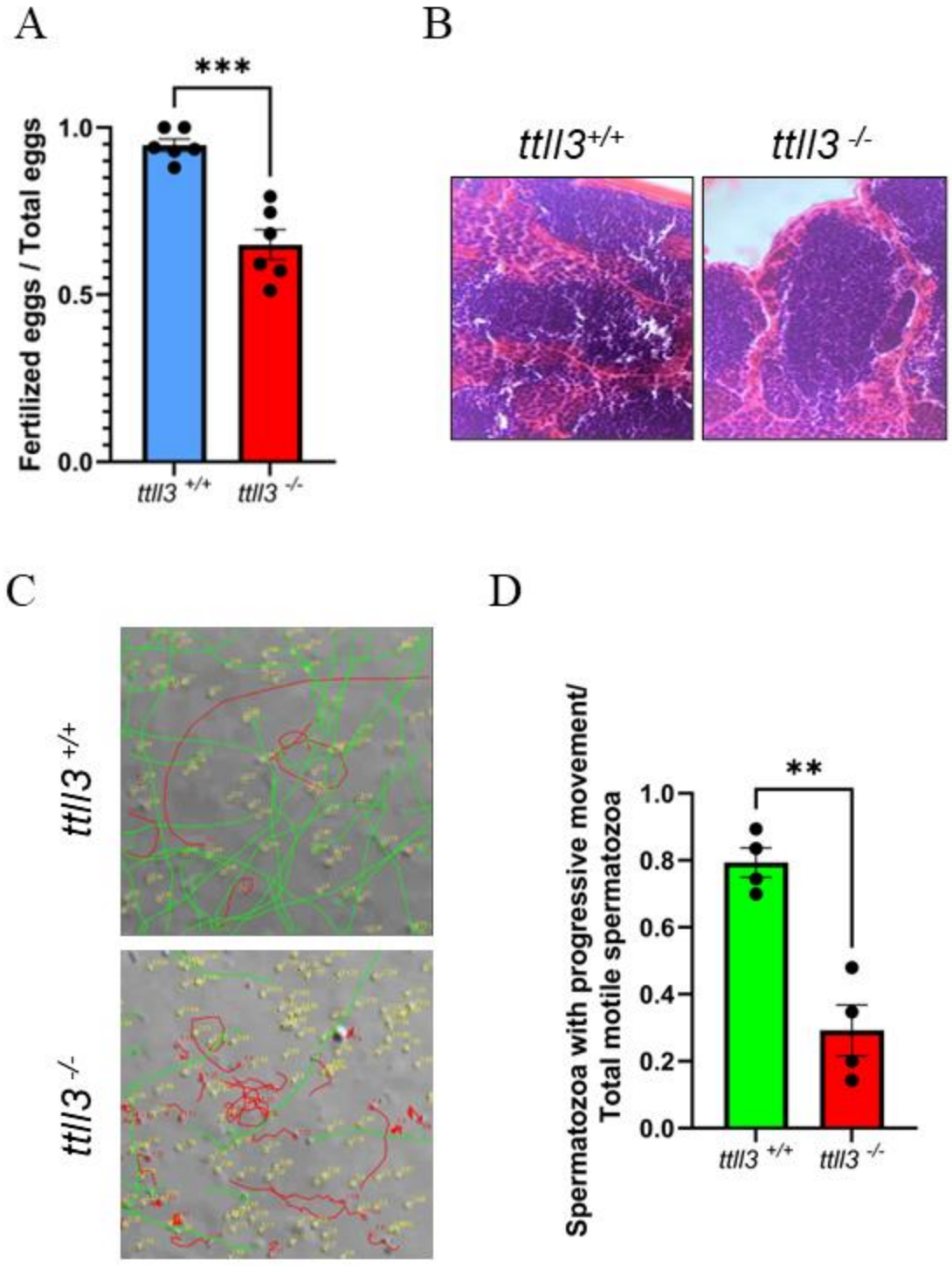
A
***
Fertilized eggs / Total eggs
1.0
0.5
0.0
ttll3 +/+
ttll3 -/-
B
ttll3+/+
ttll3 -/-
C
ttll3 +/+
ttll3 -/-
D
**
Spermatozoa with progressive movement/
Total motile spermatozoa
1.0
0.8
0.6
0.4
0.2
0.0
ttll3 +/+
ttll3 -/-

CHAPTER 3

MICROTUBULE α-TUBULIN ACETYLATION REGULATES ZEBRAFISH AGGRESSION, SOCIAL BEHAVIOURS, AND STRESS RESPONSE[1]

[1] Amirthagunanathan S., Kaya N., Tseng WC., Priyal P., Akella JS., Gaertig J., and Dougan ST. To be submitted to the Journal of Aging Studies

ABSTRACT

Neurons regulate vertebrate behavior and stress response. Microtubules play an important role in neurogenesis and neuronal functions. Microtubule posttranslational modifications (PTMs) provide microtubule diversity to fine-tune microtubule functions by altering the physical properties of microtubules and associated MAPs. Major microtubule PTMs acetylation, detyrosination, and glutamylation are enriched in neurons. Microtubule acetylation is carried out by *atat1*. Mice *Atat1* mutants exhibit defects in the hippocampus and striatum that play important roles in behavior and stress response. The role of microtubule acetylation in behavior and stress response is not understood. Our study demonstrates that loss of *atat1* results in defects in touch response in zebrafish embryos. These mutant embryos do not show any defects in sensory or motor neurogenesis. Adult *atat1* mutants also exhibit altered aggression and social behavior, indicating the role of microtubule acetylation in normal animal behavior. This *atat1* mutant also showed a reduced survival under environmental stress conditions. Larva of this mutant also showed reduced cortisol levels in response to stress conditions indicating an alteration in the HPA axis. We find that loss of microtubule acetylation leads to altered behavior and stress response in zebrafish

INTRODUCTION

Animal behaviors and stress responses are important for organisms to survive and thrive, and neurons play important roles in modulating behaviors and stress responses. Microtubules are essential in neurogenesis, establishing and maintaining neuronal

structures, axonal transportation, and functions. Any changes in microtubule function could alter normal brain development and functions (Lasser et al., 2018).

Diversification of simple polymer of α- and β-tubulins is crucial in carrying out many complex biological processes within the same cellular environments. Different tubulin isotypes and posttranslational modifications generate the microtubule diversity needed to carry out these functions (Janke, 2014). Neurons are enriched in many of these microtubule posttranslational modifications. Major microtubule PTMs like acetylation, glutamylation, and detyrosination are present in neurons.

Microtubule acetylation occurs at lysine 40 of α-tubulin (L'Hernault and Rosenbaum, 1983, L'Hernault and Rosenbaum, 1985, LeDizet and Piperno, 1987). Unlike other microtubules PTMs, α-tubulin acetylation occurs on the luminal surface of the microtubules (Nogales et al., 1999). The major enzyme that carries out the microtubule is α-tubulin acetyltransferase (ATAT1) (Akella et al., 2010, Shida et al., 2010). Additional proteins have also been shown to carry out α-tubulin acetylation in vitro (Ohkawa et al., 2008, Creppe et al., 2009, Conacci-Sorrell et al., 2010, Ouyang et al., 2021). Deacetylation of this site is performed by HDAC6, SIRT2, and smaller extend by HDAC5 (Hubbert et al., 2002, North et al., 2003, Cho and Cavalli, 2012). Microtubule acetylation alters microtubule physical properties. Acetylated microtubules show resistance to chemical depolymerization and mechanical stress (Xu et al., 2017, Portran et al., 2017, LeDizet and Piperno, 1987, Akella et al., 2010). Acetylated microtubules also show preferential association with kinesin-1 and dynein and reduce their motility (Reed et al., 2006, Alper et al., 2014, Balabanian et al., 2017). Additional site of acetylation in

α/β tubulin dimer was reported, and this modification is carried out by San acetyltransferase (Chu et al., 2011).

Microtubule acetylation is required for touch sensation. Loss of the gene that encodes α-tubulin acetyltransferase in *C.elegans*, mice, and *Drosophila* results in altered touch sensation (Akella et al., 2010, Shida et al., 2010, Morley et al., 2016, Yan et al., 2018). Both mice and *Drosophila* implicate changes in the physical properties of the microtubule network associated with mechanosensory ion channels due to the loss of microtubule acetylation. In *C.elegans*, ATAT1 plays a non-enzymatic role in the touch sense.

Atat1 mutant mice exhibited ventricular dilation with distortion in the dentate gyrus and hypoplasia in the striatum and septum (Kim et al., 2013, Li et al., 2019). Defects in neuronal migration have been implicated in hypoplasia of the striatum and septum. This mutant also showed defects in motor coordination.

These regions of the brain regulate a wide range of functions. The dentate gyrus regulates aggression, social interaction, social memory, and anxiety (Lowrey et al., 2020, Smagin et al., 2015, Anacker et al., 2018, Lewis et al., 2018, Leung et al., 2018, Zou et al., 2016). The Dentate gyrus also regulates the HPA axis, stress response, and resiliency (Schloesser et al., 2009, van Bodegom et al., 2017). Similarly, the striatum regulates social behavior (Báez-Mendoza and Schultz, 2013, Kawamichi et al., 2016). The role of microtubule acetylation in behavior and stress response is not understood.

Our data shows that *atat1* embryos showed altered touch-evoked swimming behavior, and we did not see any obvious defect in sensory or motor neurons. Our data also show that *atat1* mutant adults exhibit altered aggression behavior and mild social anxiety

compared to heterozygous siblings. Our data show that levels of microtubule acetylation increase when zebrafish larva are exposed to environmental stress conditions, and *atat1* mutant larva is more susceptible to stress conditions than wild-type larva and showed reduced survival under elevated temperatures and osmotic stress. Preliminary data also show that the cortisol level of *atat1* mutant larva has not elevated in response to an increase in temperature, while wild-type larva showed elevated cortisol levels. Our data shows the potential role of microtubule acetylation in hypothalamus-pituitary-adrenal axis response to stress.

MATERIAL AND METHODS

Zebrafish Maintenance, Embryo Collection, and Adult Tissue Collection

Zebrafish lines were maintained in Paul D. Coverdell Biomedical Center fish facility following the Animal Use Protocols (AUPs) A2014 07-005-Y3-A6, A2017 08-020-Y3-A0 and A2020 08-002-Y1-A0, approved by the Institutional Animal Care and Use Committee (IACUC) of the University of Georgia. Embryos were collected using single or multiple-pair mating and maintained at 28.5 ^{o}C in egg water (60 µg/ml Instant Ocean sea salt and 0.3 µg/ml Methylene Blue). Embryos used in experimental procedures were treated with 1-phenyl 2-thiourea to maintain optical clarity. Embryos were staged using a Leica S6E stereomicroscope (Leica Microsystems, Germany) as previously described(Kimmel et al., 1995). Appropriately aged fishes were euthanized for adult tissue collection by rapid chilling in ice water.

Genomic DNA Extraction

Genomic DNA extraction was performed with either 72hpf larva or fin clips from adult fishes. Samples were initially incubated with DNA extraction buffer (10 mM Tris pH 8.2, 10 mM EDTA, 200 mM NaCl, and 0.5% SDS) at 95 ^{o}C for 20 minutes before the addition of 200 µg/ ml proteinase K. This step was followed by incubation at 55 ^{o}C for 16 hours. Finally, proteinase K activity was terminated with incubation at 95 ^{o}C for 20 minutes. Extracted DNA was stored at -20 ^{o}C and diluted 25 times before the use as a template in PCR reactions.

Genotyping

Genotyping of the *atat1* mutant allele was performed with PCR using TALENTEST3F (5'-CATTGATAAGACCGCTACTACA-3') and TALENTEST3F (5'-GTGCATGTAGCGAACCAGAT-3') under following PCR conditions. Initial denaturation: 94^{o}C for 2 minutes, denaturation: 94^{o}C for 20 seconds, annealing: 57^{o}C for 20 seconds, extension: 72^{o}C for 30 seconds for 35 cycles and final extension: 72^{o}C for 5 minutes. PCR products were digested with *BsmI* (New England Biolabs, Ipswich, MA) and resolved in 2 % agarose gel (Lonza Bioscience).

Total RNA extraction

Total RNA extraction was performed with embryos, larva, and adult tissues. Total RNA was extracted by homogenizing the samples with TRIzol reagent (Life Technologies, Carlsbad, CA), followed by chloroform extraction and total RNA precipitation with isopropanol. Extracted total RNA preparation was treated with DNAase to eliminate any

genomic DNA extraction with TURBO DNA-*free* Kit (Life Technologies, Carlsbad, CA). Total RNA was quantified using NanoDrop 2000 (Thermo Scientific, Waltham, MA) and stored at -80 ^{o}C.

Quantitative Reverse Transcriptase-PCR (qRT-PCR)

First-strand cDNA was synthesized using the RevertAid First Strand cDNA synthesis kit (ThermoFisher Scientific, Waltham, MA) per the manufacturer's instruction. 500 ng of total RNA was used as the template for first-strand cDNA synthesis. qPCR reactions were carried out with 1 µl of first-strand cDNA as the template with primer in Table 1. The *gadph* gene was used as a control. qPCR was carried out using Bio-Rad CFX96 Touch Real-Time PCR Detection System (Bio-Rad, Hercules, CA) with PowerTrack SYBR Green Master Mix (ThermoFisher Scientific, Waltham, MA) following the manufacturer's instructions.

Immunofluorescence

Zebrafish embryos were collected at the desired stage and fixed with fresh 4% paraformaldehyde in PBT (1x PBS, 0.5% Triton X-100) overnight. Fixed specimens were gradually dehydrated with methanol series and stored in 100% methanol at -20 ^{o}C until the use. Specimens were gradually rehydrated and washed with PBT before being blocked for 2 hours in blocking reagent (2% Bovine Serum Albumin, 1% DMSO, 0.5% Triton X-100, 0.5% Normal Goat Serum in 1X PBS). Specimens were incubated with primary and secondary antibodies in blocking reagent overnight at 4 ^{o}C. Primary antibodies used were mouse monoclonal anti-monoglycylated tubulin antibody mouse

monoclonal anti-acetylated tubulin 6-11-1B (1:500) and Rabbit anti-LC3 II antibody FITC conjugated anti-mouse IgG (1:500) used as the secondary antibody. Imaging was done with either Zeiss AXIO Imager D2 compound fluorescence microscope or Zeiss LSM 880 confocal microscope (Carl Zeiss, Germany). (Carl Zeiss, Germany).

Western blots

Protein extraction was carried out by homogenizing and incubating deyolked larvae and adult tissues with Lysis buffer (RIPA buffer (Sigma-Aldrich, St. Louis, MO), NaF, Na3VO4, Protease inhibitor) followed by centrifugation to removed cell debris. Isolated protein concentration was determined by the Pierce BCA Protein Assay kit (Thermo Scientific, Waltham, MA) using the manufacturer's protocol. SDS-PAGE was carried out on 4%-20% precast gel (Bio-Rad Laboratories, Hercules, CA) with 10 µg of total protein in each sample. Resolved proteins were transferred to the Hybond-P PVDF membrane (GE Healthcare, Piscataway, NJ). Membranes were incubated at 4 ^{o}C overnight with primary antibodies at dilutions as follows: mouse monoclonal anti-monoglycylated tubulin antibody TAP952 (1:2000), Rabbit polyclonal Poly G antibody R2302 (1:1000),: mouse monoclonal anti-monoglutamylated tubulin antibody GT335 (1:1000), Rabbit polyclonal Poly E antibody R2304 (1:1000) and mouse monoclonal anti-acetylated tubulin 6-11-1B (1:1000). Primary antibody incubation followed by incubation with either HRP-conjugated anti-mouse IgG or HRP-conjugated anti-rabbit IgG secondary antibody at 4 ^{o}C overnight. Following secondary antibody incubation, blots were treated with Clarity Western ECL substrate (Bio-Rad Laboratories, Hercules, CA) and detected X-OMAT LS films (Carestream, Rochester, NY).

Touched evoked swimming behavior

Touched evoked swimming behavior was performed with 54 hpf old wild-type, *atat1* mutant, and *atat1* mutants injected with mouse *atat1* mRNA at 1 cell stage as previously reported (Smith et al., 2013). Swimming behavior was recorded at a rate of 250 frames/ second. Videos were analyzed with the ImageJ Animal tracker plugin to generate each embryo's swimming path, and statistical analysis was done with GraphPad Prism.

Birefringence microscopy

Birefringence microscopy was carried out as previously described (Smith et al., 2013). Instead of polarized lenses, in this study, we used polarized films and imaged 54 hpf embryos.

Adult behavioral assay

Adult behavior assays were carried out with 6- 8 months old heterozygous and mutant siblings. Novel tank, mirror biting, social interaction and shoaling tests were performed as previously reported (Audira et al., 2018). Adult behavior assays were recorded at a rate of 60 frames/ second. Videos were analyzed with Idtracker software, and statistical analysis was done with GraphPad Prism.

Paraffin-embedded sectioning and H & E staining

Six to eight months old adult mutants and wild-type fishes were used to collect brain tissues. Collected brain tissues were fixed in fresh 4% paraformaldehyde in PBT (1x PBS, 0.5% Triton X-100) overnight. Tissues were dehydrated with a series of ethanol.

Brains were incubated in xylene 3 times and then 3 times in 100 % paraffin at 60 ^{o}C. Then the brain tissues were embedded in paraffin, and 10 μm sections were prepared. These sections were stained with standard H & E staining protocol and mounted with Permount mounting medium.

Cortisol ELISA assay

Extraction of cortisol from zebrafish larva treated with different stress conditions was performed as previously reported (Alsop and Vijayan, 2008). The cortisol levels were quantified with the Cortisol ELISA kit (Cayman chemical company, Ann Arbor, MI) per the manufacturer's instructions.

RESULTS

Acetylated α-tubulin is enriched in neurons and ciliated tissues in zebrafish embryos

Enrichment of microtubule acetylation is reported in cilia and axons of neurons (L'Hernault and Rosenbaum, 1983, Cambray-Deakin and Burgoyne, 1987). In zebrafish, acetylated α-tubulin is enriched in ciliated tissues and neurons. At 24hpf, enrichment of acetylated tubulin is observed in pronephros and neurons (Data not shown). By 48hpf, it is enriched in the olfactory placode (Figure 3.1A), pronephros (Figure 3.1B), otic vesicle (data not shown), neurons (Figure 3.1A and 3.1B), and lateral line system (Figure 3.1B). Expression of *atat1* mRNA occurs maternally and zygotically during the zebrafish embryonic development (Figure S2.1). Expression of *atat1* mRNA is observed in the adult brain, testis, ovary, kidney, heart, gut, and liver tissues (Figure S2.1). Enrichment of

acetylated microtubule in neurons indicates a potential role of this modification in neurogenesis and neuronal functions.

Mutant that lack α-tubulin acetylation shows no obvious defects in neurogenesis during development

Knockdown of *atat1* with morpholinos in zebrafish resulted in neuromuscular defects and lacked startle response to touch (Akella et al., 2010). This morphant also showed ciliary defects phenotypes like curved body axis and hydrocephaly. Our group generated a one base pair deletion *atat1* mutant line using TALEN mutagenesis and confirmed it to be null (Tseng, 2015). This *atat1* mutant does not exhibit any obvious morphological or ciliary defects during embryogenesis. We studied this mutant's primary and secondary motor neurons and found no defect or delay in neurogenesis (Figure 3.2). Treatment of *atat1* mutant embryos with nonsense-mediated mRNA degradation inhibitor NMDi14 did not result in any obvious phenotype and confirms that NMD-mediated genetic compensation is not responsible for teh discrepencey seen between *atat1* mutant and morphant.

Mutant adults did not show any morphological defects or differences in their body weight or length (Figure S2.5). *atat1* mutant adults showed reduced longevity compared to heterozygous siblings (Figure S2.6). Mouse *Atat1* mutants exhibited defects in sperm motility and male fertility (Kalebic et al., 2013). Zebrafish *atat1* mutants showed comparable male and female fertility to wild-type siblings (Data not shown).

Acetylated α-tubulin is not detected in *atat1* $^{-/-}$ zebrafish brain

In addition to *atat1*, ARD1-NAT and Elp1 and GCN5 show ability to acetylate microtuuble in vitro (Ohkawa et al., 2008, Creppe et al., 2009, Conacci-Sorrell et al., 2010, Ouyang et al., 2021) . To understand whether these proteins play a role in microtubule acetylation in zebrafish neuronal cells, we studied the acetylated tubulin levels in the *atat1* mutant brain (Figure S3.1). We did not detect any acetylated α-tubulin in zebrafish brain, confirming that *atat1* is the only α-tubulin acetyltransferase in zebrafish neuronal cells.

The *atat1* mutant embryos show reduced touch evoked swimming response

Lack of microtubule acetylation in *C.elegan*, *Drosophila*, and mice resulted in altered touch response (Akella et al., 2010, Shida et al., 2010, Yan et al., 2018, Morley et al., 2016). Zebrafish *atat1* morphants also showed no startle response to touch (Akella et al., 2010). To understand whether *atat1* mutants show touch sense defect, we carried out the touch assay with 54hpf old wild-type, *atat1* mutant, and *atat1* mutants injected with mouse *atat1* mRNA at 1 cell stage. As seen in other organisms, zebrafish *atat1* mutants showed reduced touched evoked swimming behavior (Figure 3.3). Injection of mouse mRNA into *atat1* mutant embryos rescued the reduction in touch response of *atat1* mutant (Figure 3.3). In response to touch wild type (n=37), *atat1 -/-* (n=38), and *atat1 -/- + mAtat1-yfp* mRNA (n=31) swimming on average 44.69 mm, 15.19 mm and 33.75 mm respectively.

To understand whether neurogenesis, migration, and morphogenesis of sensory neurons and motor neurons altered, we carried out wholemount immunofluorescence with

antibodies that would specifically label Rohon-Beard neuron (anti-islet-1), primary motor neuron (ZNP-1), and secondary motor neuron (Zn-8). Interestingly, We did not see any obvious defects in Rohon-Beard or primary or secondary motor neurons (Figure S3.2A & S3.2B). Microtubule acetylation also plays a role in muscle contraction (Coleman et al., 2021). We used birefringence microscopy to confirm that wild-type and *atat1* mutants had comparable muscle arrangement and did not observe any obvious defects (Figure S3.2C).

Adult *atat1* $^{-/-}$ mutants show altered behavior

Mice lacking *Atat1* show distorted dentate gyrus due to hyperplasia, which plays an important role in learning and memory (Kim et al., 2013). Another group also showed hyperplasia in the septum and striatum and ventricular dilation when *Atat1* was knocked out in mice (Li et al., 2019). This mouse *Atat1* mutant also showed defects in motor coordination. To understand the role of microtubule acetylation in normal zebrafish brain activities, we carried out a series of behavioral assays. We used sibling heterozygous and mutant fishes at room temperature.

The novel tank experiment tests fishes' general locomotor activity, exploration, and anxiety (Audira et al., 2018). In this behavior assay, we did not see any obvious difference between mutant and heterozygous siblings (Figure 3.4A). They showed comparable latency to entering the upper tank (Figure 3.4B). Both heterozygous and mutant fishes showed a comparable average swimming speed indicating normal locomotor activity (Figure 3.4D). They also showed the comparable time to enter the upper tank and a similar proportion of time spent in the upper tank (Figure 3.4C). Both

heterozygous and *atat1* mutant fishes also show a comparable freezing time ratio (Figure S3.3C). This data shows that *atat1* mutant does not display increased anxiety in a novel environment.

We also studied aggression behavior in *atat1* mutants. A mirror was placed at the experimental tank's vertical wall, and the area within 5cm from the mirror was considered the mirror biting zone. The experimental recordings were carried out after 5 min acclimatization (Audira et al., 2018). Interestingly, *atat1* mutant fishes spent significantly less time in mirror biting compared to heterozygous siblings (Figure 3.5A). On average, heterozygous (n=8) and *atat1* mutant (n=8) fishes spent 42.6 % and 27.2 % of total time in the mirror-biting zone (Figure 3.5B). When there is no mirror, heterozygous (n=8) and *atat1* mutant (n=8) fishes spent 22.5 % and 23.3 % of total time in the mirror-biting zone. The time spent by the *atat1* mutant in the mirror biting zone in the presence of the mirror is comparable to the time spent by the *atat1* mutant when there is no mirror placed in the tank (Figure 3.5B). This data indicates that zebrafish *atat1* mutant display lower aggression. No significant difference was seen in average swimming velocity, time spent in the upper tank, or freezing time between *atat1* mutant and heterozygous siblings (Figure 3.5C, 3.5D, and S3.4C).

We assessed the social interaction by dividing the experimental tank into two half by a glass plate. Experimental fishes were placed in one half while another wild type was placed in the other. After 5 minutes of acclimatization, the experimental recordings were carried out. The area within 3 cm from the glass plate is the interaction zone (Audira et al., 2018). In our study, *atat1* mutants and heterozygous siblings spent a comparable amount of time in the interaction zone (Figure3.6A).

Interestingly, *atat1* mutants showed increased freezing behavior compared to heterozygous siblings (Figure S3.5C). Mutants (n=8) and heterozygous (n=9) spend 9.7 % and 16.3 % of total time in freezing behavior, respectively. An increase in freezing time indicates a potential increase in anxiety in response to social interaction in *atat1* mutants. Average swimming speed and time spent in the upper tank did not show a significant difference between *atat1* mutants and heterozygous siblings (Figure 3.6C and 3.6D).

The shoaling test was carried out with a group of three fishes, and they were acclimatized to the tank for 5 minutes before the recordings. Interestingly, *atat1* mutants showed reduced time spent in the upper tank compared to heterozygous siblings (Figure 3.7D). Heterozygous (n=4) and mutants (n=4) fishes spent around 22.5 % and 3.6 % in the upper tank, respectively. The average shoal area, average swimming velocity, and freezing time did not show significant differences between mutant and heterozygous siblings (Figure 3.7B, 3.7C, and S3.6C).

The *atat1* mutants exhibit behaviors previously reported to be associated with reduced aggression and elevated anxiety during social situations compared to the heterozygous siblings. We did not see significant locomotor activity or anxiety differences in a novel environment.

Exposure to stress conditions results in hyperacetylation in zebrafish larva

Microtubule acetylation levels were shown to elevate in response to stress conditions (Giustiniani et al., 2009, Geeraert et al., 2010, Mackeh et al., 2014, Li et al., 2019). To understand whether the level of microtubule acetylation elevates in response to stress

conditions in zebrafish, we exposed zebrafish 5dpf larva to heat stress (35 ^{o}C), osmotic stress (100 mM NaCl), and oxidative stress (50 μM H_2O_2). We used larva maintained at 28 ^{o}C without any treatments as control. We observed hyperacetylation in response to stress conditions (Figure 3.8A). Exposure to heat, osmotic, and oxidative stress elevates the level of microtubule acetylation by 7, 3, and 1.5 fold, respectively (Figure 3.8B). Our studies confirm the occurrence of hyperacetylation in response to stress conditions, as reported previously in human and mouse cells.

atat1 mutant larva are more sensitive to temperature and osmotic stress

To understand the role of microtubule acetylation in stress response, we were exposed to a series of stress conditions. Mutants that lack *atat1* show increased mortality under levels of stress conditions at which wild-type larva survive (Figure 3.9). Exposure of *atat1* larva to 35 ^{o}C and 37 ^{o}C for 2 hours resulted in a survival rate of 93 % and 0 % compared to 100 % survival observed in wild type (Figure 3.9A). No significant difference was seen between wild-type and mutant larva under lower temperatures. Under 250 mM of sodium chloride treatment, *atat1* larva showed a 79 % survival rate compared to 98 % in wild type (Figure 3.9B.). With a higher concentration of 300 mM, both wild-type and mutant larva showed 0 % survival. There was no significant difference in survival rate between wild-type and mutant larva under concentrations lower than 250 mM. Exposure to oxidative stress did not result in any significant difference in survival under the concentrations of H_2O_2 tested (Figure 3.9C). Increased mortality observed in atat1 larva for heat and osmotic stress indicates the potential roles of microtubule acetylation in stress response and survival.

DISCUSSION

ATAT1 is the major microtubule acetyltransferase and plays an important role in ciliary and neuronal functions (Akella et al., 2010, Shida et al., 2010, Kalebic et al., 2013, Morley et al., 2016, Yan et al., 2018, Neumann and Hilliard, 2014, Even et al., 2019, Li et al., 2019). In our study, we find altered neuronal function in zebrafish *atat1*mutant. Our study finds that atat1 mutant embryos exhibit defects in touch-evoked swimming behavior. We also find that the adults of this mutant show reduced aggression and mild social anxiety. We also find that *atat1-/-* exhibits defects in stress response.

Knockdown of *atat1* in zebrafish with morpholino showed phenotypes like curved body axis, kidney cyst, and hydrocephalous brain (Akella et al., 2010). We did not see any obvious morphological defects in *atat1* mutant embryos or adults. When these mutant embryos were treated with NMDi14, an inhibitor of nonsense-mediated mRNA decay, they did not phenocopy morphant. This data shows that the discrepancy between mutant and morphants phenotypes is not due to NMD-mediated genetic compensation. The *atat* mutant males and females showed normal fertility in both males and females. A study in mice *atat1* mutant showed reduced sperm motility and fertility while other mice *atat1* mutants did not (Kalebic et al., 2013, Morley et al., 2016, Li et al., 2019). Normal fertility in our mutant indicates normal sperm morphology and motility, but a sperm motility assay must be carried out to confirm it.

Interestingly, our mutants exhibit defects in touch-evoked swimming behavior, and we did not see any obvious abnormalities in sensory neurons, primary and secondary motor neurons, or muscle arrangement. Similar phenotypes have been reported in both mice and

Drosophila (Morley et al., 2016, Yan et al., 2018). In these mutants, even though sensory and motor neurons appeared normal, mechanosensation by the sensory neurons is altered. Alteration in the physical properties of microtubules associated with mechanosensitive ion channels was implicated in the reduction in mechanosensation. We need to study further the changes in the Rohon-Beard neuron, the sensory neuron in the zebrafish embryo, and associated microtubules to confirm what was reported in the DRG neurons of other model organisms. There could be a common mechanism regulating mechanosensation through the association of acetylated microtubules in mechanosensing neurons.

Past studies have explored behavioral changes related to *atat1* mutants; the effect of lacking ATAT1 on behaviors associated with memory, aggression, and social preference is unknown (Morley et al., 2016, Yan et al., 2018, Li et al., 2019). A study of mice atat1 mutant showed distortion in the hippocampus's dentate gyrus that plays an important role in these unexplored behaviors (Kim et al., 2013). We studied novel tank, aggression, social interaction, and shoaling behaviors in out *atat1* mutants. Our study also found adult behavioral differences between *atat1* mutant and heterozygous siblings. We found that the *atat1* $^{-/-}$ fishes show reduced aggression compared to heterozygous siblings. We also found that these *atat1* mutants show mild anxiety behaviors under social interaction and shoaling studies. The *atat1* $^{-/-}$ fishes showed freezing behavior during the social interaction behavior assay and spent more time in the lower tank during shoaling behavior assay compared to heterozygous siblings. We did not see any significant difference between behaviors of *atat1* mutant and heterozygous siblings in the novel tank test. When these *atat1* mutant fishes were introduced to novel tanks, single fish at a time,

they did not exhibit any signs of anxiety or abnormal motor behavior. Their exploration behavior was comparable to heterozygous siblings.

Previous studies have shown defects in mice brain's dentate gyrus and striatum when they lack *Atat1* (Kim et al., 2012, Li et al., 2019). Studies have shown that these regions play a role in aggression, social behavior, and anxiety (Lowrey et al., 2020, Smagin et al., 2015, Anacker et al., 2018, Lewis et al., 2018, Leung et al., 2018, Báez-Mendoza and Schultz, 2013, Kawamichi et al., 2016). Interestingly, we did not find any obvious defects in the brain sections of *atat1* mutant fishes with simple hematoxylin-eosin staining. Similarly, reduced aggression and elevated anxiety levels have been reported in mutants that lack Histamine H3 receptors (Reichmann et al., 2020). This mutant showed reduced serotonergic signaling as well. To understand further what causes the behavioral changes in our mutant, we need to study neuronal activation in the brain in response to the behavior, and differences in the levels of neurotransmitters must be studied. Further studies must be done to understand how the loss of ATAT1 alters memory and learning.

Microtubule hyperacetylation in response to environmental and nutritional stress, like starvation, osmotic stress, oxidative stress, and UV radiation, has been well established (Geeraert et al., 2010, Giustiniani et al., 2009, Mackeh et al., 2014, Li et al., 2019). In our study, we found that zebrafish larva exhibits microtubule hyperacetylation in response to stress conditions like temperature and osmotic and oxidative stress. We also found that atat1 mutants larva show reduced survival under stress conditions, indicating the role of microtubule acetylation on the stress response. Most studies show hyperacetylation in response to stress leads to increased autophagy (Geeraert et al., 2010, Mackeh et al.,

2014). Further studies must be done in our *atat1* mutants to see whether the level of autophagy is changed due to the lack of microtubule acetylation.

Hypothalamic-pituitary-adrenal (HPA) axis plays an important role in stress response through the release of cortisol in zebrafish (Alsop and Vijayan, 2008). Studies have shown the importance of dentate gyrus in the HPA axis, stress response, and stress resiliency (Schloesser et al., 2009, van Bodegom et al., 2017). To understand whether loss of ATAT1 alters the HPA axis and cortisol release, we studied cortisol levels in wild-type and *atat1* mutants under stress conditions. Our preliminary data show that *atat1* mutant larva did not elevate cortisol levels under elevated temperature, while wild-type larva showed elevated cortisol levels in response to elevated temperature (Figure S3.7). This preliminary data show that the HPA axis is altered in the mutant. Further studies have to study changes in the expression of genes associated with the HPA axis and levels of neurotransmitter to understand the mechanism behind this observation.

REFERENCE

AKELLA, J. S., WLOGA, D., KIM, J., STAROSTINA, N. G., LYONS-ABBOTT, S., MORRISSETTE, N. S., DOUGAN, S. T., KIPREOS, E. T. & GAERTIG, J. 2010. MEC-17 is an α-tubulin acetyltransferase. *Nature,* 467**,** 218-222.

ALPER, J. D., DECKER, F., AGANA, B. & HOWARD, J. 2014. The motility of axonemal dynein is regulated by the tubulin code. *Biophysical journal,* 107**,** 2872-2880.

ALSOP, D. & VIJAYAN, M. M. 2008. Development of the corticosteroid stress axis and receptor expression in zebrafish. *American Journal of Physiology-Regulatory, Integrative and Comparative Physiology,* 294**,** R711-R719.

ANACKER, C., LUNA, V. M., STEVENS, G. S., MILLETTE, A., SHORES, R., JIMENEZ, J. C., CHEN, B. & HEN, R. 2018. Hippocampal neurogenesis confers stress resilience by inhibiting the ventral dentate gyrus. *Nature,* 559**,** 98-102.

AUDIRA, G., SAMPURNA, B. P., JUNIARDI, S., LIANG, S.-T., LAI, Y.-H. & HSIAO, C.-D. 2018. A versatile setup for measuring multiple behavior endpoints in zebrafish. *Inventions,* 3**,** 75.

BÁEZ-MENDOZA, R. & SCHULTZ, W. 2013. The role of the striatum in social behavior. *Frontiers in neuroscience,* 7**,** 233.

BALABANIAN, L., BERGER, C. L. & HENDRICKS, A. G. 2017. Acetylated microtubules are preferentially bundled leading to enhanced kinesin-1 motility. *Biophysical journal,* 113**,** 1551-1560.

CAMBRAY-DEAKIN, M. A. & BURGOYNE, R. D. 1987. Posttranslational modifications of alpha-tubulin: acetylated and detyrosinated forms in axons of rat cerebellum. *The Journal of cell biology,* 104**,** 1569-1574.

CHO, Y. & CAVALLI, V. 2012. HDAC5 is a novel injury-regulated tubulin deacetylase controlling axon regeneration. *The EMBO journal,* 31**,** 3063-3078.

CHU, C.-W., HOU, F., ZHANG, J., PHU, L., LOKTEV, A. V., KIRKPATRICK, D. S., JACKSON, P. K., ZHAO, Y. & ZOU, H. 2011. A novel acetylation of β-tubulin by San modulates microtubule polymerization via down-regulating tubulin incorporation. *Molecular biology of the cell,* 22**,** 448-456.

COLEMAN, A. K., JOCA, H. C., SHI, G., LEDERER, W. J. & WARD, C. W. 2021. Tubulin acetylation increases cytoskeletal stiffness to regulate mechanotransduction in striated muscle. *Journal of General Physiology,* 153.

CONACCI-SORRELL, M., NGOUENET, C. & EISENMAN, R. N. 2010. Myc-nick: a cytoplasmic cleavage product of Myc that promotes α-tubulin acetylation and cell differentiation. *Cell,* 142**,** 480-493.

CREPPE, C., MALINOUSKAYA, L., VOLVERT, M.-L., GILLARD, M., CLOSE, P., MALAISE, O., LAGUESSE, S., CORNEZ, I., RAHMOUNI, S. & ORMENESE, S. 2009. Elongator controls the migration and differentiation of cortical neurons through acetylation of α-tubulin. *Cell,* 136**,** 551-564.

EVEN, A., MORELLI, G., BROIX, L., SCARAMUZZINO, C., TURCHETTO, S., GLADWYN-NG, I., LE BAIL, R., SHILIAN, M., FREEMAN, S. & MAGIERA, M. M. 2019. ATAT1-enriched vesicles promote microtubule acetylation via axonal transport. *Science advances,* 5**,** eaax2705.

GEERAERT, C., RATIER, A., PFISTERER, S. G., PERDIZ, D., CANTALOUBE, I., ROUAULT, A., PATTINGRE, S., PROIKAS-CEZANNE, T., CODOGNO, P. & POÜS, C. 2010. Starvation-induced hyperacetylation of tubulin is required for the stimulation of autophagy by nutrient deprivation. *Journal of Biological Chemistry,* 285**,** 24184-24194.

GIUSTINIANI, J., DAIRE, V., CANTALOUBE, I., DURAND, G., POÜS, C., PERDIZ, D. & BAILLET, A. 2009. Tubulin acetylation favors Hsp90 recruitment to microtubules and stimulates the signaling function of the Hsp90 clients Akt/PKB and p53. *Cellular signalling,* 21**,** 529-539.

HUBBERT, C., GUARDIOLA, A., SHAO, R., KAWAGUCHI, Y., ITO, A., NIXON, A., YOSHIDA, M., WANG, X.-F. & YAO, T.-P. 2002. HDAC6 is a microtubule-associated deacetylase. *Nature,* 417**,** 455-458.

JANKE, C. 2014. The tubulin code: molecular components, readout mechanisms, and functions. *Journal of Cell Biology,* 206**,** 461-472.

KALEBIC, N., SORRENTINO, S., PERLAS, E., BOLASCO, G., MARTINEZ, C. & HEPPENSTALL, P. A. 2013. αTAT1 is the major α-tubulin acetyltransferase in mice. *Nature communications,* 4**,** 1-10.

KAWAMICHI, H., SUGAWARA, S. K., HAMANO, Y. H., MAKITA, K., KOCHIYAMA, T. & SADATO, N. 2016. Increased frequency of social interaction is associated with enjoyment enhancement and reward system activation. *Scientific reports,* 6**,** 1-11.

KIM, C., CHOI, H., JUNG, E. S., LEE, W., OH, S., JEON, N. L. & MOOK-JUNG, I. 2012. HDAC6 inhibitor blocks amyloid beta-induced impairment of mitochondrial transport in hippocampal neurons.

KIM, G.-W., LI, L., GORBANI, M., YOU, L. & YANG, X.-J. 2013. Mice lacking α-tubulin acetyltransferase 1 are viable but display α-tubulin acetylation deficiency and dentate gyrus distortion. *Journal of Biological Chemistry,* 288**,** 20334-20350.

KIMMEL, C. B., BALLARD, W. W., KIMMEL, S. R., ULLMANN, B. & SCHILLING, T. F. 1995. Stages of embryonic development of the zebrafish. *Developmental dynamics,* 203**,** 253-310.

L'HERNAULT, S. W. & ROSENBAUM, J. L. 1983. Chlamydomonas alpha-tubulin is posttranslationally modified in the flagella during flagellar assembly. *The Journal of cell biology,* 97**,** 258-263.

L'HERNAULT, S. W. & ROSENBAUM, J. L. 1985. Chlamydomonas. alpha.-tubulin is posttranslationally modified by acetylation on the. epsilon.-amino group of a lysine. *Biochemistry,* 24**,** 473-478.

LASSER, M., TIBER, J. & LOWERY, L. A. 2018. The role of the microtubule cytoskeleton in neurodevelopmental disorders. *Frontiers in cellular neuroscience,* 12**,** 165.

LEDIZET, M. & PIPERNO, G. 1987. Identification of an acetylation site of Chlamydomonas alpha-tubulin. *Proceedings of the National Academy of Sciences,* 84**,** 5720-5724.

LEUNG, C., CAO, F., NGUYEN, R., JOSHI, K., AQRABAWI, A. J., XIA, S., CORTEZ, M. A., SNEAD III, O. C., KIM, J. C. & JIA, Z. 2018. Activation of

entorhinal cortical projections to the dentate gyrus underlies social memory retrieval. *Cell reports,* 23**,** 2379-2391.

LEWIS, A. S., PITTENGER, S. T., MINEUR, Y. S., STOUT, D., SMITH, P. H. & PICCIOTTO, M. R. 2018. Bidirectional regulation of aggression in mice by hippocampal alpha-7 nicotinic acetylcholine receptors. *Neuropsychopharmacology,* 43**,** 1267-1275.

LI, L., JAYABAL, S., GHORBANI, M., LEGAULT, L.-M., MCGRAW, S., WATT, A. J. & YANG, X.-J. 2019. ATAT1 regulates forebrain development and stress-induced tubulin hyperacetylation. *Cellular and molecular life sciences,* 76**,** 3621-3640.

LOWREY, S., WILSON, C., JOFFE, M., PICCIOTTO, M., CONN, P. J. & LEWIS, A. 2020. Regulation of Aggressive Behavior by Mossy Cells in the Caudal Dentate Gyrus. *Biological Psychiatry,* 87**,** S330.

MACKEH, R., LORIN, S., RATIER, A., MEJDOUBI-CHAREF, N., BAILLET, A., BRUNEEL, A., HAMAÏ, A., CODOGNO, P., POÜS, C. & PERDIZ, D. 2014. Reactive oxygen species, AMP-activated protein kinase, and the transcription cofactor p300 regulate α-tubulin acetyltransferase-1 (αTAT-1/MEC-17)-dependent microtubule hyperacetylation during cell stress. *Journal of Biological Chemistry,* 289**,** 11816-11828.

MORLEY, S. J., QI, Y., IOVINO, L., ANDOLFI, L., GUO, D., KALEBIC, N., CASTALDI, L., TISCHER, C., PORTULANO, C. & BOLASCO, G. 2016. Acetylated tubulin is essential for touch sensation in mice. *Elife,* 5**,** e20813.

NEUMANN, B. & HILLIARD, M. A. 2014. Loss of MEC-17 leads to microtubule instability and axonal degeneration. *Cell reports,* 6**,** 93-103.

NOGALES, E., WHITTAKER, M., MILLIGAN, R. A. & DOWNING, K. H. 1999. High-resolution model of the microtubule. *Cell,* 96**,** 79-88.

NORTH, B. J., MARSHALL, B. L., BORRA, M. T., DENU, J. M. & VERDIN, E. 2003. The human Sir2 ortholog, SIRT2, is an NAD+-dependent tubulin deacetylase. *Molecular cell,* 11**,** 437-444.

OHKAWA, N., SUGISAKI, S., TOKUNAGA, E., FUJITANI, K., HAYASAKA, T., SETOU, M. & INOKUCHI, K. 2008. N-acetyltransferase ARD1-NAT1 regulates neuronal dendritic development. *Genes to Cells,* 13**,** 1171-1183.

OUYANG, C., LI, J., ZHENG, X., MU, J., TORRES, G., WANG, Q., ZOU, M.-H. & XIE, Z. 2021. Deletion of Ulk1 inhibits neointima formation by enhancing KAT2A/GCN5-mediated acetylation of TUBA/α-tubulin in vivo. *Autophagy,* 17**,** 4305-4322.

PORTRAN, D., SCHAEDEL, L., XU, Z., THÉRY, M. & NACHURY, M. V. 2017. Tubulin acetylation protects long-lived microtubules against mechanical ageing. *Nature cell biology,* 19**,** 391-398.

REED, N. A., CAI, D., BLASIUS, T. L., JIH, G. T., MEYHOFER, E., GAERTIG, J. & VERHEY, K. J. 2006. Microtubule acetylation promotes kinesin-1 binding and transport. *Current biology,* 16**,** 2166-2172.

REICHMANN, F., RIMMER, N., TILLEY, C. A., DALLA VECCHIA, E., PINION, J., AL OUSTAH, A., CARRENO GUTIERREZ, H., YOUNG, A. M., MCDEARMID, J. R. & WINTER, M. J. 2020. The zebrafish histamine H3

receptor modulates aggression, neural activity and forebrain functional connectivity. *Acta physiologica,* 230**,** e13543.

SCHLOESSER, R. J., MANJI, H. K. & MARTINOWICH, K. 2009. Suppression of adult neurogenesis leads to an increased HPA axis response. *Neuroreport,* 20**,** 553.

SHIDA, T., CUEVA, J. G., XU, Z., GOODMAN, M. B. & NACHURY, M. V. 2010. The major α-tubulin K40 acetyltransferase αTAT1 promotes rapid ciliogenesis and efficient mechanosensation. *Proceedings of the National Academy of Sciences,* 107**,** 21517-21522.

SMAGIN, D. A., PARK, J.-H., MICHURINA, T. V., PEUNOVA, N., GLASS, Z., SAYED, K., BONDAR, N. P., KOVALENKO, I. N., KUDRYAVTSEVA, N. N. & ENIKOLOPOV, G. 2015. Altered hippocampal neurogenesis and amygdalar neuronal activity in adult mice with repeated experience of aggression. *Frontiers in neuroscience,* 9**,** 443.

SMITH, L. L., BEGGS, A. H. & GUPTA, V. A. 2013. Analysis of skeletal muscle defects in larval zebrafish by birefringence and touch-evoke escape response assays. *JoVE (Journal of Visualized Experiments)***,** e50925.

TSENG, W. 2015. *Neural crest specification by Max's giant associated protein and regulation of microtubule's function by alpha-tubulin acetyltransferase 1 in zebrafish.* Doctor of Philosophy (PHD), University of Georgia.

VAN BODEGOM, M., HOMBERG, J. R. & HENCKENS, M. J. 2017. Modulation of the hypothalamic-pituitary-adrenal axis by early life stress exposure. *Frontiers in cellular neuroscience,* 11**,** 87.

XU, Z., SCHAEDEL, L., PORTRAN, D., AGUILAR, A., GAILLARD, J., MARINKOVICH, M. P., THÉRY, M. & NACHURY, M. V. 2017. Microtubules acquire resistance from mechanical breakage through intralumenal acetylation. *Science,* 356**,** 328-332.

YAN, C., WANG, F., PENG, Y., WILLIAMS, C. R., JENKINS, B., WILDONGER, J., KIM, H.-J., PERR, J. B., VAUGHAN, J. C. & KERN, M. E. 2018. Microtubule acetylation is required for mechanosensation in Drosophila. *Cell reports,* 25**,** 1051-1065. e6.

ZOU, D., CHEN, L., DENG, D., JIANG, D., DONG, F., MCSWEENEY, C., ZHOU, Y., LIU, L., CHEN, G. & WU, Y. 2016. DREADD in parvalbumin interneurons of the dentate gyrus modulates anxiety, social interaction and memory extinction. *Current molecular medicine,* 16**,** 91-102.

FIGURES AND FIGURE LEGENDS

Figure 3.1. The distribution of acetylated α-tubulin in 48hpf *Danio rerio* embryo. Wholemount immunofluorescence of 48hpf wild-type embryos with acetylated α-tubulin-specific 6-11-1B antibody. Acetylated α-tubulin is enriched in ciliated structures olfactory placode (Red arrow), pronephros (Yellow arrow), and neurons (Brown triangle).

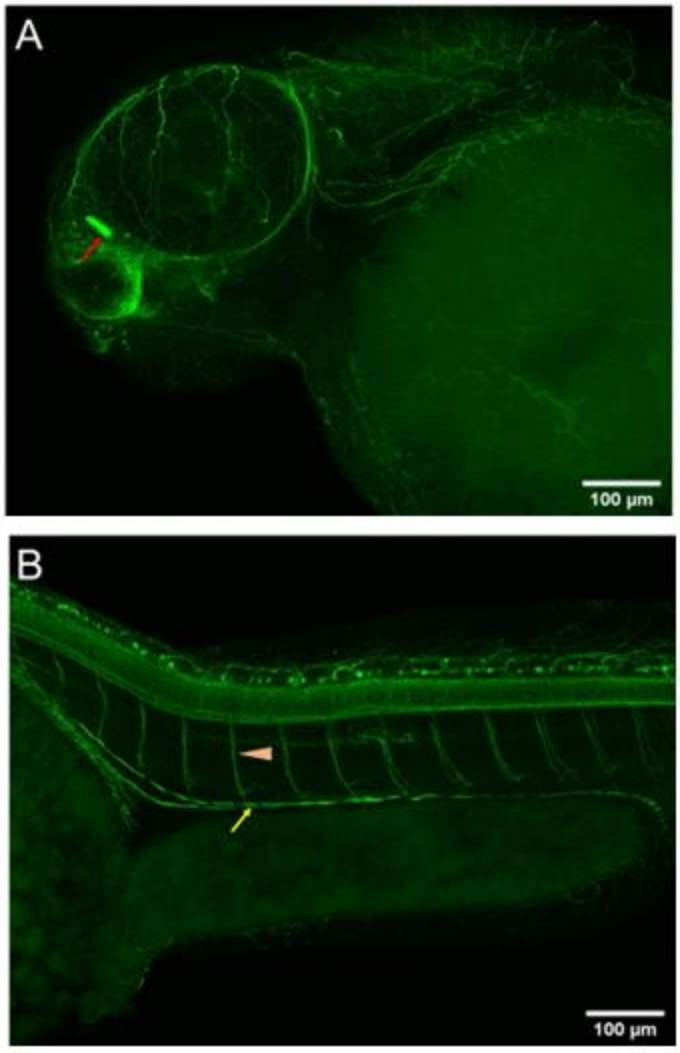
A
100 µm
B
100 µm

Figure 3.2. *atat1* mutant embryos exhibit no apparent defects in primary and secondary motor neurons. Wholemount immunofluorescence of wild-type and *atat1* $^{-/-}$ embryos at 30hpf for primary motor neurons with znp-1 and 72hpf for secondary motor neurons with zn-8.

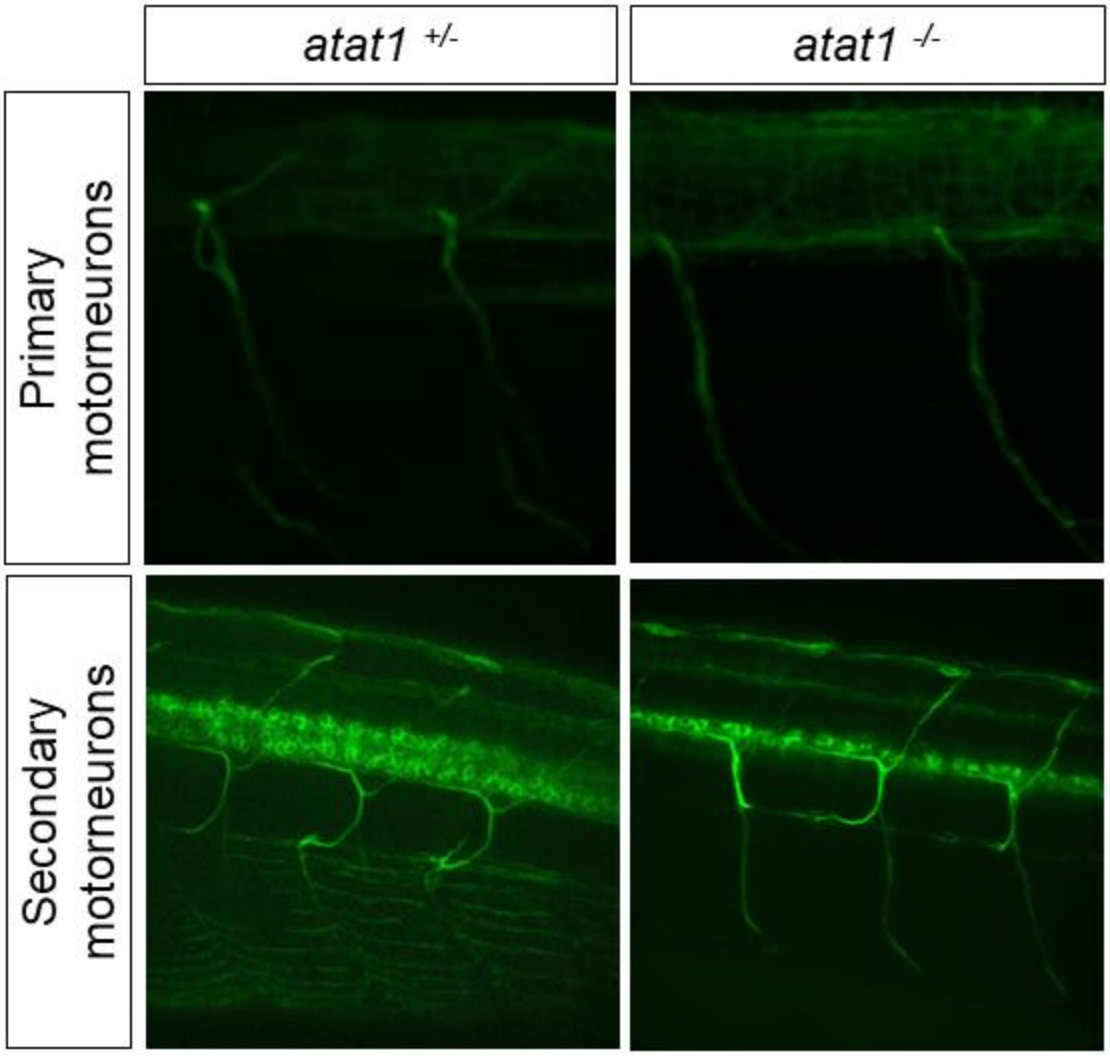
atat1 +/-
atat1 -/-
Primary motorneurons
Secondary motorneurons

Figure 3.3. Touch-evoked swimming behavior of *atat1* mutant embryos. Touch-evoked swimming behavior of *atat1* $^{+/+}$ (n=37), *atat1* $^{-/-}$ (n=38), and *atat1* $^{-/-}$ + mouse *atat-yfp* mRNA injected embryos (n=31) studied at 54hpf. (A). Representative images of swimming path of *atat1* $^{+/+}$, *atat1* $^{-/-}$, and *atat1* $^{-/-}$ + mouse *atat-yfp* mRNA injected embryos (B). Quantification of swimming path length. Videos were analyzed with the ImageJ Animal tracker plugin. All data are shown as mean ± SEM, ANOVA with Tukey's test, p-value<0.05.

A

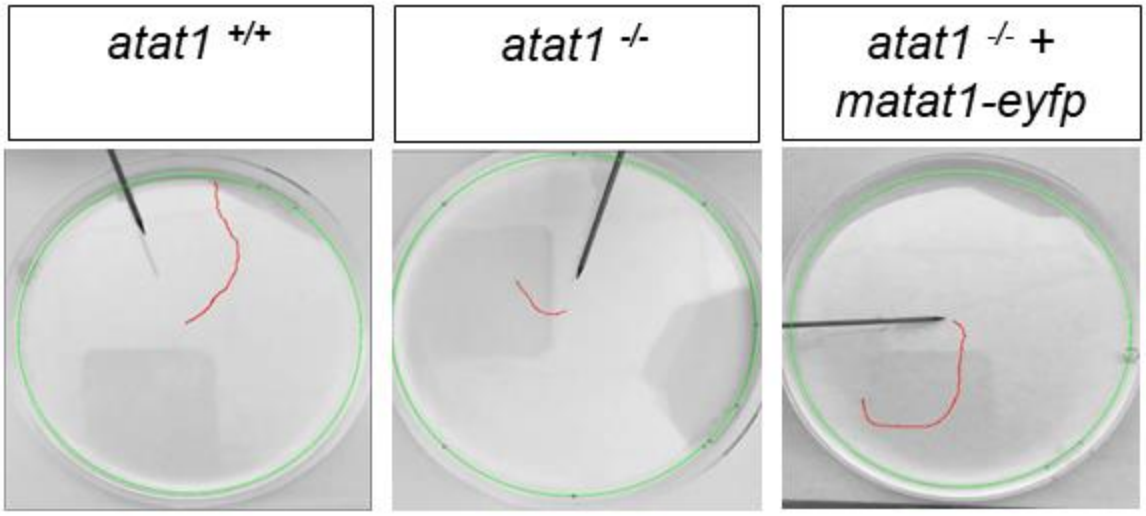
atat1 +/+
atat1 -/-
atat1 -/- +
matat1-eyfp

B

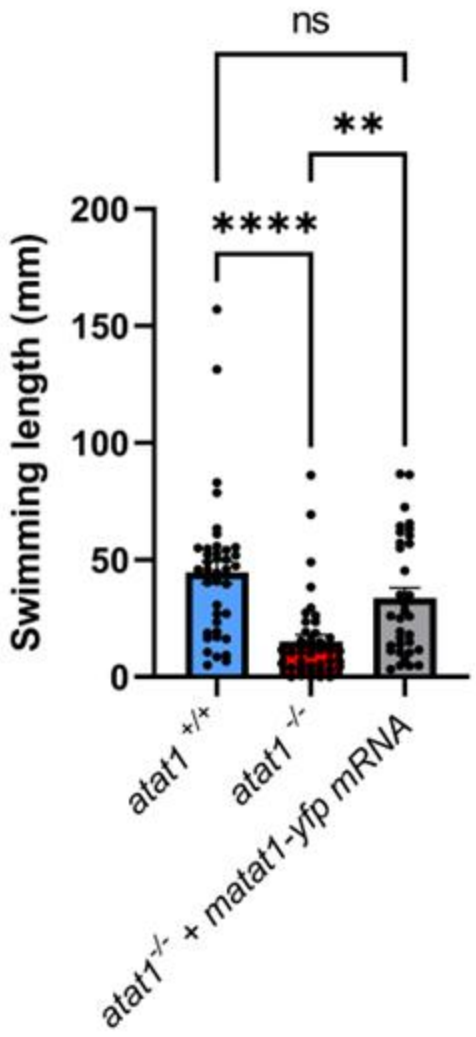
ns
**
****
200
150
100
50
0
Swimming length (mm)
atat1 +/+
atat1 -/-
atat1-/- + matat1-yfp mRNA

Figure 3.4. The behavioral response of *atat* mutants in the novel tank. Six- to eight-month-old siblings *atat1* $^{+/-}$ (n=8) and *atat1* $^{-/-}$ (n=8) fishes were introduced into the novel tank. (A). Representative images of behavior response of *atat1* $^{+/-}$ and *atat1* $^{-/-}$ in the first minute. (B). Latency to enter the upper tank by *atat1* $^{+/-}$ and *atat1* $^{-/-}$ in the novel tank. (C). The proportion of total time spent in the upper tank by *atat1* $^{+/-}$ and *atat1* $^{-/-}$ in the novel tank. (D). Average swimming velocity of *atat1* $^{+/-}$ and *atat1* $^{-/-}$ in the novel tank. Videos were analyzed with the Idtracker. All data are shown as mean ± SEM. ANOVA with Tukey's test, statistical significance- p-value<.0.05.

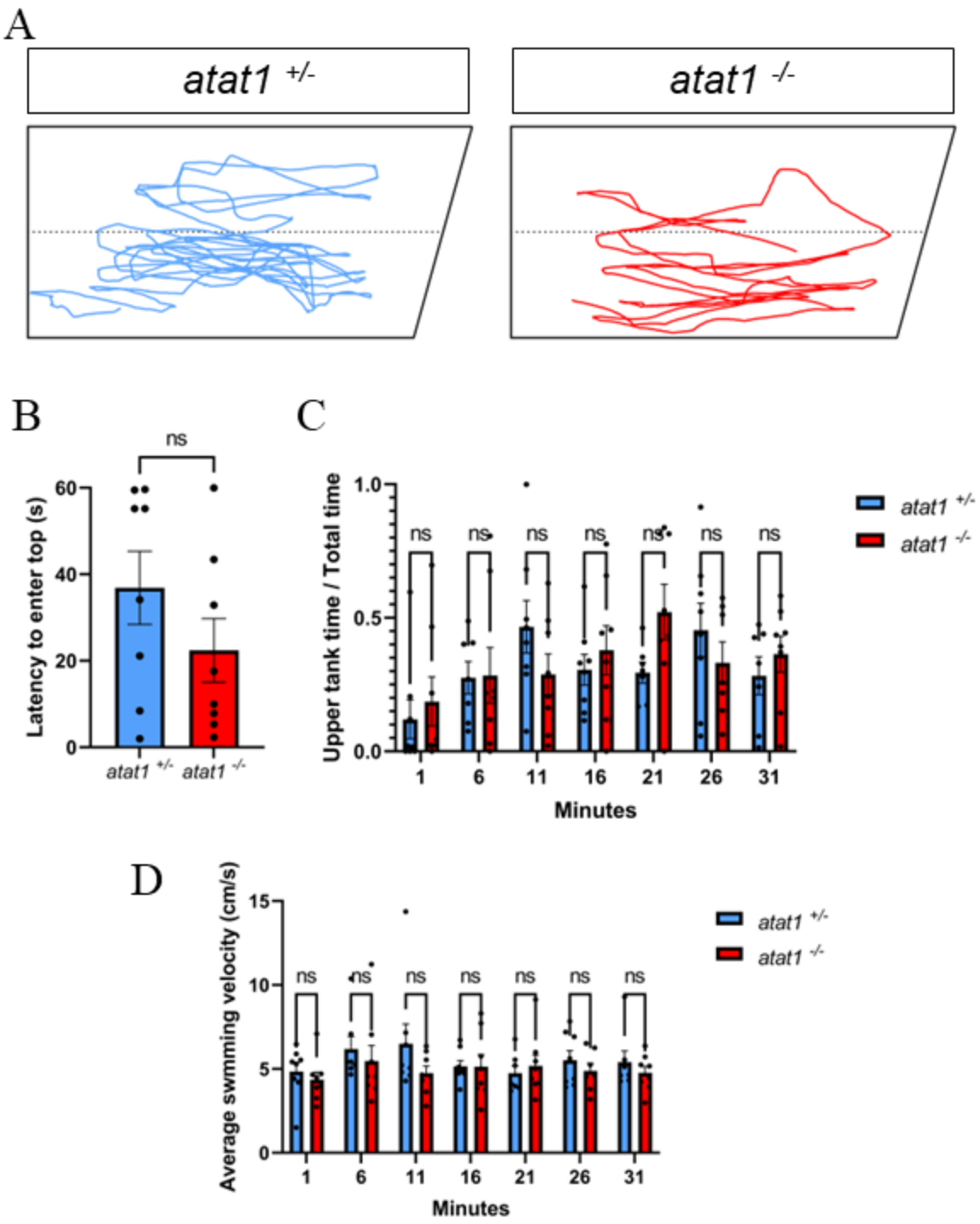
A
atat1 +/-
atat1 -/-
B
ns
Latency to enter top (s)
60
40
20
0
atat1 +/-
atat1 -/-
C
Upper tank time / Total time
1.0
0.5
0.0
ns
1
6
11
16
21
26
31
Minutes
atat1 +/-
atat1 -/-
D
Average swmming velocity (cm/s)
15
10
5
0
ns
1
6
11
16
21
26
31
Minutes
atat1 +/-
atat1 -/-

Figure 3.5. The mirror-biting behavior of *atat1* mutants. Six- to eight-month-old siblings *atat1* $^{+/-}$ (n=8) and *atat1* $^{-/-}$ (n=8) fishes were introduced to a tank with a mirror or no mirror (A). Representative images of behavior response of *atat1* $^{+/-}$ and *atat1* $^{-/-}$ with a mirror or no mirror. (B). The proportion of total time spent in the mirror-biting zone by *atat1* $^{+/-}$ and *atat1* $^{-/-}$ with a mirror or no mirror. (C). The proportion of total time spent in the upper tank by *atat1* $^{+/-}$ and *atat1* $^{-/-}$ with a mirror or no mirror. (D). Average swimming velocity of *atat1* $^{+/-}$ and *atat1* $^{-/-}$ with a mirror or no mirror. Videos were analyzed with the Idtracker. All data are shown as mean ± SEM. ANOVA with Tukey's test, statistical significance- p-value<.0.05.

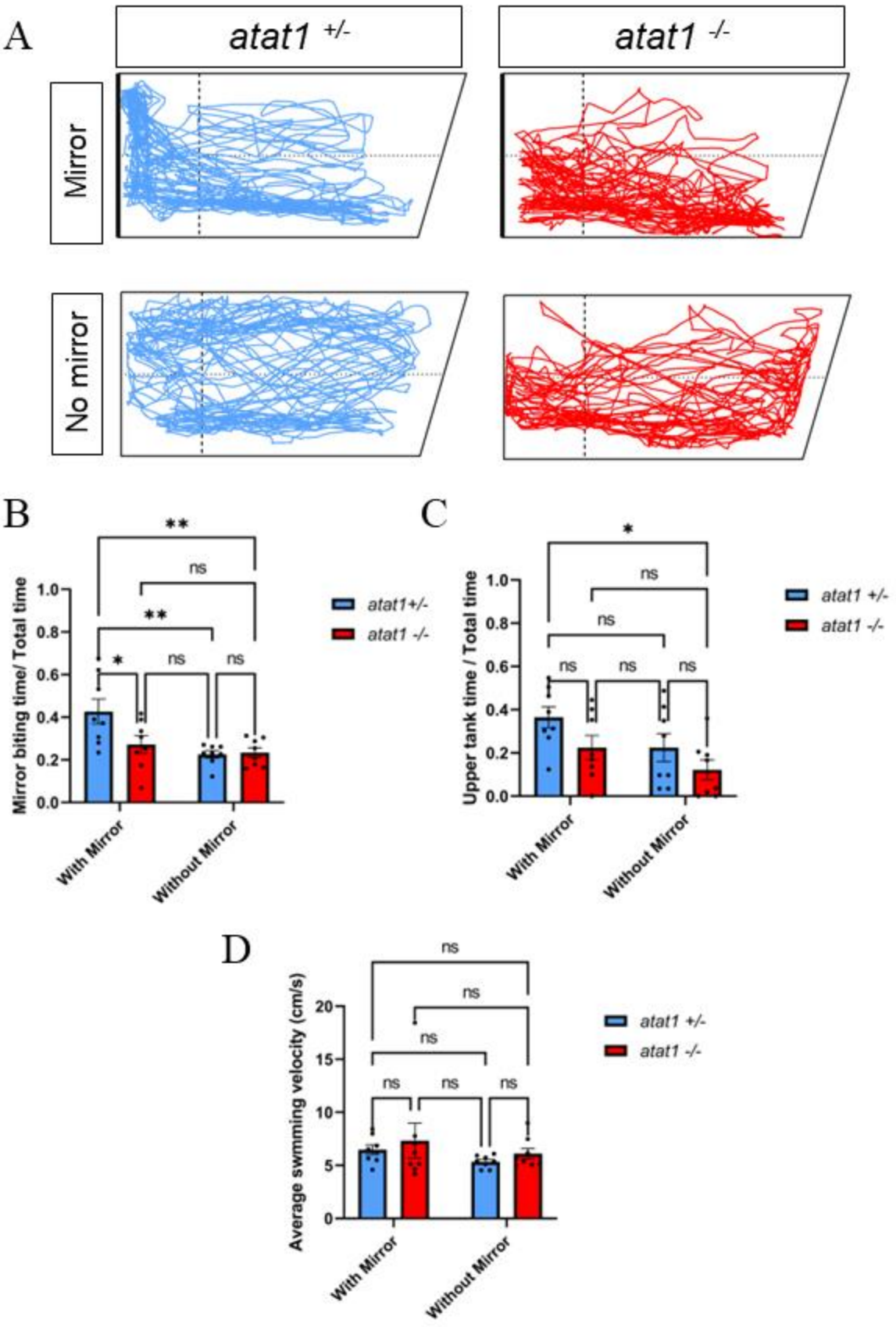
A
atat1 +/-
atat1 -/-
Mirror
No mirror
B
Mirror biting time/ Total time
atat1+/-
atat1 -/-
With Mirror
Without Mirror
C
Upper tank time / Total time
atat1 +/-
atat1 -/-
With Mirror
Without Mirror
D
Average swmming velocity (cm/s)
atat1 +/-
atat1 -/-
With Mirror
Without Mirror

Figure 3.6. The social interaction behavior of *atat1* mutants. Six- to eight-month-old siblings *atat1* $^{+/-}$ (n=9) and *atat1* $^{-/-}$ (n=8) fishes were introduced into a tank with wild-type fish separated by a transparent glass plate. (A). Representative images of social interaction behavior response of *atat1* $^{+/-}$ and *atat1* $^{-/-}$. (B). The proportion of total time spent in the interaction zone by *atat1* $^{+/-}$ and *atat1* $^{-/-}$ during social interaction. (C). The proportion of total time spent in the upper tank by *atat1* $^{+/-}$ and *atat1* $^{-/-}$ during social interaction. (D). Average swimming velocity of *atat1* $^{+/-}$ and *atat1* $^{-/-}$ during social interaction. Videos were analyzed with the Idtracker. All data are shown as mean ± SEM. ANOVA with Tukey's test, statistical significance- p-value<.0.05.

A

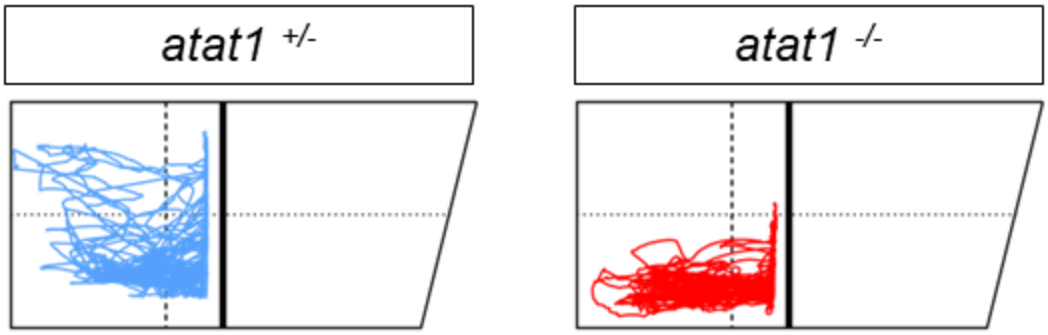
atat1 +/-
atat1 -/-

B

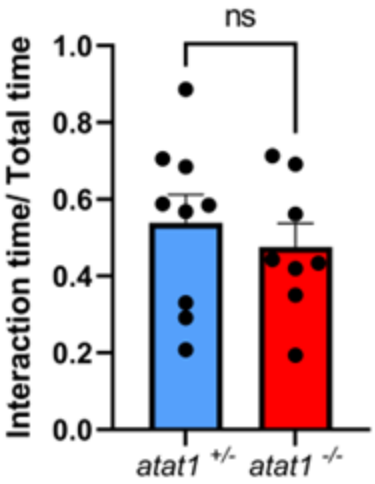
ns
Interaction time/ Total time
1.0
0.8
0.6
0.4
0.2
0.0
atat1 +/-
atat1 -/-

C

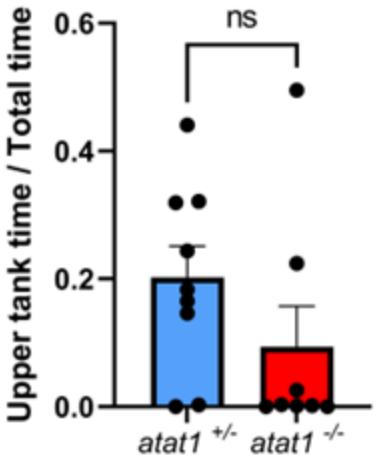
ns
Upper tank time / Total time
0.6
0.4
0.2
0.0
atat1 +/-
atat1 -/-

D

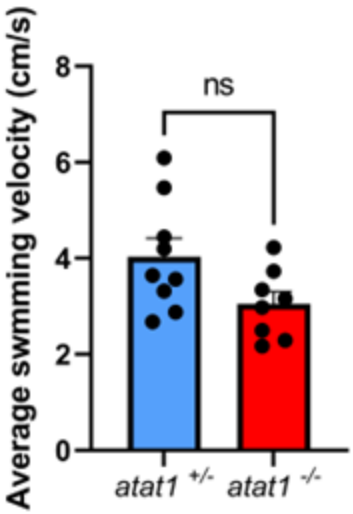
ns
Average swmming velocity (cm/s)
8
6
4
2
0
atat1 +/-
atat1 -/-

Figure 3.7. The shoaling behavior of *atat1* mutants. Six- to eight-month-old three *atat1* $^{+/-}$ (n=4) and *atat1* $^{-/-}$ (n=4) sibling fishes were introduced into a tank. (A). Representative images of shoaling behavior of *atat1* $^{+/-}$ and *atat1* $^{-/-}$. (B). Average shoaling area of *atat1* $^{+/-}$ and *atat1* $^{-/-}$. (C). Average swimming velocity of *atat1* $^{+/-}$ and *atat1* $^{-/-}$ during shoaling. (D). The proportion of total time spent in the upper tank by *atat1* $^{+/-}$ and *atat1* $^{-/-}$ during shoaling. Videos were analyzed with the Idtracker. All data are shown as mean ± SEM. ANOVA with Tukey's test, statistical significance- p-value<.0.05.

A

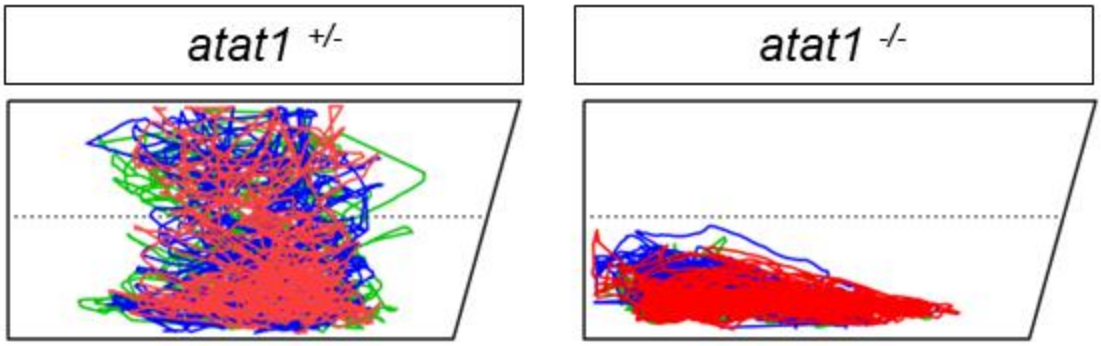
atat1 +/-
atat1 -/-

B

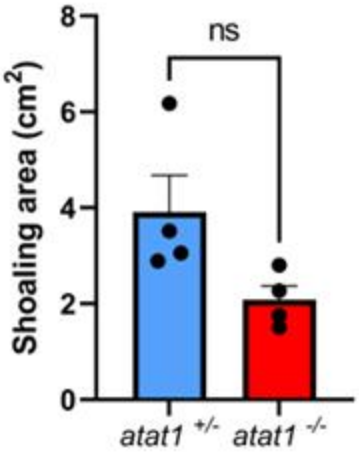
Shoaling area (cm2)
ns
0
2
4
6
8
atat1 +/-
atat1 -/-

C

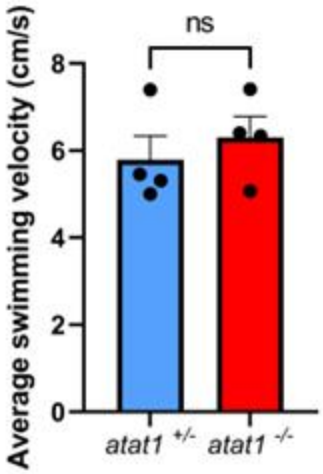
Average swimming velocity (cm/s)
ns
0
2
4
6
8
atat1 +/-
atat1 -/-

D

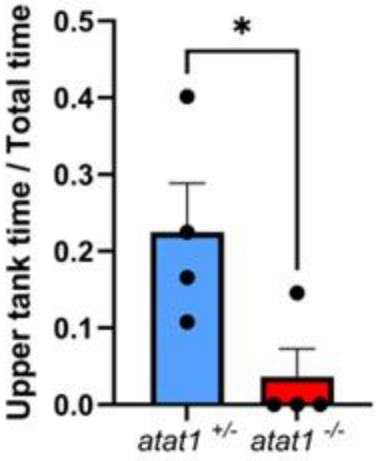
Upper tank time / Total time
*
0.0
0.1
0.2
0.3
0.4
0.5
atat1 +/-
atat1 -/-

Figure 3.8. *atat1* mutant larva show stress-induced hyperacetylation of microtubules. (A). Western blot of acetylated α-tubulin in larva exposed to elevated temperature, osmotic stress, and oxidative stress. (B). Quantification of western blot.

A

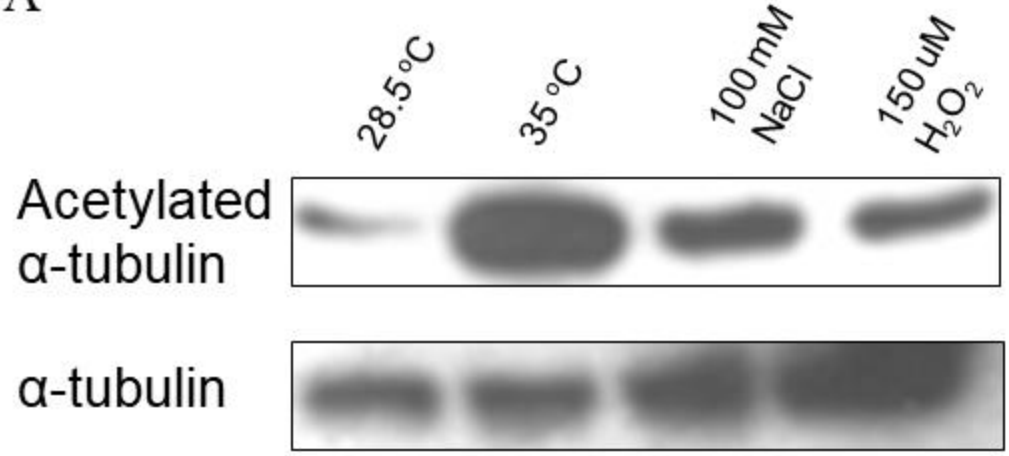
28.5 °C
35 °C
100 mM NaCl
150 uM H_2O_2
Acetylated α-tubulin
α-tubulin

B

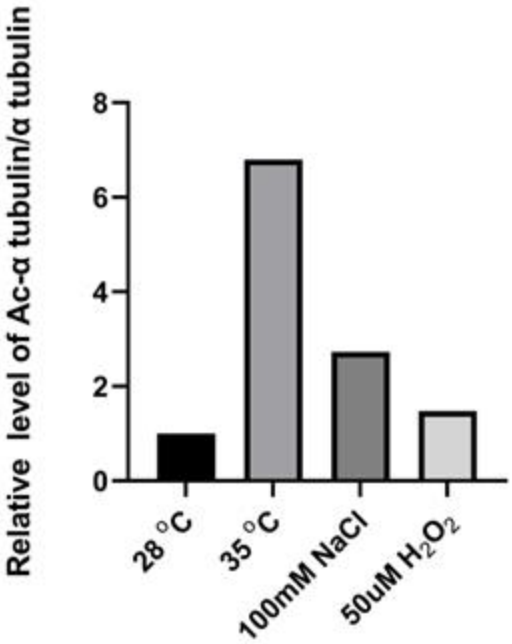
Relative level of Ac-α tubulin/α tubulin
8
6
4
2
0
28 °C
35 °C
100mM NaCl
50uM H_2O_2

Figure 3.9. *atat1* mutant larva show increased susceptibility to stress. (A). *atat1* mutant larva show reduced survival at elevated temperature. (B). *atat1* mutant larva show reduced survival under osmotic stress. (C). *atat1* mutant larva shows comparable survival under oxidative stress.

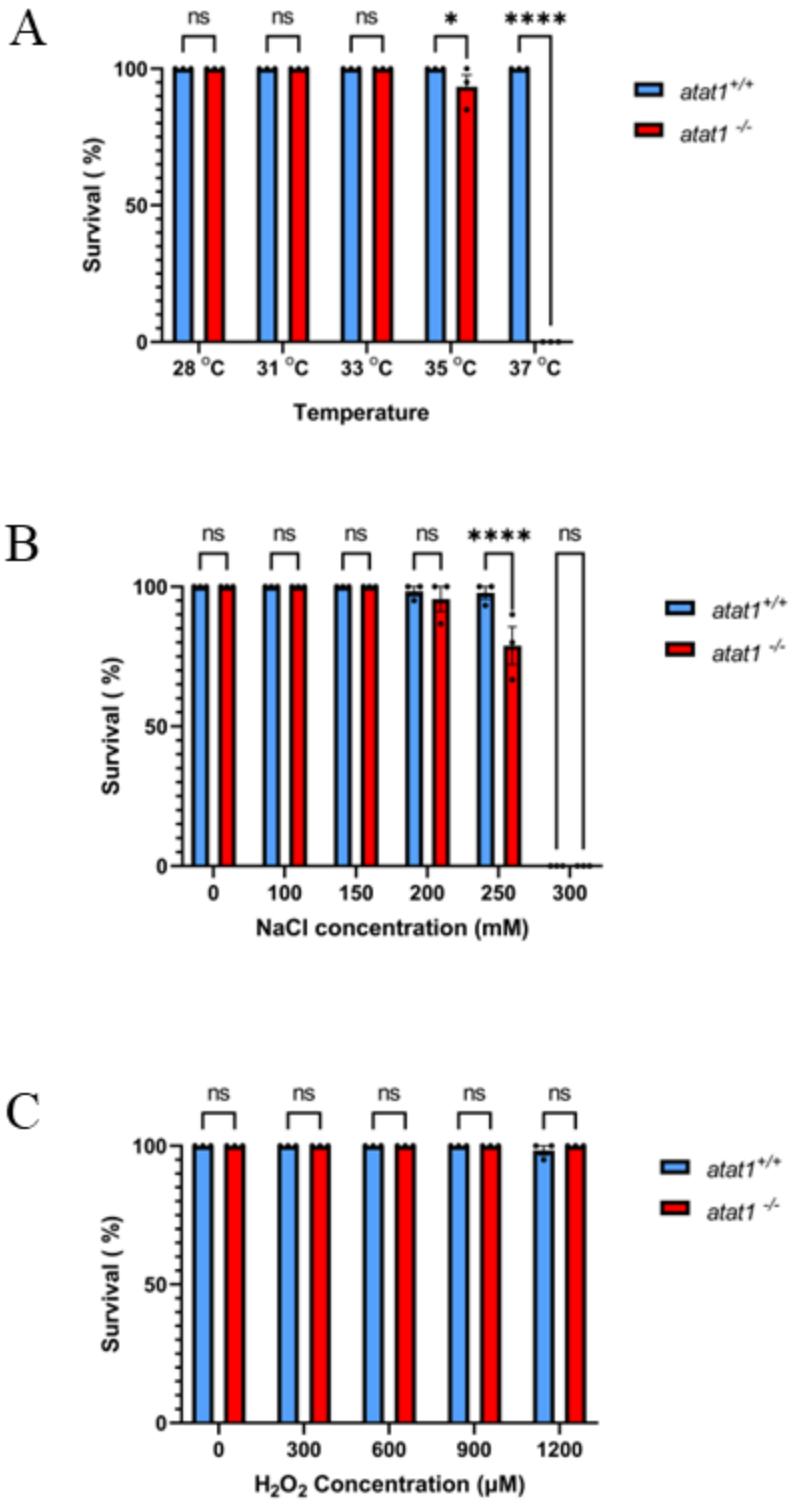
A
ns
ns
ns
*
****
100
50
0
Survival (%)
28 °C
31 °C
33 °C
35 °C
37 °C
Temperature
atat1+/+
atat1 -/-
B
ns
ns
ns
ns
****
ns
100
50
0
Survival (%)
0
100
150
200
250
300
NaCl concentration (mM)
atat1+/+
atat1 -/-
C
ns
ns
ns
ns
ns
100
50
0
Survival (%)
0
300
600
900
1200
H2O2 Concentration (µM)
atat1+/+
atat1 -/-

SUPPLEMENTAL FIGURES

Figure S3.1. *atat1* mutant brain shows no detectable acetylated α-tubulin.


atat1 +/+
atat1 -/-
Acetylated α - tubulin
α- tubulin

Figure S3.2. *atat1* mutant embryos exhibit no apparent defects in sensory or motor neurons and show normal muscle arrangement. (A). Wholemount immunofluorescence of wild-type and *atat1* $^{-/-}$ embryos at 54 hpf for Rohon-Beard neurons with islet-1 antibody (B). Wholemount immunofluorescence of wild-type and *atat1* $^{-/-}$ embryos at 54 hpf for primary motor neurons with znp-1 antibody and secondary motor neurons with zn-8 antibody. (C). Birefringence microscopy of wild-type and *atat1* $^{-/-}$ embryos at 54 hpf.

A

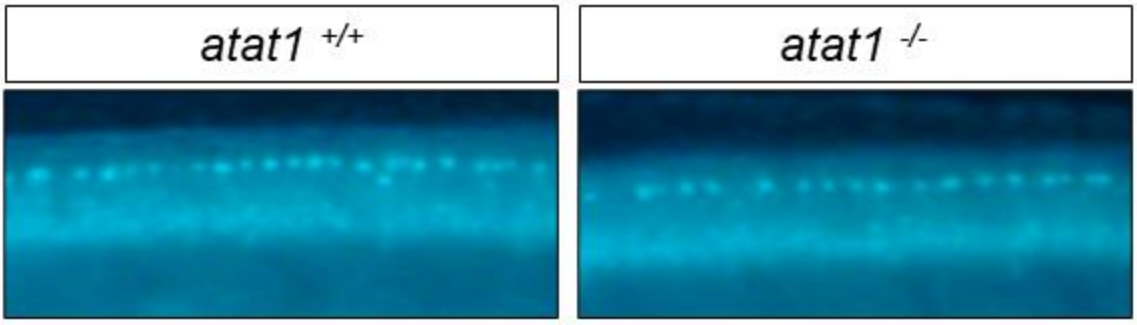
atat1 +/+
atat1 -/-

B

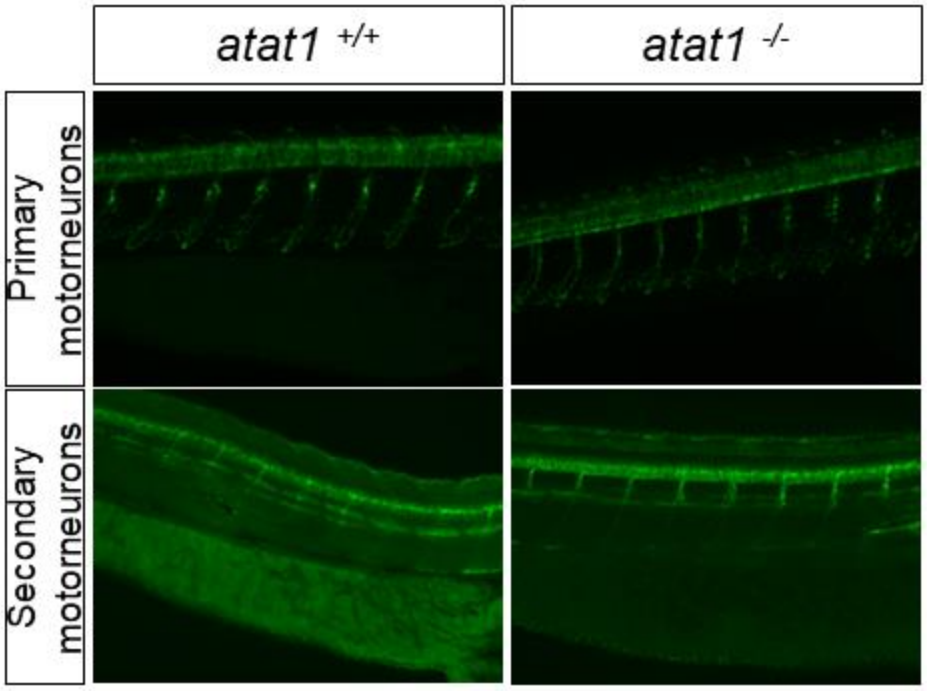
atat1 +/+
atat1 -/-
Primary motorneurons
Secondary motorneurons

C

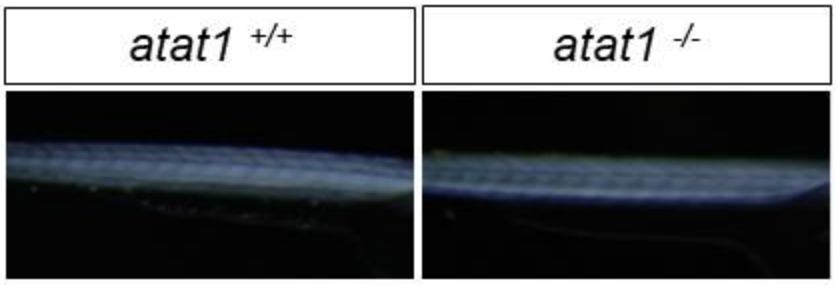
atat1 +/+
atat1 -/-

Figure S3.3. The behavioral response of *atat1* mutants in the novel tank. (A). The proportion of total time spent swimming (Velocity between 1 cm/s -10 cm/s) by *atat1* $^{+/-}$ and *atat1* $^{-/-}$ in the novel tank. (B). The proportion of total time spent in rapid movement (Velocity >10 cm/s) by *atat1* $^{+/-}$ and *atat1* $^{-/-}$ in the novel tank. (C). The proportion of total time spent in freezing movement (Velocity <1 cm/s) by *atat1* $^{+/-}$ and *atat1* $^{-/-}$ in the novel tank. All data are shown as mean ± SEM. ANOVA with Tukey's test, statistical significance- p-value<.0.05.

A

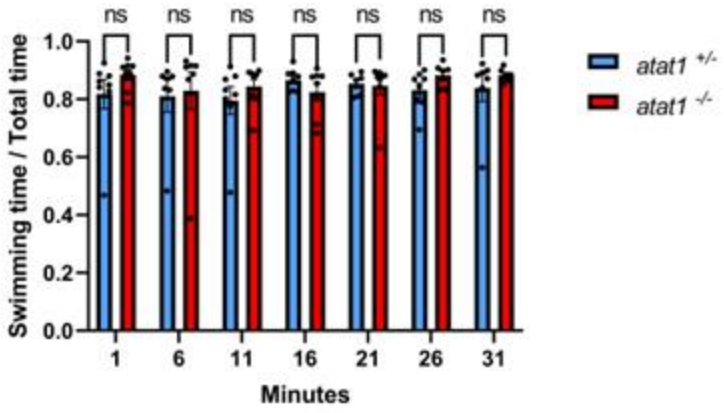
ns
Swimming time / Total time
1.0
0.8
0.6
0.4
0.2
0.0
1
6
11
16
21
26
31
Minutes
atat1 +/-
atat1 -/-

B

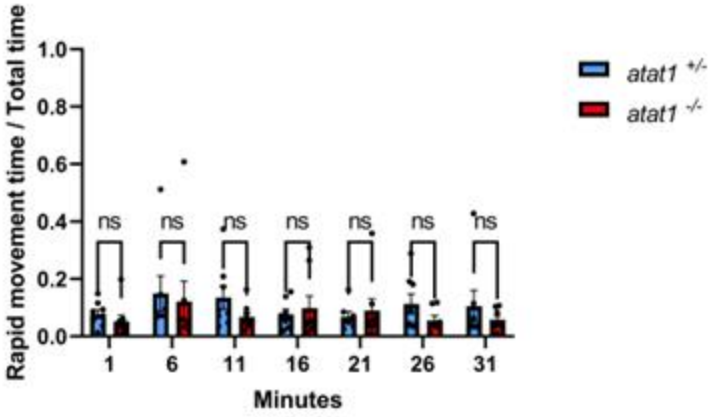
Rapid movement time / Total time
1.0
0.8
0.6
0.4
0.2
0.0
ns
1
6
11
16
21
26
31
Minutes
atat1 +/-
atat1 -/-

C

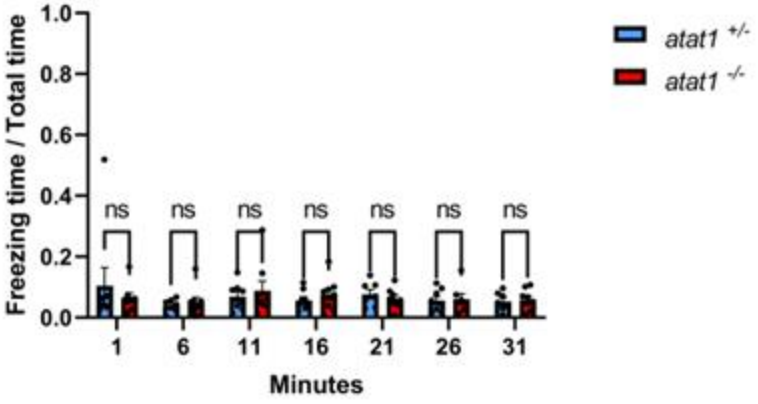
Freezing time / Total time
1.0
0.8
0.6
0.4
0.2
0.0
ns
1
6
11
16
21
26
31
Minutes
atat1 +/-
atat1 -/-

Figure S3.4. The mirror-biting behavior of *atat1* mutants. (A). The proportion of total time spent swimming (Velocity between 1 cm/s -10 cm/s) by *atat1* $^{+/-}$ and *atat1* $^{-/-}$ with a mirror or no mirror. (B). The proportion of total time spent in rapid movement (Velocity >10 cm/s) by *atat1* $^{+/-}$ and *atat1* $^{-/-}$ with a mirror or no mirror. (C). The total time spent in freezing movement (Velocity <1 cm/s) by *atat1* $^{+/-}$ and *atat1* with a mirror or no mirror. All data are shown as mean ± SEM. ANOVA with Tukey's test, statistical significance- p-value<.0.05.

A

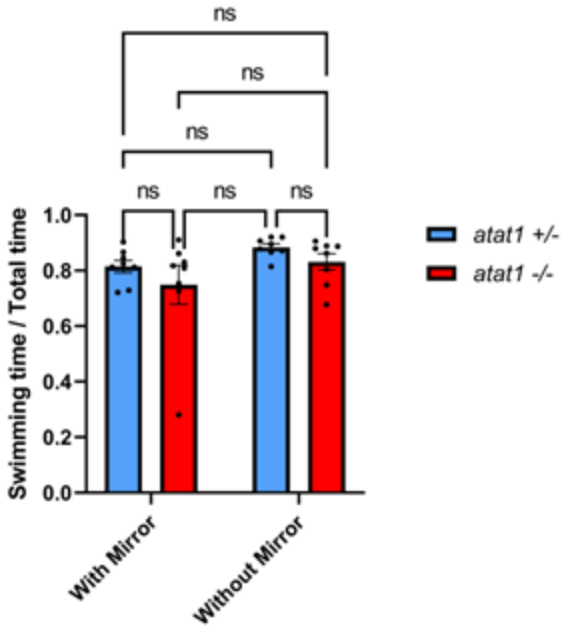
ns
ns
ns
ns
ns
ns
Swimming time / Total time
1.0
0.8
0.6
0.4
0.2
0.0
With Mirror
Without Mirror
atat1 +/-
atat1 -/-

B

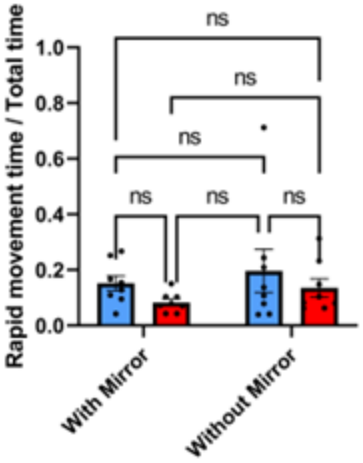
ns
ns
ns
ns
ns
ns
Rapid movement time / Total time
1.0
0.8
0.6
0.4
0.2
0.0
With Mirror
Without Mirror
atat1 +/-
atat1 -/-

C

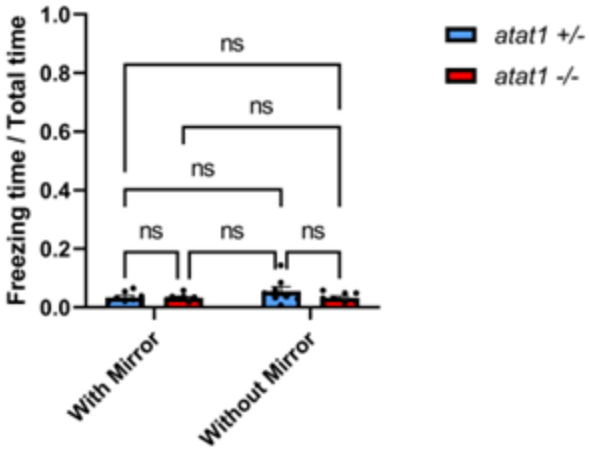
ns
ns
ns
ns
ns
ns
Freezing time / Total time
1.0
0.8
0.6
0.4
0.2
0.0
With Mirror
Without Mirror
atat1 +/-
atat1 -/-

Figure S3.5. The social interaction behavior of *atat1* mutants. (A). The proportion of total time spent swimming (Velocity between 1 cm/s -10 cm/s) by *atat1* $^{+/-}$ and *atat1* $^{-/-}$ during social interaction. (B). The proportion of total time spent in rapid movement (Velocity >10 cm/s) by *atat1* $^{+/-}$ and *atat1* $^{-/-}$ during social interaction. (C). The proportion of total time spent in freezing movement (Velocity <1 cm/s) by *atat1* $^{+/-}$ and *atat1* $^{-/-}$ during social interaction. All data are shown as mean ± SEM. ANOVA with Tukey's test, statistical significance- p-value<.0.05.

A

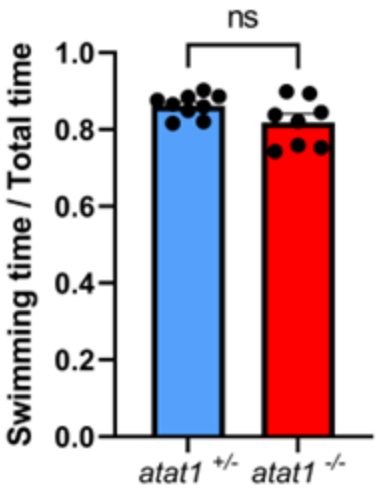
ns
Swimming time / Total time
1.0
0.8
0.6
0.4
0.2
0.0
atat1 +/-
atat1 -/-

B

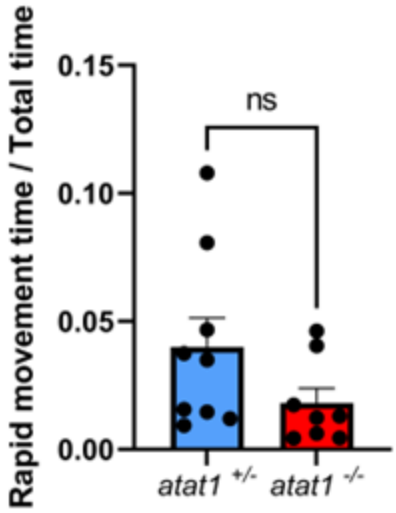
Rapid movement time / Total time
0.15
0.10
0.05
0.00
ns
atat1 +/-
atat1 -/-

C

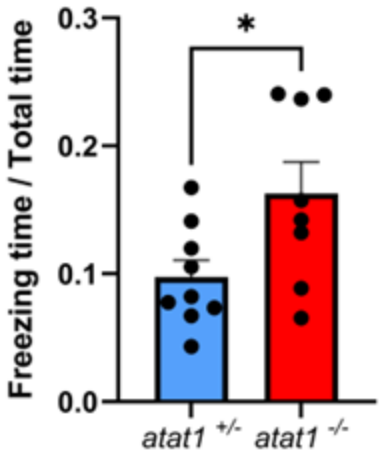
Freezing time / Total time
0.3
0.2
0.1
0.0
*
atat1 +/-
atat1 -/-

Figure S3.6. The shoaling behavior of *atat1* mutants. (A). Average interfish distance of *atat1* $^{+/-}$ and *atat1* $^{-/-}$ during shoaling. (B). Average distance to the center of *atat1* $^{+/-}$ and *atat1* $^{-/-}$ during shoaling. (C). Average farthest distance of *atat1* $^{+/-}$ and *atat1* $^{-/-}$ during shoaling. (D). Average closest distance of *atat1* $^{+/-}$ and *atat1* $^{-/-}$ during shoaling. All data are shown as mean ± SEM. ANOVA with Tukey's test, statistical significance- p-value<.0.05.

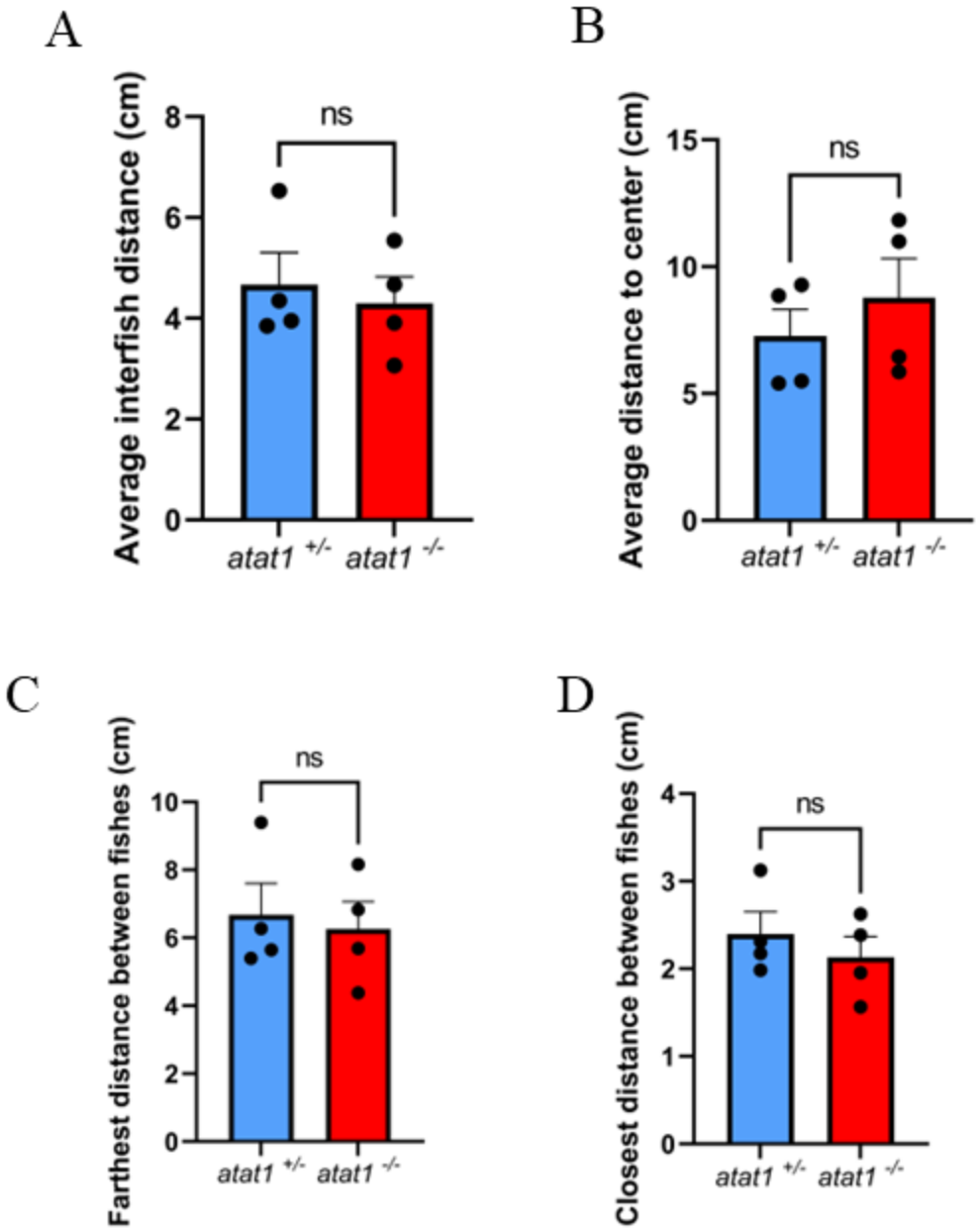
A
Average interfish distance (cm)
ns
0
2
4
6
8
atat1 +/-
atat1 -/-
B
Average distance to center (cm)
ns
0
5
10
15
atat1 +/-
atat1 -/-
C
Farthest distance between fishes (cm)
ns
0
2
4
6
8
10
atat1 +/-
atat1 -/-
D
Closest distance between fishes (cm)
ns
0
1
2
3
4
atat1 +/-
atat1 -/-

Figure S3.7. *atat1* larva does not show an elevated cortisol level in response to elevated temperature.

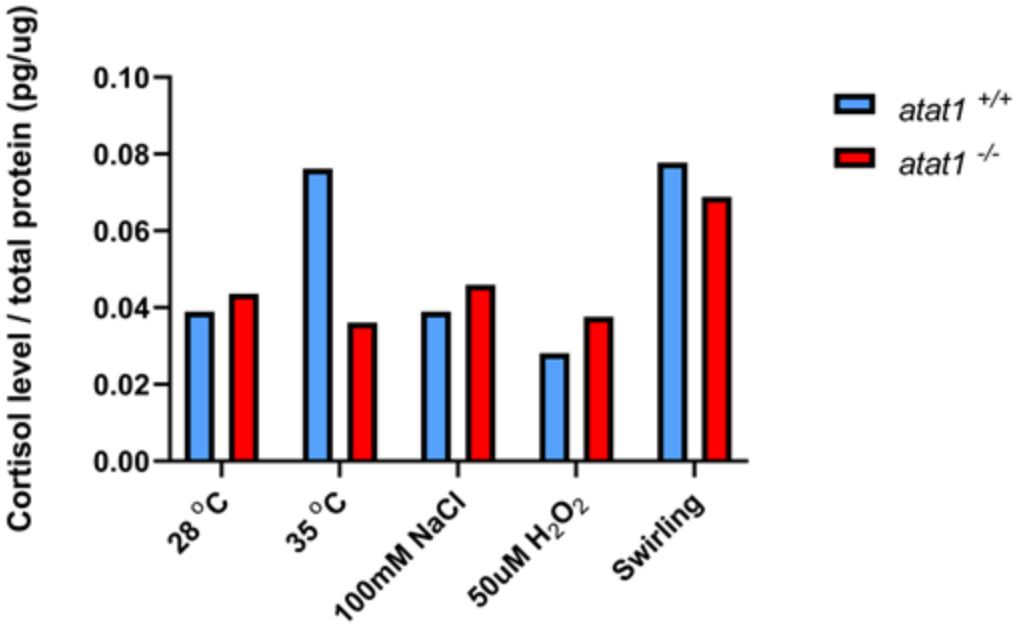
Cortisol level / total protein (pg/ug)
0.10
0.08
0.06
0.04
0.02
0.00
28 °C
35 °C
100mM NaCl
50uM H2O2
Swirling
atat1 +/+
atat1 -/-

CHAPTER 4

GENERATION OF ZEBRAFISH MUTANTS THAT LACKS MICROTUBULE PTMS DETYROSINATION/TYROSINATION AND GLUTAMYLATION USING CRISPR/CAS9 RNP MUTAGENESIS

INTRODUCTION

Microtubules are one of the key cytoskeletons in eukaryotes. Microtubules carry out a wide range of functions, including the formation of microtubule spindle during cell division, intracellular transportation, cell motility, and forming subcellular structures like the axonemal of cilia and axons in neurons. A diverse set of microtubules are generated in cells to carry out these diverse functions using different tubulin isotypes and posttranslational modifications (PTMs), collectively called "Tubulin code" (Janke, 2014). Many microtubule PTMs have been identified over the years, and the enzymes that carry out these modifications have been characterized. The C-terminal tail (CTTs) of tubulins is an active region for microtubule PTMs. Major microtubule PTMs like detyrosination and glutamylation take place in CTTs of tubulins.

Microtubule detyrosination and glutamylation are enriched in stable microtubules of ciliary axonemes and neuronal axons, indicating their potential role in ciliary and neuronal functions (Mary et al., 1996, Poole et al., 2001, Edde et al., 1990, Fouquet et al.,

1994). Depleting microtubule glutamylation resulted in short cilia length and altered axonemal architecture in many model organisms (Ikegami et al., 2010, Vogel et al., 2010, Lee et al., 2013, Wloga et al., 2008, Suryavanshi et al., 2010). In zebrafish, morpholino knockdown of *ttll6* and *ttll11* resulted in phenotypes associated with defective cilia, including curved body axis and pronephric cyst (Pathak et al., 2007, Mathieu et al., 2021). Even though microtubule detyrosination is enriched in the ciliary axoneme, its importance in ciliary function is unknown. Both microtubule glutamylation and detyrosination play important roles during neurogenesis, neuronal differentiation, and migration (Aillaud et al., 2017, Pagnamenta et al., 2019, Ikegami et al., 2006, Ikegami et al., 2007). They are also shown to play roles in axonal transportation (McKenney et al., 2016, Tas et al., 2017, Guardia et al., 2016, Lessard et al., 2019, Maas et al., 2009, Bodakuntla et al., 2021).

VASH1 and VASH2 carry out removal of terminal tyrosine of α-tubulin (Aillaud et al., 2017, Nieuwenhuis et al., 2017). Further removal of terminal residues by cytosolic carboxypeptidases (CCPs) from detyrosinated tubulin results in Δ2 and Δ3 microtubules (Paturle-Lafanechere et al., 1991, Berezniuk et al., 2013, Rogowski et al., 2010, Tort et al., 2014). Retyrosination of α-tubulin is carried out by TTL (Raybin and Flavin, 1977, Ersfeld et al., 1993). Both α- and β-tubulin undergo glutamylation, taking place in two steps. Initially, single glutamate is added to the γ-carboxyl group of glutamic acid residues of CTT of tubulin as a branching point. Microtubule glutamylation initiase enzymes TTLL4, TTLL5, and TTLL7 carry out this step (Van Dijk et al., 2007, Ikegami and Setou, 2009). Further addition of glutamates to the branching point glutamic acid by elongases belonging to Tubulin tyrosin ligase-like (TTLL) family members (Van Dijk et

al., 2007). Deglutamylation is carried out by cytosolic carboxypeptidases (CCPs) (Rogowski et al., 2010).

To understand the roles of microtubule detyrosination and glutamylation during embryogenesis and in ciliary and neuronal functions, we used CRISPR-CAS9 RNP meditated mutagenesis to generate mutants of enzymes that carry out these modifications. We generated mutant alleles of *vash1* and *vash2* that encodes the microtubule detyrosination enzymes. Double mutant of *vash1; vash2* confirms that VASH1 and VASH2 as major microtubule detyrosination enzymes in zebrafish. This double mutant shows residual levels of microtubule detyrosination potentially due to genetically encoded TUBA7l isotype lacking terminal tyrosine. These double mutants showed evidence of defects in neuronal and ciliary function. We also made mutant alleles of *ttl* that encodes the microtubule retyrosination enzyme. Unlike mice *Ttl* mutants, zebrafish mutants survived into adulthood. This mutant showed a strong increase in detyrosinated tubulin and low penetrance curved body and heart edema phenotype. We also generated mutants of microtubule glutamylation initiases *ttll4, ttll5*, and *ttll7*. These mutants and double mutants of these genes did not result in overt morphological defects. These detyrosination/ tyrosination and glutamylation mutants must be further studied to understand the effect of losing these genes on ciliary and neuronal functions and survival in zebrafish.

MATERIAL AND METHODS

Zebrafish Maintenance, Embryo Collection, and Adult Tissue Collection

Zebrafish lines were maintained in Paul D. Coverdell Biomedical Center fish facility following Institutional Animal Care, and Use Committee (IACUC) of the University of Georgia approved Animal Use Protocols (AUPs) A2014 07-005-Y3-A6, A2017 08-020-Y3-A0 and A2020 08-002-Y1-A0. Fishes were crossed in single or multiple-pair mating. Embryos were collected and raised at 28.5 ^{o}C in egg water (60 µg/ml Instant Ocean sea salt and 0.3 µg/ml Methylene Blue). Embryos used in immunofluorescence were treated with 1-phenyl 2-thiourea to maintain optical clarity. As previously described, embryos were staged using a Leica S6E stereomicroscope (Leica Microsystems, Germany) (Kimmel et al., 1995). Appropriately aged fishes were euthanized for adult tissue collection by rapid chilling in ice water.

gRNA synthesis and microinjection

gRNAs for each gene were designed using CHOPCHOP v3 online tool (Labun et al., 2019). PCR amplified (Tables) DNA templates were used for gRNA synthesis. gRNAs were synthesized with 1 µg of PCR amplicon using a MEGAshortscript^{TM} T7 transcription kit (Life Technologies, Carlsbad, CA). A ribonucleoprotein complex of gRNAs and Cas9 with nuclear localization signal (NLS) (CP01-50, PNA Bio, Newbury Park, CA) was directly microinjected into 1-cell stage wild-type zebrafish embryos. A mixture of 400 pg Cas9 with NLS, 250 pg of gRNA, and 0.1 % phenol red was used for injection. Unfertilized eggs and dead embryos were discarded around 5hpf.

Genomic DNA Extraction

Genomic DNA extraction was performed with either 72hpf larva or fin clips from adult fishes. Samples were initially incubated with DNA extraction buffer (10 mM Tris pH 8.2, 10 mM EDTA, 200 mM NaCl, and 0.5% SDS) at 95 ^{o}C for 20 minutes before the addition of 200 µg/ ml proteinase K. This step was followed by incubation at 55 ^{o}C for 16 hours. Finally, proteinase K activity was terminated with incubation at 95 ^{o}C for 20 minutes. Extracted DNA was stored at -20 ^{o}C and diluted 25 times before the used as a template in PCR reactions.

Screening of Mutants and Genotyping

Eight gRNA and Cas9 injected adult fishes (F_0) were outcrossed to wild-type fishes to obtain F1 embryos with germline transmitted mutant alleles. Adult F1 fishes were screened for mutant alleles by amplifying PCR amplicon with primers (Table), including the gRNA target sites, and products were resolved on 15% polyacrylamide gel as previously reported (VanLeuven et al., 2018). Potential mutant alleles identified in screening were confirmed with DNA sequencing (Eurofins Genomics, Louisville, KY). The same primers used for screening were used for subsequent genotyping. F1 fishes with the same mutant alleles were crossed to generate F2 generation. Adult F2 fishes were genotyped, and mutant fishes were identified to establish a mutant fish line.

Total RNA extraction

Total RNA extraction was performed with embryos, larva, and adult tissues. Total RNA was extracted by homogenizing the samples with TRIzol reagent (Life Technologies,

Carlsbad, CA), followed by chloroform extraction and total RNA precipitation with isopropanol. Total RNA preparation was treated with DNAase to eliminate any genomic DNA with TURBO DNA-*free* Kit (Life Technologies, Carlsbad, CA). Total RNA was quantified using NanoDrop 2000 (Thermo Scientific, Waltham, MA) and stored at -80 ^{o}C.

Reverse Transcriptase (RT) PCR and qRT-PCR

First-strand cDNA was synthesized using the RevertAid First Strand cDNA synthesis kit (ThermoFisher Scientific, Waltham, MA) per the manufacturer's instruction. 500 ng of total RNA was used as the template for first-strand cDNA synthesis. PCR reactions were carried out with 1 µl of first-strand cDNA. The level of glutamylation gene transcripts was determined using primers in Table 2. The *gadph* gene was used as a control. RT-PCR was carried out with PCR conditions as follows: initial denaturation- 94^{o}C for 2 minutes, 35cycles of denaturation- 94^{o}C for 20 seconds, annealing- 51^{o}C for 20 seconds, extension- 72^{o}C for 30 seconds and final extension: 72^{o}C for 5 minutes. Amplified PCR products were resolved on 2% agarose gel.

Immunofluorescence

Zebrafish embryos were fixed in fresh 4% paraformaldehyde in PBT (1x PBS, 0.5% Triton X-100) overnight incubation at 4 ^{o}C. Fixed specimens were gradually dehydrated and stored in 100% methanol at -20 ^{o}C until the use. Specimens were gradually rehydrated and washed with PBT before being blocked for 2 hours in blocking reagent (2% Bovine Serum Albumin, 1% DMSO, 0.5% Triton X-100, 0.5% Normal Goat Serum in 1X PBS). Specimens were incubated with primary and secondary antibodies in

blocking reagent overnight at 4 ^{o}C. Primary antibodies used were mouse monoclonal anti-detyrosinated tubulin antibody AA12 (1:500), mouse monoclonal anti-monoglutamylated tubulin GT355 (1:500), mouse monoclonal ZNP-1 (1:200) and mouse monoclonal ZN-8 (1:200). FITC conjugated anti-mouse IgG (1:500) was used as the secondary antibody. Imaging was done with either Zeiss AXIO Imager D2 compound fluorescence microscope or Zeiss LSM 880 confocal microscope (Carl Zeiss, Germany).

Western blots

Protein extraction was carried out by homogenizing deyolked larvae and adult tissues with lysis buffer (RIPA buffer (Sigma-Aldrich, St. Louis, MO), NaF, Na3VO4, Protease inhibitor) followed by centrifugation to removed cell debris. Protein concentration was determined using the Pierce BCA Protein Assay kit as the manufacturer's protocol (Thermo Scientific, Waltham, MA). SDS-PAGE was carried out on 4%-20% precast gel (Bio-Rad Laboratories, Hercules, CA) with 10 µg of total protein in each sample. Resolved proteins were transferred to the Hybond-P PVDF membrane (GE Healthcare, Piscataway, NJ). Membranes were incubated at 4 ^{o}C overnight with primary antibodies at dilutions as follows: mouse monoclonal anti-detyrosinated tubulin antibody AA12 (1:2000), mouse monoclonal anti-monoglutamylated tubulin antibody GT335 (1:2000), and mouse monoclonal anti-acetylated tubulin 6-11-1B (1:2000). Primary antibody incubation followed by incubation with HRP-conjugated anti-mouse IgG secondary antibody at 4 ^{o}C overnight. Following secondary antibody incubation, blots were treated with Clarity Western ECL substrate (Bio-Rad Laboratories, Hercules, CA) and detected X-OMAT LS films (Carestream, Rochester, NY).

RESULTS

Detyrosinated microtubules enriched in ciliated and neuronal tissues in developing zebrafish embryos

In *Danio rerio*, detyrosinated microtubules are enriched in ciliated and neuronal structures (Figure 4.1). At 54hpf, this modification was seen in pronephros mutlicilia, ependymal cilia and olfactory placode cilia, lateral line system, and neurons. Enrichment of detyrosinated microtubules in ciliary structures and neurons in multiple tissues suggests a potential role of this modification in the assembly and maintenance of cilia and in neurogenesis and neuronal functions. Genes encoding detyrosination enzymes *vash1* and *vash2* and tyrosination enzyme *ttl* are expressed maternally and zygotically (Figure S4.1A). All these genes were expressed in the brain, testis, ovary, kidney, heart, gut, and liver tissues (Figure S4.1B).

Generation of *vash1*, *vash2,* and *ttl* mutants using CRISPR/Cas9 mutagenesis

To understand the roles of microtubule detyrosination and tyrosination in zebrafish embryonic development, ciliogenesis, ciliary function, neurogenesis, and neuronal functions, we generated mutants of *vash1*, *vash2,* and *ttl* genes. We used CRISPR-Cas9 RNP-based mutagenesis to increase the efficiency of generating mutants (Figure 4.2). We injected in vitro synthesized gRNA specific for target genes, mixed it with Cas9 protein, and injected the mixture into 1- cell stage embryos.

To generate a mutant of *vash1,* we designed gRNA to target exon 1, and the indel should take place in the vasohibin domain (Figure 4.3A). We identified three mutants alleles, a 5

bp insertion (*vash1*^{ga243}), a 7 bp deletion allele (*vash1*^{ga244}) and a 2 bp deletion allele (*vash1*^{ga245}). Further studies were carried out with *vash1*$^{ga243\ -/-}$. These *vash1* mutant embryos or adults showed no obvious morphological defects (Figure 4.4).

We targeted exon 1 of *vash2* to generate *vash2* mutant (Figure 4.3B). We identified three mutants alleles, a 25 bp deletion (*vash2*^{ga246}), a 10 bp deletion allele (*vash2*^{ga247}) and a 14 bp deletion allele (*vash2*^{ga250}). Further studies were carried out with *vash2*$^{ga250\ -/-}$. These *vash2* mutant embryos or adults did not show any obvious morphological defects (Figure 4.4)

We also generated *ttl* mutants by targeting exon 1 of the *ttl* gene (Figure 4.3C). We identified three mutants alleles, a 17 bp insertion (*ttl*^{ga253}), an 8 bp insertion allele (*ttl*^{ga254}), and a 51 bp insertion allele (*ttl*^{ga256}) that has a premature stop codon. *ttl*$^{ga256\ -/-}$ used for further studies. Most of the *ttl* mutant embryos showed no obvious morphological defects (Figure 4.4A). We observed the low penetrance of heart edema (39.1 %), in some cases with curved body axis (21.7 %), and edema in hydrocephalus phenotypes (8.7%) (Figure 4.4A). Adult mutants did not show any obvious morphological defects (Figure 4.4 B).

We generated a double mutant of both *vash1* and *vash2* genes. This *vash1*$^{ga243\ -/-}$; *vash2*$^{ga250\ -/-}$ showed low penetrance heart edema phenotypes (33.3 %), in some cases with curved body axis (18.1 %) and microcephaly (12.1 %). (Figure 4.4A). Adult mutants did not show any obvious morphological defects (Figure 4.4B).

Vasohibin-1 and Vasohibin-2 are the major microtubule detyrosination enzymes in zebrafish

To understand whether VASH1 and VASH2 are responsible for the microtubule detyrosination, we extracted proteins from the brain and testis of single and double mutants of these genes and carried out a western blot with an antibody that specifically recognizes detyrosinated microtubules. All single and double mutants showed a reduction in the level of detyrosinated microtubules compared to the wild-type level (Figure S4.2A). In testis, *vash1* single mutant, *vash2* single mutant, and *vash1*; *vash2* double mutants show 20 %, 35 %, and 88 % reduction in microtubule detyrosination compared to wild type (Figure S4.3). In brain, *vash1* single mutant, *vash2* single mutant, and *vash1*; *vash2* double mutants show 73 %, 53 %, and 90 % reduction in microtubule detyrosination compared to wild type (Figure S4.2A). The residual level of detyrosinated microtubule could be due to the gene-encoded tubulin isotypes that lack terminal tyrosine, but the presence of additional microtubule detyrosinating enzymes is also possible. A similar residual detyrosinated microtubule in *vash1* $^{-/-}$; *vash2* $^{-/-}$ mammalian cell lines was reported (Nieuwenhuis et al., 2017). This result indicates that VASH1 And VASH2 are the major enzymes responsible for most microtubule detyrosination in zebrafish.

We also carried out a western blot with an antibody that specifically recognizes detyrosinated microtubules with protein preparations from wild-type and *ttl* $^{-/-}$ brains. We found 13 times more detyrosinated microtubules in *the ttl -/- brain than* in the wild type (Figure S4.2B).

The level of detyrosination regulates the level of synaptotagmin-2 labeling in primary motor neurons

We studied primary motor neurons in single and double mutants of microtubules detyrosination genes, and we did not find any defect or delay in neurogenesis. Both primary motor neurons showed comparable progress in neurogenesis and morphogenesis (Figure 4.5). Interestingly we found that antibody labeling by znp-1 is lower in single and double mutants of vasohibin genes (Figure 4.5). Znp-1 is an antibody against synaptotagmin 2, a synaptic vesicle membrane-associated protein. This observation raises the possibility of alteration in axonal transportation in these mutants. Interestingly, *ttl* $^{-/-}$ mutant showed abnormal axonal branching compared to wild type in primary motor neurons.

Monoglutamylated microtubules enriched in ciliated and neuronal tissues in developing zebrafish embryos

In *Danio rerio*, monoglutamylated microtubules are enriched in ciliated and neuronal structures (Figure 4.6). At 54hpf, this modification was seen in pronephros mutlicilia, ependymal cilia and olfactory placode cilia, lateral line system, and neurons. Enrichment of glutamylated microtubules in ciliary structures and neurons in multiple tissues suggests a potential role of this modification in the assembly and maintenance of cilia and in neurogenesis and neuronal functions. Microtubule glutamylation initiases *ttll4, ttll5,* and *ttll7,* and elongase *ttll1* and *ttll6 are* expressed maternally and zygotically (Figure S4.4A). These glutamylation genes were expressed in the brain, testis, ovary, kidney, heart, gut, and liver tissues (Figure S4.4B).

Generation of *ttll4, ttll5,* and *ttll7* mutants using CRISPR/Cas9 mutagenesis

To understand the roles of microtubule glutamylation in zebrafish embryonic development, ciliogenesis, ciliary function, neurogenesis, and neuronal functions, we generated mutants of glutamylation initiases *ttll4, ttll5,* and *ttll7* genes.

We generated *ttll4* mutants by targeting exon 7 of the *ttll4* gene (Figure 4.7A). We identified two mutants alleles, a 7 bp deletion (*ttll4*^{ga233}) and a 13 bp insertion allele (*ttll4*^{ga235}). *ttll4*$^{ga233\ -/-}$ used for further studies. We generated *ttll5* mutants by targeting exon 6 of the *ttll5* gene (Figure 4.7B). We identified two mutant alleles, a 14 bp deletion (*ttll5*^{ga237}) and a 4 bp deletion allele (*ttll5*^{ga238}). *ttll5*$^{ga237\ -/-}$ used for further studies. We generated *ttll7* mutants by targeting exon 7 of the *ttll7* gene (Figure 4.7C). We identified a 7 bp deletion (*ttll7*^{ga242}) mutant allele.

ttll4 $^{ga233\ -/-}$, *ttll5*$^{ga237\ -/-}$, and *ttll7*$^{ga242\ -/-}$ mutant embryos or adults of this allele did not show any obvious morphological defects (Figure 4.8). The mutants of *ttll4, ttll5,* and *ttll7* males showed an increase in the number of unfertilized eggs compared to wild type in crosses with wild type females. Wild type, *ttll4* $^{ga233\ -/-}$, *ttll5*$^{ga237\ -/-}$, and *ttll7*$^{ga242\ -/-}$ males resulted in 8.4 %, 68.9 %, 23.8 %, and 21.2% of eggs being unfertilized, respectively. Double mutants of these genes were also generated. These double mutant embryos or adults of this allele did not show any obvious morphological defects (Figure 4.8). Interestingly, most eggs laid by *ttll4*$^{ga233\ -/-}$; *ttll5*$^{ga237\ -/-}$ were unfertilized. *ttll5*$^{ga237\ -/-}$; *ttll7*$^{ga242\ -/-}$ showed an increased occurrence of unfertilized eggs. Further crosses of these double mutants with wild type males and females to confirm altered fertility.

TTLL5 is the major microtubule glutamylation initiase in zebrafish brain

We extracted proteins from brain microtubule glutamylation initiases mutant brains and carried out a western blot with an antibody that specifically recognizes monoglutamylated microtubules. We found that the *ttll5* $^{-/-}$ mutant brain showed a drastic reduction in monoglutamylated tubulin compared to the wild-type (Figure S4.5). Other microtubule glutamylation initiase mutants showed no or mild reduction in monoglutamylated tubulin compared to wild type (Figure S4.5). Since both *ttll4* and *ttll7* are specific for β-tubulin, they could potentially compensate each other for the loss of one gene.

DISCUSSION

Microtubule detyrosination is one of the earliest identified microtubule PTMs (Rodriguez et al., 1973). Microtubule detyrosination is enriched in stable microtubules of neurons, cilia, and cell division spindles (Gundersen et al., 1984, Cambray-Deakin and Burgoyne, 1987, Mary et al., 1996). Even though VASH1 and VASH2 have been known for a long time as regulators of angiogenesis, their role in the detyrosination of microtubules has been discovered recently (Watanabe et al., 2004, Kimura et al., 2009, Aillaud et al., 2017, Nieuwenhuis et al., 2017). Our understanding of the roles of microtubule detyrosination on neuronal functions and cell divisions was based on overexpression of TTL, the enzyme responsible for retyrosination or knock out of small vasohibin binding protein (SVBP) or parthenolide treatment. Even though detyrosinated microtubules are enriched in cilia, the roles of this modification on ciliogenesis and ciliary functions have yet to be studied. A genetic approach to mutating these genes is important to expand further our

understanding of microtubule detyrosination's roles in different biological processes. We used CRISPR-Cas9 RNP-mediated mutagenesis to generate zebrafish mutants of *vash1*, *vash2*, and *ttl* genes.

Our study found that *vash1* or *vash2* mutants did not exhibit any obvious morphological defects in embryos or adults and showed no evidence of fertility problems (Figure 4.4). We observed lower longevity in these mutants, but further control experiments must be conducted with heterozygous and mutant siblings. Both mutants showed reductions in the levels of microtubule detyrosination (Figures S4.2 and S4.3), confirming that their role in microtubule detyrosination is conserved in zebrafish. We generated a double mutant of *vash1* and *vash2*, showing a drastic reduction in the levels of microtubule detyrosination. This double mutant showed low penetrance microcephaly, curved body, and heart edema phenotypes. The fishes that survived into adults did not show any morphological defects. They exhibited a potential reduction in fertility and longevity, but further studies must be conducted to confirm it. In mice, *Svbp* mutant shows a microcephaly phenotype, as seen in our double mutant (Pagnamenta et al., 2019). This *vash1; vash2* double mutant showed the presence of residual microtubule detyrosination. We hypothesize that residual microtubule detyrosination is due to the presence of *tuba7l*, a gene-encoded zebrafish α-tubulin isotype lacking terminal tyrosine. The expression of *tuba7l* was reported in the testis; its expression in other tissues is unknown (Atienzar-Aroca et al., 2021). Similar residual microtubule detyrosination was reported in mammalian cells that lack VASH1 and VASH2 (Nieuwenhuis et al., 2017). The presence of other proteins that could carry out microtubule detyrosination could also be responsible for this residual microtubule detyrosination seen in double mutants. Even though we assume these mutant alleles to be

null based on sequencing, the lack of antibodies against VASH1 and VASH2 makes it possible that these alleles could not be null.

We also generated *ttl* mutants to understand the role of excessive microtubule detyrosination in biological functions. These mutants showed 13 fold increase in the level of microtubule detyrosination. The *ttl* mutant showed low penetrance curved body and heart edema phenotypes, and adults did not show any obvious morphological defects. Interestingly, mice *Ttl* mutant exhibited much more severe phenotypes. These mutant mice died within 24 hours, and aberrant axonal differentiation and axonal projection were observed in their corticothalamic loop (Erck et al., 2005). The exact reason for the discrepancy between our ttl mutant and mice mutant is unclear, and one possibility could be that our mutant is not null. The lack of antibodies specific to zebrafish TTL makes it hard to confirm whether it is null.

In our vasohibin mutants, we studied primary motor neurons with a specific antibody. The *vash1*, *vash2,* and *vash1; vash2* mutants show normal neurogenesis and morphogenesis. Interestingly, synaptotagmin 2 levels were reduced in primary motor neurons of *vash1*, *vash2,* and *vash1; vash2* mutants. Even though most *ttl* mutants had normal-looking primary motor neurons, some had abnormal axon branching. These observations raise the possibility of these genes regulating axon branching and axonal transport. Studies show the importance of detyrosinated microtubules in Kinesin-1 and tyrosinated microtubule in kinesin-3 and kinesin-5 motor activity (Tas et al., 2017, Guardia et al., 2016, Kahn et al., 2015). Further studies have to be done with these mutants to elucidate their role in axonal transport and axonal branching. Using the

transient transgenesis approach, we could transiently express fluorescently tagged motor proteins, and axonal cargos could be used to study axonal transport.

Microtubule glutamylation has been shown to play a role in neuronal and ciliary functions. To understand the role of microtubule glutamylation in zebrafish embryogenesis and ciliary and neuronal functions, we generated mutants of microtubule glutamylation initiases. We generated mutants for *ttll5*, α-tubulin glutamylation initiase, and *ttll4* and *ttll7*, β-tubulin glutamylation initiases. We also generated double mutants of these mutants. The single and double mutant embryos or adults showed no obvious phenotypes.

Interestingly *ttll5, ttll4; ttll5,* and *ttll5;ttll7* mutants exhibited some evidence of fertility problems. Further studies must be done with all mutants to confirm the fertility problem. Studies have shown that mice *ttll5* mutants exhibited sperm motility problems (Lee et al., 2013). Additionally, *ttll1, ttll6, ttll9,* and *ttll11* mutants in various model organisms showed ciliary defects (Vogel et al., 2010, Wloga et al., 2008, Suryavanshi et al., 2010, Pathak et al., 2007, Konno et al., 2016, Mathieu et al., 2021). Further studies need to be conducted to study changes in ciliary and neuronal functions in our single and double mutants.

REFERENCE

AILLAUD, C., BOSC, C., PERIS, L., BOSSON, A., HEEMERYCK, P., VAN DIJK, J., LE FRIEC, J., BOULAN, B., VOSSIER, F. & SANMAN, L. E. 2017. Vasohibins/SVBP are tubulin carboxypeptidases (TCPs) that regulate neuron differentiation. *Science,* 358**,** 1448-1453.

ATIENZAR-AROCA, R., AROCA-AGUILAR, J.-D., ALEXANDRE-MORENO, S., FERRE-FERNÁNDEZ, J.-J., BONET-FERNÁNDEZ, J.-M., CABAÑERO-VARELA, M.-J. & ESCRIBANO, J. 2021. Knockout of myoc Provides Evidence for the Role of Myocilin in Zebrafish Sex Determination Associated with Wnt Signalling Downregulation. *Biology,* 10**,** 98.

BEREZNIUK, I., LYONS, P. J., SIRONI, J. J., XIAO, H., SETOU, M., ANGELETTI, R. H., IKEGAMI, K. & FRICKER, L. D. 2013. Cytosolic carboxypeptidase 5 removes α-and γ-linked glutamates from tubulin. *Journal of Biological Chemistry,* 288**,** 30445-30453.

BODAKUNTLA, S., YUAN, X., GENOVA, M., GADADHAR, S., LEBOUCHER, S., BIRLING, M. C., KLEIN, D., MARTINI, R., JANKE, C. & MAGIERA, M. M. 2021. Distinct roles of α-and β-tubulin polyglutamylation in controlling axonal transport and in neurodegeneration. *The EMBO journal,* 40**,** e108498.

CAMBRAY-DEAKIN, M. A. & BURGOYNE, R. D. 1987. Posttranslational modifications of alpha-tubulin: acetylated and detyrosinated forms in axons of rat cerebellum. *The Journal of cell biology,* 104**,** 1569-1574.

EDDE, B., ROSSIER, J., LE CAER, J.-P., DESBRUYERES, E., GROS, F. & DENOULET, P. 1990. Posttranslational glutamylation of α-tubulin. *Science,* 247**,** 83-85.

ERCK, C., PERIS, L., ANDRIEUX, A., MEISSIREL, C., GRUBER, A. D., VERNET, M., SCHWEITZER, A., SAOUDI, Y., POINTU, H. & BOSC, C. 2005. A vital role of tubulin-tyrosine-ligase for neuronal organization. *Proceedings of the National Academy of Sciences,* 102**,** 7853-7858.

ERSFELD, K., WEHLAND, J., PLESSMANN, U., DODEMONT, H., GERKE, V. & WEBER, K. 1993. Characterization of the tubulin-tyrosine ligase. *The Journal of cell biology,* 120**,** 725-732.

FOUQUET, J. P., KANN, M. L., EDDE, B., WOLFF, A., DESBRUYERES, E. & DENOULET, P. 1994. Differential distribution of glutamylated tubulin during spermatogenesis in mammalian testis. *Cell motility and the cytoskeleton,* 27**,** 49-58.

GUARDIA, C. M., FARÍAS, G. G., JIA, R., PU, J. & BONIFACINO, J. S. 2016. BORC functions upstream of kinesins 1 and 3 to coordinate regional movement of lysosomes along different microtubule tracks. *Cell reports,* 17**,** 1950-1961.

GUNDERSEN, G. G., KALNOSKI, M. H. & BULINSKI, J. C. 1984. Distinct populations of microtubules: tyrosinated and nontyrosinated alpha tubulin are distributed differently in vivo. *Cell,* 38**,** 779-789.

IKEGAMI, K., HEIER, R. L., TARUISHI, M., TAKAGI, H., MUKAI, M., SHIMMA, S., TAIRA, S., HATANAKA, K., MORONE, N. & YAO, I. 2007. Loss of α-tubulin polyglutamylation in ROSA22 mice is associated with abnormal targeting

of KIF1A and modulated synaptic function. *Proceedings of the National Academy of Sciences,* 104**,** 3213-3218.

IKEGAMI, K., MUKAI, M., TSUCHIDA, J.-I., HEIER, R. L., MACGREGOR, G. R. & SETOU, M. 2006. TTLL7 is a mammalian β-tubulin polyglutamylase required for growth of MAP2-positive neurites. *Journal of Biological Chemistry,* 281**,** 30707-30716.

IKEGAMI, K., SATO, S., NAKAMURA, K., OSTROWSKI, L. E. & SETOU, M. 2010. Tubulin polyglutamylation is essential for airway ciliary function through the regulation of beating asymmetry. *Proceedings of the National Academy of Sciences,* 107**,** 10490-10495.

IKEGAMI, K. & SETOU, M. 2009. TTLL10 can perform tubulin glycylation when co-expressed with TTLL8. *FEBS letters,* 583**,** 1957-1963.

JANKE, C. 2014. The tubulin code: molecular components, readout mechanisms, and functions. *Journal of Cell Biology,* 206**,** 461-472.

KAHN, O. I., SHARMA, V., GONZÁLEZ-BILLAULT, C. & BAAS, P. W. 2015. Effects of kinesin-5 inhibition on dendritic architecture and microtubule organization. *Molecular biology of the cell,* 26**,** 66-77.

KIMMEL, C. B., BALLARD, W. W., KIMMEL, S. R., ULLMANN, B. & SCHILLING, T. F. 1995. Stages of embryonic development of the zebrafish. *Developmental dynamics,* 203**,** 253-310.

KIMURA, H., MIYASHITA, H., SUZUKI, Y., KOBAYASHI, M., WATANABE, K., SONODA, H., OHTA, H., FUJIWARA, T., SHIMOSEGAWA, T. & SATO, Y. 2009. Distinctive localization and opposed roles of vasohibin-1 and vasohibin-2

in the regulation of angiogenesis. *Blood, The Journal of the American Society of Hematology,* 113**,** 4810-4818.

KONNO, A., IKEGAMI, K., KONISHI, Y., YANG, H.-J., ABE, M., YAMAZAKI, M., SAKIMURA, K., YAO, I., SHIBA, K. & INABA, K. 2016. Ttll9−/− mice sperm flagella show shortening of doublet 7, reduction of doublet 5 polyglutamylation and a stall in beating. *Journal of Cell Science,* 129**,** 2757-2766.

LABUN, K., MONTAGUE, T. G., KRAUSE, M., TORRES CLEUREN, Y. N., TJELDNES, H. & VALEN, E. 2019. CHOPCHOP v3: expanding the CRISPR web toolbox beyond genome editing. *Nucleic acids research,* 47**,** W171-W174.

LEE, G.-S., HE, Y., DOUGHERTY, E. J., JIMENEZ-MOVILLA, M., AVELLA, M., GRULLON, S., SHARLIN, D. S., GUO, C., BLACKFORD, J. A. & AWASTHI, S. 2013. Disruption of Ttll5/stamp gene (tubulin tyrosine ligase-like protein 5/SRC-1 and TIF2-associated modulatory protein gene) in male mice causes sperm malformation and infertility. *Journal of Biological Chemistry,* 288**,** 15167-15180.

LESSARD, D. V., ZINDER, O. J., HOTTA, T., VERHEY, K. J., OHI, R. & BERGER, C. L. 2019. Polyglutamylation of tubulin's C-terminal tail controls pausing and motility of kinesin-3 family member KIF1A. *Journal of Biological Chemistry,* 294**,** 6353-6363.

MAAS, C., BELGARDT, D., LEE, H. K., HEISLER, F. F., LAPPE-SIEFKE, C., MAGIERA, M. M., VAN DIJK, J., HAUSRAT, T. J., JANKE, C. & KNEUSSEL, M. 2009. Synaptic activation modifies microtubules underlying

transport of postsynaptic cargo. *Proceedings of the National Academy of Sciences,* 106**,** 8731-8736.

MARY, J., REDEKER, V., LE CAER, J.-P., ROSSIER, J. & SCHMITTER, J.-M. 1996. Posttranslational Modifications in the C-terminal Tail of Axonemal Tubulin from Sea Urchin Sperm (∗). *Journal of Biological Chemistry,* 271**,** 9928-9933.

MATHIEU, H., PATTEN, S. A., ARAGON-MARTIN, J. A., OCAKA, L., SIMPSON, M., CHILD, A. & MOLDOVAN, F. 2021. Genetic variant of TTLL11 gene and subsequent ciliary defects are associated with idiopathic scoliosis in a 5-generation UK family. *Scientific reports,* 11**,** 1-15.

MCKENNEY, R. J., HUYNH, W., VALE, R. D. & SIRAJUDDIN, M. 2016. Tyrosination of α-tubulin controls the initiation of processive dynein–dynactin motility. *The EMBO journal,* 35**,** 1175-1185.

NIEUWENHUIS, J., ADAMOPOULOS, A., BLEIJERVELD, O. B., MAZOUZI, A., STICKEL, E., CELIE, P., ALTELAAR, M., KNIPSCHEER, P., PERRAKIS, A. & BLOMEN, V. A. 2017. Vasohibins encode tubulin detyrosinating activity. *Science,* 358**,** 1453-1456.

PAGNAMENTA, A. T., HEEMERYCK, P., MARTIN, H. C., BOSC, C., PERIS, L., USZYNSKI, I., GORY-FAURÉ, S., COULY, S., DESHPANDE, C. & SIDDIQUI, A. 2019. Defective tubulin detyrosination causes structural brain abnormalities with cognitive deficiency in humans and mice. *Human molecular genetics,* 28**,** 3391-3405.

PATHAK, N., OBARA, T., MANGOS, S., LIU, Y. & DRUMMOND, I. A. 2007. The zebrafish fleer gene encodes an essential regulator of cilia tubulin polyglutamylation. *Molecular biology of the cell,* 18**,** 4353-4364.

PATURLE-LAFANECHERE, L., EDDE, B., DENOULET, P., VAN DORSSELAER, A., MAZARGUIL, H., LE CAER, J. P., WEHLAND, J. & JOB, D. 1991. Characterization of a major brain tubulin variant which cannot be tyrosinated. *Biochemistry,* 30**,** 10523-10528.

POOLE, C. A., ZHANG, Z.-J. & ROSS, J. M. 2001. The differential distribution of acetylated and detyrosinated alpha-tubulin in the microtubular cytoskeleton and primary cilia of hyaline cartilage chondrocytes. *The Journal of Anatomy,* 199**,** 393-405.

RAYBIN, D. & FLAVIN, M. 1977. Enzyme which specifically adds tyrosine to the α chain of tubulin. *Biochemistry,* 16**,** 2189-2194.

RODRIGUEZ, J., ARCE, C., BARRA, H. & CAPUTTO, R. 1973. Release of tyrosine incorporated as a single unit into rat brain protein. *Biochemical and Biophysical Research Communications,* 54**,** 335-340.

ROGOWSKI, K., VAN DIJK, J., MAGIERA, M. M., BOSC, C., DELOULME, J.-C., BOSSON, A., PERIS, L., GOLD, N. D., LACROIX, B. & GRAU, M. B. 2010. A family of protein-deglutamylating enzymes associated with neurodegeneration. *Cell,* 143**,** 564-578.

SURYAVANSHI, S., EDDÉ, B., FOX, L. A., GUERRERO, S., HARD, R., HENNESSEY, T., KABI, A., MALISON, D., PENNOCK, D. & SALE, W. S.

2010. Tubulin glutamylation regulates ciliary motility by altering inner dynein arm activity. *Current biology,* 20**,** 435-440.

TAS, R. P., CHAZEAU, A., CLOIN, B. M., LAMBERS, M. L., HOOGENRAAD, C. C. & KAPITEIN, L. C. 2017. Differentiation between oppositely oriented microtubules controls polarized neuronal transport. *Neuron,* 96**,** 1264-1271. e5.

TORT, O., TANCO, S., ROCHA, C., BIÈCHE, I., SEIXAS, C., BOSC, C., ANDRIEUX, A., MOUTIN, M.-J., AVILÉS, F. X. & LORENZO, J. 2014. The cytosolic carboxypeptidases CCP2 and CCP3 catalyze posttranslational removal of acidic amino acids. *Molecular biology of the cell,* 25**,** 3017-3027.

VAN DIJK, J., ROGOWSKI, K., MIRO, J., LACROIX, B., EDDÉ, B. & JANKE, C. 2007. A targeted multienzyme mechanism for selective microtubule polyglutamylation. *Molecular cell,* 26**,** 437-448.

VANLEUVEN, A. J., PARK, S., MENKE, D. B. & LAUDERDALE, J. D. 2018. A PAGE screening approach for identifying CRISPR-Cas9-induced mutations in zebrafish. *Biotechniques,* 64**,** 275-278.

VOGEL, P., HANSEN, G., FONTENOT, G. & READ, R. 2010. Tubulin Tyrosine Ligase–Like 1 Deficiency Results in Chronic Rhinosinusitis and Abnormal Development of Spermatid Flagella in Mice. *Veterinary pathology,* 47**,** 703-712.

WATANABE, K., HASEGAWA, Y., YAMASHITA, H., SHIMIZU, K., DING, Y., ABE, M., OHTA, H., IMAGAWA, K., HOJO, K. & MAKI, H. 2004. Vasohibin as an endothelium-derived negative feedback regulator of angiogenesis. *The Journal of clinical investigation,* 114**,** 898-907.

WLOGA, D., ROGOWSKI, K., SHARMA, N., VAN DIJK, J., JANKE, C., EDDÉ, B., BRÉ, M.-H., LEVILLIERS, N., REDEKER, V. & DUAN, J. 2008. Glutamylation on α-tubulin is not essential but affects the assembly and functions of a subset of microtubules in Tetrahymena thermophila. *Eukaryotic cell,* 7**,** 1362-1372.

TABLES AND TABLE DESCRIPTIONS

Table 4.1. Primer used for the synthesis of gRNAs targeting microtubule detyrosination and tyrosination genes

Primer name	Sequence (5'→3')
vash1_ex1_gRNA Forward	GAATTAATACGACTCACTATAGGGGCCCGCATA CACCCCGAGTTTTAGAGCTAGAAATAGCAAG
vash2_ex1_gRNA Forward	GAATTAATACGACTCACTATAGGGTCTACTGATC TTGGCCGGTTTTAGAGCTAGAAATAGCAAG
ttl_ex1_gRNA Forward	GAATTAATACGACTCACTATAGGAATCGGCTGC CTTTTGGAGTTTTAGAGCTAGAAATAGCAAG
gRNA_Reverse	AAAAGCACCGACTCGGTGCCACTTTTTCAAGTTG ATAACGGACTAGCCTTATTTTAACTTGCTATTTC TAGCTCTAAAAC

Table 4.2. Primer used for the synthesis of gRNAs targeting microtubule glutamylation initiase genes

Primer name	Sequence (5'→3')
ttll1 gRNA 1	GAATTAATACGACTCACTATAGGACACGGGCTA CCGGCTGAGTTTTAGAGCTAGAAATAGCAAG
TTLL4 ex7 gRNA1 Forward	GAATTAATACGACTCACTATAGGGGCCGGAAGG ACAGACTTGTTTTAGAGCTAGAAATAGCAAG
TTLL5 ex6 gRNA1 Forward	GAATTAATACGACTCACTATAGGCTCTACAAAA ACATCCAGGTTTTAGAGCTAGAAATAGCAAG
TTLL6 ex3 gRNA 1 Forward	GAATTAATACGACTCACTATAGGGTGTTGGAGG GCTCCGCGGTTTTAGAGCTAGAAATAGCAAG
TTLL6 ex3 gRNA 2 Forward	GAATTAATACGACTCACTATAGGCGGTGTGAGC CTGATCCAGTTTTAGAGCTAGAAATAGCAAG
TTLL7 ex6 gRNA1	GAATTAATACGACTCACTATAGGTGACTCACCC ATGGCCCAGTTTTAGAGCTAGAAATAGCAAG
gRNA_Reverse	AAAAGCACCGACTCGGTGCCACTTTTTCAAGTTG ATAACGGACTAGCCTTATTTTAACTTGCTATTTC TAGCTCTAAAAC

Table 4.3. Primer used for RT-PCR

Primer Name	Forward (5'→3')	Reverse (5'→3')	Reference
ttll1 cdna	CAACAAGCTCTCGCAGATCA	TAGCCGTAACACTCGAAGCA	This study
ttll4 ex5ex8	CTTCAGCACTGCCAATGAAA	TTGGACAGGTTCCTCCAAAG	This study
ttll5 ex13ex17	AAACCCTGGCTCTTGGAAGT	TACTCCTCCTGGACCCTCCT	This study
ttll6 ex8ex11	ACGGAAACTCTCCAGCTTCA	TGCATCAGCTCCATACTTGC	This study
ttll7 ex9ex11	TGTCTGCTTTGAGGTGTTGG	TTCCTCCCTTCTGCGTTCTA	This study
ttll1 short geno	CGTCAGCTCGTAGTGGTTGG	TCAGTGTGTGTGTGTCGTTCTC	This study
ttll4 ex7 geno	CAAAGCGTGCCTGCATCT	CCTGTCAGTCGAGTATTAACAAGTATG	This study
ttll5 ex6 geno	CTCTCATCGCTTTCCAGGTC	ACGTCTGTGGTACGATGCTG	This study
ttll6 ex3 geno	AGCGCTCAGTGAGTGAAGTG	GGCTACTGGCAGTGGGATT	This study

ttll7 ex6 geno	TGAAGGAGCTGAAACGAAA	ACACAAGGCCATAAAGGATG	This study
ttll4 long	GCTTTCCTCAGCAGCTTGAT	TTCAAGGCCATTCGAGAGTT	This study
ttll5 long	GCAATGGATCAAACTGAGCA	GCTGAGCCAAACACACTCAC	This study
ttll6 long F	AGCTCGCTCAGTCTTCATCA	GAAATGCTTTAACTGTTGTGCAG	This study
ttll7 long	GCACTAATTTACGCTCAGTCCA	CAACTAACCTCCAGCCAACAA	This study

Table 4.4. Primer used for genotyping of mutants

Primer Name	Forward (5'→3')	Reverse (5'→3')	Reference
vash1 ex4ex5	TTGGAGGCTGTTATCCTTGG	ATGCTTCCACTCGATCTGCT	This study
vash2 ex1ex5	CCTGATGGACAGGAGATGGT	AAGTGGTGCCCAGAGAATTG	This study
ttl ex2ex4	CTGTGTCGCAAAGCATCACT	CATGCACTTGGCCTTGATTA	This study
vash1_geno	CCTGCCTGTAAACGAGGAGA	CTCGGGTTCCCCGTATTCT	This study
vash1_geno_2	AGTGCCCTTCATCATTAACAGG	ATCTGTACCTTGGGCAGGTC	This study
vash2_geno	TAACAATGACCGGACCAAGC	GGAGGATTCAGCAGCAGGA	This study
ttl_geno	CAATTACATCAGTGTTAAATTTTGATT	AAGAAAGACAACCCTCGCTTT	This study
vash1_long	TCCATCACGGCTCCTCAC	ATCTGTACCTTGGGCAGGTC	This study
vash1_long_2	GCTGATATGACCATGACTCTGAA	ACTCACTACTCAACAGGATAACTCA	This study
vash2_long	AATGCTGGGCGATCATAAGT	CCTGTCCATCAGGGTGAACT	This study

ttl_long	ACACAGCACACCATT GCTTC	TATGCTGAGGTCGCCA AGAT	This study

FIGURES AND FIGURE LEGENDS

Figure 4.1. The distribution of detyrosinated α-tubulin in 54hpf *Danio rerio* embryo. Wholemount immunofluorescence of 54hpf wild-type embryos with detyrosinated α-tubulin-specific AA12 antibody. (A.) Detyrosinated α-tubulin is enriched in olfactory placode (Red arrow). (B). Detyrosinated α-tubulin is enriched in pronephros (Yellow arrow), and neurons (Blue arrow).

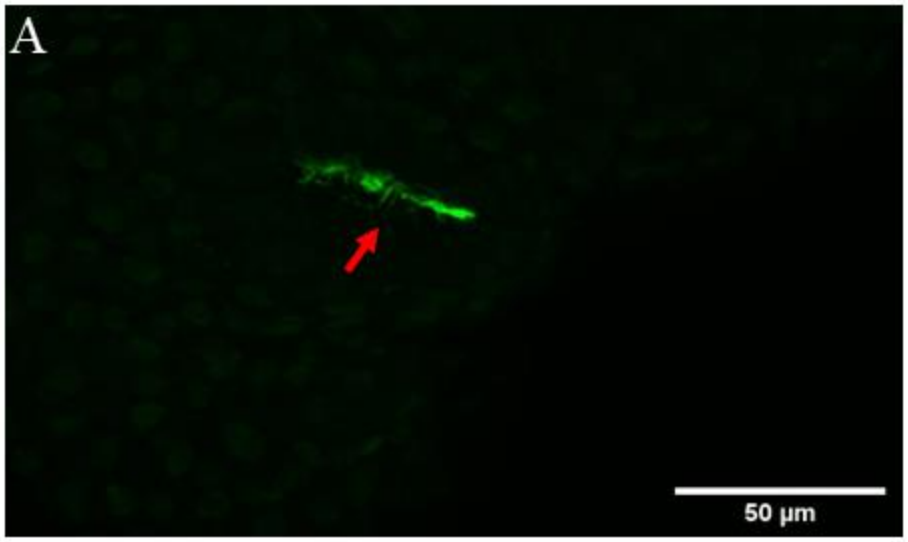
A
50 µm

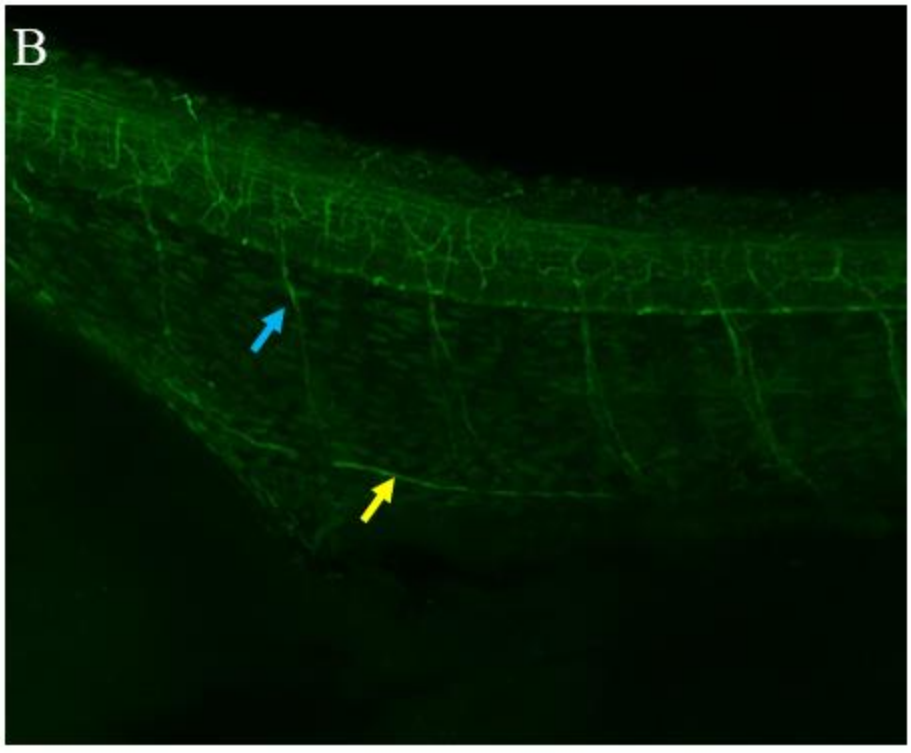
B

Figure 4.2. Schematic diagram of CRISPR-CAS9 RNP mediated mutagenesis in zebrafish. 1-cell zebrafish embryos were injected with in-vitro synthesized gRNA with Cas9 protein. A PAGE-based screening was carried out at F_0, F_1, and F_2 generations to confirm mutagenesis, germline transmission, and identification of homozygous mutant fishes, respectively.

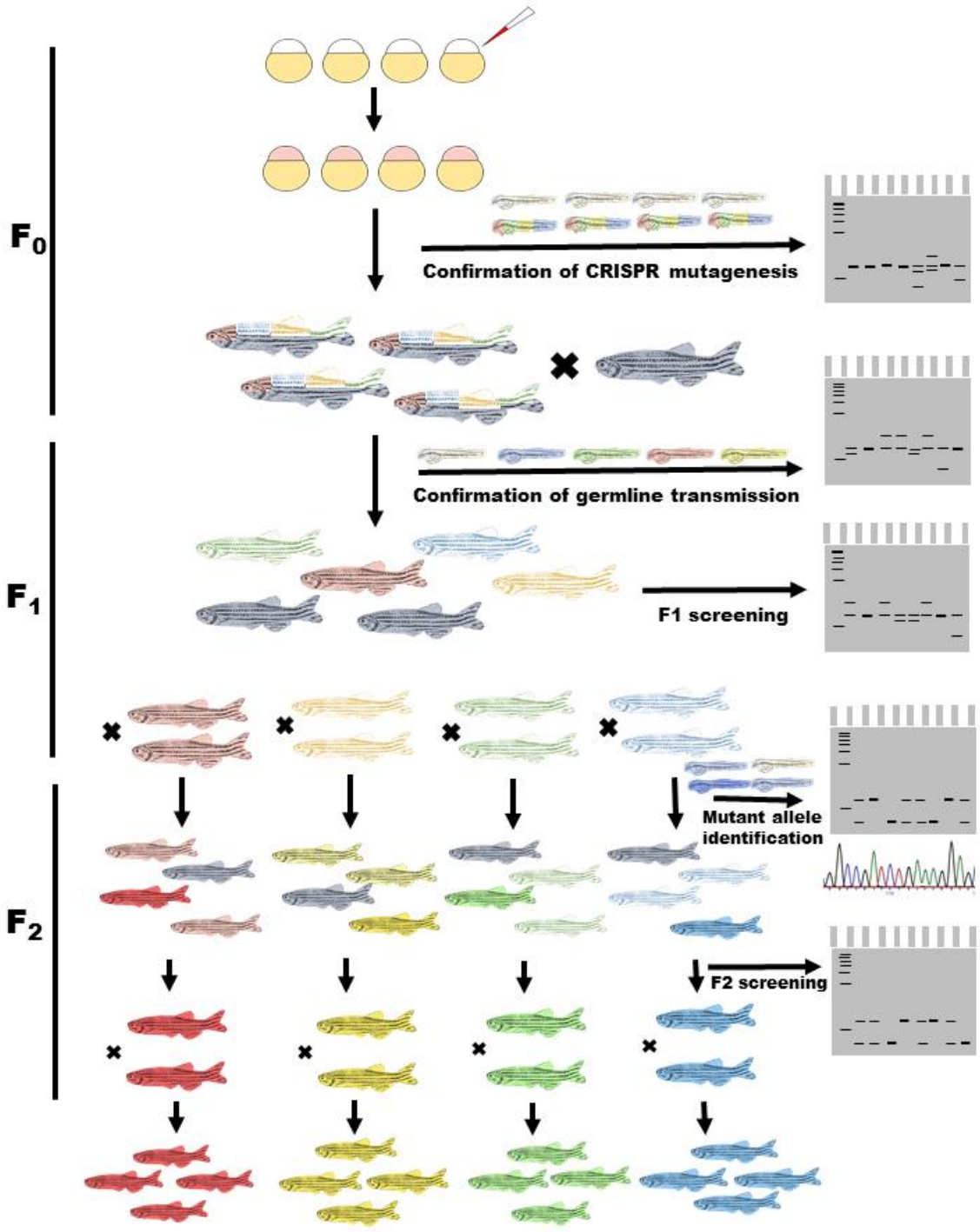
F0
Confirmation of CRISPR mutagenesis
Confirmation of germline transmission
F1
F1 screening
Mutant allele identification
F2
F2 screening

Figure 4.3. Generation of *vash1, vash2, and ttl* mutant zebrafish lines using CRISPR/Cas9 mediated mutagenesis. (A). Schematic representation of *vash1* gene and VASH1 protein. Three mutant alleles, *vash1*^{ga243} (5 nucleotide insertion), *vash1*^{ga244} (7 nucleotide deletion), and *vash1*^{ga245} (2 nucleotide deletion) were identified in F1 screening. Red arrows represent the gRNA target sites. (B). Schematic representation of *vash2* gene and VASH2 protein. Three mutant alleles, *vash2*^{ga246} (25 nucleotide deletion), *vash2*^{ga247} (10 nucleotide deletion), and *vash2*^{ga250} (14 nucleotide deletion) were identified in F1 screening. Red arrows represent the gRNA target sites. (C). Schematic representation of *ttl* gene and TTL protein. Three mutant alleles, *ttl*^{ga253} (17 nucleotide insertion), *ttl*^{ga254} (8 nucleotide insertion), and *ttl*^{ga256} (51 nucleotide insertion), were identified in F1 screening. Red arrows represent the gRNA target sites.

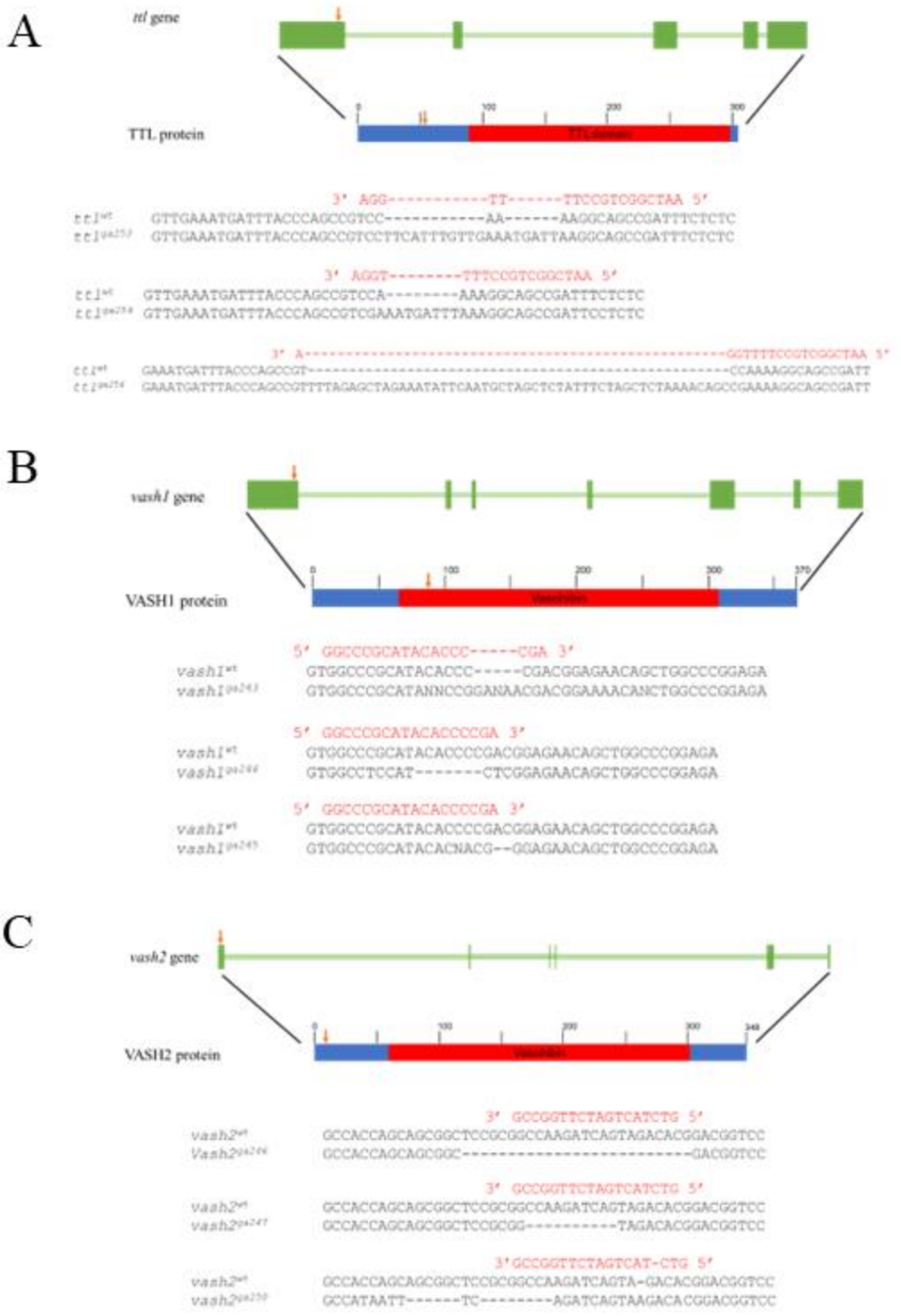
A
ttl gene
TTL protein
3' AGG----------TT------TTCCGTCGGCTAA 5'
ttl^wt GTTGAAATGATTTACCCAGCCGTCC----------AA------AAGGCAGCCGATTTCTCTC
ttl^tm253 GTTGAAATGATTTACCCAGCCGTCCTTCATTTGTTGAAATGATTAAGGCAGCCGATTTCTCTC
3' AGGT--------TTTCCGTCGGCTAA 5'
ttl^wt GTTGAAATGATTTACCCAGCCGTCCA--------AAAGGCAGCCGATTTCTCTC
ttl^tm258 GTTGAAATGATTTACCCAGCCGTCGAAATGATTTAAAGGCAGCCGATTCCTCTC
3' A----------GGTTTTCCGTCGGCTAA 5'
ttl^wt GAAATGATTTACCCAGCCGT----------CCAAAAGGCAGCCGATT
ttl^tm274 GAAATGATTTACCCAGCCGTTTTAGAGCTAGAAATATTCAATGCTAGCTCTATTTCTAGCTCTAAAACAGCCGAAAAGGCAGCCGATT
B
vash1 gene
VASH1 protein
5' GGCCCGCATACACCC-----CGA 3'
vash1^wt GTGGCCCGCATACACCC-----CGACGGAGAACAGCTGGCCCGGAGA
vash1^tm243 GTGGCCCGCATANNCCGGANAACGACGGAAAACANCTGGCCCGGAGA
5' GGCCCGCATACACCCCGA 3'
vash1^wt GTGGCCCGCATACACCCCGACGGAGAACAGCTGGCCCGGAGA
vash1^tm244 GTGGCCTCCAT-------CTCGGAGAACAGCTGGCCCGGAGA
5' GGCCCGCATACACCCCGA 3'
vash1^wt GTGGCCCGCATACACCCCGACGGAGAACAGCTGGCCCGGAGA
vash1^tm245 GTGGCCCGCATACACNACG--GGAGAACAGCTGGCCCGGAGA
C
vash2 gene
VASH2 protein
3' GCCGGTTCTAGTCATCTG 5'
vash2^wt GCCACCAGCAGCGGCTCCGCGGCCAAGATCAGTAGACACGGACGGTCC
Vash2^tm246 GCCACCAGCAGCGGC----------GACGGTCC
3' GCCGGTTCTAGTCATCTG 5'
vash2^wt GCCACCAGCAGCGGCTCCGCGGCCAAGATCAGTAGACACGGACGGTCC
vash2^tm247 GCCACCAGCAGCGGCTCCGCGG----------TAGACACGGACGGTCC
3'GCCGGTTCTAGTCAT-CTG 5'
vash2^wt GCCACCAGCAGCGGCTCCGCGGCCAAGATCAGTA-GACACGGACGGTCC
vash2^tm250 GCCATAATT------TC--------AGATCAGTAAGACACGGACGGTCC

Figure 4.4. Double mutant of microtubule detyrosinases and retyrosination mutant exhibit low penetrance morphological defects. (A). Bright-field images of 48hpf wild type, *vash1* $^{-/-}$, *vash2* $^{-/-}$, *vash1* $^{-/-}$*; vash2* $^{-/-}$, and *ttl* $^{-/-}$ embryos. (B) Bright-field images of six to eight months old wild type, *vash1* $^{-/-}$, *vash2* $^{-/-}$, *vash1* $^{-/-}$*; vash2* $^{-/-}$, and *ttl* $^{-/-}$ male and female fishes.

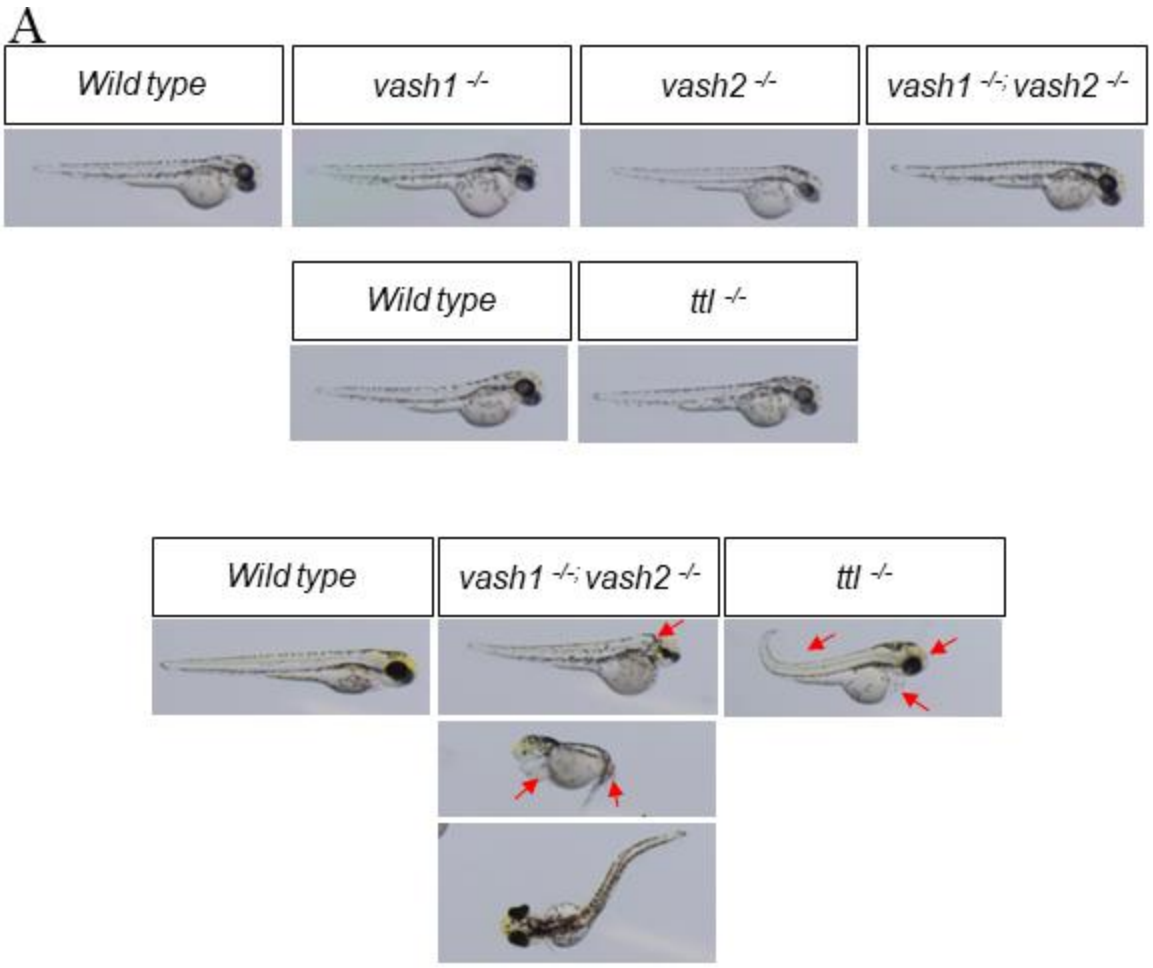
A
Wild type
vash1 -/-
vash2 -/-
vash1 -/-; vash2 -/-
Wild type
ttl -/-
Wild type
vash1 -/-; vash2 -/-
ttl -/-
B
Wild type
vash1 -/-
vash2 -/-
vash1 -/-; vash2 -/-
Wild type
ttl -/-

Figure 4.5. Single and double mutants of microtubule detyrosinases exhibit reduced labeling by anti-synaptotagmin 2 antibody in primary motor neurons without any +morphological defects. Wholemount immunofluorescence of wild-type, *vash1* $^{-/-}$, *vash2* $^{-/-}$, *vash1* $^{-/-}$*; vash2* $^{-/-}$, and *ttl* $^{-/-}$ at 30hpf for primary motor neurons with znp-1.

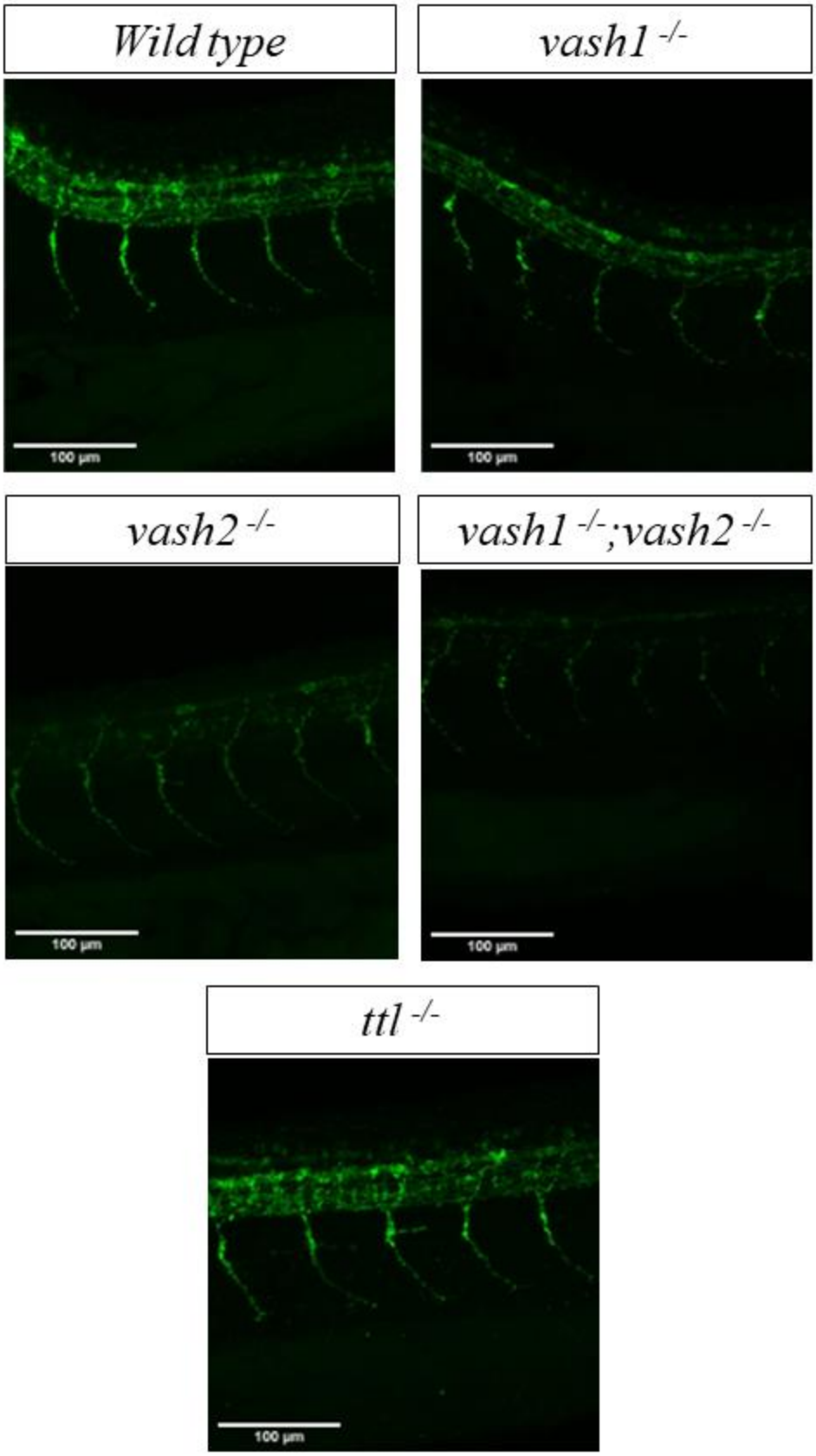
Wild type
vash1 -/-
100 µm
100 µm
vash2 -/-
vash1 -/-;vash2 -/-
100 µm
100 µm
ttl -/-
100 µm

Figure 4.6. The distribution of monoglutamylated microtubules in 54hpf *Danio rerio* embryo. Wholemount immunofluorescence of 54hpf wild-type embryos with monoglutamylated microtubule specific GT355 antibody. (A.) Monoglutamylated microtubules are enriched in the olfactory placode (Red arrow). (B). Monoglutamylated microtubules are enriched in pronephros (Yellow arrow) and neurons (Blue arrow).

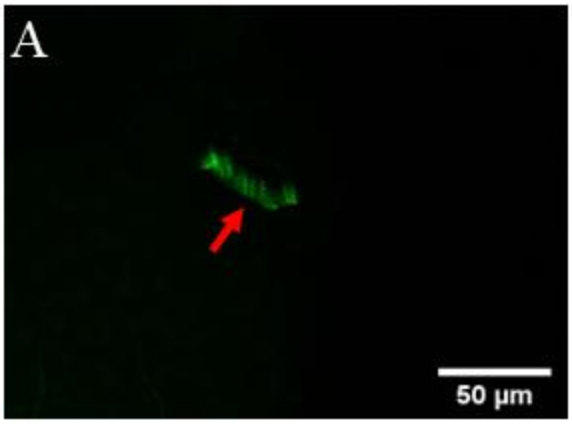
A
50 µm

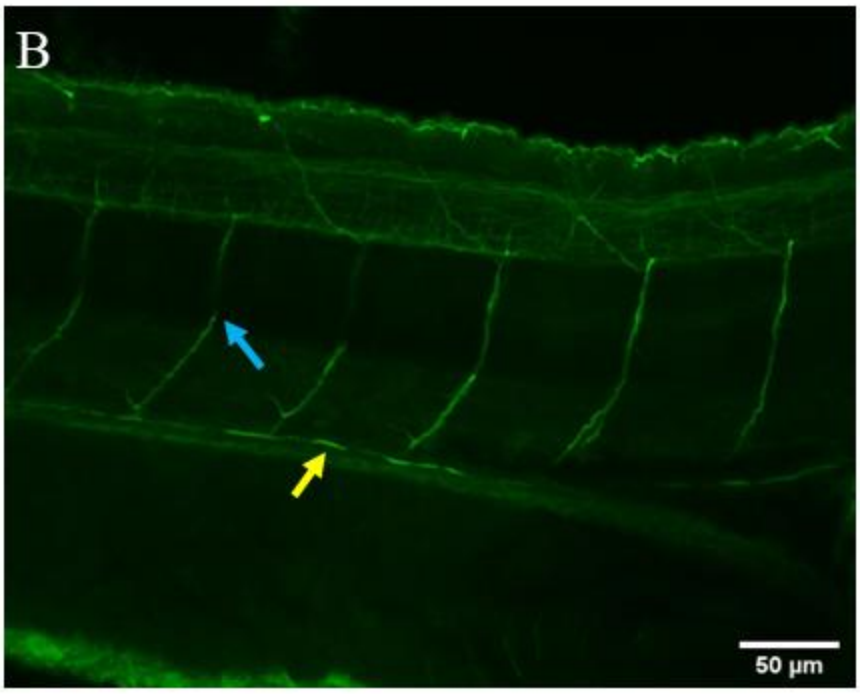
B
50 µm

Figure 4.7. Generation of *ttll4, ttll5, and ttll7* mutant zebrafish lines using CRISPR/Cas9 mediated mutagenesis. (A). Schematic representation of the *ttll4* gene and TTLL4 protein. Two mutant alleles, $ttll4^{ga233}$ (7 nucleotide deletion), and $ttll4^{ga235}$ (13 nucleotide insertion), were identified in F1 screening. Red arrows represent the gRNA target sites. (B). Schematic representation of the *ttll5* gene and TTLL5 protein. Two mutant alleles, $ttll5^{ga237}$ (14 nucleotide deletion), and $ttll5^{ga238}$ (4 nucleotide deletion), were identified in F1 screening. Red arrows represent the gRNA target sites. (C). Schematic representation of the *ttll7* gene and TTLL7 protein. One mutant allele, $ttll7^{ga242}$ (7 nucleotide deletion), *was* identified in F1 screening. Red arrows represent the gRNA target sites.

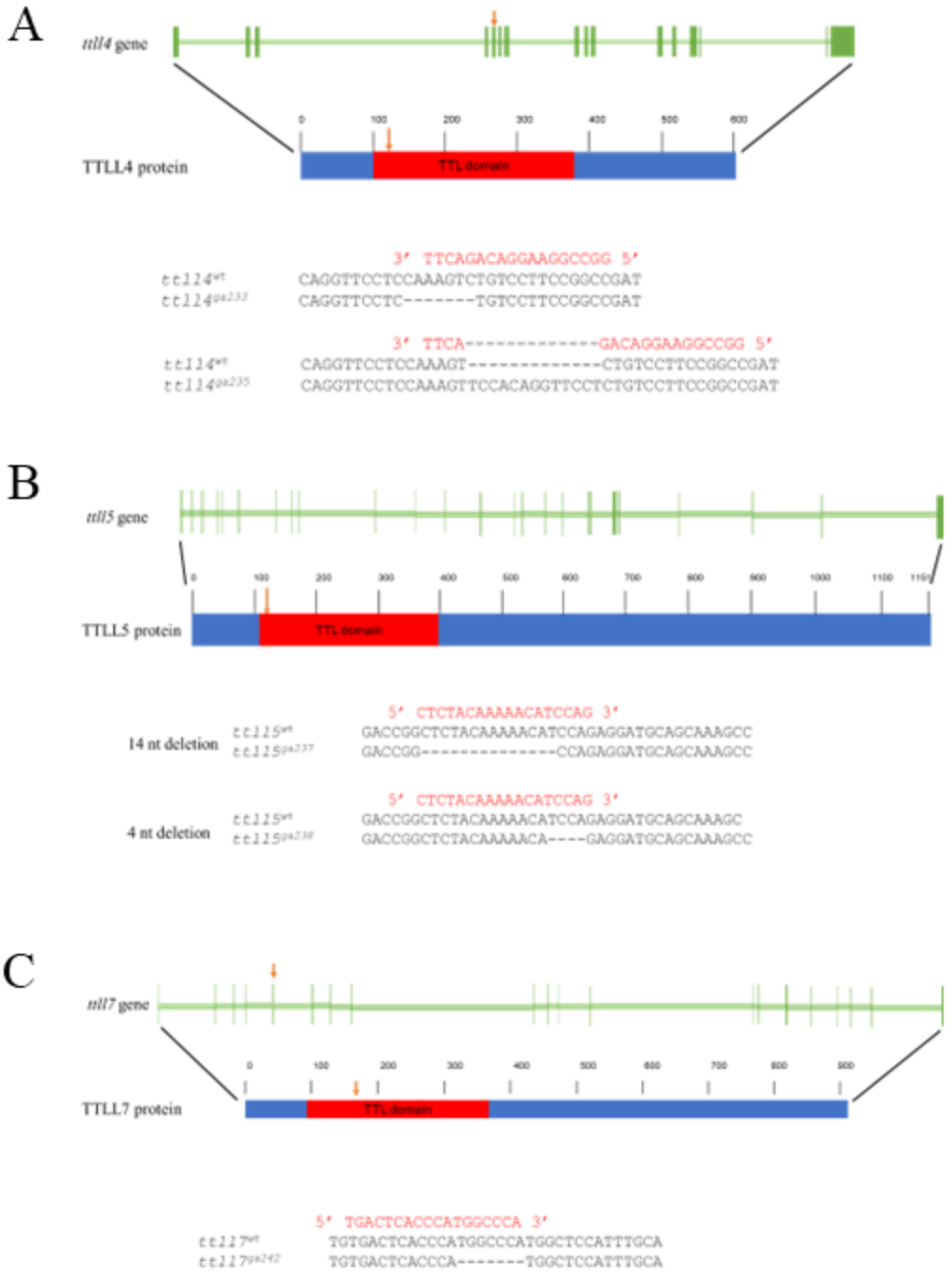
A
ttll4 gene
0
100
200
300
400
500
600
TTLL4 protein
TTL domain
3′ TTCAGACAGGAAGGCCGG 5′
ttll4wt CAGGTTCCTCCAAAGTCTGTCCTTCCGGCCGAT
ttll4gw233 CAGGTTCCTC-------TGTCCTTCCGGCCGAT
3′ TTCA----------GACAGGAAGGCCGG 5′
ttll4wt CAGGTTCCTCCAAAGT----------CTGTCCTTCCGGCCGAT
ttll4gw235 CAGGTTCCTCCAAAGTTCCACAGGTTCCTCTGTCCTTCCGGCCGAT
B
ttll5 gene
0
100
200
300
400
500
600
700
800
900
1000
1100
1150
TTLL5 protein
TTL domain
5′ CTCTACAAAAACATCCAG 3′
14 nt deletion
ttll5wt GACCGGCTCTACAAAAACATCCAGAGGATGCAGCAAAGCC
ttll5gw237 GACCGG----------CCAGAGGATGCAGCAAAGCC
5′ CTCTACAAAAACATCCAG 3′
4 nt deletion
ttll5wt GACCGGCTCTACAAAAACATCCAGAGGATGCAGCAAAGC
ttll5gw238 GACCGGCTCTACAAAAACA----GAGGATGCAGCAAAGCC
C
ttll7 gene
0
100
200
300
400
500
600
700
800
900
TTLL7 protein
TTL domain
5′ TGACTCACCCATGGCCCA 3′
ttll7wt TGTGACTCACCCATGGCCCATGGCTCCATTTGCA
ttll7gw242 TGTGACTCACCCA-------TGGCTCCATTTGCA

Figure 4.8. Single and double mutants of microtubule glutamylation initiases do not exhibit any apparent defects. (A). Bright-field images of 48hpf wild type, *ttll4* $^{-/-}$, *ttll5* $^{-/-}$, *ttll7* $^{-/-}$, *ttll4* $^{-/-}$*; ttll5* $^{-/-}$, *ttll4* $^{-/-}$*; ttll7* $^{-/-}$, and *ttll5* $^{-/-}$*; ttll7* $^{-/-}$ embryos. (B) Bright-field images of six to eight months old wild type, *ttll4* $^{-/-}$, *ttll5* $^{-/-}$, *ttll7* $^{-/-}$, *ttll4* $^{-/-}$*; ttll5* $^{-/-}$, *ttll4* $^{-/-}$*; ttll7* $^{-/-}$, and *ttll5* $^{-/-}$*; ttll7* $^{-/-}$ male and female fishes.

A

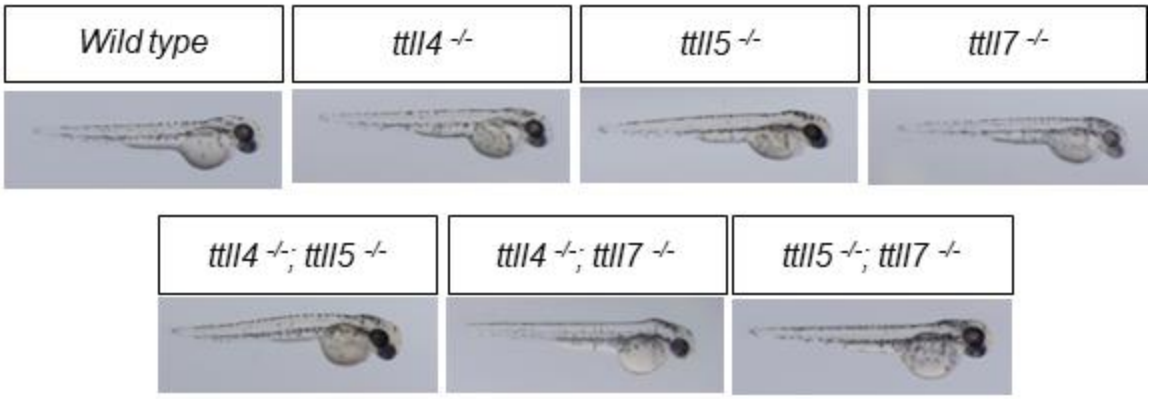
Wild type
ttll4 -/-
ttll5 -/-
ttll7 -/-
ttll4 -/-; ttll5 -/-
ttll4 -/-; ttll7 -/-
ttll5 -/-; ttll7 -/-

B

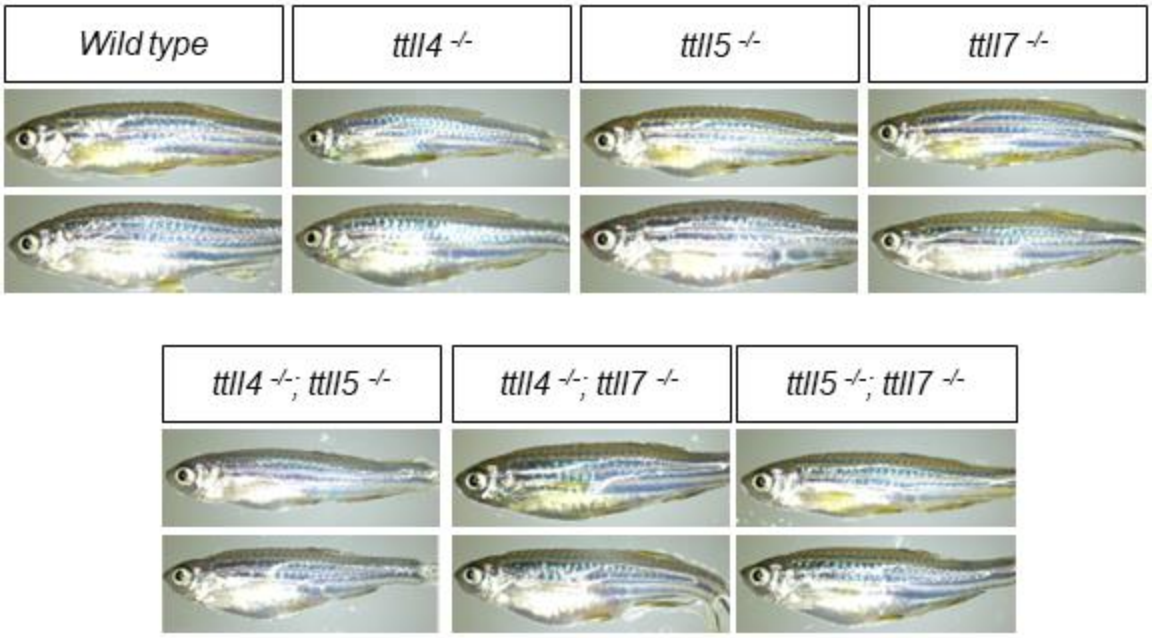
Wild type
ttll4 -/-
ttll5 -/-
ttll7 -/-
ttll4 -/-; ttll5 -/-
ttll4 -/-; ttll7 -/-
ttll5 -/-; ttll7 -/-

SUPPLEMENTAL FIGURES

Figure S4.1. Expression of *vash1, vash2,* and *ttl* expression in *Danio rerio*. RT-PCR was carried out with total RNA extracted from wild-type embryonic developmental stages, larval stages, and adult tissues. Expression of *gadph* was used as a reference, and No reverse transcriptase control was carried out for all samples to test genomic DNA contamination. (A). Microtubule detyrosination genes *vash1*, *vash2,* and retyrosination gene *ttl* were expressed maternally at the 8-cell stage. All three genes were expressed zygotically during embryonic stages (8hpf to 72hpf) and larval stages (96hpf-144hpf). (B). Microtubule detyrosination genes *vash1*, *vash2,* and retyrosination gene *ttl* were expressed in zebrafish adult tissues- Brain, testis, ovary, kidney, heart, gut, and liver.

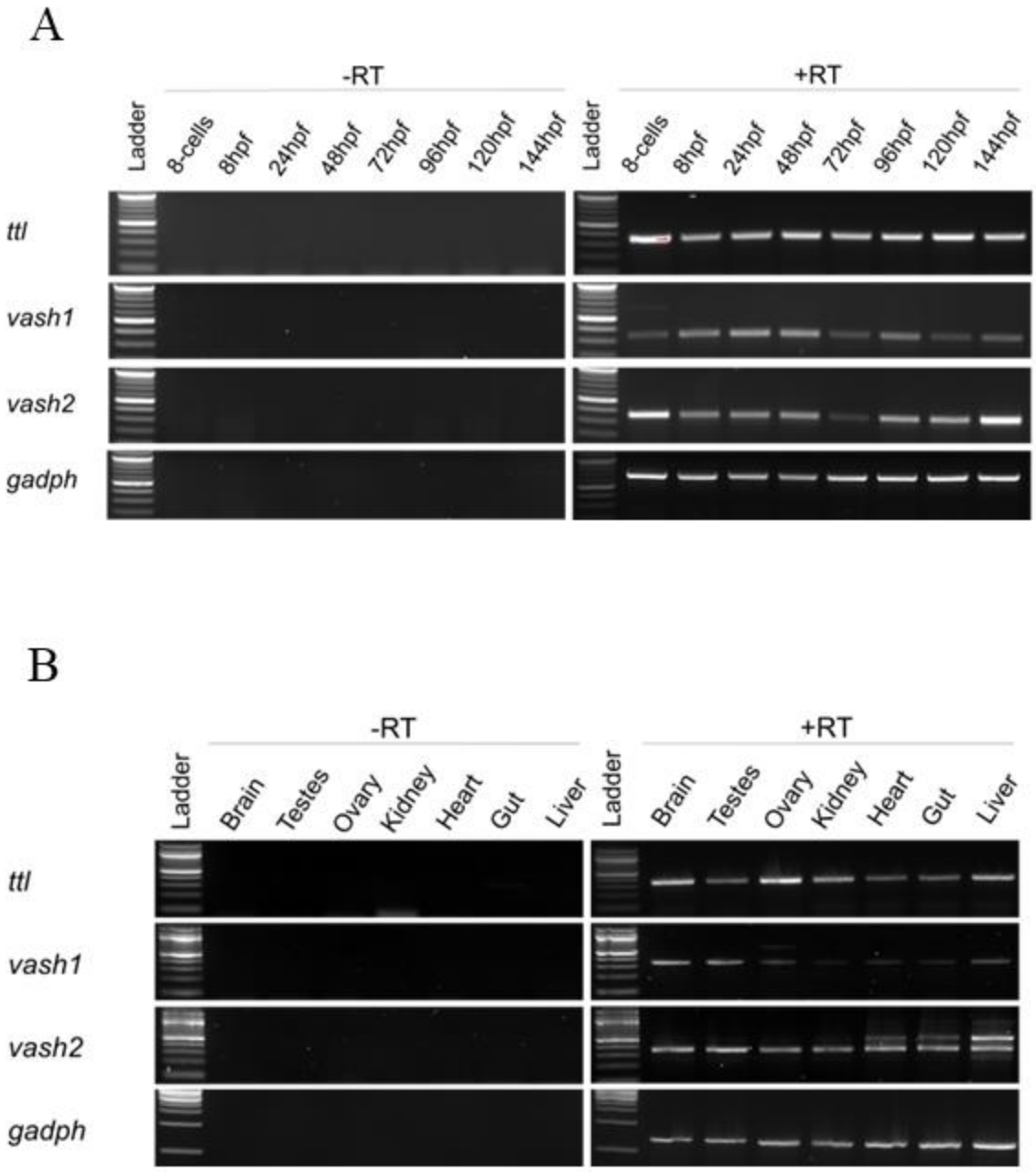
A
-RT
+RT
Ladder
8-cells
8hpf
24hpf
48hpf
72hpf
96hpf
120hpf
144hpf
ttl
vash1
vash2
gadph
B
-RT
+RT
Ladder
Brain
Testes
Ovary
Kidney
Heart
Gut
Liver
ttl
vash1
vash2
gadph

Figure S4.2. Microtubule detyrosination and tyrosination mutant brains show alteration in the level of detyrosinated microtubules. (A). Western blot of detyrosinated α-tubulin for wild-type, *vash1* $^{-/-}$, *vash2* $^{-/-}$, and *vash1* $^{-/-}$*; vash2* $^{-/-}$ and quantification (B). Western blot of detyrosinated α-tubulin for wild-type and *ttl* $^{-/-}$ quantification.

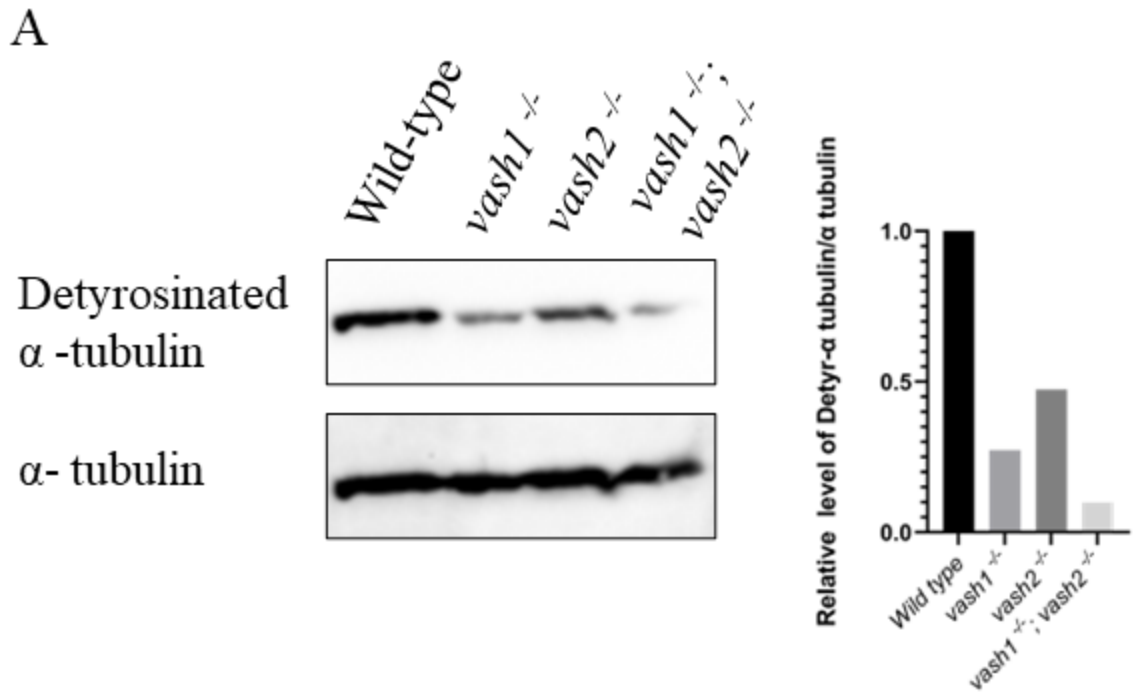
A
Wild-type
vash1 -/-
vash2 -/-
vash1 -/-; vash2 -/-
Detyrosinated α -tubulin
α- tubulin
Relative level of Detyr-α tubulin/α tubulin
1.0
0.5
0.0
Wild type
vash1 -/-
vash2 -/-
vash1 -/-; vash2 -/-

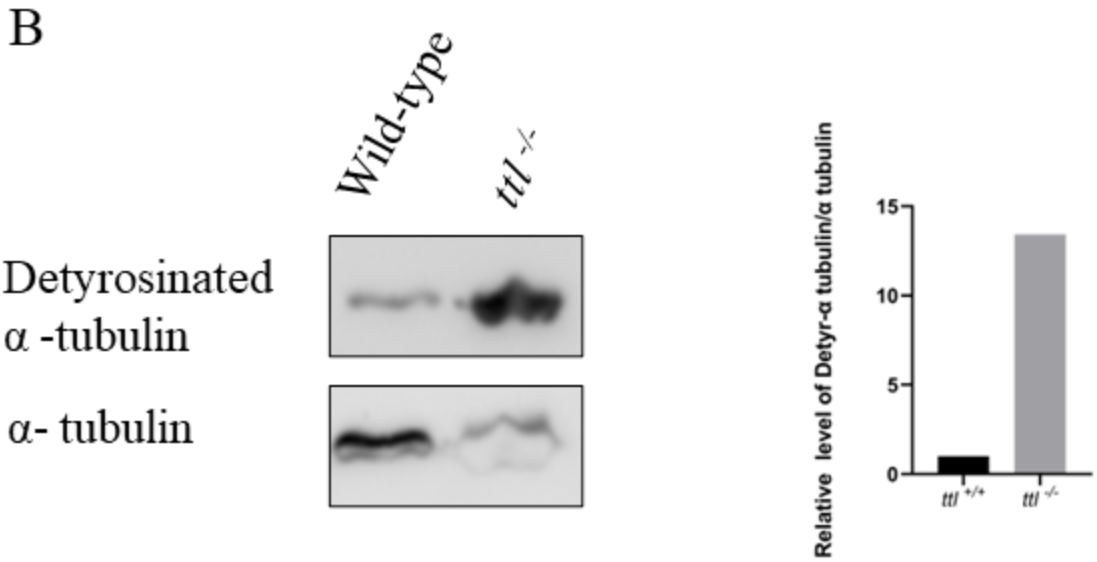
B
Wild-type
ttl -/-
Detyrosinated α -tubulin
α- tubulin
Relative level of Detyr-α tubulin/α tubulin
15
10
5
0
ttl +/+
ttl -/-

Figure S4.3. Microtubule detyrosination and tyrosination mutant testes show alteration in the level of detyrosinated microtubules. (A). Western blot of detyrosinated α-tubulin for wild-type, *vash1* $^{-/-}$, *vash2* $^{-/-}$, and *vash1* $^{-/-}$*; vash2* $^{-/-}$ (B). Quantification of western blot.

A

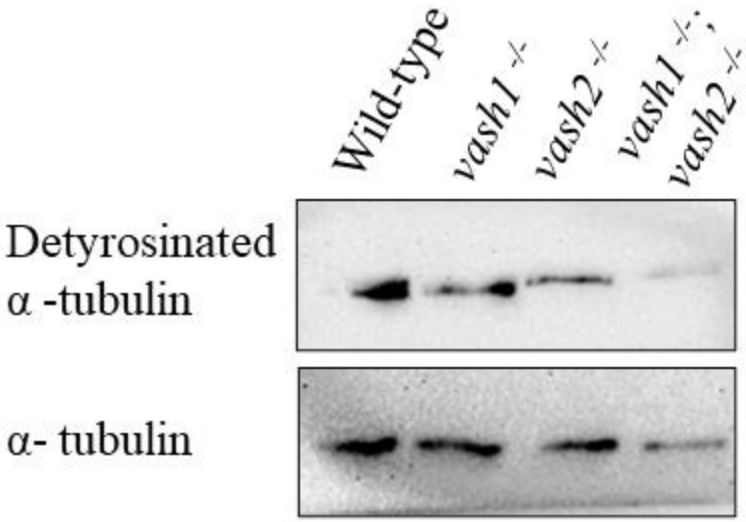
Wild-type
vash1 -/-
vash2 -/-
vash1 -/-; vash2 -/-
Detyrosinated α -tubulin
α- tubulin

B

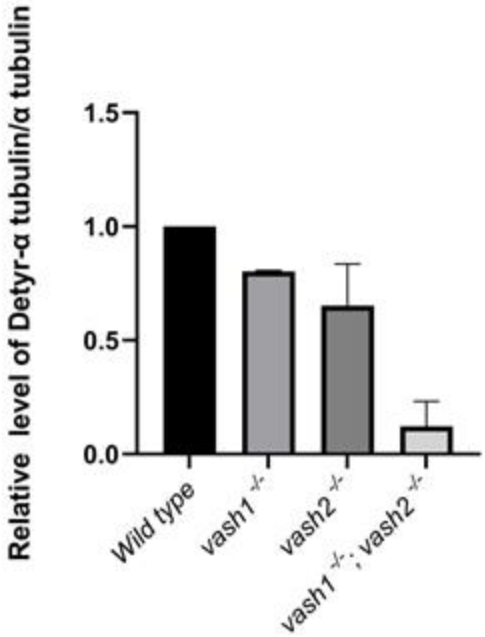
Relative level of Detyr-α tubulin/α tubulin
1.5
1.0
0.5
0.0
Wild type
vash1 -/-
vash2 -/-
vash1 -/-; vash2 -/-

Figure S4.4. Expression of *ttll1, ttll4, ttll5, ttll6* and *ttll7* expression in *Danio rerio*. RT-PCR was carried out with total RNA extracted from wild-type embryonic developmental stages, larval stages, and adult tissues. Expression of *gadph* was used as a reference, and No reverse transcriptase control was carried out for all samples to test genomic DNA contamination. (A). Microtubule detyrosination genes *vash1*, *vash2,* and retyrosination gene *ttl* were expressed maternally at the 8-cell stage. All three genes were expressed zygotically during embryonic stages (8hpf to 72hpf) and larval stages (96hpf-144hpf). (B). Microtubule detyrosination genes *vash1*, *vash2,* and retyrosination gene *ttl* were expressed in zebrafish adult tissues- Brain, testis, ovary, kidney, heart, gut, and liver.

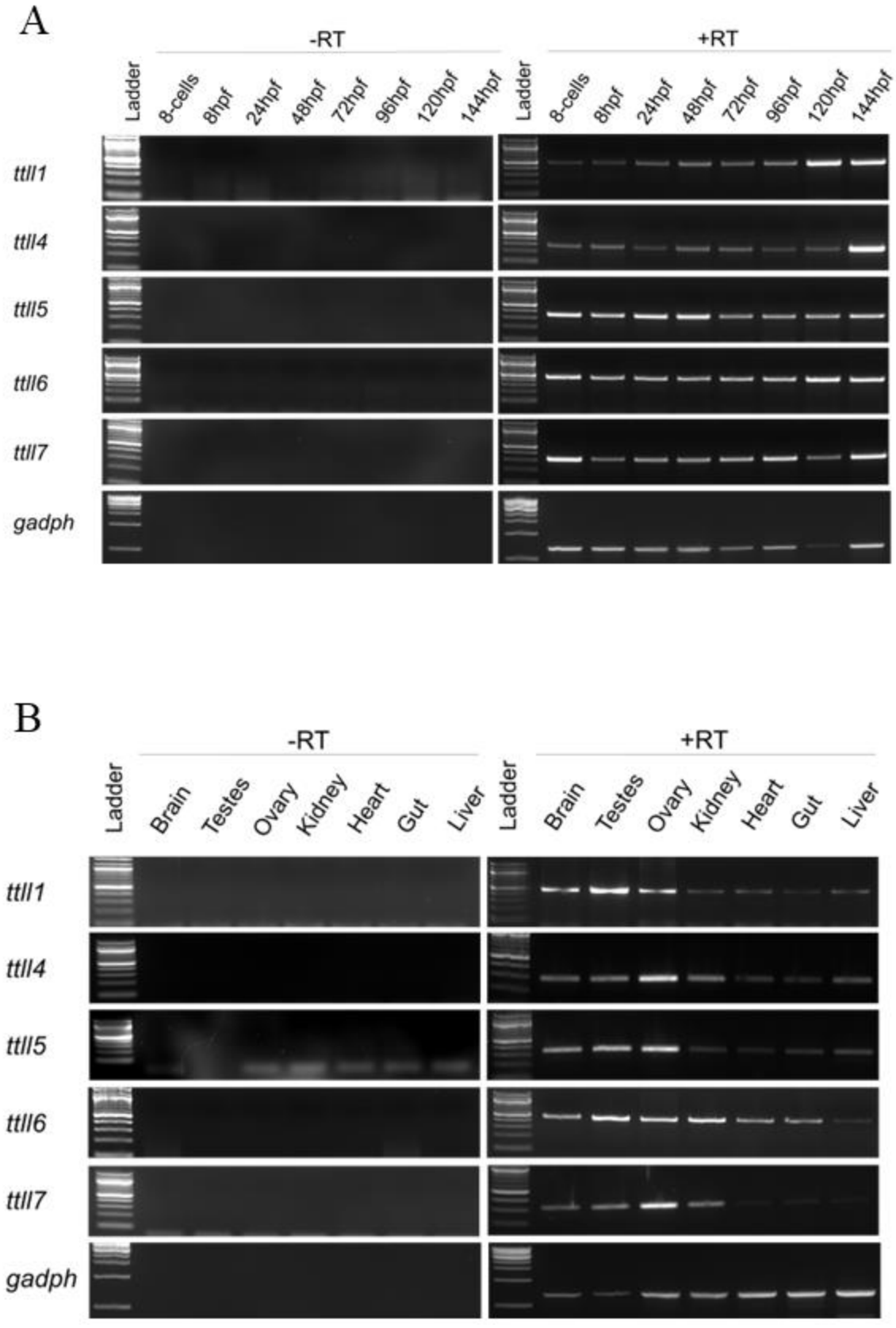
A
-RT
+RT
Ladder
8-cells
8hpf
24hpf
48hpf
72hpf
96hpf
120hpf
144hpf
ttll1
ttll4
ttll5
ttll6
ttll7
gadph
B
-RT
+RT
Ladder
Brain
Testes
Ovary
Kidney
Heart
Gut
Liver
ttll1
ttll4
ttll5
ttll6
ttll7
gadph

Figure S4.5. Microtubule glutamylation initiase mutants' brains show alteration in the level of monoglutamylated microtubules. (A). Western blot of detyrosinated α-tubulin for wild-type, *ttll4* $^{-/-}$, *ttll5* $^{-/-}$, and *ttll7* $^{-/-}$ (B). Quantification of western blot.

A

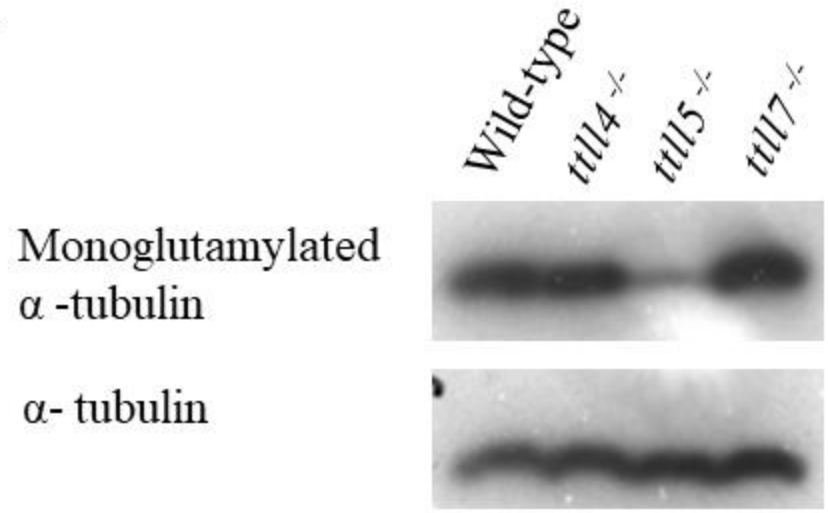
Wild-type
ttll4 -/-
ttll5 -/-
ttll7 -/-
Monoglutamylated
α -tubulin
α- tubulin

B

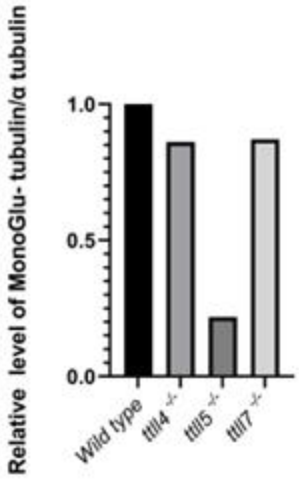
Relative level of MonoGlu- tubulin/α tubulin
1.0
0.5
0.0
Wild type
ttll4 -/-
ttll5 -/-
ttll7 -/-

CHAPTER 5

CONCLUSIONS AND FUTURE DIRECTIONS

In this collection of work, we identified the importance of microtubule acetylation and glycylation in the formation of chromosomal bouquet configuration that plays the role of the initial asymmetry breaking event during zebrafish oogenesis. We also showed that lack of acetylation leads to reduced aggression and mild social anxiety in zebrafish adults. The *atat1* mutant also showed an altered stress response. We also generated mutants of *vash1* and *vash2*, genes of microtubule detyrosination, *ttl* gene for microtubule retyrosination. Interestingly *vash1; vash2* double mutant, and *ttl* mutants show low penetrance curved body axis and heart edema phenotypes. The *vash1; vash2* double mutant also shows microcephaly as well. We found that *vash1* and *vash2* single and double mutants showed reduced synaptotagmin 2, a synaptic vesicle-associated membrane protein. We also generated mutant lines of *ttll4*, *ttll5,* and *ttll7* gene of microtubule glutamylation initiases to understand the role of microtubule glutamylation in development, ciliary and neuronal functions.

Loss of microtubule glycylation results in reduced survival and sperm motility in zebrafish

Microtubule glycylation is a microtubule PTM exclusively found in the axoneme of cilia (Levilliers et al., 1995). It is initiated by TTLL3 and TTLL8 and extended by TTLL10 (Rogowski et al., 2009, Ikegami and Setou, 2009). Zebrafish lack TTLL8, making TTLL3 the only initiase (Pathak et al., 2011). In previous morpholino studies, zebrafish ttll3 morphants showed ciliary defects like curved body axis, kidney cyst, and hydrocephalous phenotypes (Wloga et al., 2009, Pathak et al., 2011). We made a mutant line of *ttll3* using CRISPR-Cas9 mediated mutagenesis. The *ttll3* mutant embryos or adults did not exhibit any obvious morphological defects. Interestingly, this mutant showed subfertility and reduced progressive sperm motility. Mice *Ttll3* and *Ttll8* double mutants exhibited subfertility and reduced progressive motility due to alteration in the configuration of outer and inner dynein (Gadadhar et al., 2021). We need to study the sperm flagella using cryo-EM to confirm zebrafish mutant show similar changes as mice mutant. Zebrafish *ttll3* mutants also have reduced survival. The exact mechanism behind this observation is not known. But studies have attributed *ttll3* in colon cancer and retinal degeneration which have the potential ti impacts survival (Rocha et al., 2014, Bosch Grau et al., 2017). Further studies of *ttll3* $^{-/-}$ using histological methods and chemical or transgenic induced cancer studies to understand the low survival rate.

Elevation of microtubule acetylation in glycylation mutant

Past studies have shown that reduction in microtubule glycylation elevates the levels of microtubule glutamylation and microtubule acetylation (Rogowski et al., 2009, Wloga et

al., 2009). Studies also showed a reduction in microtubule acetylation elevates microtubule glycylation (Tseng, 2015, Łysyganicz et al., 2021). We found elevated levels of microtubule acetylation and glutamylation in *ttll3* mutant testis. Both microtubule glutamylation and glycylation take place in glutamate residues of the C-terminal tail of both α- and β- tubulin and they share several glutamate residues (Edde et al., 1990, Alexander et al., 1991, Rüdiger et al., 1992, Mary et al., 1994, Redeker et al., 1998, Garnham et al., 2017). These shared sites of modifications would explain the increase in the levels of glutamylation when the levels of glycylation are reduced due to increased sites for glutamylation. On the other hand increase in microtubule acetylation is interesting because they take place in different sites and have potential functional significance. An increase in the microtubule acetylation potentially compensates for the changes due to the loss of microtubule glycylation and could explain the lack of phenotype exhibited in *ttll3* mutant embryos.

The double mutant that lacks microtubule acetylation and monoglycylation exhibits defects in oogenesis

The presence of the Balbiani body determines the establishment of the animal-vegetal pole during oogenesis (Billett and Adam, 1976). Initial asymmetry breaking occurs during the zygotene stages of meiosis I. At this stage, the pole at which chromosomal bouquet formation occurs becomes the site for accumulating the Balbiani body precursors and future vegetal pole (Elkouby et al., 2016). A novel zygotene stage cilium plays an important role in proper chromosomal bouquet formation (Mytlis et al., 2022). In our study, we found that microtubule PTMs acetylation and glycylation play an important

role in chromosomal bouquet formation during oogenesis. Our study found that *atat1; ttll3* have reduced female fecundity and fertility and increased apoptosis in ovaries. We also found that chromosomal bouquet configuration is expanded in double mutants compared to double heterozygous of single mutant oocytes. Zygotene stage cilium plays an important role in forming a normal chromosomal bouquet, and these cilia are enriched with microtubule acetylation and monoglycylation. Interestingly, zygotene cilia in the double mutants did not exhibit any alteration in the establishment and maintenance of these cilia.

Understanding the mechanism behind this finding requires further studies. Zygotene cilia play a role in anchoring centrosome that plays a critical role in telomere movement (Mytlis et al., 2022). Telomere movement occurs by exerting force on the centrosome through perinuclear microtubules by the SUN-KASH complex associated with telomeres (Shibuya et al., 2014). These modifications have been shown to alter microtubule properties like stability, rigidity, and flexibility (LeDizet and Piperno, 1987, Akella et al., 2010, Xu et al., 2017, Portran et al., 2017, Wall et al., 2020). Based on the enrichment of these modifications only in zygotene cilia and anchoring role, we hypothesize the alteration that we see in chromosomal bouquet formation is due to the alteration in physical properties of a ciliary axoneme that anchor the centrosome. The changes in the physical properties would result in unproductive force exertion on the centrosome and increased centrosome vibration. To test this hypothesis, we need to study the physical properties of microtubules that lack acetylation and glycylation compared to microtubules with both modifications and that lack one PTM. We also need to study whether there is an increased vibration of the centrosome and a delay or reduction in the velocity of

telomere movement. We could do this live imaging of ovaries with transgenically tagged chromosomal bouquet formation components.

Lack of microtubule acetylation causes behavioral changes

Past studies have shown behavioral defects like touch response and motor coordination in *atat1* mutants (Akella et al., 2010, Shida et al., 2010, Morley et al., 2016, Yan et al., 2018). The *atat1* mutant embryos show a defect in touch-evoked swimming behavior. This mutant showed no obvious defects in sensory neurons, motor neurons, or muscle arrangement. In mice and *Drosophila*, defects in microtubules associated with mechanosensory ion channels implicated in touch defects. We must conduct further experiments to understand whether similar defects occur in zebrafish *atat1* mutant.

We also found that loss of microtubule acetylation alters zebrafish aggression and social behavior. The *atat1* mutants showed reduced aggression compared to wild heterozygous siblings. In social interaction and shoaling assay, we also found that *atat1* mutants exhibit anxiety - less time spent in the upper tank and increased freezing behaviors. In the novel tank experiment, *atat1* mutants comparable anxiety, exploration, and motor behavior. The dentate gyrus and striatum of *Atat1* mutant mice have shown defects; these regions are known to regulate aggression and social behavior (Kim et al., 2013, Li et al., 2019). Preliminary histological analysis of the analogous region in zebrafish does not exhibit obvious defects, further analysis with many individual fishes. Similar behavior is also shown in zebrafish histamine H3 receptor mutant (Reichmann et al., 2020). We need to study further regions activated when *atat1* mutants undergo these behavioral assays using

c-fos or rpS6 as neuronal activation markers. Alterations in neurotransmitter levels could also be studied.

Mutant that lack microtubule acetylation exhibits defect in stress response

Microtubule hyperacetylation has been shown in response to stress (Giustiniani et al., 2009, Geeraert et al., 2010, Mackeh et al., 2014, Li et al., 2019). We found that zebrafish larva shows hyperacetylation under stress conditions. We also found that *atat1* mutants showed reduced survival under certain stress conditions, indicating microtubule acetylation's role in stress response. Our preliminary data show an alteration in elevation cortisol in response to some stress in this mutant. To understand how the loss of ATAT1 alters the HPA axis, we need to study the levels of HPA axis gene expression and neurotransmitter levels. Another possibility for altered stress response could be the alteration in sensing the stress condition. Studying the behavior changes under stress conditions would allow us to shed light on this area.

Generation of microtubule detyrosination mutants

Microtubule detyrosination is enriched in neuronal axons and ciliary axonemes (Cambray-Deakin and Burgoyne, 1987, Mary et al., 1996). Posttranslational removal of terminal tyrosine is carried out by VASH1 and VASH2 (Aillaud et al., 2017, Nieuwenhuis et al., 2017). TTL carries out the retyrosination (Raybin and Flavin, 1977). We generated mutants of enzymes that carry out microtubule detyrosination and retyrosination. We found that *vash1*, *vash2*, and *vash1*; *vash2* mutants show a reduction in the levels of microtubule detyrosination compared to wild type. Interestingly, we found

some residual microtubule detyrosination in *vash1*; *vash2* double mutants. We hypothesized that this residual detyrosination is due to a gene-encoded isotype lacking terminal tyrosine. Other possibilities are the presence of additional microtubule detyrosinases and our mutants being not null. A similar residual detyrosinated microtubule was reported in human cell lines (Nieuwenhuis et al., 2017). The *vash1*; *vash2* double mutants show low penetrance curved body axis, heart edema, and microcephaly phenotype. Interestingly, defective microtubule detyrosination has been shown to associate with microcephaly and cognitive deficiency in humans (Pagnamenta et al., 2019). We also found that levels of synaptotagmin-2, a synaptic vesicle membrane-associated protein, reduced in single and double mutants, indicating potential defects in axonal transportation. The *ttl* mutant showed a drastic increase in the level of microtubule detyrosination. The *ttl* mutant showed low penetrance curved body and heart edema phenotype, but most embryos and adults were normal. Interestingly, mice *Ttl* mutant showed a much more severe phenotype where mutants died postnatal (Erck et al., 2005). To further understand the roles of these modifications in neuronal function, we need to carry out whole-mount immunofluorescence, behavioral assays, and transient transgenesis-based assays to study axonal transport.

Microtubule detyrosination is enriched in cilia, but its importance in ciliary function is unknown. With whole-mount immunofluorescence, live imaging of ciliary beating, TEM, and Cryo-EM, we should be able to study the roles of microtubule detyrosination on ciliary functions.

Generation of microtubule glutamylation initiation mutants

Microtubule glutamylation occurs in the C-terminal tail of both α- and β-tubulin (Edde et al., 1990). This modification is carried out by tubulin tyrosine kinase-like (TTLL) family proteins (Janke et al., 2005). Microtubule glutamylation is initiated by TTLL4, TTLL5, and TTLL7 and elongated by other members of TTLL family proteins (Ikegami et al., 2006, Van Dijk et al., 2007). This modification is enriched in the ciliary axoneme and neuronal axons (Edde et al., 1990, Fouquet et al., 1994). Understanding the roles of microtubule glutamylation initiase *ttll4*, *ttll5*, and *ttll7* on these biological functions is yet to be studied in zebrafish. We generated mutants of these microtubule glutamylation initiases. The *ttll5* mutant, the only α-tubulin glutamylation initiase, showed a drastic reduction in monoglutamylated tubulin. The reduction in level of monoglutamylation was minor in β-tubulin glutamylation initiatiases, *ttll4* and *ttll7*, indicationg potential compensatory role between these mutants. These mutants and double mutants of these genes did not exhibit obvious morphological defects in embryos or adults. Preliminary observations show potential fertility problems in *ttll5, ttll4*; *ttll5*, and *ttll5*; *ttll7*. Mice *Ttll5* mutants exhibited male fertility problems and reduced sperm motility (Lee et al., 2013, Bedoni et al., 2016). Further studies with single male or female mutant crosses with wildtype fishes confirm fertility problems and sperm motility assays to understand defects in flagella. With the employment of techniques like whole-mount immunofluorescence, live imaging of ciliary beating, TEM, and Cryo-EM, we should be able to study the roles these modifications play on ciliary functions. In mice it has been shown that microtubule glutamylases play role in neurite growth, reduced axonal transportation and synaptic transmission (Ikegami et al., 2006, Ikegami et al., 2007,

Lessard et al., 2019). We could also employ whole-mount immunofluorescence, behavioral assays, and transient transgenesis-based assays to study axonal transport to understand the neuronal function of these genes.

Interaction between microtubule PTMs

In a cellular environment, these modifications do not occur exclusively on individual regions of microtubules, and these modifications occur in an overlapping fashion. In the case of neuronal axons, they harbor microtubule acetylation, glutamylation, and detyrosination. Ciliary axonemes are enriched in microtubule acetylation, glutamylation, glycylation, and detyrosination. So in cellular environments, they carry out functions together, potentially having overlapping or interacting functions. In zebrafish, morphants of *ttll3* and *ttll6* exhibited a more severe ciliary defect phenotype than single morphants or one injected with the mismatch morpholino (Pathak et al., 2011). Our study also shows the role of microtubule acetylation and glycylation during oogenesis. A recent study with an antibody that recognizes glutamylated and detyrosinated microtubules shows enrichment in the hippocampal region (Vu et al., 2017). This study show differential enrichment of microtubule PTMs in different types of neurons. In Alzheimer's diseased brain, the level of microtubules glutamylation and detyrosination was increased. Since we possess mutants lacking these four microtubules PTMs, we could use them to understand their interactions to carry out cellular functions and how the lack of these modifications individually and in combination alters physical properties and preferential association of microtubule associate proteins (MAPs) using the same techniques. We could also study how the lack of these modifications individually and in combination would affect the

ciliary axoneme and neuronal axon and the transportation of materials along with them. Studying these mutants will allow us to expand our knowledge of the role of microtubule PTMs and their interaction in carrying out cellular functions.

REFERENCES

AILLAUD, C., BOSC, C., PERIS, L., BOSSON, A., HEEMERYCK, P., VAN DIJK, J., LE FRIEC, J., BOULAN, B., VOSSIER, F. & SANMAN, L. E. 2017. Vasohibins/SVBP are tubulin carboxypeptidases (TCPs) that regulate neuron differentiation. *Science,* 358**,** 1448-1453.

AKELLA, J. S., WLOGA, D., KIM, J., STAROSTINA, N. G., LYONS-ABBOTT, S., MORRISSETTE, N. S., DOUGAN, S. T., KIPREOS, E. T. & GAERTIG, J. 2010. MEC-17 is an α-tubulin acetyltransferase. *Nature,* 467**,** 218-222.

ALEXANDER, J. E., HUNT, D. F., LEE, M. K., SHABANOWITZ, J., MICHEL, H., BERLIN, S. C., MACDONALD, T. L., SUNDBERG, R. J., REBHUN, L. I. & FRANKFURTER, A. 1991. Characterization of posttranslational modifications in neuron-specific class III beta-tubulin by mass spectrometry. *Proceedings of the National Academy of Sciences,* 88**,** 4685-4689.

BEDONI, N., HAER-WIGMAN, L., VACLAVIK, V., TRAN, V. H., FARINELLI, P., BALZANO, S., ROYER-BERTRAND, B., EL-ASRAG, M. E., BONNY, O. & IKONOMIDIS, C. 2016. Mutations in the polyglutamylase gene TTLL5, expressed in photoreceptor cells and spermatozoa, are associated with cone-rod degeneration and reduced male fertility. *Human molecular genetics,* 25**,** 4546-4555.

BILLETT, F. & ADAM, E. 1976. The structure of the mitochondrial cloud of Xenopus laevis oocytes.

BOSCH GRAU, M., MASSON, C., GADADHAR, S., ROCHA, C., TORT, O., MARQUES SOUSA, P., VACHER, S., BIECHE, I. & JANKE, C. 2017. Alterations in the balance of tubulin glycylation and glutamylation in photoreceptors leads to retinal degeneration. *Journal of cell science,* 130**,** 938-949.

CAMBRAY-DEAKIN, M. A. & BURGOYNE, R. D. 1987. Posttranslational modifications of alpha-tubulin: acetylated and detyrosinated forms in axons of rat cerebellum. *The Journal of cell biology,* 104**,** 1569-1574.

EDDE, B., ROSSIER, J., LE CAER, J.-P., DESBRUYERES, E., GROS, F. & DENOULET, P. 1990. Posttranslational glutamylation of α-tubulin. *Science,* 247**,** 83-85.

ELKOUBY, Y. M., JAMIESON-LUCY, A. & MULLINS, M. C. 2016. Oocyte polarization is coupled to the chromosomal bouquet, a conserved polarized nuclear configuration in meiosis. *PLoS biology,* 14**,** e1002335.

ERCK, C., PERIS, L., ANDRIEUX, A., MEISSIREL, C., GRUBER, A. D., VERNET, M., SCHWEITZER, A., SAOUDI, Y., POINTU, H. & BOSC, C. 2005. A vital role of tubulin-tyrosine-ligase for neuronal organization. *Proceedings of the National Academy of Sciences,* 102**,** 7853-7858.

FOUQUET, J. P., KANN, M. L., EDDE, B., WOLFF, A., DESBRUYERES, E. & DENOULET, P. 1994. Differential distribution of glutamylated tubulin during spermatogenesis in mammalian testis. *Cell motility and the cytoskeleton,* 27**,** 49-58.

GADADHAR, S., ALVAREZ VIAR, G., HANSEN, J. N., GONG, A., KOSTAREV, A., IALY-RADIO, C., LEBOUCHER, S., WHITFIELD, M., ZIYYAT, A. & TOURÉ, A. 2021. Tubulin glycylation controls axonemal dynein activity, flagellar beat, and male fertility. *Science,* 371**,** eabd4914.

GARNHAM, C. P., YU, I., LI, Y. & ROLL-MECAK, A. 2017. Crystal structure of tubulin tyrosine ligase-like 3 reveals essential architectural elements unique to tubulin monoglycylases. *Proceedings of the National Academy of Sciences,* 114**,** 6545-6550.

GEERAERT, C., RATIER, A., PFISTERER, S. G., PERDIZ, D., CANTALOUBE, I., ROUAULT, A., PATTINGRE, S., PROIKAS-CEZANNE, T., CODOGNO, P. & POÜS, C. 2010. Starvation-induced hyperacetylation of tubulin is required for the stimulation of autophagy by nutrient deprivation. *Journal of Biological Chemistry,* 285**,** 24184-24194.

GIUSTINIANI, J., DAIRE, V., CANTALOUBE, I., DURAND, G., POÜS, C., PERDIZ, D. & BAILLET, A. 2009. Tubulin acetylation favors Hsp90 recruitment to microtubules and stimulates the signaling function of the Hsp90 clients Akt/PKB and p53. *Cellular signalling,* 21**,** 529-539.

IKEGAMI, K., HEIER, R. L., TARUISHI, M., TAKAGI, H., MUKAI, M., SHIMMA, S., TAIRA, S., HATANAKA, K., MORONE, N. & YAO, I. 2007. Loss of α-tubulin polyglutamylation in ROSA22 mice is associated with abnormal targeting of KIF1A and modulated synaptic function. *Proceedings of the National Academy of Sciences,* 104**,** 3213-3218.

IKEGAMI, K., MUKAI, M., TSUCHIDA, J.-I., HEIER, R. L., MACGREGOR, G. R. & SETOU, M. 2006. TTLL7 is a mammalian β-tubulin polyglutamylase required for growth of MAP2-positive neurites. *Journal of Biological Chemistry,* 281**,** 30707-30716.

IKEGAMI, K. & SETOU, M. 2009. TTLL10 can perform tubulin glycylation when co-expressed with TTLL8. *FEBS letters,* 583**,** 1957-1963.

JANKE, C., ROGOWSKI, K., WLOGA, D., REGNARD, C., KAJAVA, A. V., STRUB, J.-M., TEMURAK, N., VAN DIJK, J., BOUCHER, D. & VAN DORSSELAER, A. 2005. Tubulin polyglutamylase enzymes are members of the TTL domain protein family. *Science,* 308**,** 1758-1762.

KIM, G.-W., LI, L., GORBANI, M., YOU, L. & YANG, X.-J. 2013. Mice lacking α-tubulin acetyltransferase 1 are viable but display α-tubulin acetylation deficiency and dentate gyrus distortion. *Journal of Biological Chemistry,* 288**,** 20334-20350.

LEDIZET, M. & PIPERNO, G. 1987. Identification of an acetylation site of Chlamydomonas alpha-tubulin. *Proceedings of the National Academy of Sciences,* 84**,** 5720-5724.

LEE, G.-S., HE, Y., DOUGHERTY, E. J., JIMENEZ-MOVILLA, M., AVELLA, M., GRULLON, S., SHARLIN, D. S., GUO, C., BLACKFORD, J. A. & AWASTHI, S. 2013. Disruption of Ttll5/stamp gene (tubulin tyrosine ligase-like protein 5/SRC-1 and TIF2-associated modulatory protein gene) in male mice causes sperm malformation and infertility. *Journal of Biological Chemistry,* 288**,** 15167-15180.

LESSARD, D. V., ZINDER, O. J., HOTTA, T., VERHEY, K. J., OHI, R. & BERGER, C. L. 2019. Polyglutamylation of tubulin's C-terminal tail controls pausing and motility of kinesin-3 family member KIF1A. *Journal of Biological Chemistry,* 294**,** 6353-6363.

LEVILLIERS, N., FLEURY, A. & HILL, A.-M. 1995. Monoclonal and polyclonal antibodies detect a new type of post-translational modification of axonemal tubulin. *Journal of Cell Science,* 108**,** 3013-3028.

LI, L., JAYABAL, S., GHORBANI, M., LEGAULT, L.-M., MCGRAW, S., WATT, A. J. & YANG, X.-J. 2019. ATAT1 regulates forebrain development and stress-induced tubulin hyperacetylation. *Cellular and molecular life sciences,* 76**,** 3621-3640.

ŁYSYGANICZ, P. K., POORANACHANDRAN, N., LIU, X., ADAMSON, K. I., ZIELONKA, K., ELWORTHY, S., VAN EEDEN, F. J., GRIERSON, A. J. & MALICKI, J. J. 2021. Loss of Deacetylation Enzymes Hdac6 and Sirt2 Promotes Acetylation of Cytoplasmic Tubulin, but Suppresses Axonemal Acetylation in Zebrafish Cilia. *Frontiers in Cell and Developmental Biology*, 9.

MACKEH, R., LORIN, S., RATIER, A., MEJDOUBI-CHAREF, N., BAILLET, A., BRUNEEL, A., HAMAÏ, A., CODOGNO, P., POÜS, C. & PERDIZ, D. 2014. Reactive oxygen species, AMP-activated protein kinase, and the transcription cofactor p300 regulate α-tubulin acetyltransferase-1 (αTAT-1/MEC-17)-dependent microtubule hyperacetylation during cell stress. *Journal of Biological Chemistry,* 289**,** 11816-11828.

MARY, J., REDEKER, V., LE CAER, J.-P., PROMÉ, J.-C. & ROSSIER, J. 1994. Class I and IVa β-tubulin isotypes expressed in adult mouse brain are glutamylated. *FEBS letters,* 353**,** 89-94.

MARY, J., REDEKER, V., LE CAER, J.-P., ROSSIER, J. & SCHMITTER, J.-M. 1996. Posttranslational Modifications in the C-terminal Tail of Axonemal Tubulin from Sea Urchin Sperm (∗). *Journal of Biological Chemistry,* 271**,** 9928-9933.

MORLEY, S. J., QI, Y., IOVINO, L., ANDOLFI, L., GUO, D., KALEBIC, N., CASTALDI, L., TISCHER, C., PORTULANO, C. & BOLASCO, G. 2016. Acetylated tubulin is essential for touch sensation in mice. *Elife,* 5**,** e20813.

MYTLIS, A., KUMAR, V., QIU, T., DEIS, R., HART, N., LEVY, K., MASEK, M., SHAWAHNY, A., AHMAD, A., EITAN, H., NATHER, F., ADAR-LEVOR, S., BIRNBAUM, R. Y., ELIA, N., BACHMANN-GAGESCU, R., ROY, S. & ELKOUBY, Y. M. 2022. Control of meiotic chromosomal bouquet and germ cell morphogenesis by the zygotene cilium. *Science,* 0**,** eabh3104.

NIEUWENHUIS, J., ADAMOPOULOS, A., BLEIJERVELD, O. B., MAZOUZI, A., STICKEL, E., CELIE, P., ALTELAAR, M., KNIPSCHEER, P., PERRAKIS, A. & BLOMEN, V. A. 2017. Vasohibins encode tubulin detyrosinating activity. *Science,* 358**,** 1453-1456.

PAGNAMENTA, A. T., HEEMERYCK, P., MARTIN, H. C., BOSC, C., PERIS, L., USZYNSKI, I., GORY-FAURÉ, S., COULY, S., DESHPANDE, C. & SIDDIQUI, A. 2019. Defective tubulin detyrosination causes structural brain abnormalities with cognitive deficiency in humans and mice. *Human molecular genetics,* 28**,** 3391-3405.

PATHAK, N., AUSTIN, C. A. & DRUMMOND, I. A. 2011. Tubulin tyrosine ligase-like genes ttll3 and ttll6 maintain zebrafish cilia structure and motility. *Journal of Biological Chemistry,* 286**,** 11685-11695.

PORTRAN, D., SCHAEDEL, L., XU, Z., THÉRY, M. & NACHURY, M. V. 2017. Tubulin acetylation protects long-lived microtubules against mechanical ageing. *Nature cell biology,* 19**,** 391-398.

RAYBIN, D. & FLAVIN, M. 1977. Enzyme which specifically adds tyrosine to the α chain of tubulin. *Biochemistry,* 16**,** 2189-2194.

REDEKER, V., ROSSIER, J. & FRANKFURTER, A. 1998. Posttranslational modifications of the C-terminus of α-tubulin in adult rat brain: α4 is glutamylated at two residues. *Biochemistry,* 37**,** 14838-14844.

REICHMANN, F., RIMMER, N., TILLEY, C. A., DALLA VECCHIA, E., PINION, J., AL OUSTAH, A., CARRENO GUTIERREZ, H., YOUNG, A. M., MCDEARMID, J. R. & WINTER, M. J. 2020. The zebrafish histamine H3 receptor modulates aggression, neural activity and forebrain functional connectivity. *Acta physiologica,* 230**,** e13543.

ROCHA, C., PAPON, L., CACHEUX, W., MARQUES SOUSA, P., LASCANO, V., TORT, O., GIORDANO, T., VACHER, S., LEMMERS, B. & MARIANI, P. 2014. Tubulin glycylases are required for primary cilia, control of cell proliferation and tumor development in colon. *The EMBO journal,* 33**,** 2247-2260.

ROGOWSKI, K., JUGE, F., VAN DIJK, J., WLOGA, D., STRUB, J.-M., LEVILLIERS, N., THOMAS, D., BRÉ, M.-H., VAN DORSSELAER, A. & GAERTIG, J. 2009.

Evolutionary divergence of enzymatic mechanisms for posttranslational polyglycylation. *Cell,* 137**,** 1076-1087.

RÜDIGER, M., PLESSMAN, U., KLÖPPEL, K.-D., WEHLAND, J. & WEBER, K. 1992. Class II tubulin, the major brain β tubulin isotype is polyglutamylated on glutamic acid residue 435. *FEBS letters,* 308**,** 101-105.

SHIBUYA, H., MORIMOTO, A. & WATANABE, Y. 2014. The dissection of meiotic chromosome movement in mice using an in vivo electroporation technique. *PLoS genetics,* 10**,** e1004821.

SHIDA, T., CUEVA, J. G., XU, Z., GOODMAN, M. B. & NACHURY, M. V. 2010. The major α-tubulin K40 acetyltransferase αTAT1 promotes rapid ciliogenesis and efficient mechanosensation. *Proceedings of the National Academy of Sciences,* 107**,** 21517-21522.

TSENG, W. 2015. *Neural crest specification by Max's giant associated protein and regulation of microtubule's function by alpha-tubulin acetyltransferase 1 in zebrafish.* Doctor of Philosophy (PHD), University of Georgia.

VAN DIJK, J., ROGOWSKI, K., MIRO, J., LACROIX, B., EDDÉ, B. & JANKE, C. 2007. A targeted multienzyme mechanism for selective microtubule polyglutamylation. *Molecular cell,* 26**,** 437-448.

VU, H. T., AKATSU, H., HASHIZUME, Y., SETOU, M. & IKEGAMI, K. 2017. Increase in α-tubulin modifications in the neuronal processes of hippocampal neurons in both kainic acid-induced epileptic seizure and Alzheimer's disease. *Scientific reports,* 7**,** 1-14.

WALL, K. P., HART, H., LEE, T., PAGE, C., HAWKINS, T. L. & HOUGH, L. E. 2020. C-terminal tail polyglycylation and polyglutamylation alter microtubule mechanical properties. *Biophysical journal,* 119**,** 2219-2230.

WLOGA, D., WEBSTER, D. M., ROGOWSKI, K., BRÉ, M.-H., LEVILLIERS, N., JERKA-DZIADOSZ, M., JANKE, C., DOUGAN, S. T. & GAERTIG, J. 2009. TTLL3 Is a tubulin glycine ligase that regulates the assembly of cilia. *Developmental cell,* 16**,** 867-876.

XU, Z., SCHAEDEL, L., PORTRAN, D., AGUILAR, A., GAILLARD, J., MARINKOVICH, M. P., THÉRY, M. & NACHURY, M. V. 2017. Microtubules acquire resistance from mechanical breakage through intralumenal acetylation. *Science,* 356**,** 328-332.

YAN, C., WANG, F., PENG, Y., WILLIAMS, C. R., JENKINS, B., WILDONGER, J., KIM, H.-J., PERR, J. B., VAUGHAN, J. C. & KERN, M. E. 2018. Microtubule acetylation is required for mechanosensation in Drosophila. *Cell reports,* 25**,** 1051-1065. e6.